UNIVERSITY OF BIRMINGHAM

Engine Combustion and Emission Performance of Furan Fuels in Comparison to Conventional Automotive Fuels

By

Lewis Parry

A thesis submitted to

The University of Birmingham

For the degree of

DOCTOR OF PHILOSOPHY

The University of Birmingham

School of Mechanical Engineering

April 2020

ABSTRACT

The thesis investigates biofuel and biodiesel testing with fossil diesel. Initially, 2-methylfuran (MF) and diesel fuel blends were tested under various operating conditions with a final load experiment assessing MF and 2-methyltetrahydrofuran (MTHF). Novel tests were completed with various MF blends assessing the in-cylinder performance as well as the gaseous and particulate emissions. This testing included individually varying the injection pressure, exhaust gas recirculation and combustion phasing. All experiments used a four-cylinder 2.2l compression ignition (CI) engine.

The initial investigation assessed the suitability of an MF/diesel blend, highlighting reduced particle matter (PM) when compared to diesel.

Further tests evaluated three different MF/diesel blends (5, 15 and 25% MF b/v) under different conditions at 5 bar IMEP load. As the MF percentage increased, the oxides of nitrogen (NO_x), unburnt hydrocarbons (UHC) and carbon monoxide (CO) increased while the concentration, mass and surface area of accumulation and nucleation mode particles reduced. In comparison to diesel, it was found that the 25% MF blend attained on average NO_x, UHC and CO increases of 21%, 64% and 39%, respectively. Overall particle concentration, diameter, surface area and mass reduced by 61%, 18%, 65% and 62%, respectively. Hot exhaust gas recirculation (EGR) was used to reduce combustion sensitivity. The 25% MF testing with hot EGR found the UHC and CO formation to be on average 12% and 22% lower than the diesel cold EGR results while still attaining significantly reduced particulate results.

Load testing (1.4-9 bar BMEP) was completed using three biofuels/diesel blends. These biofuels were MF, MTHF and biodiesel. They were mixed at a ratio of 25% biofuel, 75%

diesel b/v. MF combustion was sensitive at the 1.4 and 3 BMEP loads. The biodiesel and MTHF blends performed similarly to diesel, with a slightly longer ignition delay. At the higher loads, the furan blends attained reduced NO_x, CO and UHC values over diesel while also reducing PM values. Throughout the load range, it was found that in comparison to diesel, the 25% MF blend attained an increase of UHC and CO by 26% and 55% with NO_x reducing by 6%. The average particulate concentration and diameter reduced by 62% and 37%. The 25% MTHF blend was found to, on average reduce NO_x, CO and UHC by 25%, 5% and 32%, respectively. The particle concentration and diameter reduced by 5% and 16%.

The increased gaseous emissions outweighed the reduced PM of the MF/diesel blends, highlighting the challenges of using MF within a CI engine. MTHF provided comparable combustion results to diesel while providing improved NO_x, CO, UHC and PM characteristics.

ACKNOWLEDGEMENTS

Firstly, I would like to thank my primary supervisor Professor Hongming Xu for his guidance and advice throughout my PhD. I must also thank my two secondary supervisor's Dr Jose M. Herreros and Professor Miros*ł*aw L. Wyszy*ń*ski for their advice. Thanks also goes to Dr Amrit Sahu and Dr Haoye Lui for providing support during my studies. A huge acknowledgement must go to Dr Soheil Zeraati Rezaei; he has provided a wide range of assistance and advice throughout and without his support, this work could not be presented. Thanks also needs to be given to Aawishkar Dharmadhikari and Carlo Coratella for working with me during experiments and providing encouragement during countless late nights of testing. I must also thank Omid Doudstar who provided support with additional reading materials and background knowledge.

Thank you to the technician's Jack Garrod, Kevan Charlesworth, Lee Gauntlett, Peter Thornton and Carl Hingley. All of whom helped me to attain high-quality experimental setups.

I am pleased to acknowledge the contribution of the IMechE Whitworth Senior Scholarship Award in supporting this research, thanks also needs to be given to Professor Karl D Dearn for bringing the society to my attention. The Whitworth society has allowed me to focus on my studies and produce work to the best of my ability.

I am sincerely grateful for the resources provided by Jaguar Land Rover (JLR) and by Shell Global Solutions. JLR provided components for engine modifications, and Shell supplied the commercial fuel used for this investigation. Acknowledgement also needs to be given to the EPSRC for the funding this project through project reference EP/N021746/1.

On a personal note, I need to thank my family and friends for their unwavering support over the past four years; I hope this work explains the events missed. It is not possible to acknowledge everyone here, but I am indebted to you all, my thoughts are especially with those not here to read this.

Thank you to my grandparents for making me believe that all of this is possible. I am fortunate to have grown around you all and to take aspects of your personalities with me. I wish you were all here to read this.

A special thanks goes to my sister and her family that has grown since I started this project. Seeing you and my nephews has helped me take a step back and appreciate life, I hope to grow some of your qualities in time. Thank you to my brother and his partner who have provided escapism on visits to them and the courage to believe that I can accomplish any goal I apply myself too.

I cannot express how thankful I am to my parents; ultimately, you have never made me question my decisions and have always provided support without hesitation. I know you have made sacrifices to get me to this point and I cannot express how proud and thankful I am to have you both.

Finally, my utmost thanks goes to my partner Zoe who has been with me throughout this process. She has shown what hard work and self-belief can achieve. Zoe has cushioned my low points of sustained medical leave while pursuing her own PhD and she has been with me to share the high points with. The day we met will be the highlight of my experience at the University of Birmingham and I will forever owe you what you have given me over the past four years.

I wish to dedicate this thesis to Malcolm, Iain and Thomas Parry.

They have forged me into a product of my environment and this work would not be possible without their years of input.

TABLE OF CONTENTS

LIST OF FIGURES

LIST OF TABLES

LIST OF EQUATIONS

LIST OF ABBREVIATIONS

Acc	Accumulation Mode
AFR	Air-Fuel Ratio
AHR	Accumulated Heat Release
AHR50	Accumulated Heat Release 50% Crank Angle
ANOVA	Analysis of Variance
ATDC	After Top Dead Centre
BDC	Bottom Dead Centre
BMEP	Brake Mean Effective Pressure
BP	Boiling Point
BSCO	Brake Specific Carbon Monoxide
BSFC	Brake Specific Fuel Consumption
$BSNO_x$	Brake Specific Oxides of Nitrogen
BTDC	Before Top Dead Centre
BTE	Brake Thermal Efficiency
BSUHC	Brake Specific Unburnt Hydrocarbon
CA	Crank Angle
CDC	Conventional Diesel Combustion
CEGR	Cold Exhaust Gas Recirculation
CI	Compression-Ignition
CMD	Count Median Diameter
CO	Carbon Monoxide
CO_2	Carbon Dioxide
COV	Coefficient of Variation
CR	Compression Ratio
DAQ	Data Acquisition
DEGR	Dual Exhaust Gas Recirculation
DHMF	2,5-dihydroxymethylfuran
DME	Di-Methyl Ether
DOE	Design of Experiment
DPF	Diesel Particulate Filter
ECU	Engine Control Unit

EGR	Exhaust Gas Recirculation
EOC	End of Combustion
EPSRC	Engineering and Physical Sciences Research Council
FAEE	Fatty Acid Ethyl Ester
FAME	Fatty Acid Methyl Ester
FF	Fossil Fuel
FSN	Filter Smoke Number
HCCI	Homogeneous Charge Compression Ignition
HEGR	Hot Exhaust Gas Recirculation
HEPA	High-Efficiency Particulate Arrestor
HMF	5-Hydroxymethylfurfural
HPEGR	High-Pressure Exhaust Gas Recirculation
HRR	Heat Release Rate
ICE	Internal Combustion Engine
IMEP	Indicated Mean Effective Pressure
IP	Injection Pressure
ISCO	Indicated Specific Carbon Monoxide
ISF	Insoluble Organic Fraction
ISFC	Indicated Specific Fuel Consumption
$ISNO_x$	Indicated Specific Oxides of Nitrogen
ITE	Indicated Thermal Efficiency
ISUHC	Indicated Specific Unburnt Hydrocarbons
LPEGR	Low-Pressure Exhaust Gas Recirculation
LTC	Low-Temperature Combustion
MCU	Main Control Unit
MF	2-Methylfuran
MTHF	2-Methyltetrahydrofuran
NDIR	Non-Dispersive Infrared
NI	National Instruments
NIMEP	Net Indicated Mean Effective Pressure
NO	Nitric Oxide
NO_x	Oxides of Nitrogen

Nuc	Nucleation Mode
NVH	Noise, Vibration and Harshness
OEM	Original Equipment Manufacturer
P-Rate	In-Cylinder Pressure Rate of Change
PAH	Polycyclic Aromatic Hydrocarbon
PCI	Partially Premixed Combustion
PCCI	Premixed Charge Compression Ignition
PID	Proportional Integral Derivative
PM	Particulate Matter
PN	Particle Number
PPC	Partially Premixed Combustion
PPCI	Partially Premixed Compression Ignition
PSD	Particle Size Distribution
PTO	Power Take-Off
RCCI	Reactivity Controlled Compression Ignition
RED	Renewable Energy Directive
RME	Rape-Seed Methyl Ester
RON	Research Octane Number
RPM	Revolutions Per Minute
S/N	Signal to Noise
SA	Surface Area
SC	Separated Cylinder
SI	Spark Ignition
SOC	Start of Combustion
SOI	Start of Injection
TDC	Top Dead Centre
UHC	Unburnt Hydrocarbon
VGT	Variable Geometry Turbine
VOF	Volatile Organic Fraction
WLTP	Worldwide Harmonised Light Vehicle Test Procedure
WSD	Wear Scar Diameter

LIST OF FORMULAIC EXPRESSIONS

Θ	*Crank angle*
γ	*Polytropic Index*
ω	*Engine Speed*
CO	*Carbon Monoxide*
CO_2	*Carbon Dioxide*
D	*Total Engine Displacement*
Fc	*Fuel Consumption*
H	*Hydrogen*
L	*S/N Level Value*
LHV	*Fuel Lower Heating Value*
n	*The number of responses in the factor level combination*
N	*Number of engine rotations per combustion stroke*
N	*Nitrogen Element*
N_2	*Nitrogen Molecule*
NO	*Nitric Oxide*
O	*Oxygen Element*
O_2	*Oxygen Molecule*
OH	*Hydroxide*
p	*In-Cylinder Pressure*
T	*Torque*
Qn	*Net Heat Release*
V	*In-Cylinder Volume*
Y	*The response for the given factor level*

CHAPTER 1

1. Introduction

Within the automotive industry, two major linked issues are raising significant concern. The first issue is based on fossil fuel consumption. In 2019 it was estimated that the transport sector accounted for 21% of total fossil fuel (FF) consumption worldwide. This equated to 3.15 billion tonnes of oil consumed per year, with this value anticipated to rise by 0.3% every year until 2040 (Dudley, 2019). This reliance on FF comes from a lack of similar products that are readily available at a comparable price. The second issue is the effect of global warming being seen from the use of FF. In recent years there has been lots of publicity about these effects. These issues present a responsibility to investigate non-fossil-based fuels that could be used within the automotive vehicle sector.

In the long-term, it is viewed that hydrogen-powered vehicles will be the most suitable alternative to FF powered vehicles (Ahmed et al., 2016) because of the abundance of hydrogen and the favourable emissions of heat and water vapour produced (Edwards et al., 2008, IEA, 2019). It is anticipated that the hydrogen internal combustion engine (ICE) will be the bridging technology between FF use and hydrogen fuel cell vehicles (Gillingham, 2018). Currently, the use of hydrogen as a fuel in mass-produced automotive vehicles is limited by significant safety concerns (Lipman, 2020). This means that suitable intermediary alternatives need to be found to reduce current FF consumption and greenhouse gas production while hydrogen technology progresses to a suitable state.

Electric power has become dominant in the automotive sector with vehicles being produced as solely electric or as a hybrid with an FF ICE. However, similar to the use of hydrogen propulsion, electric power is not entirely suitable for the automotive market yet

as there are significant weaknesses regarding vehicle performance, consumer requirements, charging infrastructure, technology progression and waste management. The issue of range and customer expectations is highlighted by comparing the range of a Tesla Model S and a Ford Mondeo. The Tesla Model S has a range of 183-249 miles when cruising at 75 mph (Straubel, 2014), whereas its competitor, a 2-litre diesel Euro6 Ford Mondeo has a range of 1464 miles with combined urban and extra-urban usage (FoMoCo, 2018). The rise of electric vehicles has been heavily backed by governments. However, they have failed to implement the correct infrastructure of charging points in the UK to compensate for this range deficit (Grote et al., 2019). Other concerns include limited knowledge of battery cells, meaning technology progression is difficult, expensive and dangerous (Bullis, 2015), along with issues regarding suitable means of recycling and disposing of batteries (Zhao and You, 2019).

From this analysis, it can be seen that both hydrogen and battery technology are not yet suitable alternatives to FF's in automotive vehicles. The most logical short-term solution is to use liquid biofuels. This is an ideal solution as a suitable biofuel would make most vehicles a suitable candidate for renewable fuels without significant modification. A large amount of time and economic resources have been invested into current internal combustion engine technology. Therefore, it is worthwhile to use these current ICE vehicles for as long as possible until battery and the hydrogen powertrain becomes a viable option.

1.1 Background

It has been speculated that the use of biofuels will be the first step to a long-term solution in reducing FF consumption and global warming (Council, 2008, Saini et al., 2018). Biofuels can be sourced from a number of cellulosic biomass products (e.g. plants, crops,

algae), or from subjects that consume this mass as part of their diet (e.g. human waste and animal waste/fat) (Jones and Mayfield, 2012, Adewale et al., 2015).

The use of biofuels is not a new concept, however, advances in production techniques mean that many biofuels that were once overlooked as FF ICE alternatives can now be re-analysed (Román-Leshkov et al., 2007). The possibilities made apparent by this improvement were reflected in a 2009 European Renewable Energy Directive (RED) (2009/28/EC), which stated that by 2020 10% of fuel used in the transport sector needed to be acquired from renewable sources. In 2018, a revised RED (2018/2001/EU) stated that biofuel consumption needed to increase to a minimum of 27% by 2030.

As of 2019, ethanol was the dominant biofuel used in the automotive sector worldwide (Lorne, 2019). Ethanol has many benefits when used within a compression ignition (CI) engine; this includes reduced smoke and nitrogen oxides (NO_x) (Hardenberg and Schaefer, 1981). However, the use of this fuel is only being considered as a short-term solution, as ethanol's characteristics are not ideal for an ICE fuel as it has a low energy density along with other negative aspects discussed in more detail in the literature review.

When discussing biofuels, it is crucial to understand the three main categories of biomass/feedstock used to manufacture the fuel. First-generation feedstock highlights a migration from carbon fuel dependence. The typical feedstocks include starch-rich sugars, grains and seeds as well as vegetable oil. First-generation feedstocks are not desirable as they encourage competition with food agriculture and require high volumes of water (Aro, 2016). The most conventional feedstock, second-generation, is derived from non-food biomasses that originate on land. These include organic and food waste, as well as wood and straw. The growable biomass in this category attains a high yield in

terms of space consumed. Some biomasses can be grown on poor quality land, while other second-generation biomasses require food-growing land. It should be noted that the use of organic waste for feedstock (e.g. corn and sugar husks) means that the waste cannot be used as compost which will eventually reduce the fertility of land and food growing potential (Singh et al., 2017). Third generation biofuels are the most appealing economically as they have no interaction with food agriculture. They are more energy dense than the other two options and also require minimal maintenance while being completely renewable. Third generation feedstocks include algae and seaweed. These have an abundance of production space and can be watered with untreated saltwater. However, advances need to be investigated to improve their production method of third-generation biofuels (Dragone et al., 2010).

The production advances discussed by Román-Leshkov provides economic feasibility to a range of biofuels (Román-Leshkov et al., 2007). The main advantage of using biofuels within ICE's is their oxygenated nature providing additional oxygen to favour the combustion process. The effective use of these types of fuels can allow for reduced particulate matter (PM), carbon monoxide (CO) and unburnt hydrocarbons (UHC) with a marginal increase in the production of NO_x (Patil and Taji, 2013).

1.2 Research Outline

For a biofuel to become a stable product, it is required to consider availability, carbon footprint, sustainability and affordability. When investigating a biofuel that may be used within the automotive sector, it is also necessary to assess its combustion and emission characteristics. It is required to compare the performance seen between a proposed new fuel and conventional fossil fuel. It should be noted that throughout this thesis, petroleum/fossil diesel will be referred to as diesel.

An attractive biofuel that has been focussed on in this thesis is 2-methylfuran (MF). Its use has been researched extensively within a spark ignition (SI) engine because of its similar characteristics to gasoline; however, little research has been undertaken to review MF's performance within a CI engine.

In this investigation, MF's performance will be heavily researched against diesel along with a follow-up testing comparing MF's performance against 2-methyltetrahydrofuran (MTHF) and biodiesel. This will enable the author to conclude whether the other investigated biofuels could be a suitable candidate for sustainable CI usage.

1.3 Investigation Aim and Objectives

The research undertaken in this thesis was conducted by the author in the *Future Engines and Fuels* lab within the University of Birmingham. The on-engine experiments that will be discussed were completed with an inline four-cylinder CI engine; however, some of the tests were conducted with one cylinder's gas flow and fuel delivery separated from the other three.

The aim of this thesis was to investigate possible substitutes to diesel within a CI engine. The main focus of the research was to investigate the performance of MF within a CI engine. The impact and novelty of the research is reinforced by the financial support provided by the Engineering and Physical Sciences Research Council (EPSRC) through project reference EP/NO21746/1. The objectives that were completed to ensure a thorough investigation include:

1. Evaluation of the suitability of MF and diesel blends in a compression ignition engine, taking into account the engine performance and exhaust emissions. An initial screening type study supported by statistical analysis of a single 2-

methylfuran and diesel blend was carried out. The analysis was used to find the optimum engine settings of set inputs to satisfy set reviewed outputs. The importance of each input regarding the outputs was assessed. Additional analysis was also undertaken to compare the performance of the blend and neat diesel at the optimum condition.

2. Understanding the interactions between MF fuel properties and engine parameters. Testing included varying MF/diesel blend ratios along with altering fixed engine parameters. Detailed analysis of the gaseous emissions produced was investigated. A follow-up analysis was carried out with the same parameters and blends while evaluating the particulate matter emitted.
3. Evaluation of the engine performance and emissions of furan fuels in comparison to conventional diesel fuel and biodiesel. Load testing of an MF and diesel blend and an MTHF/diesel blend. The outcomes were compared against neat diesel and a biodiesel/diesel blend. This allowed for comparison of the furan fuels performance in regard to the current automotive fuel choice and the most likely future biofuel/diesel choice.

1.4 Thesis Outline

This investigation is divided into a total of eight chapters which systematically investigates the suitability of using furan/diesel blends within an automotive CI engine. The flow diagram below is used to display the chosen structure of this thesis and highlights their necessity. A brief overview of each of the following chapters is provided in the following section and the flow of this body of work is displayed in Figure 1-1.

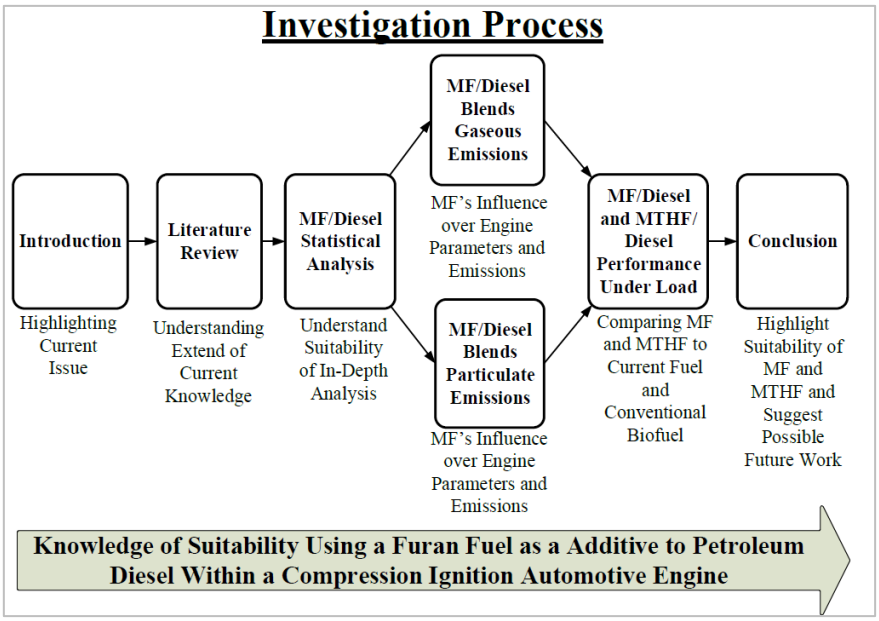

Figure 1-1 Investigation Flow Chart.

1.4.1 Chapter Overview

1.4.1.1 Chapter 2 –Literature Review

This chapter provides an overview of the relevant topics regarding the investigation. Analysis of the combustion and emissions generated from compression ignition is reviewed along with emissions regulations. Technologies that have been used to improve engine performance and reduce emissions are assessed. Currently accessible biofuels will be discussed along with a review of possible alternative biofuels. These alternatives include furan-based fuels mainly focussing on MF and MTHF.

1.4.1.2 Chapter 3 – Experimental Setup

This chapter provides detailed information about the engine test cell used, along with information regarding data acquisition and analysis. A key and unique engine conversion was also used for some experiments and will be discussed in this section.

1.4.1.3 Chapter 4 – Statistical Analysis of a 2-Methylfuran and Diesel Blend

This section completes a Taguchi based statistical analysis on a single blend ratio of 2-methylfuran and diesel. This analysis will provide an insight into the suitability of using MF within a CI engine and concludes the necessity of an in-depth evaluation.

1.4.1.4 Chapter 5 – Gaseous Emission Behaviour of 2-Methylfuran and Diesel Blends

Engine gaseous emissions are the focus of this section. Set parameters of the engine will be fixed while altering a single parameter. Various MF/diesel fuels blends (5, 15 and 25% MF b/v) will be investigated along with various engine parameters (injection pressure, injection timing and exhaust gas recirculation ratio) to understand their effect on the monitored engine outputs.

1.4.1.5 Chapter 6 - Particulate Matter Emissions of 2-Methylfuran and Diesel Blends

This section will be completed using the same test conditions and MF/diesel fuel blends as the previous chapter. This section focuses on the particulate matter emitted from the engine and evaluates the effects seen from varying the test conditions and fuels.

1.4.1.6 Chapter 7 – Load Testing with Split Injection Using Various Biofuels

This chapter assessed the performance of three different biofuel/diesel blends under increasing engine load. The biofuels analysed were MF, MTHF and biodiesel. Tests were also completed with neat diesel to serve as a baseline for comparison. Biodiesel was chosen as it is the current conventional biofuel used in CI engines in the automotive market.

1.4.1.7 Chapter 8 - Summary, Conclusion and Future Recommendations

This chapter provides an overview of the key findings from the investigations along with suggested directions for future work considering the knowledge attained from this thesis.

CHAPTER 2

2. Literature Review

The purpose of this chapter is to analyse the available literature relevant to the topic of this investigation. Reviews will be undertaken into compression ignition combustion, powertrain component advances, emissions generation, current fuels used, possible alternatives fuels, and how attempts have been made to reduce the tailpipe emissions emitted from automotive CI vehicles.

2.1 Introduction

The purpose of an ICE is to convert liquid chemical energy into mechanical energy. The popularity of the ICE in both SI and CI form has continued to grow since their creation. By 2030 it is anticipated that there will be a global vehicle fleet of approximately 2850 million vehicles with an expected 94% using an ICE either solely or as a hybrid (Lukoil, 2016). One of the significant consequences from the use of fossil fuels is the increase in global carbon emissions with liquid fuels contributing to around 3000 million metric tonnes of carbon production per year (Boden et al., 2011).

The negative impact of tailpipe emissions and the rising vehicle numbers highlights the necessity to assess possible alternative fuels in ICE's to reduce the carbon emissions generated from fossil fuel use.

2.2 Compression-Ignition Fundamentals

As the names suggest the significant differences between CI and SI engines are the modes in which combustion is initiated. The first compression ignition engine was patented in

1898 by Rudolf Diesel (Diesel, 1898). Since then the fuel used to power CI engines has been termed as diesel.

Typical compression ignition engine operation is shown in Figure 2-1. A CI cycle starts by drawing fresh air into a cylinder through a poppet valve(s). Negative pressure is generated inside the cylinder with the crankshaft rotating and moving the piston down the cylinder, drawing air into the cylinder; this is the intake stroke. The rotation of the crankshaft controls the position of the valves and closes the intake valve as the piston reaches the bottom of the cylinder. The closing of the valves results in an effectively closed cylinder with only a small amount of gas able to blow-by the gap in the piston rings. The piston then begins moving upward, compressing the gas within the cylinder; this is known as the compression stroke. As the piston reaches the top of the cylinder, high-pressure fuel is injected directly into the cylinder generating combustion. The high pressure of the combustion acts upon the piston, moving it down the cylinder and rotating the crankshaft, this is known as the combustion stroke. As the piston reaches the bottom of the cylinder, the exhaust stroke starts, and the exhaust valve opens. The motion of the piston moving up the cylinder and high pressure of the cylinder purges the spent gas to the exhaust port. Once the piston reaches the top of the cylinder, the exhaust valve closes and the cycle starts again with the intake stroke reintroducing fresh charge into the cylinder.

With SI engines the fuel can be mixed with the air before being introduced into the cylinder. Electronic excitation from a spark plug is used to begin combustion, and the fresh charge is compressed to a lesser extent. The significant differences in combustion initiation and fuel qualities play a crucial role in the varying combustion and emissions characteristics seen from SI and CI engines (Heywood, 1988).

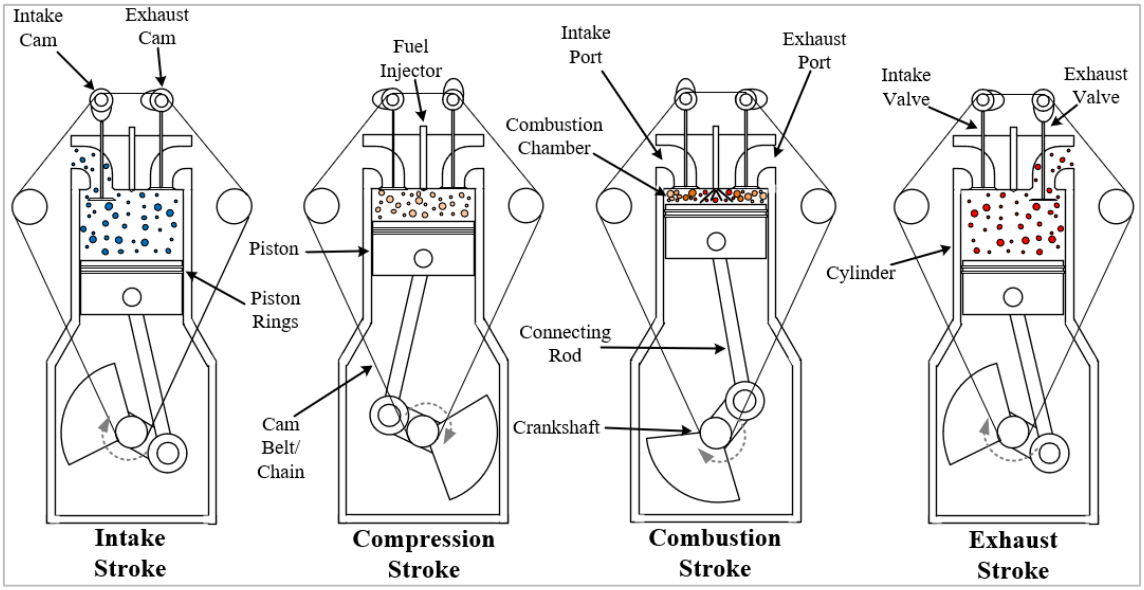

Figure 2-1 Four-Stroke Compression Ignition Cycle. Image created by the author.

2.2.1 Compression-Ignition Combustion

The conventional diesel combustion (CDC) process is a complex heterogeneous phenomenon typically requiring a compression ratio (CR) of 15-20:1 to ensure the in-cylinder gas pressure is high enough to attain combustion when fuel is injected.

Ricardo stated that there are three critical stages of combustion (Taylor, 1977). This can be seen when the combustion heat release rate (HRR) is assessed, see Figure 2-2. These stages are ignition delay, premixed combustion and finally diffusion/mixing-controlled combustion. With CI combustion, it is expected to see varying amounts of premixed and diffusion combustion; the two modes are defined by the state of dilution between the fuel and air reactants (Turns, 1995).

The ignition delay is the time between the start of injection (SOI) and the start of combustion (SOC). For CDC combustion, fuel injection usually occurs between 5-20 crank angle degrees before top dead centre (BTDC), with bottom dead centre (BDC) and top dead centre (TDC) being defined as the point at which the piston reaches the lowest

and highest point of the cylinder, respectively. When liquid fuel is injected into the cylinder, the increased charge pressure from the compression stroke and high surface area of the numerous fuel droplets encourages the fuel to vaporise and mix with the gas in the immediate vicinity. As the piston continues to rise to the top dead centre, the in-cylinder pressure and temperature increases, initiating premixed combustion. Combustion then begins with a sharp in-cylinder pressure rise, that is limited by the reactions of the reactants and products. The fuel injector is typically placed into the centre of the cylinder with the flame kernel/front travelling from the centre of the combustion chamber to the cylinder wall. This increased pressure and flame motion forces the remaining fuel and air to the outskirts of the cylinder, forcing them to interact; this is the diffusion/mixing controlled combustion. The in-cylinder temperature would now be high in the unburnt fuel zone, this temperature and the lean air/fuel mixture would prompt combustion through the rest of the unburnt mixture until the mixture becomes too lean or the flame front becomes extinguished. This flame is smothered when combustion travels towards the crevices of the combustion chamber and as it approaches the relatively cold chamber wall.

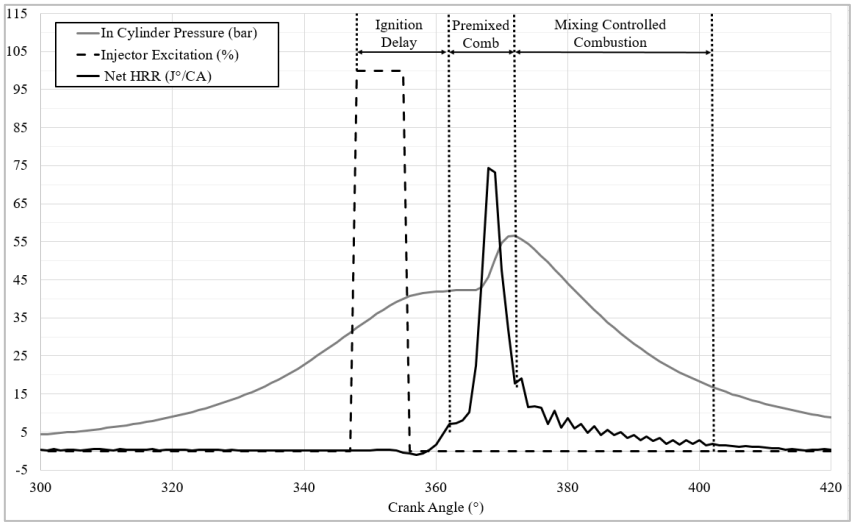

Figure 2-2 Diesel Combustion Heat Release Rate. Results from Author Testing at 5 IMEP and 1800 rpm.

2.2.2 Compression-Ignition Gaseous Emissions

Figure 2-3 displays the typical constituents of diesel-fuelled CI exhaust gas. The pollutant emissions are formed of CO, carbon dioxide (CO_2), UHC, NO_x, PM and sulphur dioxide along with other contaminants. Although these pollutant emissions only account for a small amount of the exhaust gas composition, it is essential to understand their formation mechanisms and find techniques that can reduce the hazardous pollutants produced from diesel-fuelled CI combustion.

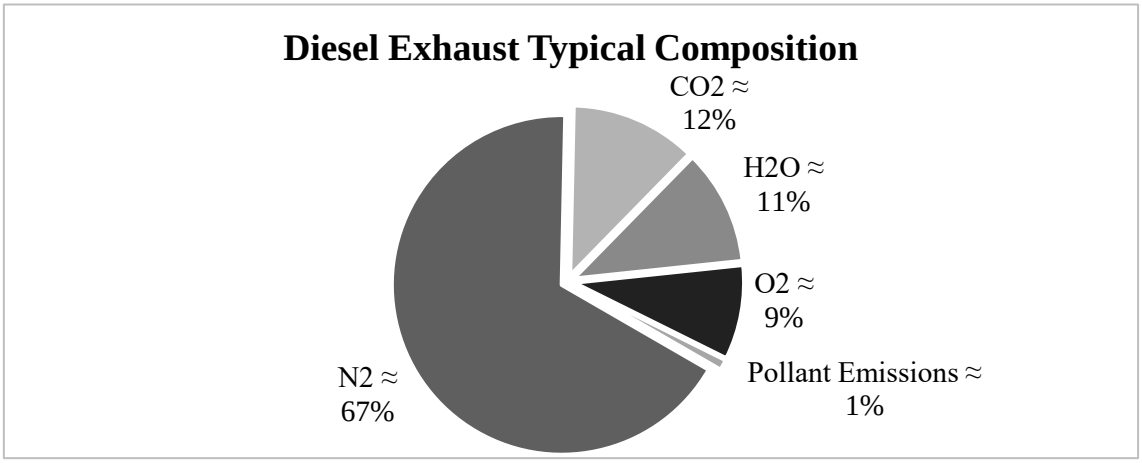

Figure 2-3 Diesel CI Engine Exhaust Gas Constituents, Adapted From (Resitoglu et al., 2015).

CO is a by-product of incomplete combustion, and CO will always be present during the combustion process (Ayandotun B. Wasiu, 2012, Iida, 1993). Carbon monoxide has several different formation mechanisms, with the majority of the formation seen during the combustion process (El-Din et al., 2019). CO is mainly generated when there is not enough oxygen within the immediate vicinity of the combustion flame front to convert the carbon fuel into CO_2. The equivalence ratio is defined as the ratio of actual air/fuel (AFR) ratio to the stoichiometric AFR and is a crucial parameter influencing CO emissions. CO typically increases as the equivalence ratio increases (Bascom et al., 1971). The amount of CO and CO_2 generated can be used to calculate combustion efficiency (Lu

et al., 2013), see Equation 2-1. It should be noted that low levels of CO can also be generated under lean, high-temperature conditions where the dissociation of CO_2 occurs; however, this is negligible.

$$Combustion\ Efficency = \frac{CO_2}{(CO + CO_2)} \quad \text{Equation 2-1}$$

UHC's are produced when the injected fuel is not able to undergo the full conversion process seen from complete combustion (Miller, 2017). Yu et al. highlighted the various scenarios where UHC can be produced; this ranges from under-mixing, cyclic misfire, cyclic variation, wall impingement and wall quenching (Yu et al., 1980). Advances in optical studies have improved the understanding of the fuel injection process. It has been found that injector dripping or fuel vaporisation within the injector sac can also increase UHC production (Musculus et al., 2007). Over-mixing UHC's are formed when the fuel injection event is commenced early during the compression stroke, and a long ignition delay is seen. This occurs through two processes; firstly, with early injection, some fuel impinges onto the cylinder wall creating a fuel film that is not possible to entirely combust because of the low temperature and lack of available air as the flame front moves to the perimeter of the combustion chamber. Secondly, the long delay results in a AFR which provides a hostile environment to attain combustion (Musculus et al., 2007). Under-mixing is typically seen during transient operation with local fuel-rich areas having low oxygen content restricting complete combustion (Bohac et al., 2006). Heywood discussed that the main area where the full combustion conversion process is not possible is at the cylinder wall and also in the crevices between the piston, cylinder wall and piston ring (Heywood, 1988). When the flame front travels towards the cylinder wall, it is extinguished by the reducing temperature and colder temperature of the cylinder wall and

head. A final reason why unburnt hydrocarbons are seen within the exhaust fumes is that it is believed that some hydrocarbons are absorbed into the lubricating oil during combustion because of the high pressure environment. Once combustion is complete, the UHC's are then desorbed and purged into the exhaust system (Andrews et al., 1993).

NO_x has been noted to cause severe issues to human health both directly and indirectly. Excessive exposure to the group of gases is known to cause respiratory problems along with contaminating water (EPA., 2016). The formation of NO_x is a crucial area to review when discussing gaseous emissions. It is seen as one of the main negatives regarding the use of diesel within a CI engine. NO_x is heavily dependent on local combustion temperature with significant formation being seen at temperatures above 1800K and the rate of NO_x production doubling at every 90K interval up to 2200K (Iglesias Fernández, 2016); this high temperature combustion is required to break the triple bond seen between two nitrogen atoms (Fluent, 2012). Once the bond is broken, a reaction occurs between the nitrogen and oxygen molecules along with the atoms that are unable to reach chemical equilibrium (Hebbar, 2014). The accepted thermal formation method for NO_x in a diesel-fuelled CI engine was put forward by Zeldovich (Tomeczek and GradoŃ, 1997) and is displayed below:

$$O + N_2 \leftrightarrow NO + N \qquad \textbf{Equation 2-2}$$

$$N + O_2 \leftrightarrow NO + O \qquad \textbf{Equation 2-3}$$

$$N + OH \leftrightarrow NO + H \qquad \textbf{Equation 2-4}$$

$$NO + HO_2 \leftrightarrow NO_2 + OH \qquad \textbf{Equation 2-5}$$

Typically, CI engines operate in oxygen-rich conditions. However, this is the global air/fuel ratio. Locally, especially during the premixed combustion, there are fuel-rich regions. PM formation is usually seen when the local equivalence ratio is above 2:1, and the combustion temperature exceeds 1575K. These local rich environments within the combustion chamber are a critical location that will generate the majority of NO_x and PM. There have been some control strategies put in place to try and reduce the amount of NO_x and PM emitted; however, as they are generated by the very nature of the combustion mode, there will always be these rich areas, and so the generation of these emissions is impossible to negate and is hard to control to a high degree.

2.2.3 Compression-Ignition Particulate Emissions

Emissions legislation considers not only gaseous emissions but also particulate matter emissions. The size and number of particles seen from vehicle exhausts have become an area that has attained attention because of their direct impact on public health as well as the growing density of major cities (Smith et al., 2009). As with gaseous emissions, particulate matter formation is governed by the combustion method and control, as well as the fuels and additives used (Burtscher and Matter, 2000).

Particulate matter is the mixture of liquid and solid particles with soot typically comprising over 50% of the overall PM (Srivastava and Agarwal, 2008). Soot is generated in the high-temperature oxygen-deprived regions of combustion with NO_x and gives a surface for the liquid particles and hydrocarbons to be absorbed onto, see Figure 2-4 for a representation of PM (Mohankumar and Senthilkumar, 2017). PM can also be considered in terms of soluble volatile organic fractions (VOF) and insoluble organic fractions (ISF). VOF is comprised of constituents like lubricating oil, partially oxidised fuel and polycyclic aromatic hydrocarbons (PAH's) (Williams et al., 1987), whereas ISF

is mainly accounted for with solid carbon/soot along with trace amounts of sulphate and nitrate (Tan et al., 2004).

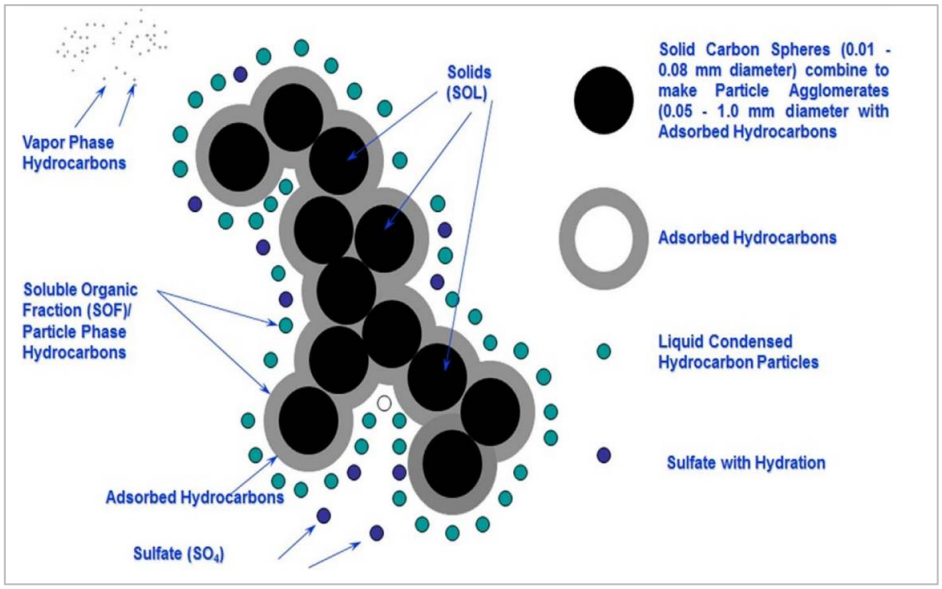

Figure 2-4 Particulate Matter Composition (Mohankumar and Senthilkumar, 2017).

Kittelson highlighted that for vehicle exhaust emissions, there are two main particle formation mode types to consider (Kittelson, 1998). There are the nucleation mode particles which are typically <50nm, and the accumulation mode particles which typically range from 50-1000nm. Overall, these are accepted sizing guides for the two modes, but as nucleation and accumulation are a definition of particle state/nature, not size, further clarification of the modes is required. Nucleation is defined as the initiation of a new thermodynamic phase producing unstructured nuclei in the gas phase (Okolieocha et al., 2015). The nuclei are generated by the formation of crystallising PAH's and VOF compounds in the luminous flame and typically have a diameter of 1.5-2nm (Mohankumar and Senthilkumar, 2017, Reijnders et al., 2018). There is a large number of nuclei particles which account for around 90% of the total particle number concentration. However, as nuclei are a gas phase substance, they only account for around 1-20% of the overall mass (Kittelson, 1998). It should be noted that a large number of

nuclei provide a large surface area which aids surface growth by allowing gaseous PAH and soot precursors to condense on their surface and agglomerate (Reijnders et al., 2018).

Typically, the majority of particle mass is found in the accumulation regime (Merkisz, 2015). Accumulation occurs from the inter-particle collision of small carbonaceous specimens. This causes the coalescence of these particles that when cool, can be considered as a solid particle (Mohankumar and Senthilkumar, 2017, Szymkowicz and Benajes, 2018). The cooling of these particles allows vapour to condense and agglomerate on the surface of the particles (Alfarra, 2004). Both of these effects will cause the particle number to reduce while increasing the mean size of the particles (Mohankumar and Senthilkumar, 2017).

The accumulation mode has acquired this name as particle removal from this regime is the least efficient (Alfarra, 2004). A large amount of time is required for accumulated particles to coagulate to form coarse-mode particles (>1000nm). This results in an insignificant amount of coarse-mode particles being generated in the exhaust system, and these are generally not taken into account for this reason (Wu, 2007).

2.2.4 Emissions Regulation

The first legislation regulating the emissions seen from automotive vehicles was put into place during the early 1960s (Hancock et al., 1985). Diesel-powered road-going vehicles sold within Europe have had to comply with the ‘Euro’ regulations since 1992. These regulations, see Table 2-1, are now on their sixth major iteration with the legislation becoming more and more stringent and Euro 6d regulations being enforced in 2020 (Christie and Ward, 2015). Although consumer expectations of ICE performance and reliability have forced manufactures to improve powertrain performance, it is emissions

legislation that has played a major factor behind manufactures having to make advances in reduced emissions production.

Table 2-1 Euro Light Duty Diesel Regulations (DieselNet, 2019).

Stage	Date	CO	UHC + NOx	NOx	Particulate Matter	Particle Number
	MM/YYYY	g/km				#/km
Euro 1	08/1992	2.72	0.97	-	0.14	-
Euro 2	01/1996	1.0	0.7	-	0.08	-
Euro 3	01/2000	0.64	0.56	0.50	0.05	-
Euro 4	01/2005	0.50	0.3	0.25	0.025	-
Euro 5a	09/2009	0.50	0.23	0.15	0.005	-
Euro 5b	09/2011	0.50	0.23	0.15	0.005	$6.0x10^{11}$
Euro 6	09/2014	0.5	0.17	0.08	0.005	$6.0x10^{11}$

2.3 Major Component Advances in Powertrain Systems Based on Combustion Technologies

2.3.1 Forced Induction

With any ICE there will always be losses when converting the chemical energy of fuel into the mechanical energy of engine rotation. Figure 2-5 displays a Sankey diagram highlighting the typical losses and efficiency values of a diesel-fuelled CI engine, the diagram shows that one of the significant losses is within the exhaust gas.

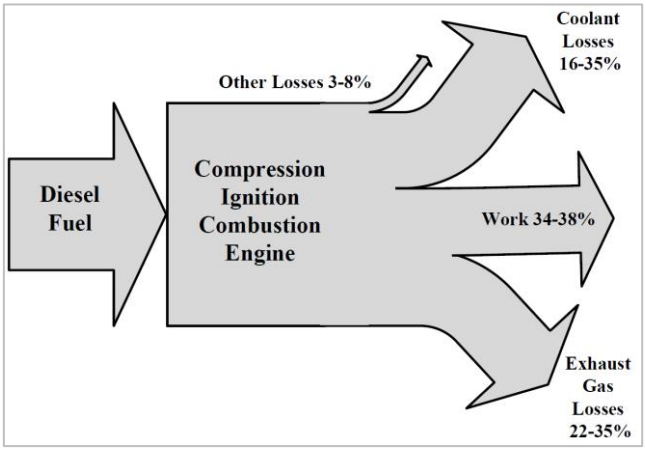

Figure 2-5 CI Engine Fuel Conversion and Losses at High Load, adopted from (Adler and Bandhauer, 2017).

The first turbocharger was patented in 1915 by A. Büchi, with the purpose of recycling energy within the exhaust system (Hiereth and Prenninger, 2007). Turbochargers typically operate by having two axially connected rotors, these are referred to as the turbine and compressor and are mounted into the exhaust and intake system engine, respectively, Figure 2-6 displays a basic schematic of a turbocharging system. The turbine rotor is rotated by the high-pressure exhaust gas generated from combustion; this in turn, rotates the compressor creating an increased gas pressure in the intake system. This increase in oxygen density and allows for more fuel to be injected into the cylinder, which can increase the attainable power and engine thermal efficiency.

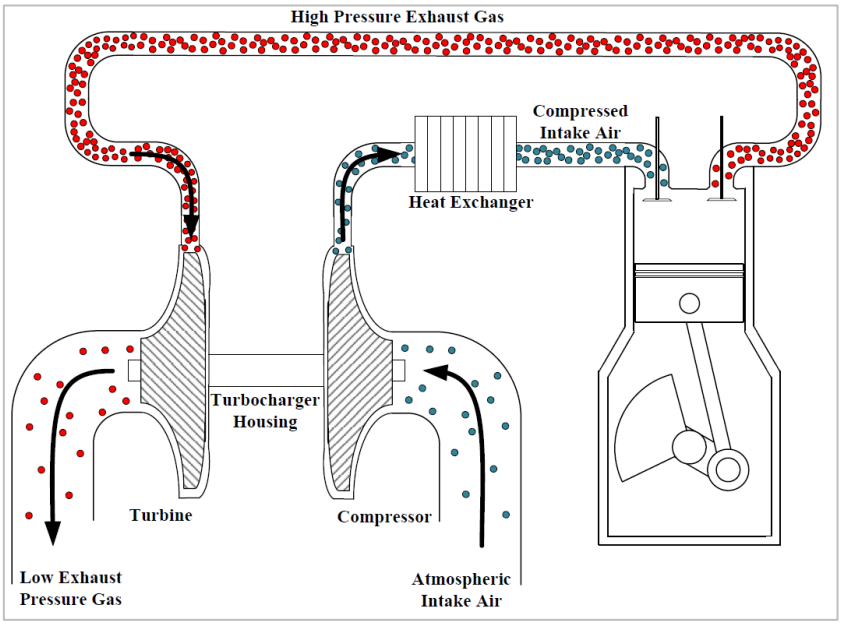

Figure 2-6 Turbocharger Schematic. Image created by the author.

One of the most important developments to the turbocharger is the design of the variable geometry system, see Figure 2-7. This design alters the nozzle angle of attack in the turbine and therefore the exhaust gas flow onto the turbine blades. By reviewing the comparison between a fixed and variable geometry turbine (VGT) in Figure 2-8, it can be seen that a variable geometry can provide a wider performance window. The additional

control of the nozzles aids in improving the low engine speed torque, turbocharger lag and also the exhaust gas recirculation (EGR) flow rate (Feneley et al., 2017), EGR operation will be discussed in further detail in section 2.3.3. Typically, the variable nozzle system is just seen in the turbine housing. However, there are cases of variable nozzles being used in the compressor housing for high-performance applications (Uchida et al., 2006).

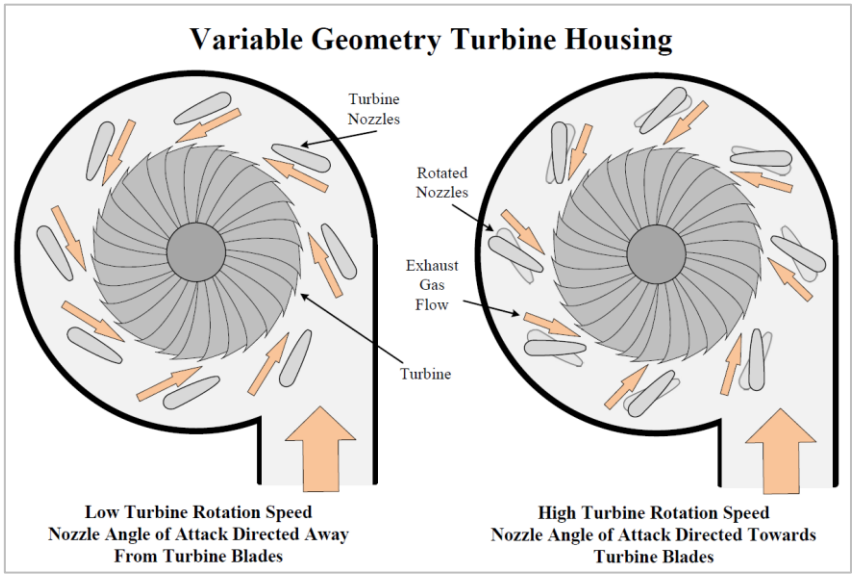

Figure 2-7 Turbocharger Variable Geometry Design**.** Image created by the author.

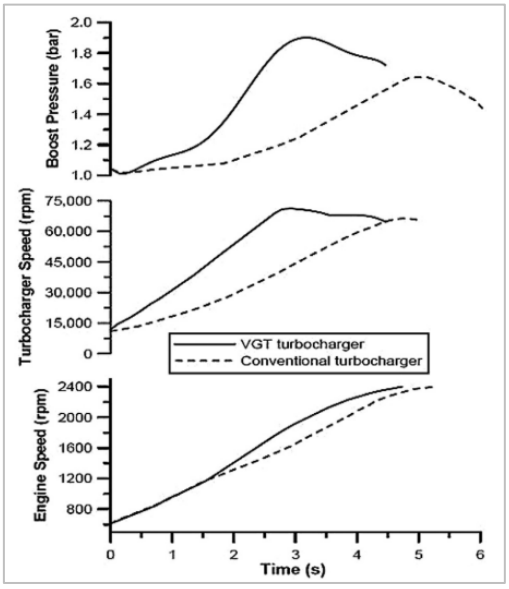

Figure 2-8 Comparison Between VGT and Fixed Geometry Turbine Performance (Feneley et al., 2017).

2.3.2 Fuel Injection

2.3.2.1 Fuel Pressurisation

One of the significant steps forward with CI ICE technology is the advancement of fuel injection systems. Previously, the most common system for low to medium size vehicles was a distributor pump. This was driven from the engine, which meant that injection pressure was in a direct relationship with engine rotational speed, with the injection timing being controlled by a pressure control valve. This resulted in very little control over injection pressure and injection timing regarding other engine operating parameters and user demand (Adey et al., 1981).

The injection system conventionally used with light-duty CI engines today is the common rail injection system. The main components are a low-pressure pump, high-pressure pump, a common rail that distributes the high-pressure fuel to the injectors and an engine control unit (ECU), see Figure 2-9. Advances in electronic and computational technology when the common rail was introduced meant that the ECU had the potential to assess many sensors and operate a range of components at a high speed. Similar to the distributor pump, the high-pressure pump is rotated by the engine crankshaft. However, a selection of valves within the low-pressure pump, high-pressure pump and common rail means that the ECU can control the fuel pressure within the common rail. The typical maximum fuel pressure that is possible to attain with a common rail system is 2500 bar, whereas a distributor injector could attain a maximum of 300 bar (Flaig, 2013). This increased overall pressure, along with the range of pressure available at a set engine speed is a considerable improvement, especially when considering a low engine speed. This high pressure allows fuel to be injected at a much finer size and also with a longer spray penetration length, giving higher potential energy to the fuel along with increased global

surface area. This aids fuel atomisation and mixture homogeneity, decreasing the formation of UHC, CO and PM (Agarwal et al., 2014).

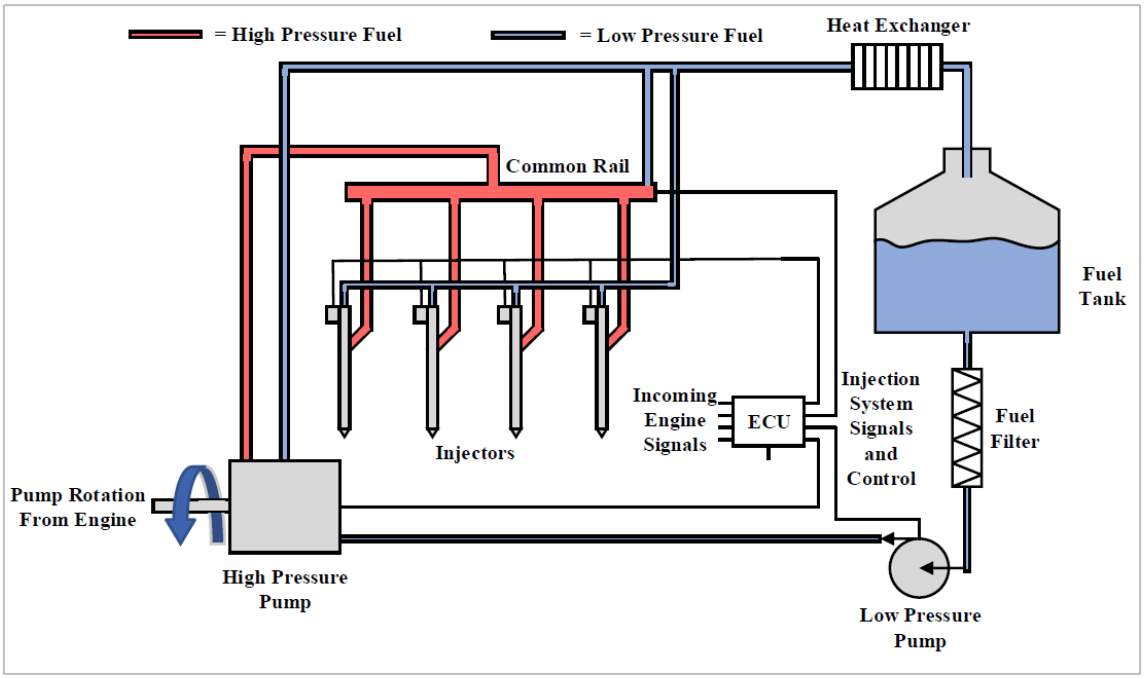

Figure 2-9 Common Rail Schematic. Image created by the author.

2.3.2.2 Injection Events

Advances in technology have meant that current injection systems can attain rapid injector rise, fall and dwell times (around 100µs), meaning that multiple injection events are now attainable (Robert Bosch Gmb, 2005, Schöppe et al., 2008). Within a CI engine, there are typically 5-7 injection events per combustion event (Tian et al., 2017). These can be categorised as either a pilot, main or post-injection events, each of which has their own in-cylinder pressure and emissions influence, see Figure 2-10. The bulk of the fuel is injected during the main injection event, and the principal purpose of this event is to generate the majority of the in-cylinder pressure that will rotate the crankshaft. Before the main injection, there are pilot injections where some fuel is injected into the cylinder to prepare the combustion chamber with a low amount of fuel. The benefit accomplished

from having pilot injections is increased mixture preparation time. This delay between injection and combustion aids in attaining more homogenous combustion, which reduces the maximum in-cylinder pressure and the pressure rate of change during combustion (P-Rate). The use of pilot injection in this regard has two significant benefits, firstly reducing combustion noise and secondly, the NO_x formation is reduced from the lower P-Rate, which results in a lower in-cylinder temperature rate of increase. (Denny et al., 2019, Du et al., 2019). The injection of additional fuel after the main injection event, post-injection, aids in increasing the amount of soot oxidation, reducing PM formation (O'Connor and Musculus, 2013). It can also be used to increase the in-cylinder gas temperature as the exhaust valve opens and can be used to initiate the regeneration of exhaust aftertreatment systems (Mohan et al., 2013).

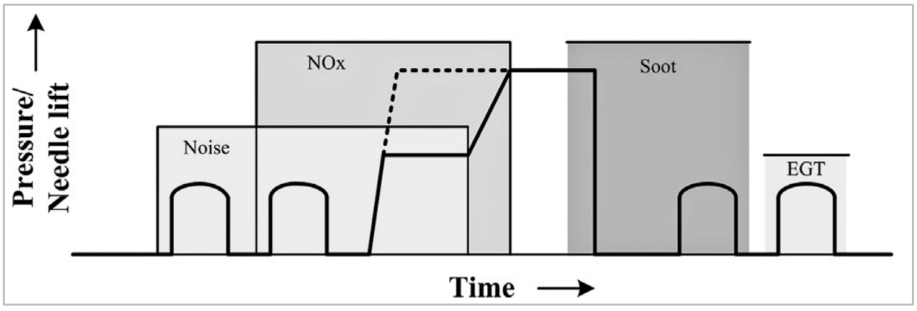

Figure 2-10 Injection Event Combustion and Emissions Interaction (Mohan et al., 2013).

2.3.2.3 Fuel Injection Timing

Injection timing controls the point during the engine cycle that combustion is initiated. Altering the injection timing will change the combustion, emissions and injector spray characteristics (Heywood, 1988). The main injection event typically occurs BTDC, but the ignition delay results in the majority of combustion occurring after top dead centre (ATDC). Heat release characteristics regarding fuel injection timing will mainly be viewed in two manners in this thesis. The crank angle (CA) of the SOI, and also as the consequent CA ATDC at which 50% of the sum apparent heat release (AHR) is attained

(AHR50). All future AHR50 values will be referred to as AHR50 *X* with *X* defining the CA ATDC.

Figure 2-11 displays the in-cylinder pressure and HRR of two different injection timings attaining the same indicated mean effective pressure (IMEP); these SOI timings were 20°BTDC and 10°BTDC both scenarios used a single injection event. By comparing the data attained, it can be seen that the earlier injection timing resulted in the majority of combustion occurring closer to TDC. This resulted in the combustion occurring in a smaller volume of the cylinder and generating a higher maximum pressure value. The high pressure attained during combustion increased NO_x formation, and the high P-Rate resulted in high combustion noise. However, the higher temperature would have aided in reducing PM, CO and UHC formation (Ahmed et al., 2019). This noise generated from a high P-Rate is attained from a high-intensity pressure wave inside the cylinder. This high P-Rate is known to cause structural issues to engine components (Ren et al., 1999). When fixed injection timing is being used, it is crucial to bear biofuels and P-Rate in-mind as biofuels typically contain oxygen which will reduce combustion duration and increase the tendency for high-intensity P-Rate values to occur (Giakoumis et al., 2016).

The AHR50 value for the 20°BTDC injection timing was 0, and a value of AHR50 12 was attained with the SOI set to 10°BTDC. This highlights that the combustion duration increased as the AHR50 value moved away from TDC. The combustion phasing was also seen to change slightly, with a value of AHR50 12, an increasing amount of diffusion combustion was attained (Wang et al., 2016).

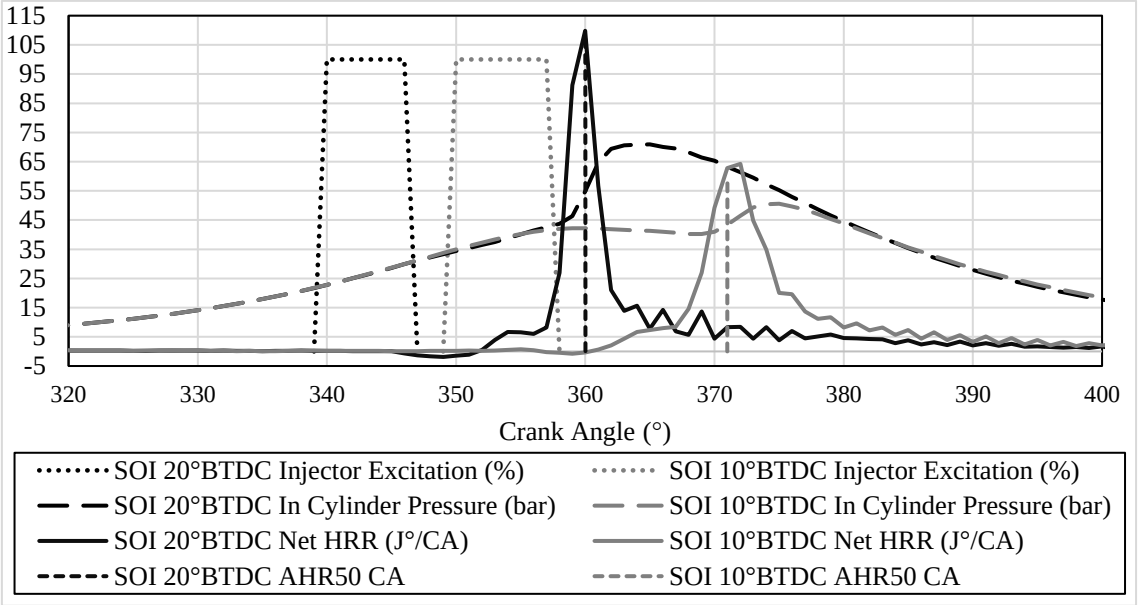

Figure 2-11 Heat Release Rate of Two Injection Timings. Results from Author, Operating at 5 IMEP and 1800 rpm.

2.3.3 Exhaust Gas Recirculation

The first production EGR system was fitted to commercial engines in 1973 (Carley, 2003), and although the design has dramatically improved, the methodology is still the same. The purpose of the EGR is to circulate spent exhaust fumes into the intake manifold and dilute the fresh charge that is entering the cylinder. When combustion occurs with no EGR, the equivalence ratio at the flame front varies greatly with local rich points attaining a combustion temperature of up to 2500K (Agarwal et al., 2017). This, in turn, generates NO_x, which as discussed, is regarded as one of the significant concerns of CI ICE exhaust emissions (Juttu et al., 2007). The introduction of spent gas ensures that there is redundant recycled combustion gas between the injected fuel and oxygen. These spent gases reduce combustion speed and temperature, lowering the amount of NO_x produced (Dangar and Rathod, 2013). The major negative of using EGR to reduce NO_x generation is that it also slightly reduces the combustion efficiency and generated power while increasing the PM and UHC emitted (Schubiger et al., 2001, Ladommatos et al., 1997, Ladommatos et al.,

1996). However, this negative of increased fuel consumption is substantially outweighed by the extent to which NO_x reduction can be attained (Hountalas et al., 2008, Maiboom et al., 2008, Zhang et al., 2013, Zheng et al., 2004).

There are three main types of EGR design on an engine. High pressure, low pressure and dual EGR, see Figure 2-12. High-pressure EGR (HPEGR) re-directs high-pressure flow from the exhaust manifold to the intake manifold (after the compressor), bypassing some exhaust gas flow before it reaches the turbocharger. Low-pressure EGR (LPEGR) directs air that has travelled through the turbocharger and possibly the after-treatment system back to the intake system before the compressor. Typical engines now use either a HPEGR or both systems in a configuration called dual EGR (DEGR) to compensate for the positive and negative aspects of the two systems (Zheng et al., 2004). HPEGR offers a fast response when operating under transient conditions; however, it is very reliant on the high pressure seen within the exhaust manifold which means it also has a direct relationship to the turbocharger turbine rotational speed (Park et al., 2010). LPEGR reduces the effects seen on the turbine but has a reduced response rate which makes it suitable for steady-state operating conditions (Zamboni and Capobianco, 2013). A significant advantage seen when using an LPEGR is that the turbocharger VGT position can be increased while still achieving a similar EGR rate. This will reduce the exhaust manifold backpressure, reducing pumping losses and fuel consumption (Park and Bae, 2014). Nearly all EGR's use an intercooler to reduce the exhaust gas temperature before the spent fumes re-enter the cylinder. This aids in reducing the intake gas temperature and in turn, the combustion temperature, again reducing NO_x formation (Park et al., 2007).

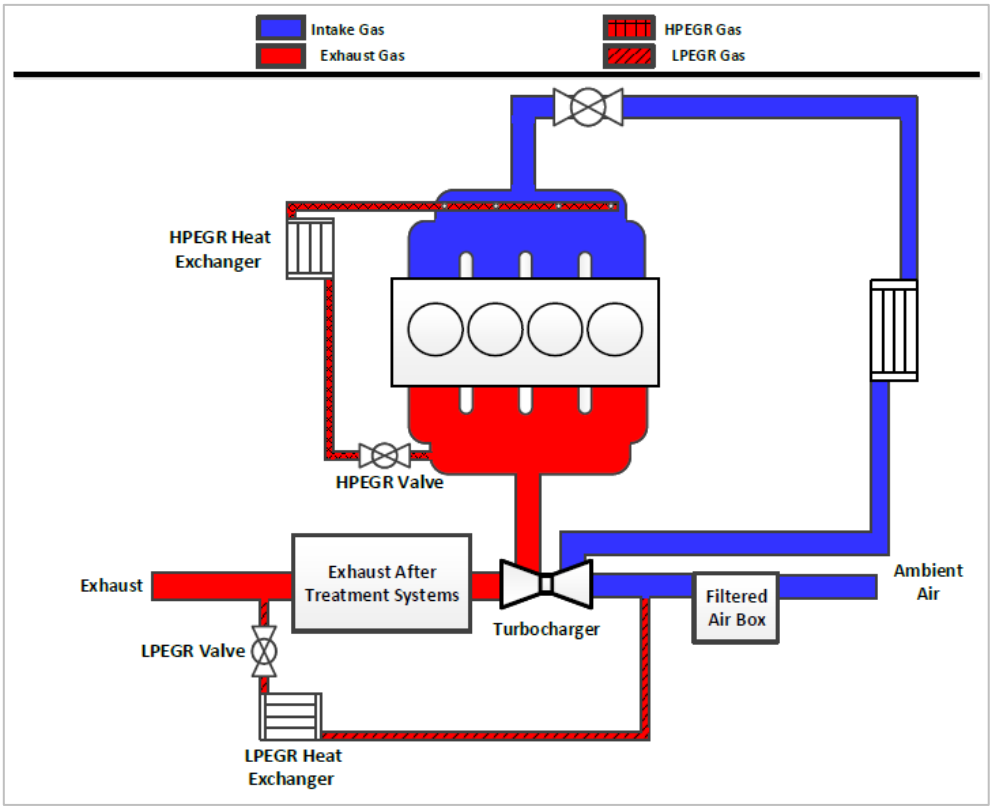

Figure 2-12 Dual EGR Schematic**.** Image created by the author.

There have been reviews into the effect of reducing EGR intercooler efficiency and increasing intake manifold gas temperature. The increase of EGR gas temperature is known as hot EGR (HEGR), and it has been found to reduce the ignition delay and combustion duration (Selim, 2003). When discussing hot EGR, it is essential to bear in mind the decreased gas density attained from the increased gas temperature; this will reduce the mass flow rate of the charge entering the cylinder (Ladommatos et al., 2000). When using low cetane fuels in CI engines, it can be required to use high amounts of EGR and little to no EGR cooling to increase the intake gas temperature. The use of HEGR at low load conditions can improve combustion efficiency and reduce cyclic variation. This technique has been used in CI engines with low cetane gasoline/diesel mixtures. Zeraati-Rezaei et al. found that a 99% reduction of NO_x and smoke could be attained when

compared to the diesel baseline, but lower injection pressures were required to reduce over-mixing and cyclic variation (Zeraati-Rezaei et al., 2017).

It should be noted that cold EGR (CEGR) is attained when the intercooler cooling circuit is fully activated. CEGR is the conventional technique used for automotive engines, and because of this, it can also be referred to as EGR.

2.3.4 Engine Control

The influence of electronic technology improvements has dramatically aided combustion efficiency and reduced the emissions generated from vehicles (Çağatay Bayindir et al., 2011, Cuatto et al., 2000, Kong et al., 2007). The advances in terms of computing power and reduced physical space means that original equipment manufacture's (OEM's) can now attain high-resolution control and implement logic on a wide range of components that were previously unavailable (Mendonca et al., 2017). ECU's have taken a significant step forward, and OEM's can now monitor engine rotation at a resolution of around 0.5-1 (CA), giving more control to calibration (Pacitti et al., 2008, Seo et al., 2006). These improvements can be applied to other areas, from injection volume to gearbox, suspension and braking system operation. Previously EGR systems would be opened by the vacuum created between the intake and exhaust manifolds (Berry and Brunt, 1996). Now it is possible to find the optimum position for the EGR valve by using potentiometers and advanced control strategies to ensure that the required position of the EGR is attained and maintained (Isermann et al., 1999).

2.4 Low-Temperature Combustion

As discussed in the previous section, CDC often causes a high amount of NO_x and PM to be generated. As regulations regarding the tailpipe emissions seen from road-going

vehicles have become more stringent, it has become necessary to investigate alternative combustion modes.

Low-temperature combustion (LTC) has the potential to provide users with significantly reduced NO_x and PM. The major drawback of LTC is the advanced injection required, which reduces combustion efficiency and increases the UHC, CO and fuel consumption. There are four major subtypes of CI LTC; these are homogeneous charge compression ignition (HCCI), partially premixed combustion (PPC), reactivity-controlled compression ignition (RCCI), and partially premixed compression ignition (PPCI). Note, PPCI is also referred to as premixed compression ignition (PCI) and premixed charge compression ignition (PCCI) but will be referred to as PPCI.

The operating principle of LTC combustion is to attain high amounts of homogeneous fuel and air throughout the cylinder before combustion occurs. The uniformity of the fuel/air mixture encourages an increase of mixing controlled combustion, and a reduced amount of oxygen-limited, high temperature, NO_x and PM generating premixed combustion (Agarwal et al., 2017). A comparison of temperature gradients seen within an RCCI and CDC combustion chamber during combustion is displayed in Figure 2-13.

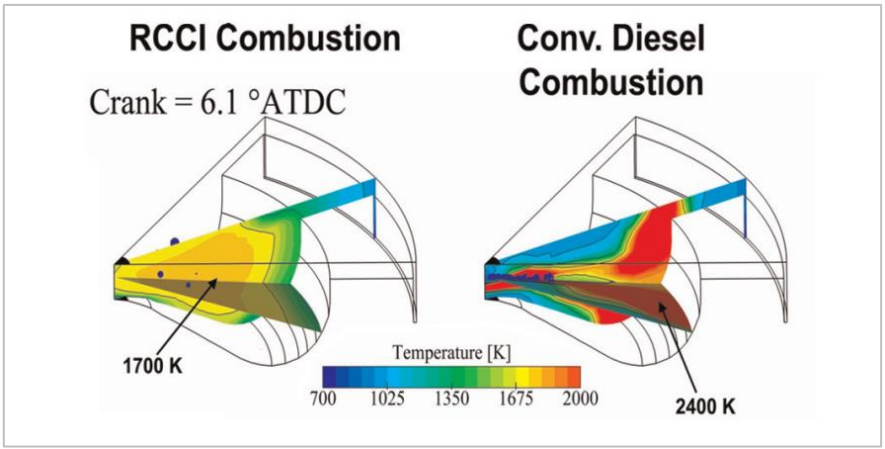

Figure 2-13 Computational Model Comparing CDC to LTC (Kokjohn et al., 2011).

When using HCCI, the aim is to prepare the cylinder with a lean, uniform air/fuel mixture before compressing the mixture to a point where it will self-ignite. Fuel can either be injected directly into the cylinder or at the intake port. To ensure that a homogenous mixture is attained with direct injection, it is necessary to inject fuel at the early stages of the compression stroke, usually from 300-100°BTDC (Sjöberg et al., 2002). HCCI is not a popular alternative as it is knock prone at high engine loads as the engine will operate at a higher in-cylinder temperature that will reduce the ignition delay. HCCI combustion is most effectively controlled by either altering the amount of EGR seen within the combustion chamber or by altering the intercooler efficiency of the EGR and altering the in-cylinder gas temperature (Machrafi, 2010).

PCI is generally regarded as a derivative of HCCI and is considered as the link between HCCI and CDC, which means it is possible to attain the combustion and emissions of either mode to suit the user and regulations (Gao et al., 2011). Combustion is controlled via a selection of engine parameters (e.g. EGR, injection pressure, intake gas pressure) to try and attain a uniform fuel/air mixture; however, the SOI has the most influence over the SOC.

RCCI is an advanced LTC technique that controls combustion behaviour via the reactivity of the fuels used. Advanced injection timing is used to inject a low reactivity/cetane number fuel, e.g. gasoline, then a high reactivity fuel, e.g. diesel is injected to initiate combustion at the desired point. RCCI is considered to be an effective LTC mode as it can provide high brake thermal efficiency (BTE) while still providing reduced NO_x and PM over other LTC methods (Li et al., 2015). The primary benefit of RCCI over other methods is that a variety of fuels can be used for the low reactivity fuel, e.g. butanol, methanol, ethanol and natural gas (Benajes et al., 2015, Dahodwala et al., 2015, Li et al.,

2014, Nieman et al., 2012, Qian et al., 2015). The major drawback of this configuration is the increased production and maintenance costs brought about by having two separate fuel injection systems.

PPCI is a combustion mode that is mainly associated with light-duty engines and is attained by using high amounts of EGR, high injection pressure and advanced injection timing. PPCI is typically able to attain a partially homogenous mixture. It has been suggested that PPCI combustion is single-stage combustion that is similar to the premixed phase of CDC combustion, however, unlike HCCI the combustion is not seen throughout the combustion chamber and is not as localised as CDC with DI (Kimura et al., 1999). This means that the emissions seen from the PPCI are also a mid-point between HCCI and CDC, with PPCI providing an increase in NO_x and PM and decrease in UHC and CO when compared to HCCI (Cao et al., 2009).

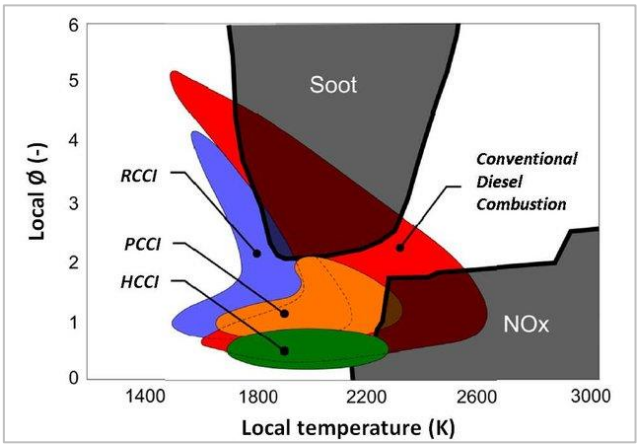

Figure 2-14 Diesel Combustion Modes Soot and NO_x Comparison (Agarwal et al., 2004).

By reviewing Figure 2-14, it can be seen that the LTC operation modes provide a reduced area in the engine operating conditions that are known to generate PM/soot and NO_x. These alternatives do provide a vast improvement on the emissions generated, but it also needs to be stated that there are the following challenges regarding the use of LTC:

1. High combustion noise and reduced combustion rate control
2. Poor cold start ability
3. Cycle to cycle and cylinder to cylinder variations
4. Overall engine control, especially combustion control at high engine speed and load
5. Limited power density
6. Reduced combustion efficiency
7. Increased CO and UHC emissions
8. A lack of highly accurate combustion and chemical reaction models

2.5 Diesel in Compression Ignition Engines

Originally petroleum diesel fuel oil was a straight-run product that was attained from the distillation of crude oil. As the demand for petroleum diesel has increased, various cracking techniques have been developed to produce diesel constituents (Speight, 2011b). The most typical method to manufacture petroleum diesel is to boil crude oil at a range of 746-896K; this produces a mixture of carbon chains within the oil that range from around 8-21 carbon atoms per molecule (Speight, 2011a).

Before 2007 the allowable content for sulphur in road-going diesel fuel was 500ppm in America and Europe; after this, the content was reduced to 15ppm (Stanislaus et al., 2010). This legislation has aided in reducing the harmful pollutants seen from the high sulphur fuels. The reduced sulphur content has also allowed for component advances to be implemented that would otherwise fail or become heavily contaminated (Speight, 2011b, Speight, 2011a). The significant advance is the reduced size of injector nozzles that would not have been possible with high sulphur fuels. Injectors nozzles are expected to have decreased to a size of approximately 100μm, with an increased number of nozzles

to aid in mixture distribution (Wang, 2012). With high sulphur fuels, small nozzles would have experienced deposits on the nozzle or sac that would have been blocked or fouled, manipulating the spray penetration length and direction.

The fuel characteristics used in an engine constitute a significant role in governing the combustion and emissions characteristics produced. The possibility to synthesize fuels means that there is an opportunity to investigate and improve fuel characteristics.

2.6 Oxygenated Biofuels for Compression Ignition Engines

Fossil fuels have been the most predominant fuel in ICE vehicles because of its ease to source, minimal cost and appealing chemical properties. Over recent years alternatives to FF usage has become more apparent because of growing concerns over global warming as well as increased costs from reducing oil stores. This has resulted in an increased focus on possible biofuels for ICE usage, this coupled with advances in biofuel production methods means that there is also a more comprehensive range of available fuels to investigate (Chheda et al., 2007). This section reviews biofuels, taking into account biodiesel, ethanol, 2-methylfuran and 2-methyltetrahydrofuran. The characteristics of these fuels are displayed below in Table 2-2, with an in-depth analysis provided in the subsequent sections.

Table 2-2 Fuel Properties.

(Barabás and Todoruț, 2011, Chen et al., 2013, Eldeeb and Akih-Kumgeh, 2018, Heuser et al., 2013, Pace, 2014, Santa Cruz Biotechnology, 2015, Wang et al., 2013, Xiao et al., 2019)

Parameters	Diesel	Gasoline	Biodiesel	Ethanol	MF	MTHF
Carbon Range / Chemical Formula	C_{12}-C_{25} (Chen) $C_{17}H_{32}O_2$*	C_4-C_{12} (Chen)	C_{12}-C_{24} (Chen) $C_{19}H_{35}O_2$# (Barabás)	C_2H_6O	C_5H_6O	$C_5H_{10}O$
Research Octane Number	20-30 (Xiao)	96.8 (Wang)	-	109 (Wang)	103 (Wang)	86 (Eldeeb and Akih-Kumgeh)
Motor Octane Number	-	85.7 (Wang)	-	90 (Wang)	86 (Wang)	-
Cetane Number	52 (Xiao)	10-15 (Xiao)	47-52 (Chen)	8 (Xiao)	9 (Xiao)	15 (Heuser)
Oxygen Content (%)	0 (Xiao)	0 (Wang)	10.8 (Xiao)	34.78 (Wang)	19.51 (Wang)	18.6 (Heuser)
Stoichiometric Air/Fuel Ratio	14.3 (Xiao)	14.7 (Wang)	12.54 (Xiao)	8.95	10.05	10.64
Density at 20ºC (kg/cm^3)	826 (Xiao)	744.6 (Wang)	871 (Xiao)	790.9 (Wang)	913.2 (Wang)	867 (Heuser)
Water Solubility	Negligible (Xiao)	Negligible (Xiao)	Negligible (Xiao)	Miscible (Xiao)	Negligible (Xiao)	Negligible (Pace)
Latent Heat of Vaporisation (kJ/kg) at 25ºC	270-301 (Xiao)	373 (Wang)	200 (Chen)	919.6 (Wang)	358 (Wang)	-
Lower Heating Value (MJ/kg)	42.5 (Chen)	42.9 (Wang)	38.81 (Chen)	26.9 (Wang)	31.2 (Wang)	32.8 (Eldeeb and Akih-Kumgeh)
Initial Boiling Point (ºC)	180-370 (Chen)	32.8 (Wang)	262-359 (Chen)	78.4 (Wang)	64.7 (Wang)	80 (Heuser)
Auto-Ignition Temperature (ºC)	246 (Chen)	420 (Chen)	363 (Chen)	434 (Chen)	-	270 (Santa Cruz Biotechnology)
Normalised C Value	1*	-	1	1	1	1
Normalised H Value	1.8838*	-	1.8421	3	1.2	2
Normalised O Value	0.059*	-	0.105	0.5	0.2	0.2

N.B. * = Normalised values of diesel supplied by Shell and used to calculated Diesel Formula

#Biodiesel formula used to calculate Normalised Ratios. Referenced Biodiesel is Rapeseed Methyl Ester.

2.6.1 Biodiesel

The use of biofuel in a compression ignition engine is not a new concept. In 1937 G. Chavanne attained a patent in Belgium (patent 422,877) for separating the fatty acids and glycerine of vegetable oil to produce a diesel-like fuel, referred to as biodiesel (Anastasov, 2009). This fuel was used to power a commercial bus between Brussels and Lovain in 1938 (Knothe et al., 2010).

Nowadays biodiesel is typically made via transesterification which has built from the process put forward by Chavanne. Before transesterification, the biomass is filtered and has the majority of the water removed. A catalyst (usually a mixture of methanol or ethanol and sodium hydroxide or potassium hydroxide) is mixed with the filtered biomass oil to react with the triglyceride oil molecules within the biomass; this produces the biodiesel and a small amount of waste glycerine. If ethanol is used in the catalyst, fatty acid ethyl ester (FAEE) is formed, and if methanol is used, then fatty acid methyl ester (FAME) is created (Huang et al., 2015). A notable characteristic of biodiesel is the high conversion yield attainable when optimised oils, catalysts and methods are used, with up to 99% conversion yield being reported (Venkat Reddy et al., 2006).

The positive results attained from the use of first-generation biodiesel feedstocks has moved the focus onto second and third generation feedstocks to ensure that biodiesel production do not compete with the farming of food crops. A review by Bhuiya et al. highlighted the typical results attained by using second-generation biodiesels as a blend with fossil diesel in comparison to using neat diesel. The key findings highlight reduced engine power from a lower heating value of biodiesels, this in turn, increased fuel consumption. Biodiesels has an improved lubricity and reduced soot formation, both of which can aid in reducing carbon build up and wear on components. The oxygen content

of biodiesel is one of the main reasons regarding some of the major differences between the second-generation biodiesel results assessed and fossil diesel. The oxygen content of biodiesel can aid in reducing UHC formation by improving combustion efficiency and increasing premixed combustion, this in turn, increases the NO_x formation and reduces the PM emitted by oxidising particles and precursors. Typically, CO and CO_2 are seen to decrease and increase, respectively, this is a result of the increased combustion efficiency. However, CO and CO_2 have both been seen to decrease with the use of biodiesel, which is a result of improved combustion efficiency and a reduced carbon to hydrogen ratio. The use of second-generation biodiesel as an additive with fossil diesel has many positives, however, there are concerns regarding the use of pure biodiesel within a CI engine because of the higher viscosity of biodiesel. This may greatly affect the emissions emitted because a reduced fuel spray penetration length and increased fuel droplet size, this is especially important when considering premixed combustion. However, when considering LTC combustion modes, this fuel characteristic may be favourable as it may reduce the wall impingement and provide reduced CO, UHC and PM values (Bhuiya et al., 2016). A comparative analysis of a selection of first, second and third generation biodiesels mixed with diesel at a ratio of 20%/80% (b/v) highlights similar results for the various blends, these results were in line with the second generation review discussed above (Rajak et al., 2019). The results discussed in the review by Bhuiya et al. and Rajak et al. highlighted that fatty acids within a feedstock can play a large role in biodiesel properties, these acids can be attained from any feedstock generation. Monosaturated fatty acids can aid in improving ignition quality and increasing fuel blend miscibility, this can in turn increase combustion stability. However, the use of fatty acid alkyl ester can

aid in improving the cetane number as well as long term storage suitability by reducing the formation of crystals within the biodiesel when stored at low temperatures.

Biodiesel is one of the most commonly used biofuels and is typically either used as a standalone fuel or mixed with diesel; the latter is most commonly used in the automotive sector. To signify the amount of biodiesel used in a blend a blended fuel is referred to as B*x* with the *x* being interchangeable with the volume percentage of biodiesel used, e.g. a volume mixture of 10% biodiesel and 90% diesel is referred to as B10. This reference system was put in place by the Alternative Fuels Data Centre and has been generally adopted worldwide. This system will also be used when discussing the fraction blends of MF, MTHF and biodiesel and will be referred to as MF*x*, MTHF*x* and B*x*, respectively.

Investigations into the performance of biodiesel/diesel blends in comparison to the use of neat diesel have highlighted that:

1. Depending on the blend ratio and operating conditions, UHC production has been reported to reduce by 7.4-45%, and CO can be reduced by 8.6-40%. This can be attributed to the oxygen available within biodiesel, improving combustion quality. However, the negative aspect of the increased oxygen content is reduced combustion duration, increasing NO_x formation. An increase in NO_x has been reported to range from 5.6-52% (Wan Ghazali et al., 2015).
2. Biodiesel is also capable of attaining reduced particulate emissions over fossil diesel, this can mainly be attributed to the reduced aromatic compounds and increased available oxygen. It has been reported that the particle number can linearly reduce by up to 50% with the introduction of biodiesel blends going from B0 to B100. It has also been found that along with a reduced particle number, the

average size can marginally decrease (Jaichandar and Annamalai, 2011, Shahir et al., 2015).

3. Biodiesel does have a reduced calorific value when compared to petroleum diesel and reviews have stated that there is typically a 15% increase in brake specific fuel consumption (BSFC) when using neat biodiesel (Dwivedi et al., 2011).

This highlights that although biodiesel does offer some benefits for its use, it is still necessary to review other biofuels to investigate whether more suitable alternatives are available that have fewer negative aspects.

2.6.2 Ethanol

By reviewing the data produced by the UK government in Figure 2-15, it can be seen that ethanol volume sales have been similar to biodiesel for many years and although recent trends indicate that biodiesel is becoming a predominant biofuel, it is still suitable to review the use of ethanol within a CI engine.

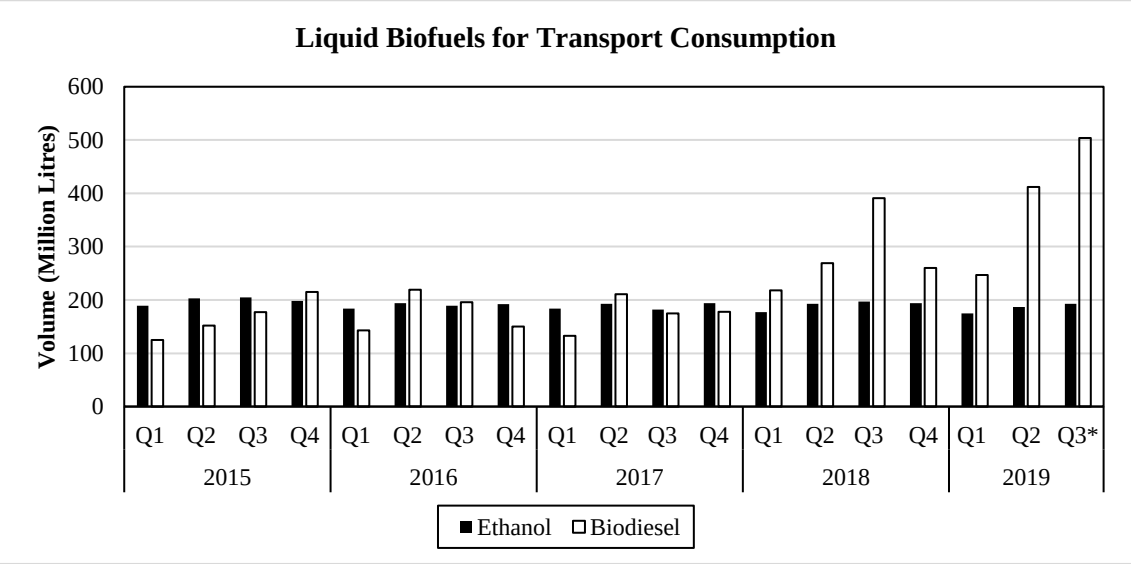

Figure 2-15 UK Transport Biofuels Consumption. N.B. * = Predicted Value (Statistics, 2019).

Ethanol feedstock is cellulose matter; this is the cellular structure of plant matter and is considered to be the most abundant organic compound on earth (Jonker, 2008). Ethanol is produced by drying and shredding the cellulose feedstock into a powder and then adding water to the powder to create a pulp/mash. An enzyme is then added to the pulp to further breakdown the cellulose into smaller particles. The mixture then undergoes a range of heat cycles and a second enzyme is added to convert the feedstock into dextrose, after which it is left to ferment and produce ethanol along with by-products. The mixture is then heated to vaporise the ethanol and separate it from the rest of the major contaminants in the batch. Once condensed, it is separated from the remaining water.

As ethanol has a much lower cetane number than diesel (ethanol = 8, diesel = 52), it would be challenging to attain combustion with pure ethanol in a mass-produced CI engine without undertaking any significant alterations. From tests completed with ethanol/diesel blends, it has been found that the low cetane number reduces the combustion stability, with issues being seen with blends as low as 15% ethanol b/v. This reduced stability promotes higher CO and UHC formation and increases as the ethanol fraction becomes greater (Sandalcı et al., 2014). As with biodiesel, the oxygenated nature of ethanol can significantly reduce PM emissions, but the inclusion of oxygen within fuel is known to reduce heating value and increase BSFC (Yahuza and Dandakouta, 2015). Even with the use of an oxygenated fuel and increased combustion speed, it was found that ethanol/diesel blends were able to reduce NO_x formation as the higher latent heat of vaporisation of ethanol decreased the in-cylinder gas temperature (Lei et al., 2010). One of the significant negatives regarding ethanol is its hygroscopic nature, which can encourage ethanol/diesel blends to separate when stored for a period of time, causing major engine in-stability (Lapuerta et al., 2007).

Bearing these factors in mind, it is apparent why biodiesel is the chosen biofuel over ethanol in CI engines. However, as discussed in the previous section, biodiesel does not have entirely favourable characteristics, and it is required to investigate other possible alternatives that can be used in a CI engine.

2.6.3 Furan Fuels

Furanoid fuels contain a central five-member furan ring. This ring is comprised of four carbon atoms and an oxygen atom. 2-methylfuran and 2-methyltetrahydrofuran are furan fuels with methyl side chains. They have been considered promising alternative fuels for a considerable time with their resistance to detonation being published in 1958 (Derfer, 1958). In 2007, a new production method was published that was suitable for furan fuel production (Román-Leshkov et al., 2007). The overall process removes five oxygen atoms from fructose to produce fuels with attractive characteristics, including a reduced boiling point (BP), water insolubility and increased research octane number (RON) (Barlow et al., 1983).

The chemical structure of MF and MTHF is very similar, which means that their production is alike with MTHF being synthesised from MF. The process to produce MF can fundamentally be broken down into two steps, see Figure 2-16. Initially fructose hexose it dehydrated to remove three oxygen atoms and create 5-hydroxymethylfurfural (HMF) and then 2,5-dihydroxymethylfuran (DHMF). DHMF is a member of the furfural biomass-derived group, which is acknowledged as a platform group used to synthesise a wide range of biofuels (Li et al., 2016). A further two oxygen atoms are then removed via hydrogenolysis to produce furfural alcohol and then MF (Román-Leshkov et al., 2007). Hydrogenation can then be used to acquire MTHF (Gathergood et al., 2018).

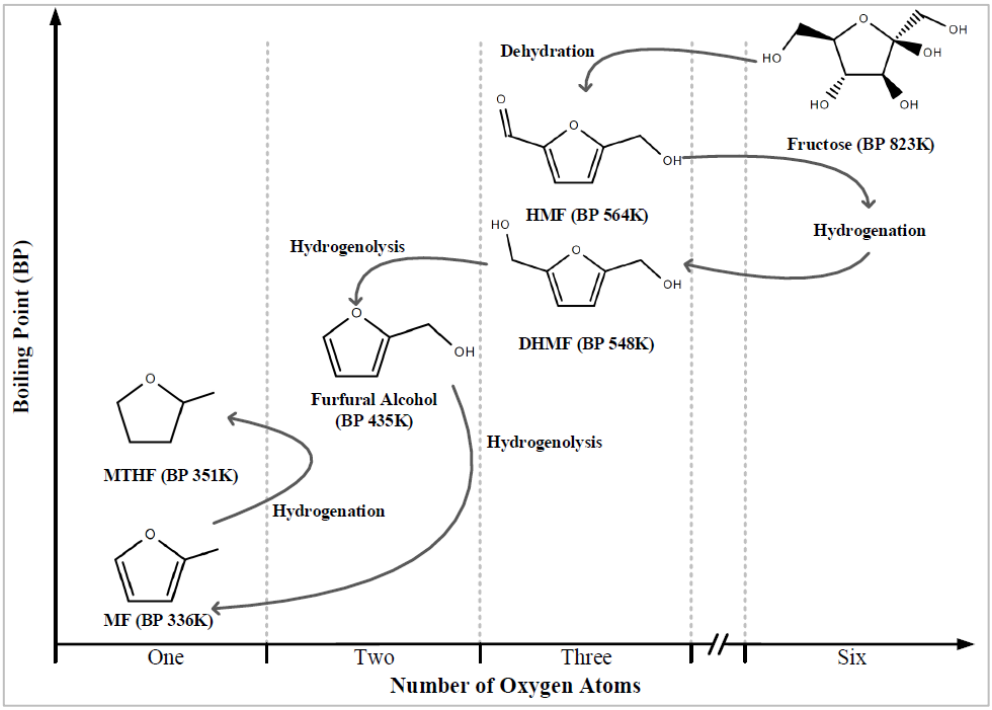

Figure 2-16 MF and MTHF Production from Fructose. Adapted From (Román-Leshkov et al., 2007) With Additional Information From (Obregón et al., 2018).

The feasibility of using second and third-generation feedstocks for the production of furan fuels is a desirable option for sustainable fuel usage. MF and MTHF are particularly appealing because of their fuel combustion characteristics (Wu et al., 2010). However, this is not the only aspect to consider when taking into account the practicality of alternative fuels. Research into furan fuels has found that they are corrosive substance. Rubber pipes and seals have been observed to swell from corrosion. However, when the seals and pipes have been converted to polytetrafluoroethylene and perfluoro-elastomer based materials, the corrosive issues have no longer been reported (Heitzig et al., 2015, Hoppe et al., 2016).

Lubricity testing of the fuels found that MTHF had a wear scar diameter (WSD) of 855µm and MF had a WSD value of approximately 330µm. The accepted maximum for diesel-based fuels is 460µm (Weinebeck, 2019, Dearn et al., 2018). The reduced lubricity of

MTHF indicates increased stress on the fuelling system, especially on rotating and high-pressure components. This would drastically reduce the life span of systems and highlights the necessity for a lubricity improver to be used when testing these fuels, especially when a common rail injection system is being used.

The higher cetane number of MTHF, when compared to gasoline and MF, means that it is more favourable to use the fuel within a CI engine. The favourable characteristics of MTHF were confirmed by a statistical analysis relating MTHF properties to the ideal CI fuel. It highlighted that many of MTHF's characteristics were in line with the proposed characteristics, these include oxygen content, aromatic content and the temperature required to for 50% of the fuel to be vapourised (Janssen et al., 2011).

Load testing with pure MTHF has been completed with a single cylinder diesel engine. The results found that at the low load point (4.3 bar IMEP) combustion was not attainable because of the cetane number of MTHF. The physical CR of 15:1 was too low for the second-lowest load point (6.8 bar) which required high amounts of forced induction to increase the practical CR to 19:1 to attain stable combustion. This load point and the two higher points (9.4 & 14.8 bar IMEP) were compared to neat diesel. The MTHF values at each of the load point provided significantly reduced soot with increases of CO and UHC. These characteristics can be directly attributed to the cetane number of MTHF forcing injection to be advanced, increasing the ignition delay and cylinder wall impingement. The CO and UHC formation of MTHF was seen to reduce dramatically as the load, and in-cylinder temperature increased. The percentage difference compared to neat diesel at 6.8 bar found that CO and UHC was 120% and 150% greater, respectively. This was reduced at the two highest loads with the percentage difference for UHC and CO being 50% and 100%, respectively. The soot formation was reduced by 92.5% at 6.8 IMEP, and

78% at 14.8 bar IMEP as MTHF was able to oxidise soot (Janssen et al., 2010). The performance of MTHF with an exhaust aftertreatment system was also evaluated. It was found that a diesel particle filter (DPF) was able to regenerate at temperatures 100°C lower when pure MTHF was used. The oxidation of soot at a lower temperature was attributed to the additional oxygen content available with MTHF soot. The reduced soot formed by the use of MTHF would also increase the time required between DPF regenerations. Less fuel would also be required to attain the regeneration temperature, and it would occur faster because of the additional oxygen available within the soot (Bhardwaj et al., 2013).

The statistical analysis of the ideal proposed characteristics highlighted that the most significant discrepancy between MTHF and the ideal values was the low cetane value of MTHF. To overcome this issue, a high cetane fuel was added to MTHF. A volume blend of 30% di-n-buthylether and 70% MTHF was tested under the load testing conditions previously discussed. The ignition delay was still prevalent in the blend when compared to neat diesel, but this was significantly reduced over pure MTHF. This ignition delay of the blend was still able to provide greatly reduced soot over neat diesel along with similar CO and UHC formation. The increased cetane value of the fuel blend, when compared to neat MTHF, was able to maintain a long enough ignition delay to improve mixture homogeneity, but it was short enough to reduce the wall impingement from pure MTHF use (Janssen et al., 2011).

The performance of MF within an ICE has been reviewed by several researchers. However, the majority of investigations have focussed on SI engines because of the similar motor octane number with gasoline. Results have found that low blends of MF/gasoline can provide positive performance enhancements within an SI engine. Wei

et al. completed engine speed sweep testing, fuelling the engine with a 10% MF/ 90% gasoline (b/v) blend, concluding that UHC and CO could be reduced. It was also found that the increased energy density of MF aided in reducing combustion duration, increasing thermal efficiency and reducing BSFC (Wei et al., 2014). An in-depth load test of pure MF was completed on a single cylinder engine by Wang et al. ranging from 3.5-8.5 bar IMEP. At the highest load, it was found that the combustion duration reduced by 7 CA when compared to neat gasoline. This reduced combustion duration along with the compact molecular structure of MF aiding in reducing detonation. The negative aspect of reduced combustion duration was increased NO_x formation. An increase was seen throughout the engine load range with a 64% increase over gasoline at the highest load. The reduced combustion duration did improve combustion efficiency through the load range and reduced the UHC formation by 73% at the highest load. The oxygen content of MF was also able to oxidise soot and reduce the accumulation and nucleation particle concentration by 36% and 77% in that order. The investigation also found an increased thermal efficiency of up to 3% and reduced fuel consumption by 30% (Wang et al., 2013). Hoppe et al. were able to complete testing with an engine that could be fitted with two different piston designs. One was able to attain a CR of 8.5:1, and the other provided a value of 13.5:1. The results found that the knock resistance of MF was able to provide increased thermal efficiency of up to 21%. They also found that the reduced combustion duration and lower enthalpy of vaporisation were also able to improve the combustion stability and cold start ability (Hoppe et al., 2016). Pan et al. noted the increased NO_x formation and reviewed the effect of altering the EGR level from 0-15%. At full load and with a CR of 9:1, it was found that the CO and UHC increased as the EGR level increased with both neat gasoline and neat MF. The increased combustion stability of MF meant

that the CO and UHC results were lower than gasoline at each respective EGR point. The results also found that as the EGR level increased, the NO_x formation of both fuels reduced. However MF had a more considerable influence on NO_x formation and provided a more significant value range from 0-15% EGR, this resulted in MF producing reduced NO_x over gasoline from 11-15% EGR (Pan et al., 2014).

Xiao et al. have completed initial investigations reviewing the use of MF within a CI engine. The first investigation completed load testing from 1.3-11.3 bar BMEP with MF10-MF40. Results found that the low cetane number and high auto-ignition temperature of MF increased the ignition delay and combustion resistance. This resulted in high levels of combustion instability at high MF blend ratios when operating at low load conditions. The oxygen content of MF aided in reducing the combustion duration, which in turn increased NO_x and BTE. The reduced combustibility of MF increased the UHC and CO production as the MF blend increased (Xiao et al., 2016). A review into particulate generation and unregulated emissions of blends ranging from MF10-30% found that 1,3-butadiene and benzene reduced with increasing load and MF fraction. Acetaldehyde was found to reduce when the load increased with higher MF ratios. The higher combustion temperature of MF blends found that particle mass and size decreased as the blend ratio increased. However, this resulted in a higher particle concentration as MF fraction increased. At low loads and high blend ratios, it was seen that both concentration and mass would increase because of combustion instability (Xiao et al., 2017). An investigation into the use of pilot injection with MF blends found that the increase of pilot volume reduced the UHC and CO emission by increasing the combustion efficiency. When comparing the results to neat diesel, it was found that MF30 was able to significantly reduce the nucleation and accumulation particle number because of the

increased preparation time and the increased oxidation available from MF (Xiao et al., 2018). A study comparing the characteristics of biodiesel mixed with MF (blends from 10-30% b/v) highlighted very similar trends to the testing seen with diesel and MF blends. The ignition delay increased, and combustion duration decreased as MF blend increased, reducing combustion duration and increasing NO_x. Low loads were problematic for high MF/biodiesel blends, and high amounts of UHC and CO were seen at these points. The benzene, 1,3-butadiene and acetaldehyde also reduced as MF fraction increased, apart from the MF30 at low load. The MF/biodiesel testing also produced lower benzene and 1,3-butadiene emissions values than the MF/diesel blends at each load point (Xiao et al., 2019).

2.7 Summary and Research Novelties

2.7.1 Summary

The investigation undertaken in this thesis will focus on the in-cylinder and emissions performance of 2-methylfuran/diesel blends within a compression ignition engine, along with analysis into MTHF and biodiesel blends with diesel. It is apparent that the use of fossil fuels is no longer acceptable with concerns being raised regarding energy security and the emissions emitted. In the long term, it is believed that hydrogen-powered vehicles will be the sustainable option with battery power being the intermediary technology until hydrogen power is suitable for mass production. However, battery power still has issues regarding consumer expectations, raw material usage and recyclability. This means that alternative fuels are required to be reviewed until battery power becomes more suitable for consumer and legislation requirements.

Advances in biofuel production mean that many previously attractive but production extensive and expensive fuels have become suitable to review comprehensively. Furan

ring fuels can supply desirable fuel qualities while being manufactured from products like sweetcorn husks and seaweed.

A review into combustion engine fundamentals has been completed which has highlighted the basics of compression ignition combustion and the emissions that are generated. This has been followed by advances made by automotive manufacturers to attain more control over engine performance and emission generated. The test engine used for this body of work has been taken into account for this review to provide the reader with an understanding of the engine parameters altered during testing, their effect on engine performance and their applicability to mass-produced vehicles.

Current alternative fuels have also been reviewed, which has highlighted their positive aspects and shortcomings when compared to diesel fuel performance. The critical issues seen with ethanol usage is its low energy density, increased UHC and CO production over gasoline and its hygroscopic nature with water causing ethanol and fossil fuel mixes to separate when stored for an extended period. Biodiesel is a more accepted CI alternative, but it still does not meet consumer demand as it is more expensive, increases fuel consumption, and it provides difficulties for manufacturers by increasing NO_x formation. Two appealing furan fuels are MTHF and MF. MTHF has been researched more extensively in compressions ignition engines, with results highlighting the low cetane number and oxygen content of MTHF. The low cetane number increases combustion instability while the oxygen content aids significantly in reducing particulate emissions. MF has been widely reviewed in SI engines and has proven to be a viable alternative in that ICE form.

2.7.2 Research Novelties

From this review, it has been found that furan fuels offer many favourable characteristics for their use within an ICE and recent production advances mean that thorough investigations are now economically viable. The overall aim of these investigations is to assess possible biofuels that would reduce fossil fuel dependence. A range of publications have been released regarding the use of furans with SI engines, however, there has been limited focus concerning CI engines. By using low cetane oxygenated furan fuels with a CI engine, it may be possible to reduce particle formation while maintaining low levels of UHC and CO emissions. Therefore, the overall aim of this thesis is to fill the knowledge gap regarding the use of furan fuels (MF and MTHF) as a fuel component within CI engines, this thesis will take into account the in-cylinder performance as well as the gaseous and particulate emissions in an effort to conclude if using furan fuels within a CI engine could aid in reducing the automotive industries dependence on fossil fuels.

This thesis will study the in-cylinder combustion patterns, fuel economy, gaseous and particulate performance of various MF (MF5, MF15 and MF25) and MTHF (MTHF25) fuel blends with diesel under a range of operating conditions. Comparisons will be completed against fossil diesel initially and also a biodiesel/diesel blend (B25) in a load test. The purpose of these comparisons is to understand furan fuels performance against the current automotive fuel as well as biodiesel as this is the fuel that will be the conventional biofuel/diesel choice for compression ignition engines if no other alternatives are found. The novelties of these experiments that will give depth and additional range to the current information available includes:

- Exploring by statistical analysis, the suitability of using MF within a CI engine in terms of engine performance, fuel economy and emissions.

- A study of the interactions between engine technologies (injection pressure and timing, cold EGR and hot EGR) and MF fuel blends aiming to evaluate the potential of MF as an efficient and clean (gaseous and particle emissions) alternative fuel.
- An investigation of the performance of MF and MTHF (both furan fuel components) fuel blends at a range of engine loads in comparison to diesel and biodiesel (B25). This study will review in-cylinder combustion characteristics, fuel economy as well as gaseous and particulate emissions.

CHAPTER 3

3. Experimental System

3.1 Introduction

This chapter discusses the experimental systems, equipment and techniques used to complete the investigations undertaken, this includes a description of the engine configuration and engine test cell used. A single engine was used for this investigation; however, two different engine configurations were used and will be discussed in further detail in this section.

3.2 Base engine

The engine experiments were completed with a mass-produced 2.2l light-duty Ford Duratorq L316 engine; the specifications are shown in Table 3-1. This engine is an inline 4-cylinder compression ignition engine fitted with a VGT and a common rail direct injection system. The OEM injectors were piezoelectric; however, as a non-OEM injector driver was used, solenoid injectors had to be fitted to allow for suitable control.

Table 3-1 Engine Specifications.

Component	Specification
Stroke	94.6 mm
Bore	86 mm
Connecting Rod Length	155 mm
Compression Ratio	16.6:1
Swept Volume	2198 cc
Injectors	7 Holes (0.15mm diameter), Solenoid

Figure 3-1 displays a schematic of the base experimental set up of the Duratorq engine. To ensure that results were suitable for real-world applications, the engine was kept as

close to its original design as possible. However, some components had to be removed to reduce the complexity of the system and increase the robustness of the engine; these components included the alternator, air-conditioning compressor as well as the coolant, vacuum and power steering pumps. To aid in additional control and experimental scope, a ball valve was placed on to the EGR intercooler.

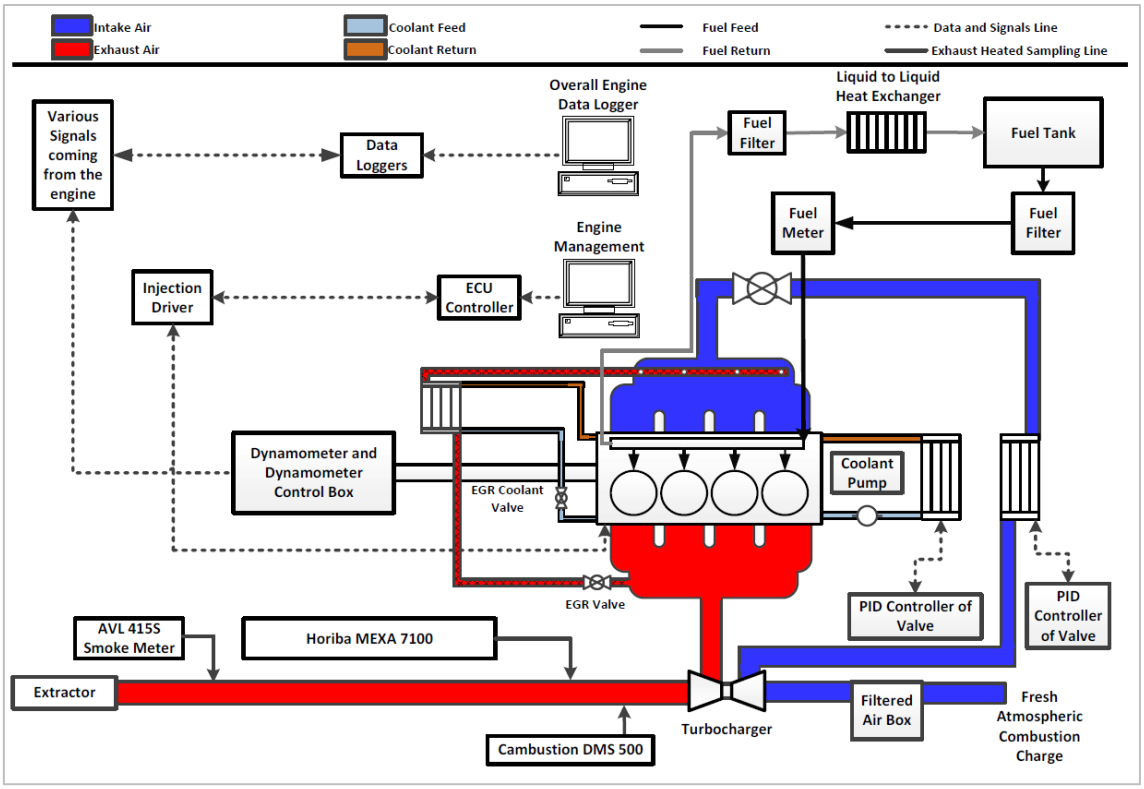

Figure 3-1 Base Engine Configuration.

3.2.1 Dynamometer and Dynamometer control

The dynamometer used was a reversible eddy current Froude Engineering EC38TA (shown in Figure 3-2), this had a maximum torque of 477.5 Nm, that used closed-loop cooling with a dry gap rotor. The dynamometer was electronically interfaced and controlled through a Schneck 2000 D/W system. This was capable of monitoring engine torque through a load cell, and rotational speed via a toothed wheel, the front panel of the control unit is shown in Figure 3-3.

The Duratorq engine was connected to the EC38TA by the OEM dual mass flywheel, clutch and power take-off unit (PTO). The PTO and dynamometer were then connected through a conventional driveshaft.

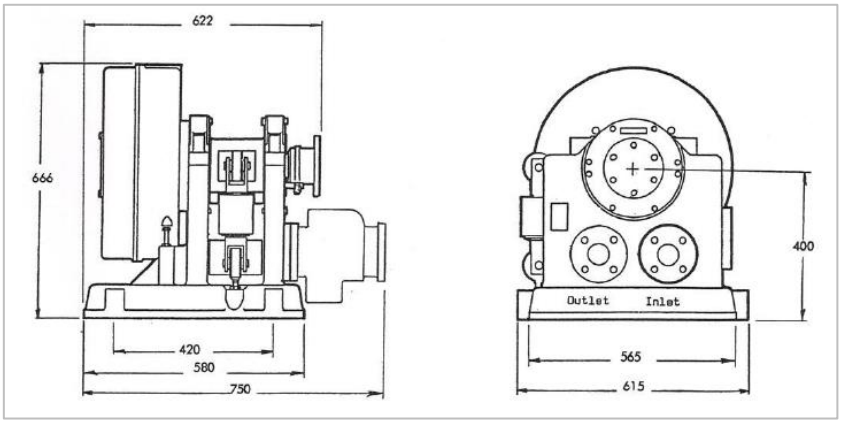

Figure 3-2 Froude Engineering ECT38TA Dynamometer (Zhang, 2011).

Figure 3-3 Schneck 2000 D/W Control Unit.

3.2.2 Engine Control

The ECU used to control the performance of the engine was an M250 open ECU manufactured by Pi-Innovo, this was linked to a Pi-Innovo S070 solenoid injector driver. The ECU came equipped with two H-bridge circuits which were used to control the position of the EGR valve and VGT, an external H-bridge, manufactured by Axiomatic (AX10060X), was used to set the position of the intake valve.

The author communicated to the open-ECU and injector controller through a computer program. The software used to do this was version 2.3.3 of Accurate Technologies ATI Vision. This used a calibration file and strategy file to suitably control the engine. Using this program meant that the operator could control a range of engine components, increasing the spectrum of available research areas. The typical ATI user interface used throughout the testing is shown in the appendix. The calibration file would stay the same for all types of engine testing, but the strategy would change depending on the engine configuration used.

The dynamometer was not able to rotate the engine, so to start the engine a battery and the OEM starter motor were used. The starter motor was controlled through LabVIEW via a National Instruments (NI) USB-6218 board which was able to engage a selection of relays and electrical flow paths to connect the 12v battery to the starter motor and initiate engine rotation. When a signal was received from the crankshaft or cam sensor, the ECU would batch inject into all of the cylinders. When the crankshaft and cam signals became synchronised, injection would then become sequential. Base fuel injection maps were used to control the injection timing, quantity and pressure (along with all other aspects) when starting the engine. Once the engine had been running for around a minute, the author would then override these maps to warm up the engine in a controlled manner and then set the first testing point. The use of ATI Vision and the open ECU allowed the author to set the demand of various valves and motors as well as the timing and duty cycle of various engine components.

3.2.3 Engine Fluid Temperature Control

Many of the conditions within the test cell were maintained and regulated to ensure that the engine and associated components were operating in a safe and repeatable manner.

To further ensure accurate and reproducible values, much of the control was undertaken by computers and controllers instead of the OEM mechanical components. The main alteration was to the intercoolers and plumbing architecture, with two GL320-1428-5 E J Bowman shell and tube liquid intercoolers being used. The first intercooler was introduced into the engine cooling system. This allowed for the control of the engine coolant temperature, which also controlled the OEM EGR intercooler coolant temperature and the lubricating oil temperature. The second intercooler was used to control the intake air temperature after the fresh intake charge had passed through the compressor. The cooling liquid used for these intercoolers was ambient water, and this liquid was also integrated with additional intercoolers discussed in the following sections. This ambient water was gravity fed from a large tank situated above the test cell.

Both cooling systems used separate closed-loop Fuji Electric PXG.4E proportional integral derivative (PID) controllers that allowed the author to set the required engine coolant and intake gas temperatures individually. The intercooler efficiency was controlled with electro-pneumatic transducer's manufactured by Johnson Controls (EP-8000-4). These were connected to Northvale Korting 3-way valves (75AM-M26824-15/20DN). The PID's monitored the actual temperature of the coolant and gas and output current between 4-20mA, this electric current controlled the position of the Northvale valves, controlling the intercooler efficiency of the systems. The set target temperatures for the PID's were 25°C for the intake air after the turbine compressor and 89°C for the engine coolant once the coolant had passed through the engine.

3.3 Engine Conversion to include a Separated Cylinder

The overall knowledge of MF performance within a CI engine was limited. Most of the investigations undertaken in this thesis were the first of their kind and would include

ranging sweeps of engine variables. As MF has a low cetane number, it was known that combustion would become more challenging to attain as the MF blend ratio increased.

It was decided to convert the conventional four-cylinder engine to a novel configuration that had a separated cylinder (SC) for some of the tests. Three cylinders would be fuelled by neat diesel, and a separated cylinder would be externally fuelled by the MF/diesel blends. This allowed for the three cylinders to run safely while the test point for the separated cylinder was being set. The conversion was required as MF was expensive in small volumes, it may have been corrosive and because the low cetane number may have caused the engine to stall. If the engine were to stall it would take at least one hour to restart the engine, purge the emissions equipment and let the engine reach a steady-state again before continuing testing. This configuration did require additional care to be taken to ensure the combustion performance of all the cylinders was similar; however, this conversion did give more flexibility and control when the engine began to respond poorly to certain test scenarios. The following section describes the steps undertaken to convert the configuration of the engine.

3.3.1 Overview of the Single Cylinder Conversion

Completing such a significant conversion to the system was challenging from a packaging perspective. It was decided to separate the fourth cylinder from the first three as this cylinder was at the opposite side to the dynamometer, ECU and original EGR, meaning that the fourth cylinder had the most available space. The experimental set up is displayed below in Figure 3-4 and is discussed in more detail in the following section.

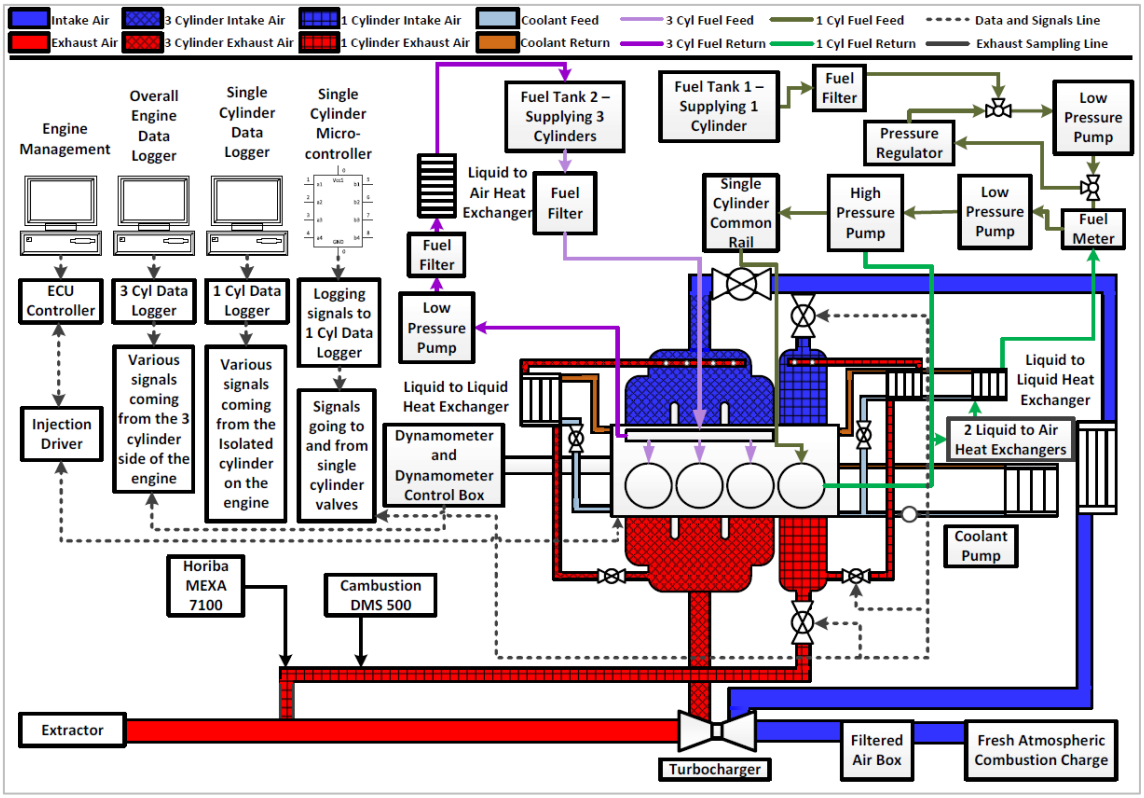

Figure 3-4 Separated Cylinder Experimental Setup Schematic.

The first step undertaken in the conversion was the alteration of the ECU strategy. The updated strategy allowed for the first three cylinders to be run by the injection volume and timing values set by the author in their respective map/lookup tables. The SC could then run with author set override values. The overall values used for the SC injection timing and volume added together the value used for the other three cylinders and the override value. For example, if the injection timing for the three cylinders was set to 10°BTDC and the SC was set with an override value of 1°BTDC, then the separated cylinder would have an injection timing value of 11°BTDC.

This logic could be implemented separately for the injection timing and volume of the SC. However, if split injection was used, it resulted in the override values being applied to all injection timings and volumes. This meant that the ECU did not offer enough

flexibility to complete comprehensive split injection tests and that only a single injection strategy would be suitable for SC testing.

3.3.2 Gas Flow Separation

3.3.2.1 Intake Gas

The next stage in the conversion was to alter the intake and exhaust manifold while integrating a new HPEGR system for the separated cylinder. The new manifolds were used to separate the gas flow between the first three cylinders and the SC. This was done to allow for more control of the gas pressure in the separated system and to ensure that there was no cross-contamination of the neat diesel exhaust gas from the three cylinders entering the separated cylinder when the three cylinder EGR valve was open.

The primary material choice for this conversion was 316-grade stainless steel. This was chosen as it is durable, relatively lightweight and has non-reactive qualities. These points were crucial as they created a robust system that could generate repeatable and reliable results.

For the intake manifold conversion, a plate was put between the manifold runners of the third and fourth cylinder to give the fourth cylinder a separate manifold. The top section of the separated manifold was then removed and replaced with a plate and pipe. Another pipe was then used to connect the intercooler of the compressed intake gas and the separated manifold; this acted as the SC intake pipe. This meant that the gas flow to the separated cylinder was independent, while the other three cylinders were still supplied fresh charge as usual. Integrated into the SC intake pipe was a valve to control the SC fresh gas flow rate. A coupling for the EGR along with fittings for temperature, pressure and EGR ratio monitoring was also mounted to the intake pipe manifold. The manifold

and SC intake pipe is shown as standalone components in Figure 3-5 and fitted to the engine in Figure 3-6.

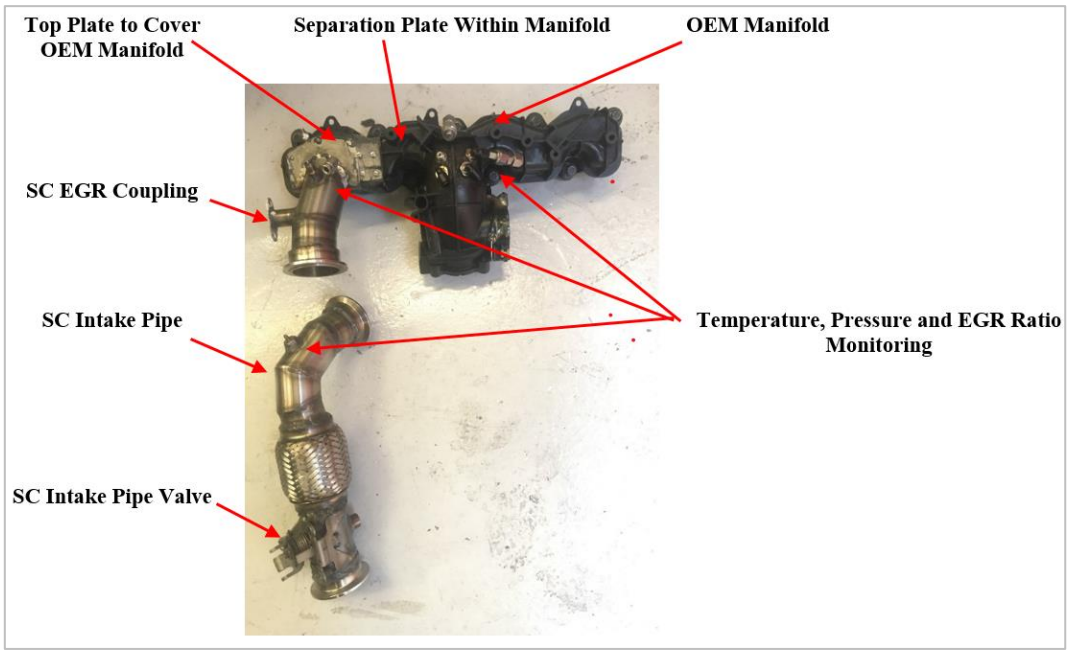

Figure 3-5 Intake Manifold Used with Separated Cylinder along with Separated Cylinder Intake Pipe.

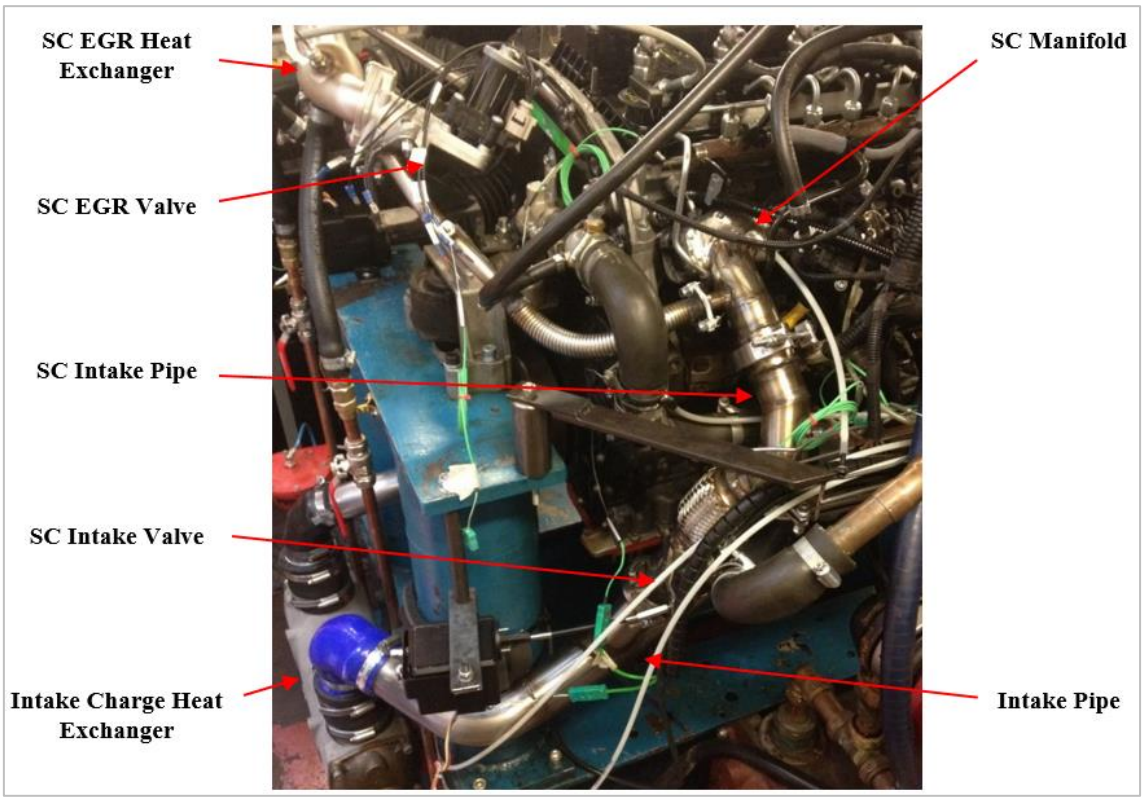

Figure 3-6 Separated Cylinder Intake and Intake Side EGR System Mounted to Engine.

3.3.2.2 Exhaust Gas

The exhaust gas flow was separated by cutting the OEM manifold where the third and fourth cylinder runners met and then welding plates over the openings to create two separate manifolds, see Figure 3-7. The SC exhaust manifold then had two pipes welded onto it. One connected to the SC EGR and the other connected to the exhaust of the other cylinders, see Figure 3-8. There was limited space between the exhaust turbine and engine, and there was a necessity for numerous sampling points of the SC gas before it was reintroduced to the conventional exhaust system. This meant that the SC exhaust pipe had to bypass the turbine housing. This required a valve to be installed on to the SC exhaust pipe to control backpressure and mimic the exhaust gas pressure seen before passing through the turbine. The SC exhaust pipe had sampling points added for temperature, pressure and emissions systems. The SC exhaust pipe fitted onto the engine is shown in Figure 3-8.

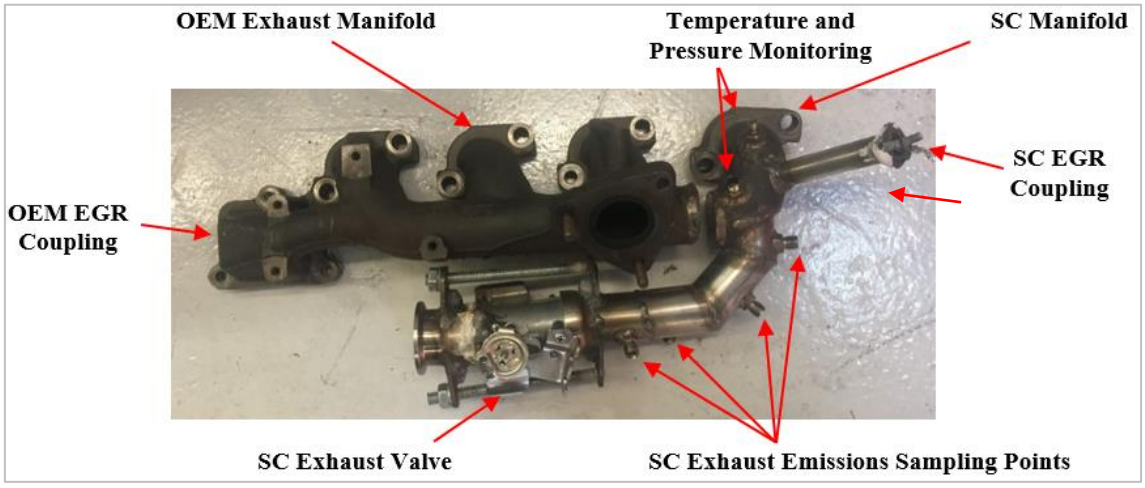

Figure 3-7 Exhaust Manifold and Pipe Used with Separated Cylinder.

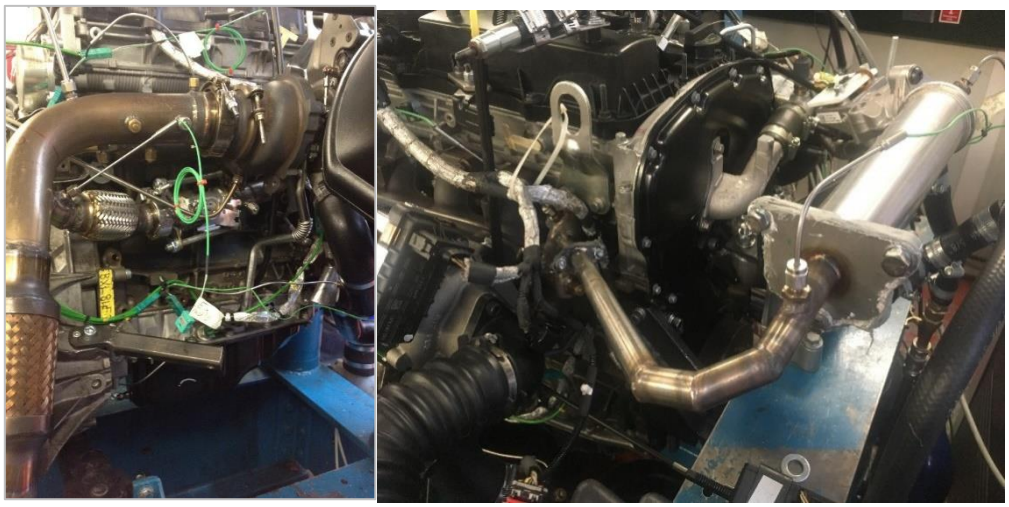

Figure 3-8 Separated Cylinder Exhaust and Exhaust Side EGR System Mounted to Engine.

3.3.2.3 EGR Gas

As discussed, an EGR for the SC system was fitted which operated separately to the OEM EGR system. This system included a liquid to air shell and tube intercooler (Ford part number 6C1Q-9F464-BD). The liquid cooling connections of the intercooler were fitted with ball valves to control coolant flow and intercooler efficiency. The coolant liquid was plumbed into the ambient water system used for the GL320-1428-5 E J Bowman shell intercoolers discussed earlier. Similar to the SC intake and exhaust system, a valve was used on the EGR to control gas flow along with a selection of temperature and pressure sensors to alter and monitor the EGR functions. Figure 3-8 shows the SC EGR system mounted to the engine and Figure 3-9 shows the separated cylinder gas flow system for clarity.

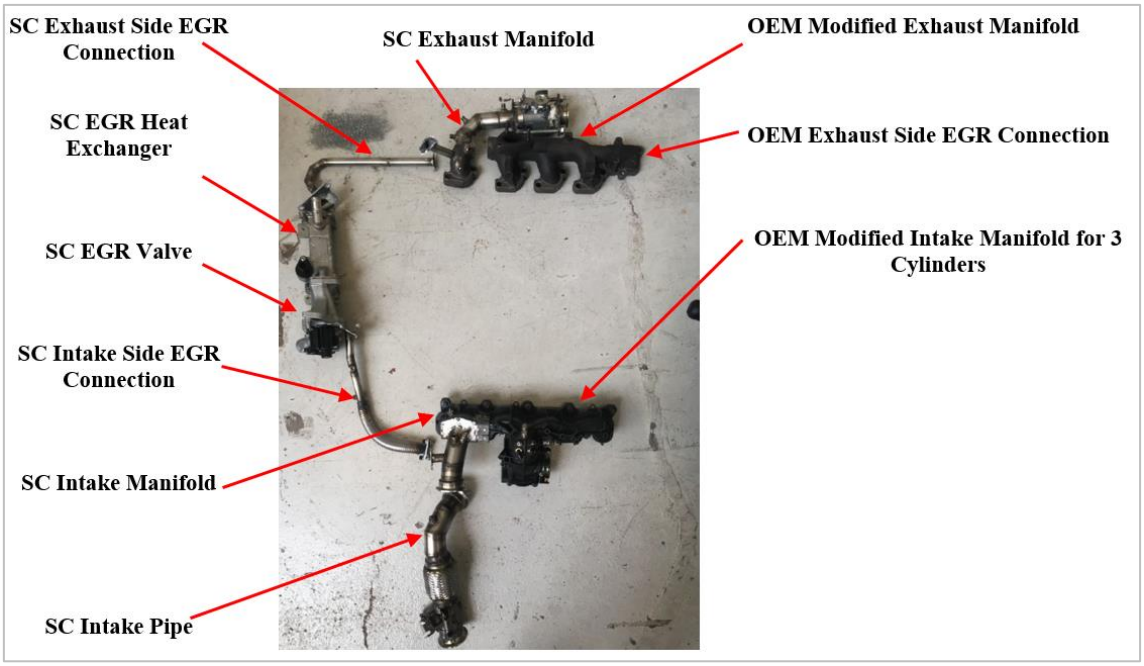

Figure 3-9 Separated Cylinder Intake and Exhaust Manifold with EGR System.

3.3.2.4 Gas Flow Control

As discussed, each new subsection of the conversion was fitted with a valve to control the gas flow through the SC system. Mechatronics was included in the conversion to safely control and monitor the position of these valves during the engine's operation.

The main component of the mechatronics control system was an Arduino Mega R3 microcontroller. This microcontroller was coded and had an electronic circuit manufactured that allowed the individual control of the valve positions. The valves used were an Actuonix PQ12 linear actuator for the EGR valve and A.R.A (U.S. patent number 4,656,407) linear actuators for the exhaust and intake manifold valves. The microcontroller would also send reference voltage to a data logger so that it was possible to safely monitor and log the position of the valves while running the engine. A schematic of the control system is displayed in the appendix.

3.3.3 Separated Cylinder Fuel Injection System

As the separated cylinder was using a different fuel to the other three cylinders, it required a different fuel injection system. The fuelling for the first three cylinders would come from the OEM on engine common rail system, the fuelling for the separated cylinder was supplied via a modified Autoelektonika – STPiW2 diesel injection test bench. The system was originally designed for the testing of high-pressure diesel pumps and fuel injectors. To ensure the system would be suitable for prolonged engine tests, some improvements were required. Firstly, as MTHF is known to be corrosive, all rubber pipes were converted to 316 stainless steel pipes. Secondly, an external fuel tank was fitted along with a fuel consumption meter (discussed in the next section); finally, an improved fuel cooling system was added to the SC fuel delivery system. An overview of the injection system is displayed in Figure 3-10.

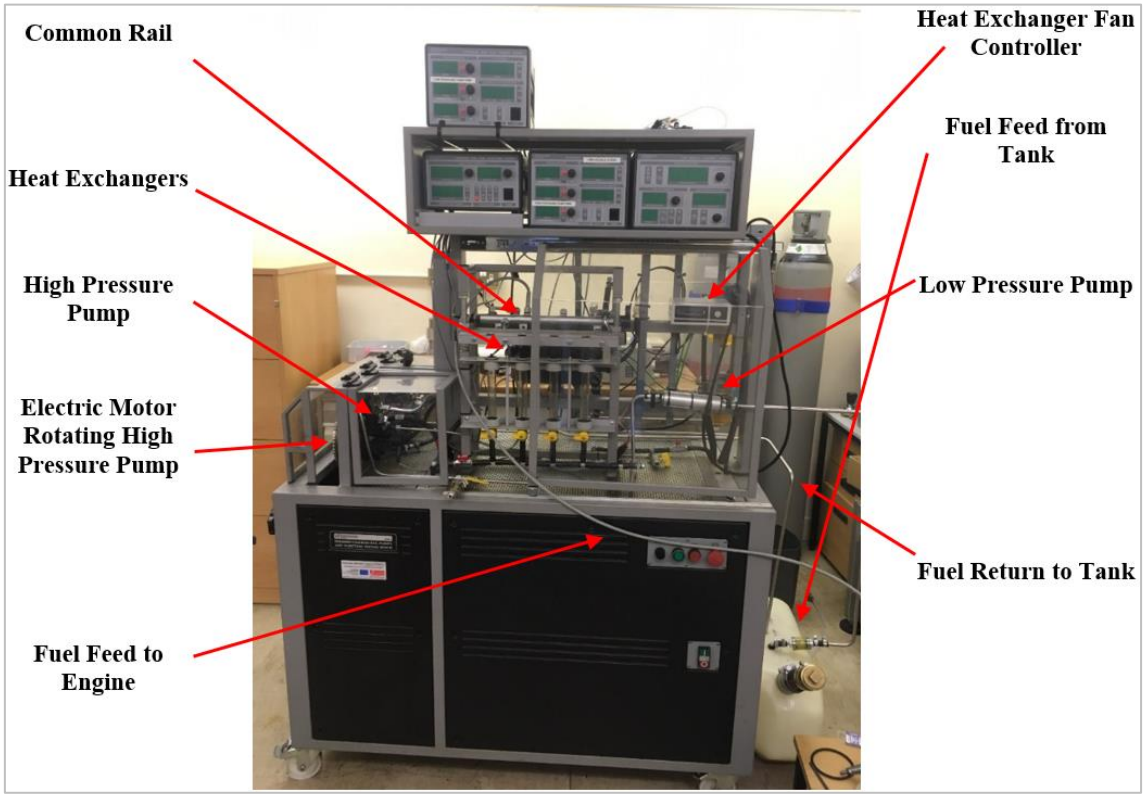

Figure 3-10 Autoelektonika – STPiW2 Diesel Injection Test Bench.

The engine experiments would continue for many hours, and because of this, additional fuel cooling strategies were employed to maintain a low and constant fuel temperature. Firstly, two liquid to air intercoolers and a large fan were fitted to the system. The fan was controlled by using an Arduino Uno microcontroller that allowed the fan speed to be monitored and altered by the user, thus altering the heat rejection rate. A schematic of the system can be found in the appendix. Secondly, a liquid to liquid intercooler was manufactured. The cooling liquid used with this exchanger was the ambient water which was used for the liquid to liquid bowman intercoolers discussed earlier. This ambient water passed into a sealed tank which had a wound pipe in it. The pipe connected to the injection system, allowing the heat of the fuel flowing through the pipe to be dissipated to the ambient water. The flow rate of the cooling water was controlled with two ball valves operated by the author. The flow diagram for the fuel injection system is displayed in Figure 3-11.

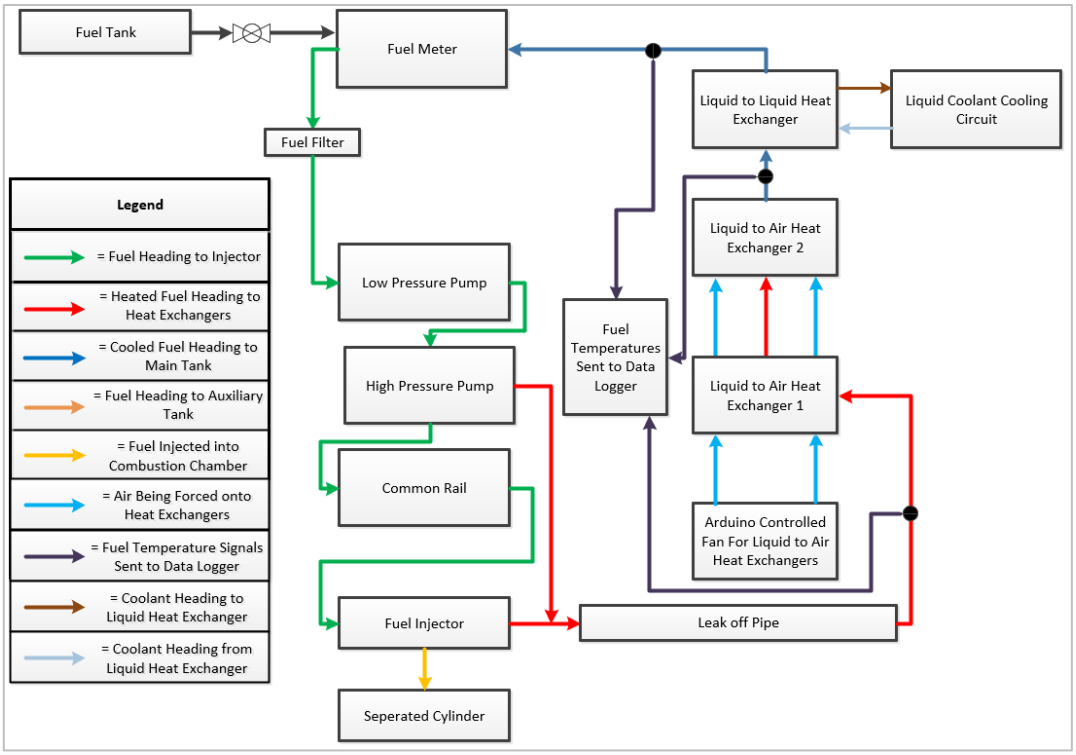

Figure 3-11 Single Cylinder Fuel Injection Schematic.

3.4 Fuel Consumption Measurement

Depending on the testing being completed, an AVL 733s fuel meter was either fitted to the fuelling system of the conventional four-cylinder system or the SC external fuel injection system displayed in Figure 3-11.

For the SC conversion, there were two separate fuel tanks used. The first fuel tank fed the first three cylinders' neat diesel, and any fuel that was returned from the on-engine common rail, high-pressure pump or leak off pipes went through an AVL 752-60 fuel cooler and back into the tank, no fuel meter was used for the first three cylinders during the SC testing. The second tank (shown in Figure 3-11) was used for filling the fuel meter, which fed fuel to the SC injection system. The fuel meter had a small reservoir within it which was mounted onto a load cell that was regularly calibrated. Fuel was delivered to the engine from the reservoir and fuel that was not injected from the system was returned to the fuel meter via the intercoolers discussed in the previous section. The fuel meter was able to monitor the weight reduction of the reservoir over a set period and calculate the fuel consumption. The fuel consumption was monitored over 180 seconds for all of the tests.

When tests were completed with the conventional 4-cylinder configuration, a single tank was used. Fuel was delivered to all of the cylinders via the AVL-733s fuel meter; any rejected fuel was passed through the AVL 752-60 fuel cooler and back to the fuel meter. It should be noted that the fuel cooler was a liquid to liquid intercooler with ambient temperature water being the cooling media used. AVL software was used to communicate with the fuel meter, allowing the user to control and monitor the fuel level of the meter as well as logging the fuel consumption.

3.5 Instrumentation

The instrumentation discussed in this section highlights the primary sensors that were used to monitor the quantitative performance of the different operating conditions.

3.5.1 In-Cylinder Pressure Measurement

To attain in-cylinder pressure in reference to the crank position, an in-cylinder pressure sensor and rotary encoder were used. After the first research chapter reviewing the feasibility of using MF within a CI engine, a higher resolution encoder was fitted to the engine. The pressure sensor and encoders will be discussed in this section.

3.5.1.1 In-Cylinder Pressure Sensor

The pressure sensor used for all the investigations was a Kistler 6058A non-cooled PeizoStar transducer. The sensor was mounted into the combustion chamber via a glow plug adaptor (Kistler 6544Q192) which housed the sensor. The calibrated pressure sensor provided a linearity of $\leq \pm 0.05\%$ at the full-scale output. The linearity and sensitivity calibration values of the pressure sensor were inserted into a Kistler 5011B10Y50 charge amplifier. The use of these values and the signal drift compensation incorporated into the amplifier allowed for a repeatable and accurate in-cylinder pressure signal to be output through a BNC port.

3.5.1.2 Crank Shaft Encoder and Referencing Pressure Sensor Signal

A shaft encoder was fitted onto the end of the crankshaft with the closest cylinder being the pressure sensor mounted fourth cylinder.

The results assessed in chapter 4 used a NI PCI-6251 data acquisition (DAQ) card to gather the incoming in-cylinder pressure and encoder signals. This was then coupled with a LabVIEW program to process and display the incoming data. The pressure signal was

received from the charge amplifier, and the crank position was calculated by synchronising the cam sensor signal with an AMI-Elektronik/Art.No:41500043-00360 rotary encoder that had a resolution of 1 CA. The LabVIEW program could be used to display in-cylinder information as well as logging and saving 200 consecutive cycles when completing testing.

All testing after the initial research chapter used an AVL 365C crank encoder. The encoder and pressure sensor signals were connected to an AVL IndiModul 621 DAQ board which output information to a computer through the program AVL IndiCom. This software did not require a cam signal and could calculate the TDC CA from the measured motoring pressure. Similar to the LabVIEW in-cylinder pressure program, the AVL software was configured to display a range of information and log 200 consecutive engine cycles, however, with the AVL encoder it was possible to log in-cylinder pressure with a resolution of 0.5 CA. The capabilities of this board allowed the injector excitation to also be logged by fixing an inductive loop to the fourth cylinder injector wiring.

3.5.2 Overall Temperature and Pressure Monitoring

A selection of K-type thermocouples were used throughout the experimental setup, these thermocouples and the fittings were either supplied from RS Components or Thermal Detection. When measuring low temperatures ranging from 0°C-100°C. 1mm diameter thermocouples were chosen because of their fast response; these were mainly used to measure intake air temperatures and fluid temperatures. 3mm thermocouples were used in areas expecting temperatures above 100°C as these thermocouples are more physically robust.

Temperature sensors were placed throughout the test cell to measure gas and fluid temperatures. A selection of pressure transducers were used to measure the intake and exhaust gas pressures as well as the coolant pressure. These thermocouples and pressure transducers were connected to the NI card discussed in the previous section, which allowed the values to be displayed and logged through a LabVIEW script. These sensors also monitored the overall values of the three cylinders running diesel when using the SC configuration.

When the separated cylinder system was used there were additional thermocouples and pressure transducers used to measure the state of the SC intake, exhaust, EGR and external fuel injection systems. For the SC, a separate logging system was used. This used two PicoLog TC08's to measure the thermocouple values and a PicoLog 1012 to measure the gas pressures and valve positions of the SC system. The values seen from the PicoLog data loggers were displayed and logged with the datalogger supplier software, PicoLog 6.

All data logged from the NI card and PicoLog systems were logged at a frequency of every 100ms for 180 seconds.

3.6 Exhaust Emissions Measurement

The emissions were measured using three key pieces of equipment, a Horiba MEXA, an AVL smoke meter and also a Cambustion DMS particle analyser.

3.6.1 Gas Emissions Characterisation

Gaseous emissions were measured using a Horiba MEXA-7100-DEGR. This piece of equipment measured the gaseous emissions and output a value from each analyser every second. When logging data, a text file would be generated of the average value seen from

each analyser after 180 seconds. Before the equipment could be used for experiments, the author needed to allow the equipment to heat up sufficiently and calibrate. The MEXA used a selection of analysers to measure various gaseous emissions seen within the exhaust system; a schematic of the system is shown in Figure 3-12. A dry Non-Dispersive Infrared (NDIR) technique was used to find the amount of CO_2 and CO, and dry chemiluminescence detection was used to measure NO_x and nitric oxide (NO) levels. It should be noted that in this report, the sum value of NO and NO_x will be referred to as NO_x. The MEXA used a hot-dry flame ionisation detector to measure the content of UHC, and a magneto-pneumatic technique was used to measure the oxygen content. The AFR and lambda were calculated based upon the concentration of the various gas traces seen within the exhaust, the EGR ratio was calculated by comparing the CO_2 level seen within the exhaust gas and intake gas once EGR had been introduced. For the correct measurement of the air-fuel ratio, lambda and EGR ratio it was necessary to enter a normalised carbon, oxygen and hydrogen content value in reference to the content of the fuel/fuel blend. These normalised values needed to be entered and updated every time a different fuel or fuel blend was being used. The formula for the normalised C, H and O values of the blend fuels were calculated using the following equation and the normalised values of the fuels tested are shown in Table 2-2.

$$\begin{aligned} &Blend\ Fuel\ Normalised\ Value \\ &\quad = Fuel\ A\ Normalised\ Value * Fuel\ A\ Blend\ Ratio \\ &\quad + Fuel\ B\ Normalised\ Value * Fuel\ B\ Blend\ Ratio \end{aligned}$$

Equation 3-1

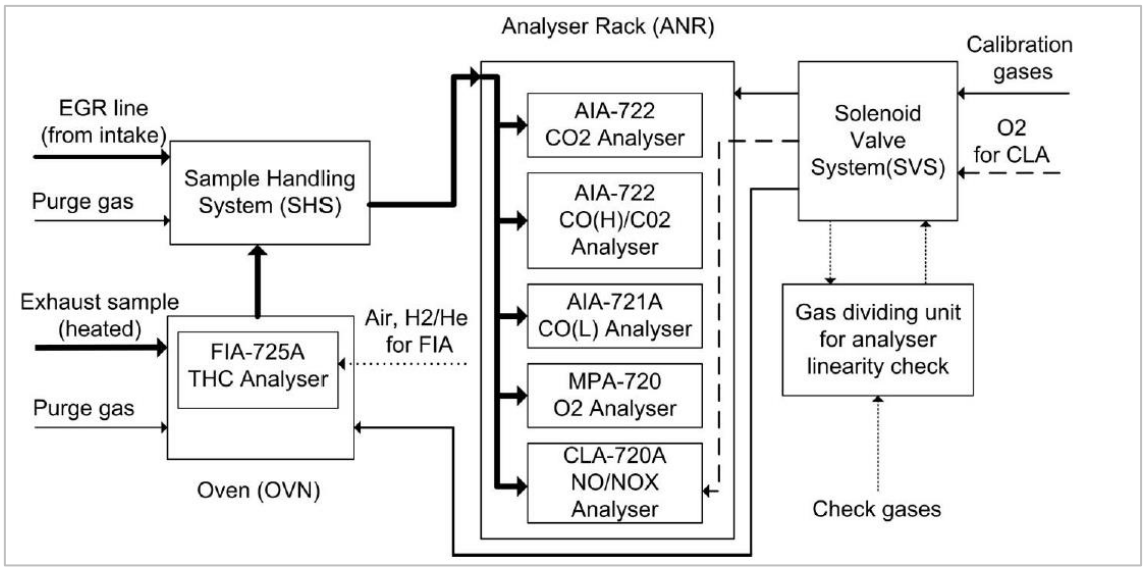

Figure 3-12 Horiba MEXA 7100 DEGR Gas Flow Schematic (Zhang, 2013).

3.6.2 Smoke Emissions

To measure the level of smoke within the exhaust gas, an AVL 415s smoke meter was employed, shown in Figure 3-13. Once the instrument was fully warmed up, it sampled exhaust gas onto a piece of filter paper and measured the gas flow. The paper was then measured via a reflectometer to calculate the opacity of the paper. The opacity gave a filter smoke number (FSN), and a value in the unit of grams/m3 could be attained when the sampling gas flow was taken into account.

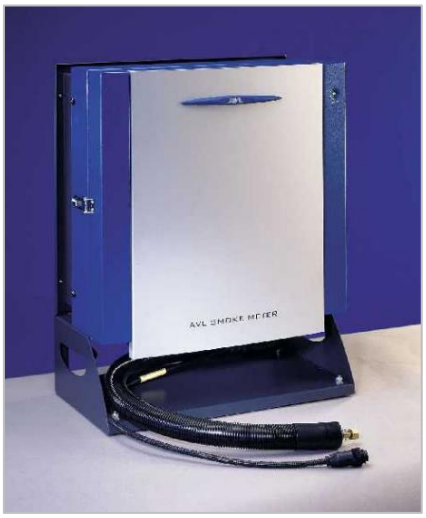

Figure 3-13 AVL 415s Smoke Meter (Schindler, 2004).

3.6.3 Particulate Size Analyser

To measure the particle size characteristics of the exhaust emissions, a Cambustion DMS500 MKII fast particulate analyser was used. The DMS500 is fitted with a two-stage dilution and sampling system that is explicitly designed for its direct use on an engine exhaust system. The first dilution point uses heated compressed air at the sampling point to remove any condensation and agglomeration. The second diluter uses a high-efficiency particulate arrestor (HEPA) to allow a wide range of aerosol concentrations to be sampled. A figure displaying the exhaust gas flow within a DMS500 is shown in the appendix. Before the treated sample enters the classifier of the DMS500, the gas enters a unipolar corona charger which uses high voltage discharge to charge the surface of each particle. The charged particles then enter the classifier, which is in a low-pressure environment (0.25 bar absolute).

The classifier is compiled of 22 electrometer detectors/rings each of which emits their own radial electrical field varying in magnetic strength, and each ring translates to a set particle size. As the particles fall down the classifier the magnetic strength of the rings increases. This results in smaller particles being attracted to the low magnetic strength rings situated towards the classifier gas inlet and the larger particles that require increased magnetic strength from the rings are situated towards the classifier gas outlet. The DMS is connected to a laptop via an ethernet cable; the user interface is shown in Figure 3-14. The software is used to alter the operating state and data logging of the DMS. The recorded data can be viewed via a Microsoft Excel add-in created by the manufacturer, this add-in can calculate the particle concentration of each measured size. Further processing can also be completed with the add-in to calculate particle mode number and

concentration along with the average particle mass, surface area (SA) and count median diameter (CMD) of both modes.

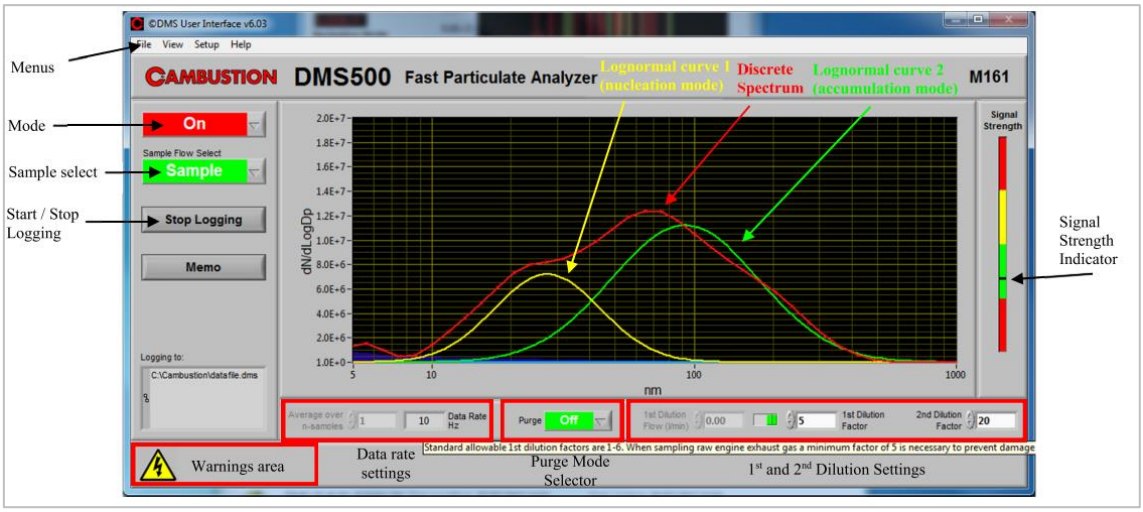

Figure 3-14 DMS500 Software User Interface (Cambustion, 2007).

3.7 Fuel Blend Preparation

As some of the test fuels were known to attain a high WSD which could damage the testing system, it was decided to add a lubricity improver (Paradyne R655) to each of the biofuels to ensure component longevity. The lubricity improver was added to the biofuels before they were mixed with the diesel at a ratio of 300 parts per million. Once the lubricity improver was added the biofuels, the biofuels were then mixed with the diesel. This blending was completed by the author mixing the fuels by volume at ambient temperature.

As discussed in the gaseous emissions review, normalised C, H O values needed to be inserted into the Horiba MEXA main control unit (MCU) to reflect the characteristics of the fuel used. This was required by the MEXA to allow the system to calculate set parameters including lambda and EGR ratio correctly. When using a blended fuel, the

normalised C, H and O values of the blend were calculated by taking into consideration the volumetric ratio of each fuel used, see Equation 3-1.

3.8 Engine Start-Up and Measurement Procedure

When undertaking testing it was necessary to start the engine in a controlled manner which was repeatable. Before starting the engine, the Horbia and DMS were both turned on and given sufficient time to warm up and calibrate. While these pieces of equipment were warming up the other pieces of equipment were also prepared e.g. the engine cooling intercooler valves were opened, the fuel tank and fuel meter was filled, the computers were turned on and used to check all of the sensors were working correctly etc. Once all of the required equipment was suitably prepared, the engine was started and allowed to warm up, this controlled warm up consisted of maintaining the engine at 24nm of torque at 1800 rpm. The injection pressure for the warm up was set to 650 bar with a single injection event used to attain an AHR50 value of 10. While warming up the engine at this low load, the functionality of all of the equipment was again checked to ensure it was working correctly, this included altering the VNT and EGR valve position, checking the operating temperatures and pressures were correct as well as the operation of the emissions equipment. The engine was kept at this low torque until the engine coolant and oil temperature had stabilised, wherever possible the emissions equipment was set to purge to reduce build up in the analysers. This warm up procedure was completed every time the engine was started.

Once the engine had warmed up it was then possible to set a testing point from the testing matrix. The user would alter the engine to attain the desired performance characteristics. Once the point had been initially set the engine performance would begin to change slightly as the engine thermally stabilised. The engine would require minor adjustments

to maintain the operating condition set point and would require further checking to ensure the engine performance had not altered again. When the engine had become stable the user would then wait for three minutes before starting testing to confirm no further alterations were required for the engine operating conditions.

Before recording a test point it was required that the emissions equipment had been purging for at least three minutes and the fuel meter had just been filled. The test data logging was completed over a period of three minutes with the data logging of various pieces of equipment being run simultaneously. Once the logging was completed the emissions equipment were set to purge for three minutes and the logging was then completed again. This process was completed a total of three times for each test point.

Additional preparation was required when running the SC engine to ensure the performance being seen within the SC was the same as the other three cylinders. To start with, the engine was run in the conventional four-cylinder mode, being fuelled by diesel. This gave the injection timing and volume values that the three cylinders running diesel would require when using the SC engine configuration. Once this was completed the engine was then ran in the SC mode but with all cylinders being fuelled with diesel, this was done to ensure that the operating conditions were still the same and that the temperatures and pressures were the same. The SC exhaust system bypassed the turbocharger which meant that the OEM EGR and VNT needed to be altered to ensure that the same pressure within the exhaust and intake manifolds of the three cylinders were the same, as well as the EGR ratio within the intake manifold. The SC EGR, intake and exhaust manifold valves were also altered to ensure that the SC pressures mimicked the other three cylinders. Once this was completed the engine testing was then commenced, the engine was then ran in the SC mode with the three cylinders being fuelled with diesel

and the single cylinder being fuelled with the test fuel. The three cylinders used the injection timing and volume values found from the initial four cylinder testing and the separated cylinder used these values as a base value with additional override values being used to attain the same in-cylinder performance as the other three cylinders. It was important to undertake this systematic methodology as the SC in-cylinder performance was very sensitive to becoming unbalanced from the performance of the other three cylinders and this would have a direct effect on all of the results attained.

3.9 Instrument Uncertainty Analysis

This section explains the uncertainty of the instruments used with the following section expanding upon this by highlighting the data post-processing and analysis. The instruments included in this analysis includes the dynamometer controller, exhaust particle size analyser, exhaust gas emissions analyser, exhaust smoke meter, fuel meter as well as the temperature and pressure sensors used through the engine test cell.

The Schneck 2000 D/W dynamometer controller was equipped with a load cell that was mounted onto the dynamometer to measure the torque. Before starting the engine, the controller was turned on, and the load cell was calibrated to ensure that the engine load displayed was 0 ± 0.1 Nm (Zhang, 2011).

Before using the Cambustion DMS500, it was necessary to turn on the system and allow it to stabilise and complete preliminary checks. During this period, the DMS500 would heat up to allow the suitable sampling of exhaust gas as well as ensuring that it was possible to attain a stable low-pressure environment within the classifier to characterize the exhaust particles. Once this was complete, it was then required to auto-zero the equipment to remove any offsets seen at each electrometer detector. Once the equipment

was being used it was also necessary to auto-zero the equipment at least every hour to ensure that accurate results were being attained as the electrometer offset would change as more exhaust particles were introduced onto each electrometer detector (Cambustion, 2007).

Similar to the DMS500, the Horiba MEXA also needed to be stabilised and calibrated before operating. Initially, the Horiba required time for the sampling lines and analysers to heat up to their set temperatures. Once this had occurred, it was then possible to calibrate each of the analysers. Span gases were used to provide known gas concentrations to the analysers and allow them to zero and calibrate. Once this was complete, the manufacture noted a gas error deviation of ±1% at full scale (Zhang, 2011).

The AVL smoke meter has gas pass through a filter paper was a sensor that reviewed the opacity of the paper to calculate the FSN. The smoke meter was configured to keep taking samples until three simultaneous samples were acquired with an FSN tolerance of 0.01. The maximum error was ≤ ± (0.005 FSN + 3 % of measurement value) (Zhang, 2011).

The AVL fuel meter operated by using a load cell to measure the mass of the tank within the fuel meter over a set period; This measured the reduction in mass and therefore, the fuel consumption. The fuel meter was calibrated periodically by emptying the tank and applying a known mass to the tank that would act upon the load cell. By using the known mass supplied by AVL the sensitivity and linearity deviation of the fuel mass consumed was 0.12% at full-scale (AVL, 1996).

The maximum temperature deviation of the K-type thermocouples used was ±1.5°C. The pressure sensors used gauge and absolute variants of Variohm EPT3100 sensors. These had a non-linearity and accuracy of ≤0.15% and ≤0.5% of their full-scale range,

respectively (Variohm, 2019). The temperature sensors either connected to a NI PCI-6251 or a PicoLog TC08 data logger, these had a 16 and 20-bit resolution, respectively (National-Instruments, 2020, PicoTech, 2020b). The pressures sensors were either connected to the NI PCI-6251 or a PicoLog 1012 data logger. The PicoLog 1012 had a 10-bit resolution (PicoTech, 2020a).

3.10 Engine Results Post Processing

This section discusses the analysis methods used for processing the data retrieved from the various pieces of test equipment.

An in-house MATLAB code was generated by the author to bring together and process the majority of the test data. The initial significant portion of the code automatically generated all of the results of each test while looking for errors and anomalies; the code would then save the results into manageable Microsoft Excel files in individual test folders. To aid with reducing the uncertainty discussed in the previous section, tests were repeated consecutively three times. This repetition allowed the second significant section of the MATLAB code to open the three results folders then and extract the data from the Excel files generated in the first portion of the code. The code would then find the average and standard deviation value of each performance aspect and create separate Excel files with the average and standard deviation values from the three tests.

The MATLAB code was able to interact with the majority of data recorded during testing. However, some files were not necessary or suitable to interact with. The code overlooked screenshots of the ATI Vision interface and an Excel file which was used to make arbitrary notes of IMEP, EGR percentage, lambda, SOI timing, injection pressure (IP) etc. as well as values attained from the smoke and fuel meters. The MATLAB code did

momentarily interact with the DMS files to notify the user of any error messages. However, the Microsoft Excel Add-In created specially by Cambustion was used to process DMS results.

3.10.1 Temperature, Pressure and SC Valve Position Post Processing

As discussed earlier, A NI card and PicoLog system were used for logging data. When the engine was being used as a conventional 4-cylinder engine, only the NI card was used. The NI card communicated through a LabVIEW interface to allow the user to log various temperature and pressure values, along with the data seen from other sensors. When the SC system was used, the PicoLog system was also employed to monitor the temperatures, pressures and valve positions seen from the SC system.

The LabVIEW and PicoLog software were configured to output a text file when recording data. The text files logged readings from the sensors every 100 milliseconds for 3 minutes. The name of the sensors was noted and placed into the MATLAB script. The script would then average the values seen from each sensor over the 3 minutes and associate the values with the noted names.

3.10.2 Gaseous Emissions Post Processing

The gaseous emissions values attained from the Horiba came through a LabVIEW interface that communicated with the MCU of the MEXA. The interface itself allowed the user to interact with the MEXA and control whether it was sampling, purging, calibrating or in a paused state waiting for the next command. The LabVIEW interface also allowed the user to log the sampled values attained. When logging the LabVIEW program would monitor the value given from each analyser over 180 seconds. At the end

of the three minutes, the program would export a text file with the average value of each analysed gaseous emission.

As discussed, the MATLAB code would process these results and create Microsoft Excel files with the average and standard deviation values of each analysed gas. The data from this file was then used along with other engine performance, fuel consumption and fuel property information to convert the exhaust emissions from ppm to g/kWh. The methodology set out by Heywood was used to complete the conversion (Heywood, 1988).

3.10.3 In-Cylinder Pressure Post Processing

As discussed earlier, the in-cylinder pressure data was acquired with two different methods.

When the LabVIEW interface was used, an output text file would contain the raw in-cylinder pressure seen at every CA for 200 consecutive cycles. The MATLAB script processed the .txt file to give values for an average cycle from the 200 recorded, as well as finding the net mean effective pressure (NIMEP) of each sample and the NIMEP coefficient of variation (COV) of the 200 cycles sampled. The in-cylinder data from AVL IndiCom was again attained from 200 cycles. However, this exported two different files. The first exported a text file with the average in-cylinder pressure and injection excitation seen over 200 cycles. The second exported a text file containing the cycle to cycle NIMEP over the 200 cycles. Both methods were capable of providing an average in-cylinder pressure along with cycle to cycle value of NIMEP that could be used to find the average NIMEP and the NIMEP COV.

To attain comparable results, in-cylinder pegging was required. Although there are various methods, the overall purpose of pegging is to normalise the fresh gas pressure by

taking into account the varying manifold pressure generated; this pressure can have a broad range when using a VGT CI engine. When using the LabVIEW interface, the MATLAB code was required to process and peg the in-cylinder pressure once the data had been recorded. The pegging value was found by subtracting the intake manifold pressure from the in-cylinder pressure at BDC. This pegging value could then be added to all raw in-cylinder pressure values recorded (Randolph, 1990). As the AVL IndiCom system is designed explicitly for on-engine diagnostics, it was capable of pegging the data while displaying live data. IndiCom used the accurate and easy to calculate method of thermodynamic pegging. This method calculated the value of thermodynamic compression between two CA's and compared them to the on-engine value attained to find the thermodynamic pegging value. The CA values chosen were 100 and 40°BTDC, which is highlighted to be suitable values for CI engines (Merker et al., 2011).

The NIMEP attained from the in-cylinder pressure can be used in conjunction with other pieces of data to provide performance characteristics that are comparable to other engine configurations. These characteristics include, indicated specific fuel consumption (ISFC), indicated thermal efficiency (ITE) along with the g/kWh of emissions.

The in-cylinder pressure was also used by the MATLAB code to calculate the net heat release using a single-zone calculation. This is an accurate and yet simple formula and is displayed in the below equation (Mauro et al., 2018). A polytopic index value of 1.32 was selected for all calculations and CA's.

$$\frac{dQ_n}{d\theta} = \frac{\gamma}{\gamma - 1}\, p\, \frac{dV}{d\theta} + \frac{1}{\gamma - 1} V\, \frac{dp}{d\theta}$$

Equation 3-2 (Heywood, 1988)

The following equations were used to calculate the BMEP, BSFC, BTE:

$$BMEP\ (bar) = \left(N * T * 2 * \frac{\pi}{D}\right) * 0.0001 \quad \textbf{Equation 3-3}$$

$$BSFC = \frac{Fc}{\omega * T} \quad \textbf{Equation 3-4}$$

$$BTE = \frac{2 * \pi * \omega * T}{Fc * LHV} \quad \textbf{Equation 3-5}$$

N.B. The LHV values of the blend fuels took into account the LHV values of the fuels used and their volumetric ratio.

3.10.4 Particulate Matter Post Processing

The Microsoft Excel add-in used to assess the particulate matter data was Cambustion Utilities v7.46. This add-in was able to read the .dms file created by the DMS logging software. Each .dms file had 90 consecutive seconds of logged data. The raw file displayed the voltage excitation and particle concentration on each ring over each logging time step (2 seconds). The add-in was capable of processing the results taking into account the sample gas flow and other parameters, finding the average value of particle size distribution (PSD) and full spectrum particle concentration. From the average value, it was also possible to find the average number concentration, particle mass, surface area, geometric median diameter and CMD of the nucleation (nuc) and accumulation (acc) mode particles.

Each .dms file underwent this process. The 3 processed DMS results of each test case were further processed to find the average and standard deviation values. Once an overall average and standard deviation was found for each test condition, the values along with the average values and standard deviation of the other test conditions were inserted on the same Excel document to allow for comparison.

3.10.5 Results Comparison

Throughout this investigation, there is comparison on an array of areas including the in-cylinder performance, gaseous and particulate emissions. These comparisons will take various areas into account, including the fuel used and operating conditions. To allow manageable comparison and data analysis, the percentage increase or decrease will be reviewed to allow for unitless evaluation. Equation 3-6 displays the percentage difference formula used in this thesis.

$$Percentage\ Difference = 100 * \left(\frac{Final\ Value - Starting\ Value}{Starting\ Value}\right)$$

Equation 3-6

3.11 Summary

This chapter highlights the experimental facility used for this thesis.

All tests were completed on a direct injection 2.2l 4-cylinder 4-stroke compression ignition engine which was equipped with a VNT and HPEGR. Two distinct engine variations were used to complete the testing discussed in the research chapters. For the first and last research chapters (chapters 4 and 7), the engine operated with the OEM intake pipe, intake manifold and exhaust manifold being used. For the second and third research chapter, a novel test configuration was created by the author. The fourth cylinder was fitted with a separated intake manifold, exhaust manifold, common rail system and HPEGR that allowed the fourth cylinder to operate under different conditions to the other three cylinders.

There was a wide range of equipment used to monitor, alter, log and characterise the performance of the engine at different operating conditions. In summary, a PI Innovo open ECU and injector driver was used to control the majority of the engine performance

with this being controlled through the program ATI Vision. The majority of the temperatures and pressures were monitored through a LabVIEW program connected to a NI card. When the separated cylinder was used, PicoLog data loggers were also included in the test system. A Kistler PiezoStar pressure transducer and Kistler pressure amplifier were used to monitor and log the in-cylinder pressure of the fourth cylinder. For the first research chapter, the pressure sensor was monitored through a LabVIEW program which cross-referenced the crank angle position from an AMI-Elektronic rotary shaft encoder and a camshaft sensor signal. For the subsequent research chapters, AVL IndiModul was used with an AVL 365C crank encoder.

The engine exhaust emissions were monitored with three pieces of equipment. An AVL smoke meter was utilised to monitor the smoke level within the exhaust, a Cambustion DMS500 was used to review the particulate matter, and a Horbia MEXA-7100-DEGR was used to review the exhaust gaseous composition.

All tests were repeated three times, and the author created an in-house MATLAB code to process the majority of the data attained automatically. The code created excel files displaying the average, standard deviation and individual values of all processed information.

CHAPTER 4

4. Statistical Analysis of a 2-Methylfuran and Diesel Blend

This chapter provides an initial study investigating the suitability of using 2-methylfuran as a fuel component within a compression ignition engine.

4.1 Introduction

As discussed in the literature review chapter, MF has very appealing chemical characteristics for its use within an ICE. Compared to the depth of knowledge concerning the use of MF within an SI engine, there is a limited number of publications covering CI applications. As the CI analysis is very restricted, the most suitable start point for an experimental campaign would be, to begin with an initial investigation to ensure that the results attained highlight the necessity for in-depth testing.

This chapter examines the combustion and emissions characteristics of a single MF/diesel blend fuel. The testing used a statistical approach to find the optimum engine settings of a selection of inputs, focussing on a range of predetermined engine outputs. The engine was then run at these settings being fuelled by the MF/diesel blend and neat diesel to understand whether the blend offered any benefits over the use of neat diesel fuel.

4.2 Experimental Procedure

The engine was run in the conventional four cylinder manner, attaining 1.4 bar BMEP at an engine speed of 1800 revolutions per minute (rpm) with a single injection per combustion event. All tests were repeated three times with the results then being averaged. It was decided only to assess one MF/diesel blend with the blend being chosen as MF10. This ratio was chosen as it was the ratio selected by EU incentive 2009/28/EC

to ensure that 10% of commercially available fuel is attained from renewable sources by 2020.

For this investigation, a Taguchi statistical analysis tool was used. The Taguchi method relies on using a developed orthogonal array experimental design of experiment (DOE) to give a reduced test matrix. The results from this reduced matrix can be used to characterise the effect each engine input had on each focussed output. By processing the data attained from the reduced matrix, the user can gain an understanding of the influence each input factor had on the monitored output factors. For this investigation, it was decided to complete testing with three different engine inputs, each operating at three different points. The engine inputs chosen were the SOI timing, IP and EGR ratio. These were chosen as they are critical operating controls for CI engines. The output factors that were focussed on were BTE, NO_x and soot. These were chosen as they are crucial performance factors for diesel-fuelled CI engines and also as it had been found that the introduction of MF played a key role in altering these areas (Xiao et al., 2016). The use of three inputs at three operating points allowed for the use of an L9 orthogonal test array to be used that would capture the influence of each input. The input parameters and orthogonal test array are shown in Table 4-1.

Table 4-1 Design Parameters and Control Factor Values For Testing Carried Out at 1.4 bar BMEP and 1800 RPM

Engine Input	Input Level 1	Input Level 2	Input Level 3
EGR Ratio (%)	32	42	52
Injection Timing (°BTDC)	7.5	10	12.5
Injection Pressure (bar)	350	500	650

4.3 Results and Discussion

4.3.1 Signal to Noise Ratio Analysis

The tests displayed in Table 4-2 were completed, and the analysis was carried out to find the Signal-to-Noise (S/N) ratio. Calculating this ratio can allow for further evaluation comparing how different engine input levels (signals of SOI, IP and EGR), affected the monitored outputs (noise of BTE, NO_x and soot). Before calculating the S/N ratio, it was necessary to bear in mind the ideal response of the output. For BTE a higher value should be targeted, whereas low values of NO_x and soot are preferred. For the S/N ratios to reflect this BTE was calculated using Equation 4-1, whereas NO_x and soot were calculated using Equation 4-2. It is important to note that once the correct S/N ratio equation is used, a higher S/N ratio is preferred as this demonstrates a greater positive influence over the focussed output. The output results and S/N ratios of the L9 test array are shown in Table 4-2.

$$Larger\ the\ better\ S/N\ Ratio\ Input\ values = -10 * \log(\Sigma(1/Y2)/n) \quad \textbf{Equation 4-1}$$

$$Larger\ the\ better\ S/N\ Ratio\ Input\ values = -10 * \log(\Sigma(Y2)/n)) \quad \textbf{Equation 4-2}$$

Table 4-2 Taguchi Analysis Initial Experiment Results and S/N Ratios.

	Experiment Conditions			Results			Calculated S/N Ratios		
Experiment	EGR (%)	SOI Timing (°BTDC)	Injection Pressure (bar)	BTE mean (%)	NO_x mean (g/kWh)	Soot mean (FSN)	BTE S/N ratio	NO_x S/N ratio	Soot S/N ratio
1	32	12.5	350	24.53	6.947319	0.048	27.79	44.89	26.37
2	32	10	500	24.06	5.900043	0.025	27.62	43.88	32.02
3	32	7.5	650	23.14	4.071716	0.0113	27.28	41.09	38.79
4	42	12.5	500	23.91	5.323504	0.029	27.57	43.83	30.54
5	42	10	650	23.55	4.165623	0.021	27.44	41.82	33.16
6	42	7.5	350	22.98	1.897684	0.023	27.22	35.65	32.61
7	52	12.5	650	23.80	3.015482	0.0166	27.53	40.41	35.55
8	52	10	350	24.16	1.810453	0.045	27.66	36.28	26.91
9	52	7.5	500	22.73	1.353738	0.0156	27.13	33.60	36.03

For the next stage of the analysis, it was necessary to review which engine inputs gave the greatest range of S/N ratio and thus, the most significant influence over the monitored outputs. For this to be completed, the results of each output needed to be averaged with other inputs that were at the same operating point. For example, when assessing the BTE, the 32% EGR S/N ratio value was found by averaging the BTE S/N ratio of experiments 1, 2 and 3. For soot analysis, the influence of 650 bar IP required the mean of the soot S/N ratio from experiments 3, 5 and 7. Graphs displaying the results of the input factors in reference to the output factors can be seen in Figure 4-1.

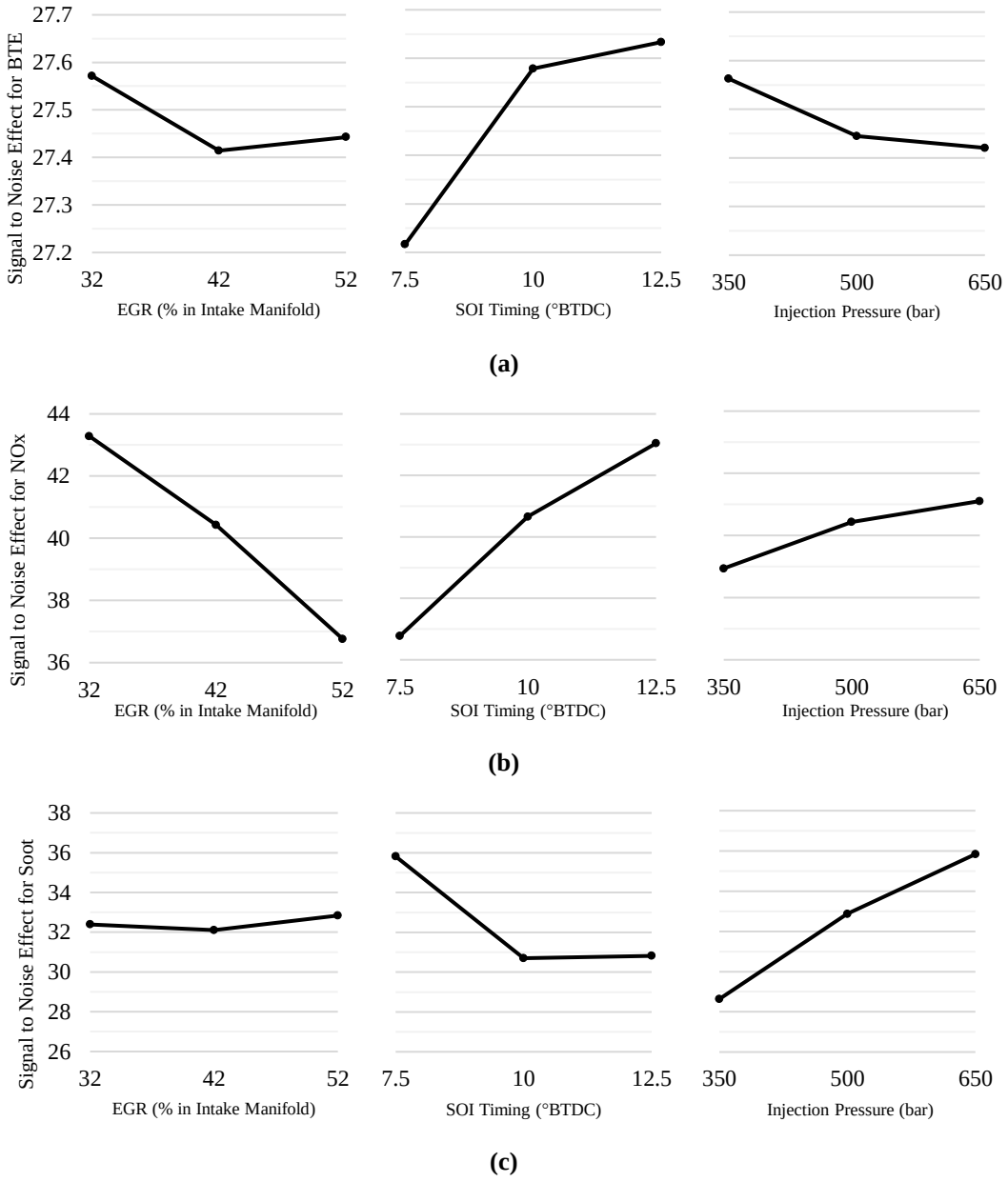

Figure 4-1 **(**a) - Engine Operating Parameter effect on S/N ratio of BTE. (b) - Engine Operating Parameter effect on S/N ratio of NO_x. (c) - Engine Operating Parameter effect on S/N ratio of NO_x. Engine Operating at 1.4 bar BMEP and 1800 rpm.

In Figure 4-1a, it can be seen that the BTE is greatly affected by injection timing with EGR and IP having a similar range of influence. The increased values of EGR and injection pressure encouraged more homogenous combustion reducing the peak HRR values seen and reducing the BTE emitted. Injection timing is known to have a significant impact over BTE as it controls when the combustion event begins and the combustion

phasing. An injection timing event moving closer to TDC from ATDC reduces the combustion duration and increases brake thermal efficiency. The earlier timings used reduced the injection volume required to attain 1.4 bar BMEP, increasing BTE. These findings fall in line with the results that have been found by others (Hountalas et al., 2008, Sluder et al., 2001). The use of a Taguchi DOE allowed for observations and conclusions to be made concerning the influence of the engine inputs as well as the most suitable engine operating conditions that would provide the optimum engine settings for a single output. As BTE is targeted to be as large as possible it can be concluded that the engine conditions that would provide the best value for this would be 32% EGR, SOI at 12.5°BTDC and setting IP to 350 bar.

Figure 4-1b highlights that the injection pressure had the lowest interaction with NO_x generation. As expected, the EGR and SOI had a large amount of influence over the NO_x produced (Pierpont et al., 1995, Suryawanshi and Deshpande, 2005). The SOI reduced the NO_x as the injection event delayed moving closer to TDC from BTDC. This can be credited to the combustion event occurring later in the engine cycle, increasing combustion duration and reducing local combustion temperature. The EGR S/N ratio range highlights the efficiency of using EGR as a NO_x control method. It was found that the most suitable engine inputs for minimum NO_x generation were 52% EGR with SOI set to 7.5°BTDC and an injection pressure of 350 bar. The obtained trends and optimal EGR and injection setting conditions for BTE and NO_x are mostly opposed, which demonstrate the well-known BTE-NO_x trade-off.

Figure 4-1c displays the effect of engine conditions on soot production. The EGR ratio is shown to have a minimal effect on production within the studied range. However, the injection pressure presents the greatest S/N ratio range. The injection timing from 7.5-

10°BTDC has a very steep gradient in comparison to 10-12.5°BTDC. This highlights that there is an exponential growth in soot formation as the combustion event moves closer to TDC, this compliments data seen by other researchers, this can be accredited to fine fuel particles entraining during premixed combustion (Raeie et al., 2014, Zhang and Kook, 2012). The opposite effect of NO_x and soot emissions when the injection timing is modified presents the well established soot-NO_x trade-off. The most suitable engine conditions for minimum soot would be 52% EGR, injection timing set to 7.5°BTDC and an injection pressure of 650 bar.

4.3.2 Confirmation Experiment

The Taguchi analysis allowed for conclusions to be made regarding the optimum condition for a single output, further analysis would be required for conclusions to be made that would take all of the engine outputs into account. Before this, a confirmation experiment needed to be undertaken to examine if the S/N ratio analysis and proposed engine conditions found in the previous section were correct. The NO_x generated was focussed on for this confirmation assessment as it is key parameter when discussing the use of CI engines, as discussed, these optimal engine settings found for minimum NO_x were 52% EGR, SOI at 7.5°BTDC and 350 bar IP. The engine was run with the conditions found in the S/N ratio analysis, and the results of brake specific NO_x ($BSNO_x$) production are compared in Table 4-3. The results found from the confirmation experiment highlighted the success of the S/N ratio analysis, with the proposed operating condition from the S/N ratio analysis attaining a 14.3% reduction of $BSNO_x$ when compared to the lowest $BSNO_x$ value attained in the initial nine tests. This showed that the initial nine experiments were capable of correctly characterising the engine responses and the S/N ratio analysis could find suitable engine operating conditions for the engine output.

Table 4-3 $BSNO_x$ g/kWh Production of Each Test. Engine Operating at 1.4 bar BMEP and 1800 rpm.

$BSNO_X$ (g/kWh)									
Test 1	**Test 2**	**Test 3**	**Test 4**	**Test 5**	**Test 6**	**Test 7**	**Test 8**	**Test 9**	**NO_X Optimal**
4.238	3.452	2.447	3.030	2.398	1.119	1.752	1.100	0.780	0.683

4.3.3 Analysis of Variance

Further detailed evaluation was required to take all three of the outputs into account to find an optimum overall engine operating condition. To find the optimum condition, it was decided to use an Analysis of Variance (ANOVA) investigation. This investigation could be used to find the quantitative importance of each input factor for each output factor independently, e.g. the importance of SOI, IP and EGR when considering BTE. By attaining quantitative values, it would then be possible to find the optimum overall engine setting that took into account all of the outputs at the same time. For this analysis, the weight of each output was considered equal when finding the optimal engine settings, although weighting factors could be introduced to focus on key outputs.

The ANOVA study was completed by using the average S/N ratio values for each level calculated in section 4.3.1 and displayed in Figure 4-1.

The influence of each input was then calculated for each of the outputs using the following method:

1. Table 4-4 displays the averaged S/N ratios when focussing on NO_x formation; these values were then multiplied by the number of levels in Table 4-4, these multiplied values are shown in Table 4-5. These tables are shown to demonstrate

the ANOVA calculation process of a set output. This process was repeated twice to find the influence of each input factor in regard to BTE and soot.

2. The influence of an input factor was found by subtracting the levels S/N ratio from each other and multiplying the value attained by the power of the number of levels minus 1. This formula is shown in Equation 4-3, and the total of EGR, SOI and IP in regards to NO_x are shown in Table 4-5.

$$((L1 - L2)^2) + ((L1 - L3)^2) + ((L2 - L3)^2)$$

Equation 4-3

3. The total of an output (e.g. EGR) could then be compared to the sum total of all of the outputs to find the influence ratio of the focussed output. This was completed for all inputs and is shown at the bottom of Table 4-5 for the NO_x ANOVA analysis.

Table 4-4 Control Factor NO_x S/N Ratios.

		NOx S/N Ratio		
		EGR	**SOI**	**IP**
Level	**1**	-43.299751	-43.04747	-38.946994
	2	-40.4373678	-40.66658	-40.441499
	3	-36.7718399	-36.78613	-41.11169

Table 4-5 NOx ANOVA Study.

		Influence of Factor		
		EGR	**SOI**	**IP**
Level	**1**	-123.873	-129.142	-116.841
	2	-121.312	-122	-121.3245
	3	-110.316	-110.358	-123.3351
Total of Each Control Factor		576.7046	539.3779	66.317512
Total of All Factors		1182.4		
Influence of Each Factor		48.77	45.62	5.61

The methodology described was completed for each output factor. These weighting factors, along with the optimal setting for a single output, were then tabulated to allow for manual cross-referencing to find the optimal engine setting to satisfy all outputs simultaneously, this is displayed in Table 4-6.

By reviewing Table 4-6, it can be seen that NO_x production was primarily controlled by the amount of EGR used, with a 49% influence. However, variation in EGR ratio had little influence over BTE and soot with EGR having an influence of 11% and 0.6%, respectively. It was decided to use the NO_x EGR value for the optimum overall setting. Regarding the injection timing, it was noted that BTE was very dependent on fuel injection timing with an 80% variation and an ideal setting of 12.5°BTDC. However, NO_x and smoke both had around a 40% dependence on SOI timing with an ideal setting of 7.5°BTDC. This meant that there was a similar dependence of 12.5 and 7.5°BTDC SOI. To ensure that the BTE, NO_x and smoke had been taken into account, it was decided that the best SOI timing value would be 10°BTDC. The injection pressure used for the optimum setting was 650 bar as smoke was seen to be 60% dependant on the pressure of

the injected fuel. NO_x and BTE each had a less than 10% dependence, so their optimum IP setting was not considered.

The initial S/N ratio analysis found the most suitable settings for the three individual engine outputs; the ANOVA analysis allowed for the importance of each input on each output to be found. By joining these two types of data analysis together, it was possible to conclude that the most suitable operating condition that would satisfy all output conditions simultaneously at the same time was 52% EGR, an SOI of 10°BTDC and IP of 650 bar.

Table 4-6 Optimal Engine settings for Performance Criteria's and the Influence of each Setting.

	Optimum EGR Setting (%)	**Optimum SOI Setting (°BTDC)**	**Optimum IP Setting (bar)**		**EGR Influence on Factor (%)**	**SOI Influence on Factor (%)**	**IP Influence on Factor (%)**
Max BTE	32	12.5	350		10.91	80.07	9.01
Min NO_X	52	7.5	350		48.77	45.61	5.6
Min Smoke	52	7.5	650		0.62	39.14	60.22
Optimum Setting Satisfying All Outputs	52	10	650		-	-	-

4.3.4 Optimum Confirmation Experiment

Engine testing was completed at the optimum engine operating point found by the ANOVA analysis. The data displayed in Figure 4-2 shows that the initial nine tests were capable of providing suitable results for one or two of the outputs at each test point but not all of them. Test number 9 provided the most suitable values out of the initial test matrix. It can be seen that test 9 was able to provide lower $BSNO_x$ and smoke than the

optimum response, however, the BTE can be seen to be very low. The optimum setting was found to have a slight increase in NO_x and soot when compared to test 9, but this is disproportionate to the increase in BTE attained. This highlights that the statistical analysis was successful at finding the optimum engine settings that took into account all of the outputs.

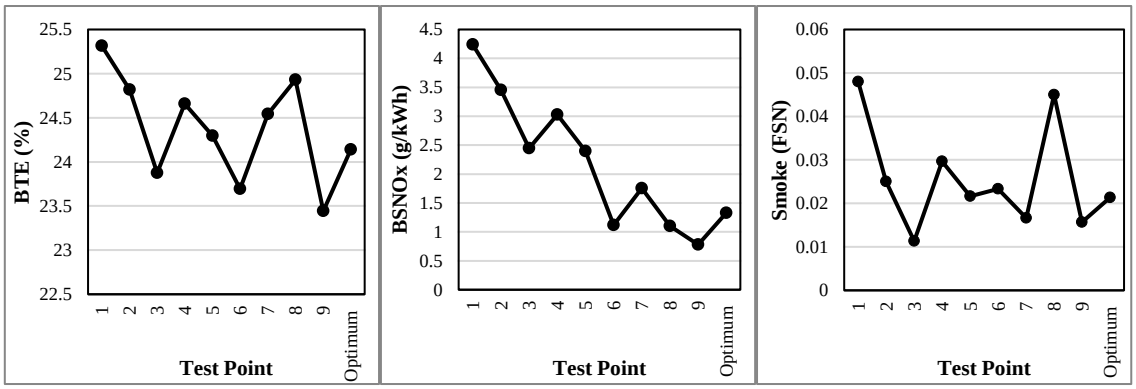

Figure 4-2 Engine Outputs Comparing Initial Tests and Optimum Engine Set Point. Engine Operating at 1.4 bar BMEP and 1800 rpm.

4.3.5 Optimum Comparison to Neat Diesel

The objective of this initial investigation was to understand whether using a 2-methylfuran/diesel blend within a CI engine could provide any benefit over using neat diesel. Statistical analysis was used to characterise the engine operating performance efficiently. Once the optimum operating point (defined by the fixed load and engine speed of 1.4 bar BMEP and 1800 rpm along with the optimal EGR, IP and SOI found in the analysis) for using an MF/diesel blend was found, it was then required to run the engine with neat diesel at the same engine operating condition. There was a limited amount of MF used in the blend ratios, and broad steps were used in the Taguchi test plan input factor values. Taking these factors into account, it is suitable to assume that if the statistical DOE were to be repeated with neat diesel, then the optimum engine operating conditions would be the same as the MF10 conditions.

4.3.5.1 In-Cylinder Combustion Characteristics

The in-cylinder pressure and HRR generated by the two different fuels at the optimum operating point is displayed in Figure 4-3. Table 4-7 displays data comparing critical combustion areas. The CA for 10%, 50% and 90% cumulative HRR are the same for MF10 and diesel. However, Figure 4-3 highlights that MF10 has a slight ignition delay which was not captured by the 1 CA resolution of the crank encoder used for the first investigation. The delay is visible to see within the premixed combustion phase and highlights the ignition delay that was brought about by the decreased cetane number of MF. The cetane number and slight shift in combustion phasing meant that the maximum in-cylinder pressure of MF10 was reduced, reducing the temperature of the combustion. This is a positive effect as it would aid in reducing the knocking phenomena within the engine and also allow for a higher compression ratio to be used, which would allow for a higher BTE to be attained. However, this shift in combustion phasing did reduce the combustion efficiency of MF10. The significant difference seen in Table 4-7 is the increased fuel consumption, this can be attributed to the reduced combustion pressure, along with the reduced lower heating value of MF which would require more fuel to be injected to attain the same BMEP.

There are some minor differences seen with the HRR in Figure 4-3, with a slight reduction in diffusion combustion and a slight increase in premixed combustion. It is anticipated that as the MF fraction of tested fuels increases, the mixing-controlled combustion will increase because of the decreased cetane number, latent heat of vaporisation and high auto-ignition temperature reducing the MF's tendency to ignite.

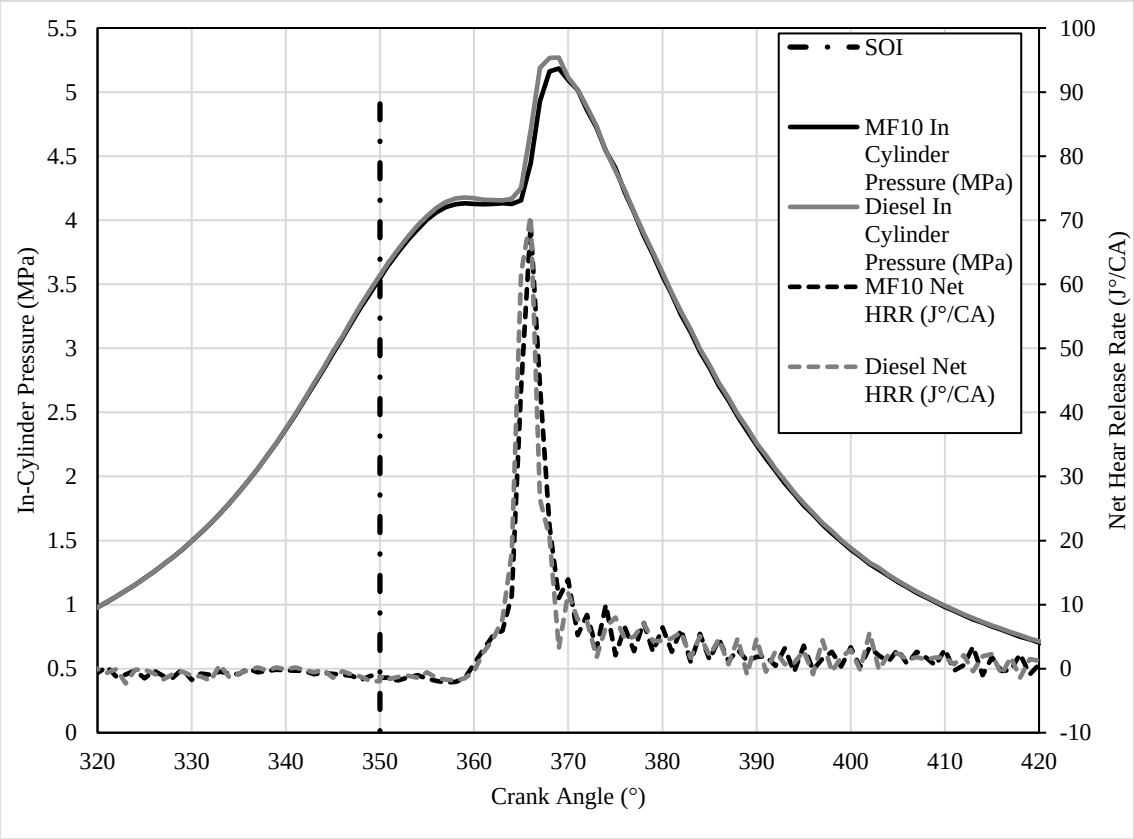

Figure 4-3 MF10 and Diesel In-Cylinder Pressure and HRR Comparison. Engine Operating at 1.4 bar BMEP, 1800 rpm, 52% EGR, SOI 10°BTDC, IP 650 bar.

Table 4-7 Combustion Analysis of MF10 and Diesel. Engine Operating at 1.4 bar BMEP, 1800 rpm, 52% EGR, SOI 10°BTDC, IP 650 bar.

Fuel	BTE (%)	HRR10 (°)	HRR50 (°)	HRR90 (°)	Combustion Duration (°)	Combustion Efficiency (%)	BSFC (g/kWh)
MF10	24.42	364	366	377	20	96.17	356.31
Diesel	24.85	364	366	377	20	97.29	340.85
Diesel Percentage Increase	1.76	0	0	0	0	1.15	-4.53

4.3.5.2 Emissions Characteristics

4.3.5.2.1 Particulate Emissions

Figure 4-4, Figure 4-5 and Figure 4-6 display the PSD, mode concentration and mode mass of MF10 and neat diesel, respectively. From Figure 4-4, it can be seen that there was a significant difference in the number of particles created between the two fuels. MF10 was seen to reduce particles in both the nucleation and accumulation mode. The oxygen content of 2-methylfuran is mainly responsible for the significant reduction of particle emissions; this can be ascribed to the oxidation of particles and particle precursors. The oxygen content of MF limits particle production during diffusion combustion (Xiao et al., 2016), this is a significant contributor in reducing particle number. The reduction in particle density is displayed in Figure 4-5, which highlights a substantial drop in the number concentration of particles in both modes. When comparing MF10 particle generation to that of neat diesel, it was calculated that there was a total concentration reduction of 35.45%, which consisted of a 30.15% reduction in the nucleation mode and a 56.6% reduction in accumulation mode. This overall reduction was accompanied by a similar reduction in particle mass, displayed in Figure 4-6.

Table 4-8 displays some of the critical performance values of the particle emissions, this demonstrates the overall trend of reduced particulates from the use of MF10, including the reduction in CMD with nucleation size reducing by 14.58% and accumulation size reducing by 6.33%. It should be noted that the reduction in the average particle size is not the result of a higher number of particle emissions of smaller size but a reduced number of particles being generated which in turn reduces the number of particle interactions which results in reduced particle size.

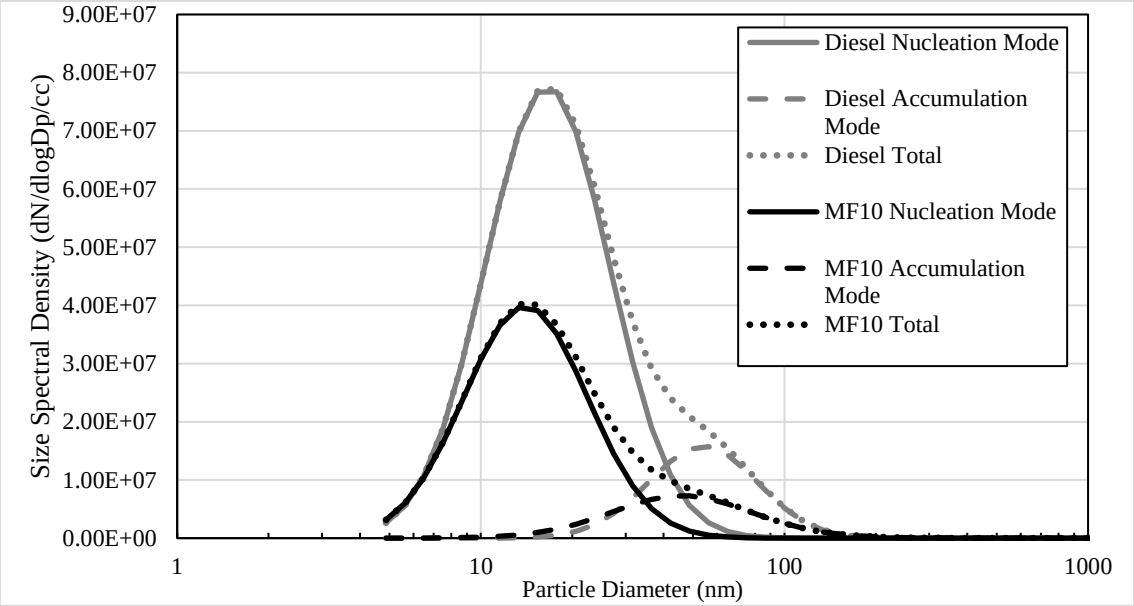

Figure 4-4 Optimum Engine Condition Emissions Particle Size Spectral Density. Engine Operating at 1.4 bar BMEP, 1800 rpm, 52% EGR, SOI 10°BTDC, IP 650 bar.

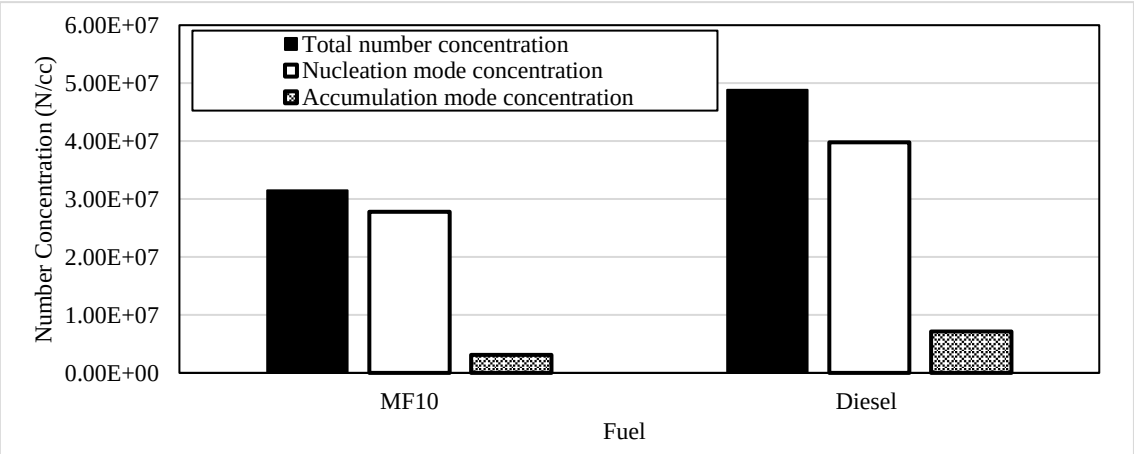

Figure 4-5 Optimum Engine Condition Emissions Number Concentration Comparison. Engine Operating at 1.4 bar BMEP, 1800 rpm, 52% EGR, SOI 10°BTDC, IP 650 bar.

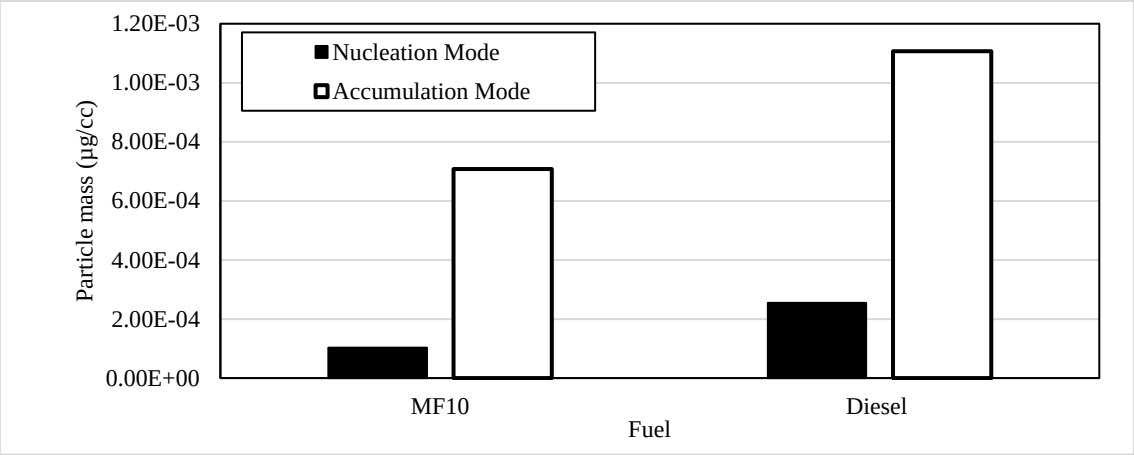

Figure 4-6 Optimum Engine Condition Emissions Particle Mass. Engine Operating at 1.4 bar BMEP, 1800 rpm, 52% EGR, SOI 10°BTDC, IP 650 bar.

Table 4-8 Comparison of Particulates Between MF10 and Diesel. Engine Operating at 1.4 bar BMEP, 1800 rpm, 52% EGR, SOI 10°BTDC, IP 650 bar.

	Total n/cc	Geometric Mean Diameter (nm)	Nucleation Mode Count Median Diameter (nm)	Nucleation Mode Concentration (n/cc)	Nucleation Mode Geometric Standard Deviation	Nucleation mode mass (µg/cc)	Accumulation Mode Count Median Diameter (nm)	Accumulation Mode Concentration (n/cc)	Accumulation Mode Geometric Standard Deviation	Accumulation mode mass (µg/cc)
MF10	3.15E+07	16.7	14.2	2.78E+07	1.57	1.03E-04	50.3	3.10E+06	1.75	7.08E-04
Diesel	4.88E+07	18.8	16.6	3.98E+07	1.60	2.55E-04	53.7	7.15E+06	1.51	1.11E-03
MF10 Percentage Decrease Over Diesel	35.45	11.17	14.58	30.15	1.88	59.60	6.33	56.64	-15.6	36.22

4.3.5.2.2 Gaseous Emissions

From the gaseous emissions displayed in Table 4-9, it can be seen that the reduced in-cylinder pressure (and thus in-cylinder temperature) generated by the ignition delay of MF10 resulted in a 17% reduction of $BSNO_x$ emissions compared to diesel. As discussed

in the combustion comparison, the ignition delay did also decrease combustion efficiency; this resulted in MF10 attaining increases of brake specific CO (BSCO) and brake specific UHC (BSUHC) when compared to diesel. It is thought that at higher loads, and higher intake air and combustion temperatures, the combustion efficiency of MF/diesel blended fuels will be closer or equivalent to that of neat diesel. This would allow for a higher amount of oxidation to occur, and the negative offset of BSUHC and BSCO generation would reduce.

Table 4-9 Comparison of Gaseous Emission and Smoke Number. Engine Operating at 1.4 bar BMEP, 1800 rpm, 52% EGR, SOI 10°BTDC, IP 650 bar.

	Smoke (FSN)	**BSNO$_x$ (g/kWh)**	**BSUHC (g/kWh)**	**BSCO (g/kWh)**	**CO_2 (g/kWh)**
MF10	0.0021	1.331898	3.89005	17.04661	611.9753
Diesel	0.047	1.609403	2.912047	11.53189	592.5203
Diesel Percentage Increase over MF10 (%)	95.53	17.24	-33.58	-47.82	-3.28

4.4 Conclusion

The purpose of this chapter was to assess the suitability of using the biofuel 2-methylfuran within a CI engine to conclude whether further investigations were appropriate. Research into the use of biofuels is required to reduce the automotive industries dependence on FF and the resulting greenhouse gases emitted from burning FF's. This initial investigation was successful at using statistical analysis with the fuel MF10 at a fixed BMEP of 1.4 bar and 1800 rpm. The analysis characterised a set of inputs (EGR, IP, SOI) to find their relationship to several predetermined outputs (BTE, NO_x, smoke), intending to find the optimum inputs to provide the best possible values of the outputs simultaneously. There

were two sets of statistical analysis completed; the first was an S/N ratio analysis to understand what the ideal engine inputs were to satisfy each of the engine outputs individually. Secondly, an ANOVA analysis was used to find which inputs had the most influence on the focussed outputs. It was then possible to understand quantitatively which input factors were the most important and as the ideal engine inputs for each individual output had already been found it was then possible to conclude which engine inputs conditions would be the most suitable to take all of the outputs into account. To ensure the analysis was effective, two confirmation tests were undertaken. The first focussed on the S/N ratio analysis, which correctly predicted the engine conditions required to provide reduced $BSNO_x$. The second focused on the ANOVA analysis, which provided conditions for an overall optimum, taking all focussed outputs into account. The results found that both forms of investigation had been successful in characterising engine performance when fuelled with MF10, and they had both been able to provide improved engine conditions depending on the focussed outputs.

Tests were run with the overall optimum engine operating inputs, with the engine being fuelled with MF10 and neat diesel to allow for comparison. This engine condition was 1800 rpm, 1.4 bar BMEP, 52% EGR, 650 bar IP and an SOI of 10°BTDC. By comparing the results, it was found that:

1. The low ignitability of MF10 created a higher ignition delay which at the low load engine operating condition reduced the maximum combustion pressure (by 0.85 bar), and then in-cylinder combustion temperature, which reduced the $BSNO_x$ by 17.24%
2. The ignition delay and cetane number reduced combustion efficiency by 1.15%

3. The reduced efficiency and the lower heating value of MF increased the BSFC by 4.53%. The lower combustion efficiency and increased ignition delay of MF10 increased the BSCO by 33.58% and BSUHC by 47.82% at this specific low load engine operation condition
4. A significant overall difference between the two fuels was seen from the particulate emissions. Overall, the total number concentration reduced by 35.45%. The particle number concentration of the two modes was seen to reduce with nucleation falling by 30.15% and accumulation reducing by 59.6%

The outcomes from this initial investigation highlight that the use of an MF and diesel blend within a CI engine is a viable option. Overall, some positives can be attained by using MF within a CI engine. However, further investigation is required to assess the use of higher MF blend ratios, higher operating loads, as well as different control methods to try and reduce the negative aspects discussed in this chapter.

CHAPTER 5

5. Gaseous Emission Behaviour of 2-Methylfuran and Diesel Blends

This chapter studies in detail the gaseous emissions emitted from a selection of 2-methylfuran and diesel blends. To understand the performance of the fuels under different conditions, testing sweeps were completed where the engine performance was fixed while a set engine parameter was swept through a range of values, e.g. EGR from 0-30%; an in-depth test matrix is shown in the appendix. For these tests, IMEP was focussed on over BMEP as the single-cylinder experimental setup was used. Testing in reference to IMEP was more suitable as it took into account the SC in-cylinder pressure as a performance parameter instead of the overall engine torque. The was preferred as the in-cylinder performance of the three cylinders and the SC may not have been identical.

5.1 Introduction

A selection of experiments were undertaken to investigate the effect of altering a single engine variable with a range of MF/diesel blend fuels. The parameters chosen were IP, AHR50 (as a result of modifying the SOI) as well as EGR; in this case, the study was extended to assess the effect of CEGR and HEGR. The parameters SOI, IP and EGR were chosen as they were all found to be critical areas in the gaseous and PM performance analysis in the previous chapter. HEGR was also included in this testing sweep as it has been found that HEGR may improve the combustion stability of low cetane fuels in a CI engine (Zeraati-Rezaei et al., 2017).

It was decided to fix the AHR50 (consequence or output parameter) for these tests rather than the SOI (input parameter) as it had already been found that the cetane number, auto-

ignition temperature and latent heat of vapourisation temperature of MF would play a key role in altering the ignition delay of MF/diesel blends. This would significantly alter the combustion characteristics giving results that would not be suitable to compare.

5.2 Experimental Procedure

These experiments were completed with the separated cylinder system discussed in the experimental setup chapter. This was done to allow the author more flexibility when setting the test conditions while reducing fuel consumption by only supplying one cylinder with the blend fuel, while the other three cylinders were fuelled with neat diesel.

The fuel blends chosen were MF5, MF15 and MF25. Initial screening tests were completed with these blends and MF35; this found that MF25 was the suitable upper blend ratio limit at 1800 rpm and 5 bar IMEP as combustion stability became a significant problem past this blend ratio at this load and engine speed. The blends were mixed with 300ppm of lubricity improver added to the MF, then diesel was added to attain the required MF/diesel blend ratio. The results of these tests were compared to neat diesel to give a baseline result with real-world applicability. It should be noted that for the HEGR tests, MF5 was not investigated as preliminary tests found that the low MF blend would provide no significant difference in results from the neat diesel testing.

Each parameter experiment was completed over two consecutive days with an engine speed of 1800 rpm and a load of 5 bar IMEP attained with a single injection event and the experimental procedure discussed in section 3.8.

Before tests were completed, the engine was run until the oil and coolant temperature had stabilised. The initial tests were completed with neat diesel in all cylinders to attain the engine operating values. To ensure the engine remained balanced, the three diesel-fuelled

cylinders were operated at these values; the separated cylinder used these values and the override values of SOI and injection volume to attain the same test condition. An overview of the test matrix used in this section is displayed in Table 5-1.

Table 5-1 Fixed Parameter Test Plan Overview

Parameter	Minimum Value	Maximum Value	Increments	Fuels Tested
AHR50 CA	0°	12°	3°	D, MF5, MF15, MF25
Injection Pressure	500 bar	1100 bar	150 bar	D, MF5, MF15, MF25
Cold EGR	0%	30%	7.5%	D, MF5, MF15, MF25
Hot EGR	0%	30%	7.5%	D, MF15, MF25

In-depth test plans can be found in the appendix.

5.3 Results

5.3.1 Oxides of Nitrogen

NO_x has been noted to cause severe issues to human health both directly and indirectly. Excessive exposure to the group of gases is known to cause respiratory problems along with contaminating water (EPA., 2016). The formation of NO_x is a key area to assess when discussing gaseous emissions. It is seen as one of the main negatives regarding the use of diesel within a CI engine. As discussed previously, NO_x formation occurs when high in-cylinder temperatures are attained that are capable of breaking the triple bond of nitrogen.

The AHR50 tests showed that the use of MF/diesel blends within a CI engine increased the level of indicated specific NO_x ($ISNO_x$) seen in the exhaust gas for the medium load engine operation condition used during testing. This outcome was opposite to the low load condition in the previous chapter. The $BSNO_x$ was reduced with the addition of MF in the previous chapter as the SOI was maintained at a fixed value. The low cetane

number, higher latent heat of vaporisation and higher auto-ignition temperature of MF increased the ignition delay (defined as the CAD from SOI to AHR10 CA). In the previous chapter, this delay resulted in the combustion occurring in a greater cylinder volume during the cycle, reducing combustion pressure/temperature (Xiao et al., 2016).

The overall trend of each AHR50 combustion phasing test point displayed that the $ISNO_x$ value increased as the MF blend ratio increased. The higher MF blends promoted increased premixed combustion (with cetane number being a controlling factor (Ickes, 2009)) and the higher in-cylinder oxygen availability, partially controlled by fuel oxygen content, promoted the rapid oxidation of the fuel and then a high-pressure rate that resulted in higher local temperature and $ISNO_x$ emission formation. The data displayed in Table 5-2 highlights that on average, MF25 generated 68% more $ISNO_x$ in comparison to diesel. It was noted that as the MF blend fraction increased, the combustion duration decreased, resulting in a more significant proportion of the fuel burnt in premixed combustion compared to diesel fuel. The reduction of combustion duration and increase in premixed combustion at this load can be seen to increase the maximum pressure seen during combustion which would then, in turn, increase the temperature, giving a larger window of opportunity for more NO_x to be produced during combustion. The diffusion combustion phase is typically oxygen-limited, so the use of an oxygenated fuel will provide more oxygen and decrease the amount of oxygen starvation seen during diffusion combustion promoting fuel oxidation and increasing in-cylinder pressure and temperature.

Table 5-2 ISNOx Formation in Relation to Combustion Pressure and Duration. Engine Operating at 5 bar IMEP, 1800 rpm, 10% EGR, AHR50 8.

	Diesel Average	MF5 Average	MF15 Average	MF25 Average
$ISNO_x$ (g/kWh)	0.57	0.72	0.68	0.96
Maximum In-Cylinder Pressure (MPa)	6.15	6.17	6.24	6.25
Combustion Duration (°)	19.53	19.53	18.33	17.33
Ignition Delay (°)	16.06	16.21	17.84	20.23

The results of the $ISNO_x$ emitted from the injection pressure testing are shown in Figure 5-1. MF5 and MF15 follow a similar trend to the AHR50 where the $ISNO_x$ is shown to be most dependant on increasing the content of MF. However, when MF25 was tested, it was found that the injection pressure had a significant influence over the NO_x formation, providing a general trend of reducing $ISNO_x$ as injection pressure increased. Typically, when using neat diesel, $ISNO_x$ increases when a higher IP is used as more fuel is burnt during the premixed combustion phase. This can be attributed to an increased spray penetration length and improved mixture homogeneity (Yoon et al., 2019). However, with the MF blends homogeneity is not as great an issue as MF combustion self-supplies oxygen and is not as dependant on the oxygen within the cylinder, the low cetane number results in an increased ignition delay which can improve mixture homogeneity and mixing controlled combustion. Hildingsson found that combustion efficiency can reduce when using low cetane number fuels at high injection pressures in CI engines (Hildingsson et al., 2009). The higher injection pressure can be accredited to air/fuel over-mixing within the cylinder, that would result in wall impingement from the fuel. By comparing the combustion efficiency in Figure 5-2, this statement can be seen to be true for the MF/diesel blends tested. The boiling point of MF is 64.7°C which is considerably lower than that of diesel. The results seen from 500 bar injection pressure with MF15 and MF25 are very similar. This highlights that at this low injection pressure, the boiling point does

not yet play a key role in reducing NO_x. However, when the injection pressure of MF25 is increased, NO_x and combustion efficiency reduces. This can be attributed to the smaller fuel droplet size attained from higher injection pressures and the increased ignition delay of higher MF blends. These two factors provide smaller fuel droplets and a longer residence time within the cylinder before combustion: this allows the MF/diesel mixture to evaporate and mix at a higher rate, providing a more homogenous air/fuel mixture. This effect of homogeneity attained by MF25 at 1100 bar IP provides the lowest $ISNO_x$ seen throughout the IP parameter sweep. This demonstrates that the injection pressure is a critical factor in reducing $ISNO_x$ with high MF blends. The uniform mixture attained outweighs the negative aspects seen to increase NO_x, being consistent with the decrease in combustion efficiency (see Figure 5-2).

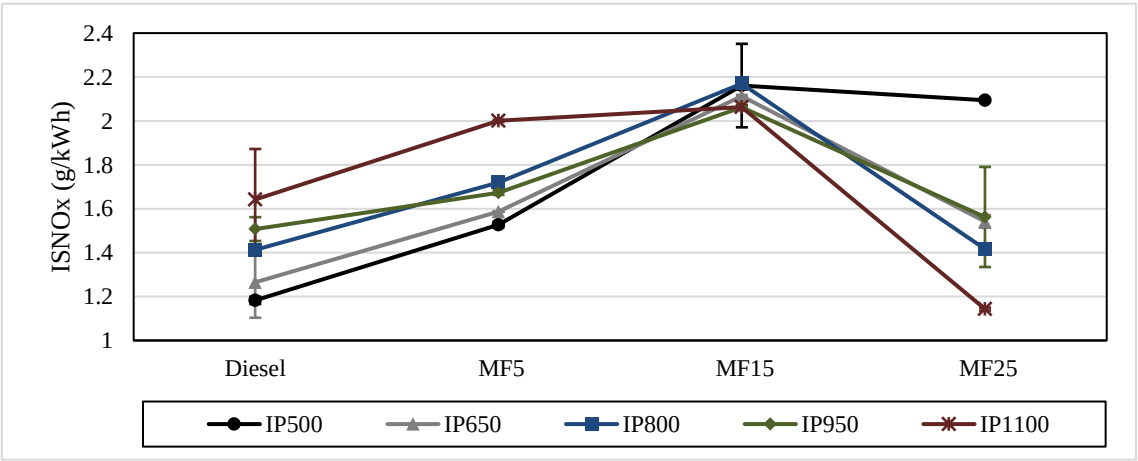

Figure 5-1 $ISNO_x$ formation from Injection Pressure Testing. Engine Operating at 5 bar IMEP, 1800 rpm, 10% EGR, AHR50 8.

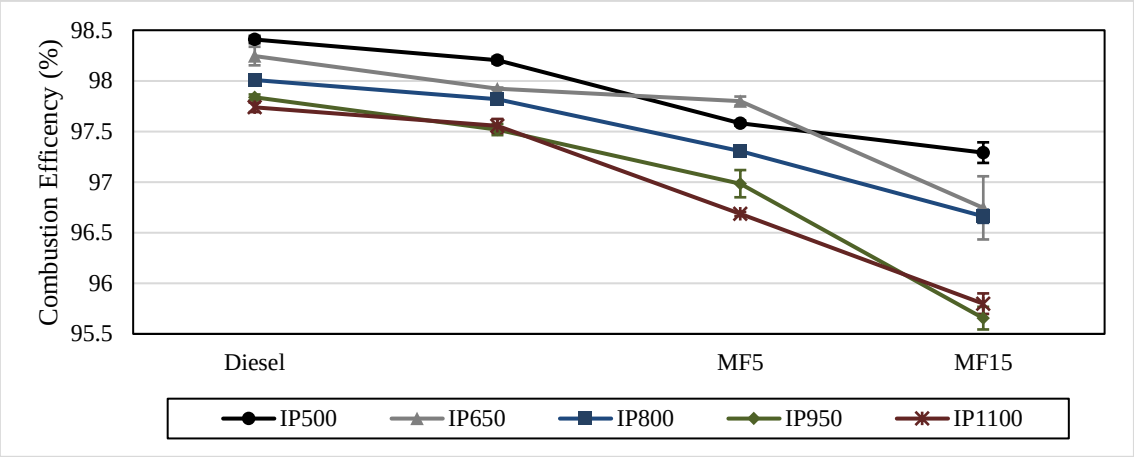

Figure 5-2 Combustion Efficiency of Each Fuel from Injection Pressure Testing. Engine Operating at 5 bar IMEP, 1800 rpm, 10% EGR, AHR50 8.

The use of exhaust gas recirculation is a well-known NO_x control method. Tests were completed monitoring the impact of the amount of exhaust gas introduced into the intake manifold, with studies undertaken using both hot and cold EGR. The results displayed in Figure 5-3 and Figure 5-4 show that the use of EGR with MF blends was a successful technique in reducing the amount of NO_x produced. NO_x reduction saturated past 22.5% EGR with very little difference in $ISNO_x$ production when compared to 30% EGR in both hot and cold form. The values of $ISNO_x$ seen with low amounts of EGR were similar between the hot and cold EGR tests. However, with the hot EGR, the NO_x levels were seen to be marginally higher for each EGR ratio from 15% onwards. Figure 5-5 highlights that with the lower EGR ratios the hot EGR had little effect on the intake manifold temperature but as the ratio increased the manifold temperature increased dramatically which reduced the ignition delay and mixture preparation time, increasing NO_x formation.

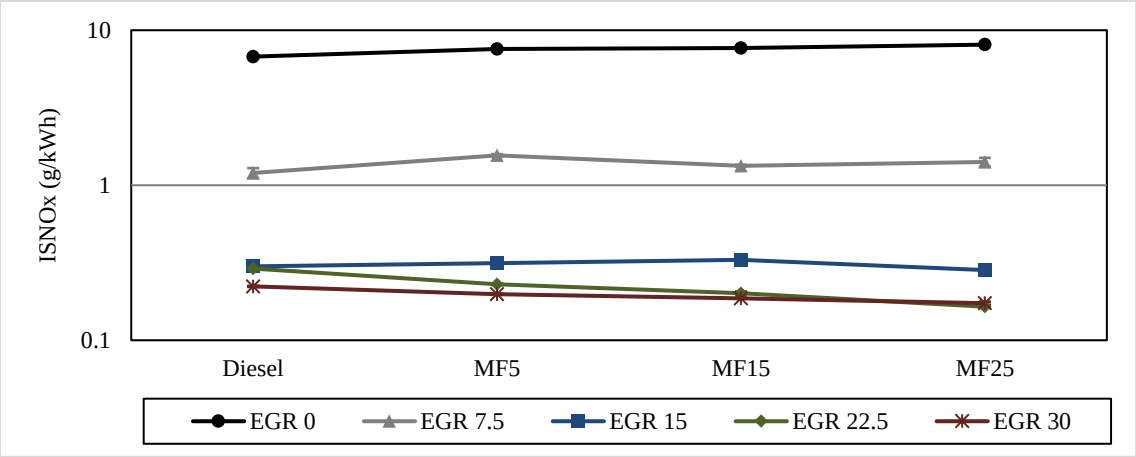

Figure 5-3 Cold EGR Testing $ISNO_x$ Levels. Engine Operating at 5 bar IMEP, 1800 rpm, IP 650 bar, AHR50 8.

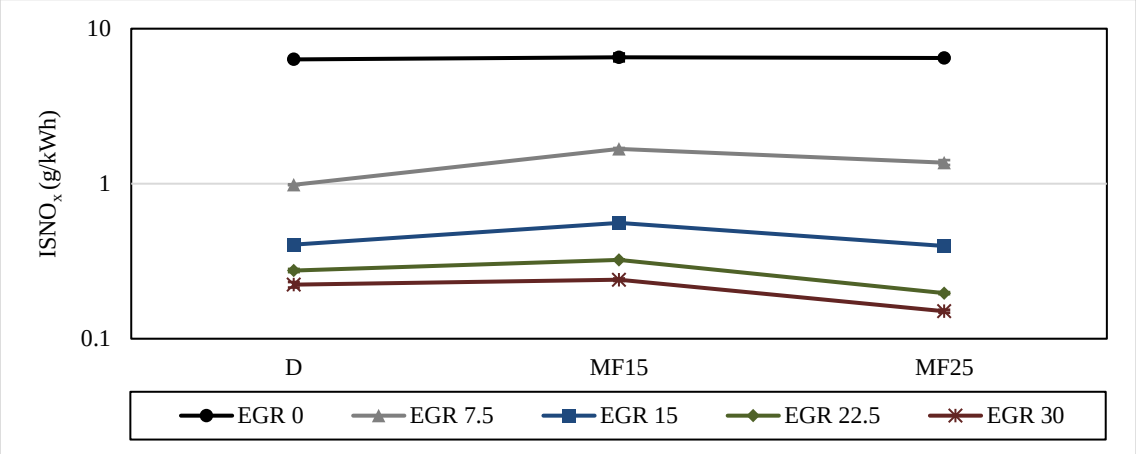

Figure 5-4 Hot EGR Testing $ISNO_x$ Levels. Engine Operating at 5 bar IMEP, 1800 rpm, IP 650 bar, AHR50 8.

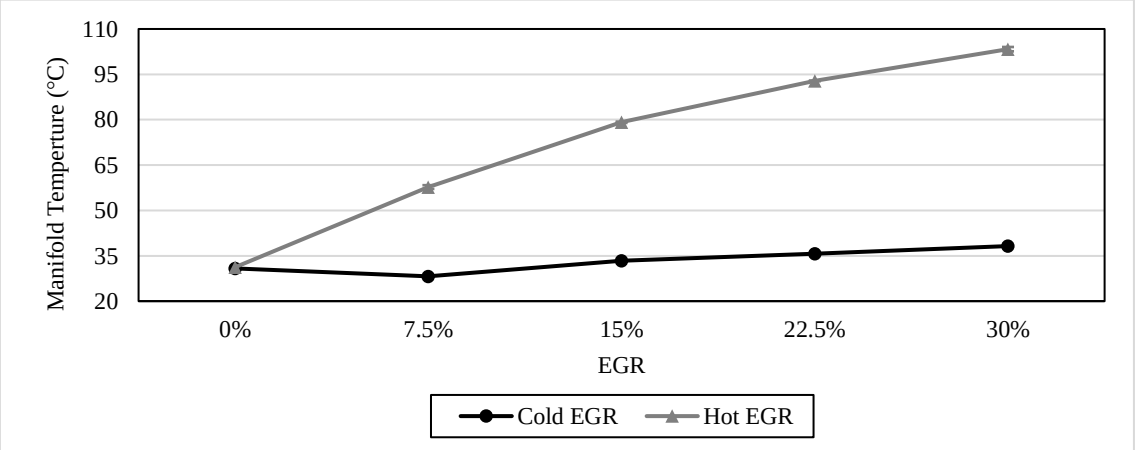

Figure 5-5 Manifold Temperature with increasing Hot and Cold EGR. Engine Operating at 5 bar IMEP, 1800 rpm, IP 650 bar, AHR50 8.

5.3.2 Unburnt Hydrocarbons

It is required to attain an understanding regarding the use of MF/diesel blends and the production of UHC's. This knowledge is necessary as UHC's are a regulated emission, and excess exposure to these hydrocarbons can create health problems. The results from the AHR50 testing found a gradual increase of indicated specific UHC (ISUHC) as the MF fraction increased. The average value of each fuel is displayed in Figure 5-6 and highlights a 48% increase of ISUHC when the MF25 average and diesel average are compared. This trend is very similar to that of the injection pressure testing with ISUHC showing no significant dependence on injection pressure. Similar to the $ISNO_x$, ISUHC formation was found to be more dependant over the fraction of MF used rather than the engine test sweeps.

Unburnt hydrocarbons are seen in the exhaust when particles of fuel undergo no or partial combustion. When the MF fraction of the blends increase, the low cetane number of MF makes the combustion process more and more sensitive to being prematurely extinguished at the cool perimeter of the cylinder. This would generate a higher number of unburnt hydrocarbons in the exhaust system. The higher latent heat of vaporisation of MF compared to diesel could reduce local in-cylinder temperature and then also impede hydrocarbon oxidation.

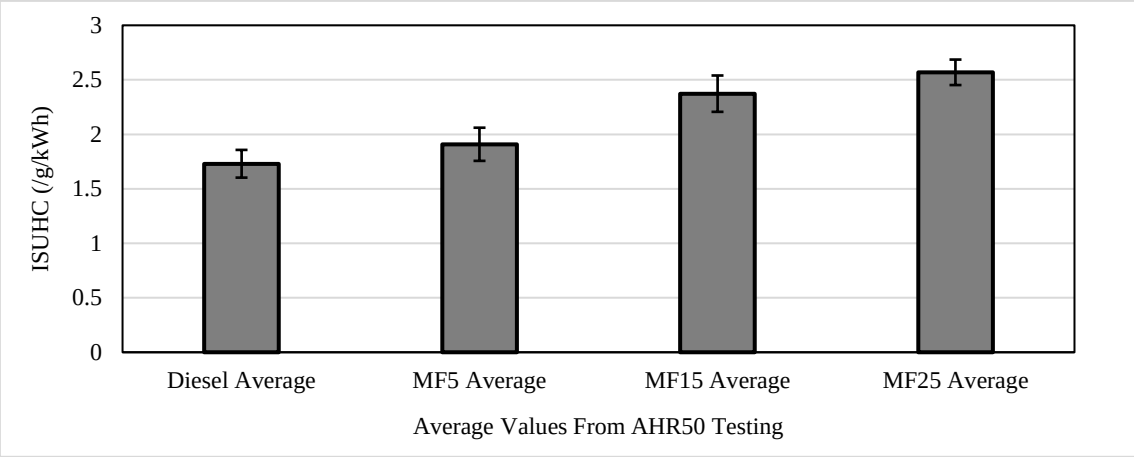

Figure 5-6 AHR50 Testing Comparing Average ISUHC Value for Each Fuel. Engine Operating at 5 bar IMEP, 1800 rpm, IP 650 bar, 15% EGR.

It is typically expected that the use of oxygenated fuels within a CI engine will reduce the amount of UHC available in the exhaust as the oxygenated fuel will promote post-combustion oxidisation within the combustion chamber (Sharma et al., 2008). Reduced hydrocarbon results were seen by Xiao et al. when completing load testing of MF/diesel blends. \the UHC values were found to be consistently lower than diesel with similar blend ratios to this investigation being used (Xiao et al., 2016). As all of the tests completed in this chapter were at a load 5 bar IMEP, it can be concluded that this load was too low to allow for the entertainment of post-combustion oxidation and that this phenomenon may occur at higher loads which would also increase in the combustion efficiency of MF blends.

Hot EGR was decided to be evaluated for this investigation when it became apparent that MF blends with higher MF content were sensitive to high amounts of cold EGR. This use of high MF blends and high CEGR increased the net IMEP COV of the combustion cycles, creating individual cycles that were very combustion inefficient, producing high amounts of ISUHC. The benefit of using HEGR is that it increases the intake gas

temperature; this increased temperature increases the rate at which the injected fuel vaporises, the increasing gas temperature and vaporisation aid in promoting combustion. HEGR also increases the combustion chamber wall temperature (Abd-Alla, 2002), this temperature increase may also aid in reducing the rate of premature quenching seen with low cetane fuels. Figure 5-7 and Figure 5-8 display the UHC generated from using CEGR and HEGR, respectively, the ISUHC produced by MF25 at 30% CEGR was omitted from the results for clarity as high combustion instability was attained, at 30% CEGR the ISUHC value was 24.99 g/kWh. By comparing each fuel using CEGR and HEGR, it can be seen that the use of HEGR can attain reduced ISUHC values at each EGR setting, which in turn reduced the HEGR UHC value range.

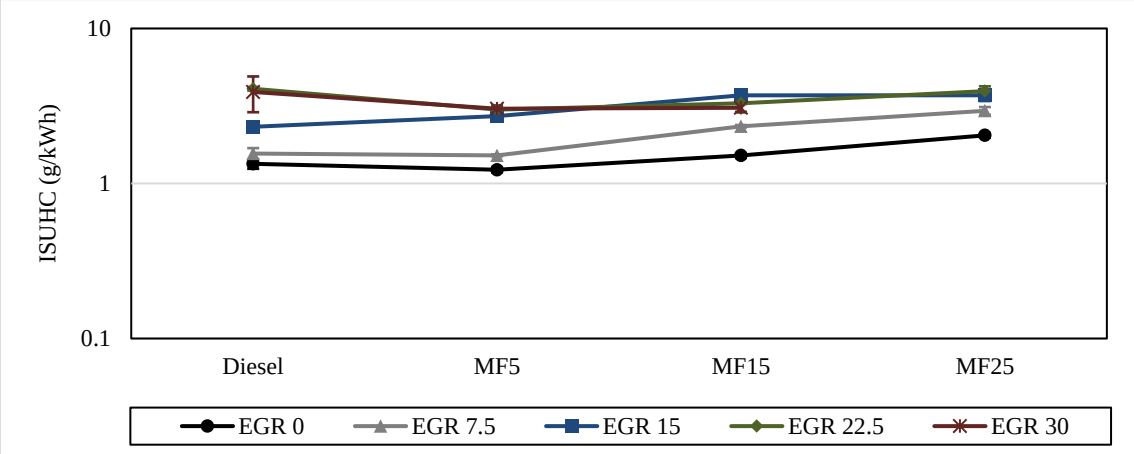

Figure 5-7 Cold EGR ISUHC Formation. Engine Operating at 5 bar IMEP, 1800 rpm, IP 650 bar, AHR50 8.

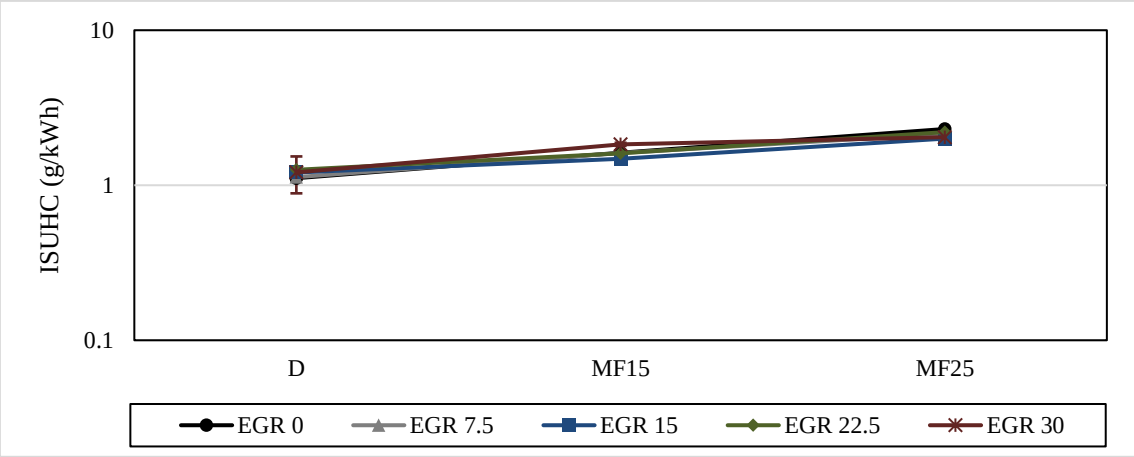

Figure 5-8 Hot EGR ISUHC Formation. Engine Operating at 5 bar IMEP, 1800 rpm, IP 650 bar, AHR50 8.

To assess the hypothesis that a higher load will reduce the ISUHC generated, it is suitable to compare the UHC results seen between the hot and cold EGR testing. This is because an effect seen from higher engine loads is higher in-cylinder temperature; this can be somewhat simulated with the use of hot EGR. Table 5-3 displays some critical characteristics of MF15, with 30% CEGR and 30% HEGR. The results show that hot EGR was capable of reducing the ISUHC generated by 39%, most likely due to the increased in-cylinder temperature associated with increased engine load. This is also reflected in a reduction in the net IMEP COV, which reduced the amount of inefficient combustion cycles discussed in the previous chapter. The ISFC was also drastically reduced by the improved atomisation supplied by the increased temperature within the cylinder. The improvements in both NIMEP COV and ISFC meant that less fuel was injected into the cylinder with a more complete combustion event, resulting in reduced ISUHC production. This displays that MF blends at higher loads could produce similar ISUHC values compared to diesel fuel combustion; however, tests at higher loads need to be undertaken to confirm this.

Table 5-3 UHC Generation Comparison Between MF15 with 30% Hot and Cold EGR. Engine Operating at 5 bar IMEP, 1800 rpm, IP 650 bar, AHR50 8.

	Intake Manifold Temperature (°C)	NIMEP COV (%)	ISUHC (g/kWh)	ISFC (g/kWh)
MF15 with 30% Cold EGR	41.72	7.40	3.07	174.33
MF15 with 30% Hot EGR	98.05	4.92	1.85	132.28
MF15 30% CEGR percent decrease over MF15 30% CEGR (%)	-135.01	33.51	39.73	24.12

5.3.3 Carbon Monoxide

Carbon monoxide is generated when complete combustion is not achieved. When complete combustion is accomplished, the injected carbon products react with oxygen to produce H_2O and CO_2, CO is formed from partial oxidation during the combustion process. This is formed instead of CO_2 because of oxygen starvation during combustion, which means that there is not enough O_2 available to form carbon dioxide. From this understanding, it can be concluded that the formation of CO is significantly dependant on the local equivalence ratio. CI engines typically always operate under excess O_2 conditions and CO is typically very low in comparison to SI engines. However, the CO formation will be evaluated because the local equivalence ratio may not reflect the global oxygen excess that is seen and because future emission regulations will be less tolerant of CO's production from automotive vehicles. Typically, the CO emissions seen from neat diesel is particularly low at medium and high loads as the combustion temperature exceeds 1100°C which aids in reducing the time required to oxidise CO_2 (Su, 2010).

The average value of indicated specific CO (ISCO) formed by each fuel blend from the IP testing is shown in Figure 5-9. The figure displays the increase in ISCO within the exhaust gas as the fraction of MF increases.

If an oxygenated fuel is used for combustion at favourable engine operation conditions, then low CO levels can be attained. This can be ascribed to the fuel self-supplying oxygen during the combustion process. This reduces the demand for oxygen within the cylinder, helping to promote complete combustion (Turner et al., 2011).

The average lambda value of each fuel during the IP tests is shown in Figure 5-10. This displays that as the MF content increases, as does the amount of oxygen within the exhaust. This highlights that there is another issue with the specific characteristics of MF, causing the CO to increase.

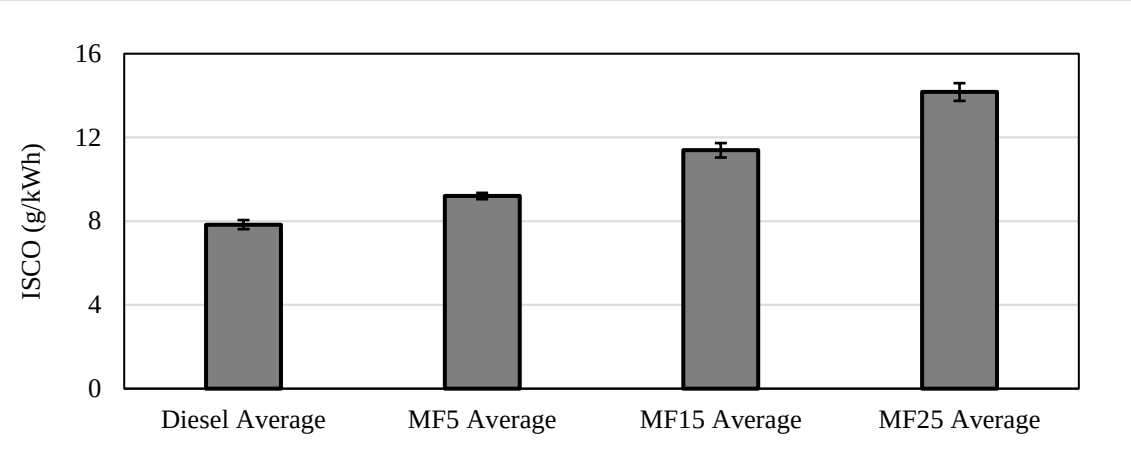

Figure 5-9 MF Injection Pressure Testing Average Values of ISCO. Engine Operating at 5 bar IMEP, 1800 rpm, 15% EGR, AHR50 8.

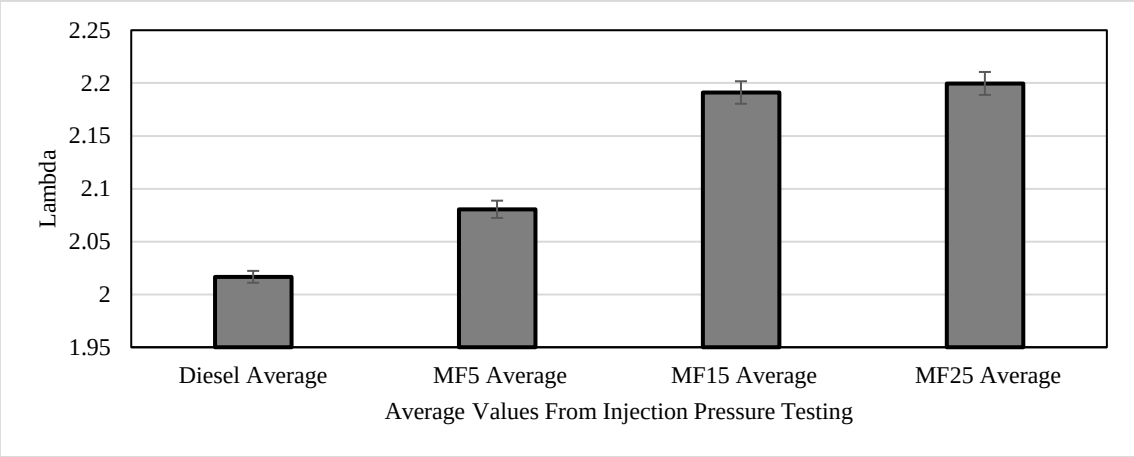

Figure 5-10 MF Injection Pressure Testing Average Values of Lambda. Engine Operating at 5 bar IMEP, 1800 rpm, 15% EGR, AHR50 8.

The increase of ISCO seen with the increase of MF fraction can be partially attributed to the lower cetane number of MF for two reasons. Firstly, as described in the NO_x analysis, there is reduced combustibility with MF/diesel blends when compared to neat diesel. When the flame front reaches adverse conditions, i.e. the perimeter of the cylinder, the flame would be more susceptible to being prematurely extinguished, producing more CO products and then reducing the amount of CO_2 generated. The second reason also linked to the cetane number is the increased ignition delay of MF. This increased residence time within the cylinder would increase the amount of fuel impinging on the surfaces of the combustion chamber where compete combustion is not possible to attain.

Figure 5-11 displays the effect of injection pressure on ISCO formation with the use of MF25. For all of the fuels, it was found that higher injection pressure did increase the CO generation, but MF25 was found to have the highest ISCO value range. The effect of CO production with increasing injection pressure and increasing MF usage can be hypothesised to have two major influences. The primary reason is that MF is more viscous fuel than diesel. Increased viscosity is known to aid in increasing spray penetration length (Chang and Farrell, 1997). This, coupled with the ignition delay, would again increase

the amount of fuel fouling on the cylinder wall. The secondary reason is that diesel has lower volatility than MF. This characteristic of diesel would be a prominent factor at low/medium loads like the tests undertaken. With the blend fuels, this could result in the diesel and MF separating, with the diesel pooling during injection while the highly volatile MF would entrain with the fresh charge in the cylinder. This could make a diesel lean and MF rich mixture towards the outer cylinder, decreasing the local cetane number of the mixture at the cylinder perimeter again reducing combustion efficiency and increasing ISCO. With MF25 and IP 950/1100 bar, the high injection pressure increased spray penetration, which increased the intake gas interaction and possibly created an MF rich mixture towards the outer of the cylinder. Both of these interactions could be reducing combustion efficiency, promoting CO production.

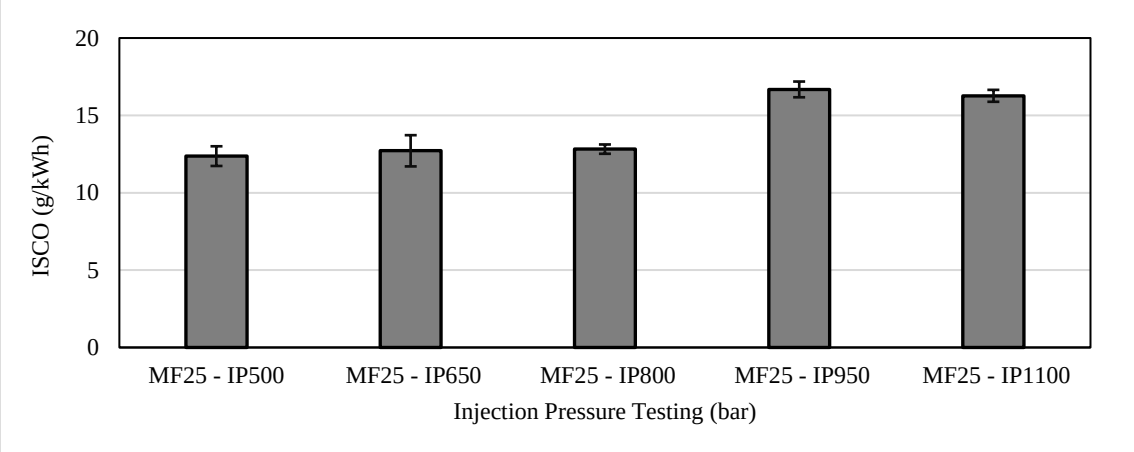

Figure 5-11 ISCO Level Increase with MF25 and Increased Injection Pressure. Engine Operating at 5 bar IMEP, 1800 rpm, 15% EGR, AHR50 8.

Figure 5-12, and Figure 5-13 display the ISCO generated during the CEGR and HEGR testing, respectively. By assessing the CEGR results, it can be seen that there are two typical trends seen. Firstly, when assessing the ISCO of a single fuel, it can be seen that the ISCO value increases as the CEGR ratio increases; this can be attributed to the

reduction of oxygen available within the cylinder reducing the combustion efficiency. Secondly, it can be seen that there is a slight increase in the ISCO values attained as the MF fraction increases, this can be ascribed to the reduction of cetane number reducing combustion susceptibility and increasing combustion inefficiency. By comparing the CEGR and HEGR diesel results can be seen that the use of HEGR aided in reducing the ISCO formation, especially when higher amounts of HEGR were introduced. The range of ISCO attained from CEGR testing varied from 5.81-20.31 g/kWh, whereas when HEGR was used this range was reduced to 5.61-13.90 g/kWh. This benefit can be attributed to the increase of gas temperature entering the cylinder, which would increase combustion susceptibility and decrease the amount of combustion quenching seen at the cylinder wall. MF25 is a noteworthy testing case displayed in Figure 5-13, overall this presents a very narrow ISCO range (12.88-13.9 g/kWh), and when compared to the MF25 CEGR testing, it was only the 0% CEGR results that were able to attain a lower value than this. This reduced range can be attributed to the balance between low cetane number and manifold temperature. At low HEGR values, the ISCO value of MF25 is primarily controlled by the low cetane number reducing combustion efficiency. The increase in HEGR value increases the manifold temperature. This increase of manifold temperature has more significant control over the reduction of available oxygen as the EGR ratio increases and the reduced cetane number of the fuel, both of which would reduce combustion efficiency. The oxygenated nature of MF would also aid in reducing the ISCO value as MF would supply oxygen to the combustion event and would be less sensitive to the available oxygen within the cylinder.

The results attained from the MF25 HEGR testing highlight that the use of HEGR is a suitable control method to aid in reducing the amount of ISCO generated during

combustion, and that is it a control method that should be considered when using low cetane fuels in a CI engine.

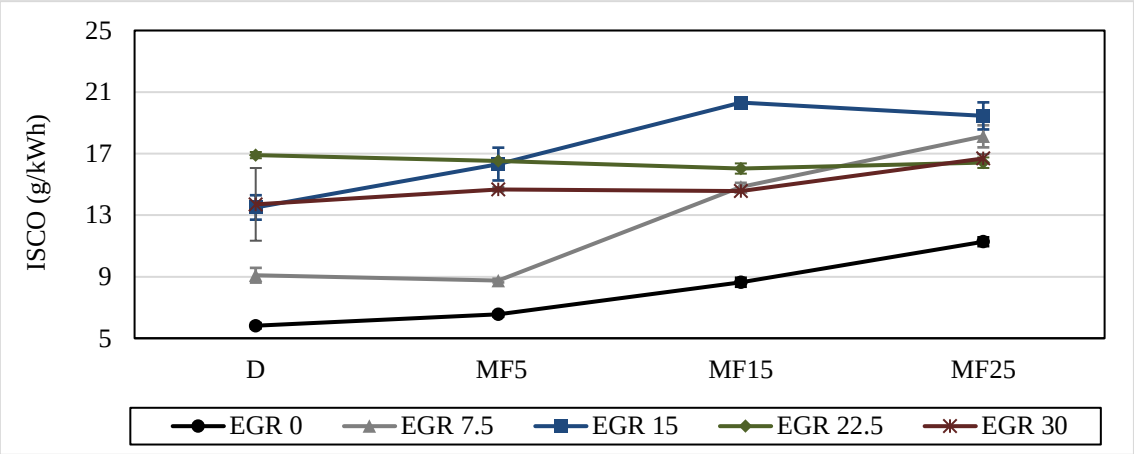

Figure 5-12 CEGR ISCO Formation. Engine Operating at 5 bar IMEP, 1800 rpm, 650 bar IP, AHR50 8.

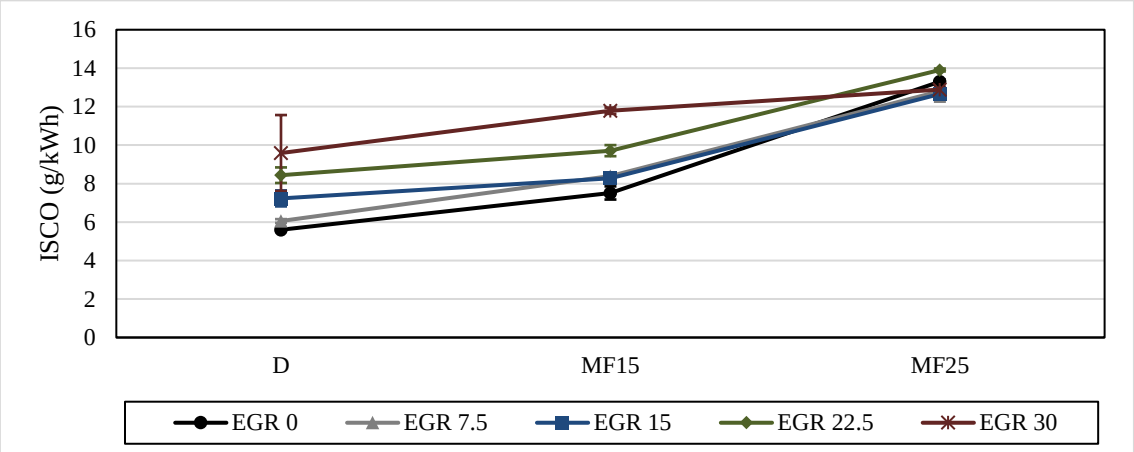

Figure 5-13 HEGR ISCO Formation. Engine Operating at 5 bar IMEP, 1800 rpm, 650 bar IP, AHR50 8.

5.3.4 Gaseous Emissions of MF25 Hot EGR compared to neat diesel Cold EGR

From the analysis undertaken in this chapter so far, it has been found that ISNO$_x$, ISCO and ISUHC typically increases as the MF fraction and CEGR ratio increases. However, by using HEGR, it was found that the increased manifold temperature aided in reducing combustion instability and therefore, CO and UHC formation. This section focuses on

comparing the diesel CEGR and MF25 HEGR combustion characteristics and resulting gaseous emissions.

Table 5-4 displays the differences seen from the combustion characteristics between diesel and MF25 using CEGR as well as MF25 using HEGR. The NIMEP COV can be seen to increase as the EGR ratio increases for each fuel; this can be expected as the combustion speed reduces from the reduced available oxygen attained from the increased EGR ratio. At MF25 30% CEGR, it can be seen that the NIMEP COV value becomes very high and highlights the combustion stability issues previously described. It should be noted that not only does MF25 with HEGR attain a reduced mean NIMEP COV value over diesel using CEGR, it also has a 14% reduced range, displaying that using HEGR is very effective at reducing cycle to cycle variation with low cetane fuels. It should also be noted that it is typically accepted for NIMEP COV to be less than 5% (Stone, 1999) with drivability issues being seen when NIMEP COV exceeds 10% (Maurya and Agarwal, 2011). Values over 5% were seen when using the SC configuration because of packaging restrictions requiring the intake and exhaust pipes to be a quarter of the size of the OEM intake and exhaust pipes. This increased the amplitude of the pressure waves within the SC manifolds during operation and consequently the NIMEP COV, typically when using a single cylinder experimental system the manifolds used have high volumes to dampen the pressure fluctuations seen within the manifolds (Buchman and Winter, 2017).

By comparing the ignition delay it can be seen that MF25 with CEGR had the most prolonged mean ignition delay, the use of HEGR significantly reduced the average ignition delay of MF25 by 4.5 CA. It was found that the MF25 HEGR average ignition delay was only 2.6 CA greater than the diesel mean with CEGR. This highlights the positive effect seen by using HEGR to increase the gas temperature entering the cylinder

to improve combustion initiation. This increased in-cylinder temperature would have also aided in reducing the wall quenching seen, both of these factors resulted in HEGR improving the ISFC of MF25 with a 15% reduction of mean ISFC when compared to the CEGR mean value, HEGR also produced a similar mean value to the ISFC attained from diesel using CEGR.

Table 5-4 Fuelling and EGR Strategy Combustion Comparison. Engine Operating at 5 bar IMEP, 1800 rpm, IP 650 bar, AHR50 8.

	EGR Ratio (%)	Max Pressure (MPa)	Pressure Max Rate of Change (MPa)	NIMEP COV (%)	Combustion Duration (CA)	Ignition Delay (CA)	ISFC (g/kWh)
Diesel CEGR	**0**	5.84	0.67	5.29	17.67	11.40	183.17
	7.5	5.77	0.58	5.30	18.67	13.35	171.48
	15	5.52	0.41	5.83	20.67	15.03	160.55
	22.5	5.39	0.34	6.07	20.67	16.30	160.23
	30	5.26	0.25	6.62	20.33	17.60	155.74
	Average	5.56	0.45	5.82	19.60	14.74	166.24
MF25 CEGR	**0**	6.09	0.75	4.74	15.00	14.70	218.51
	7.5	5.80	0.52	5.36	17.33	16.75	210.89
	15	5.48	0.31	6.76	18.67	20.70	189.02
	22.5	5.34	0.20	8.73	20.67	25.80	176.83
	30	4.39	0.12	50.14	25.00	31.60	227.72
	Average	5.42	0.38	15.15	19.33	21.91	204.60
MF25 HEGR	**0**	5.95	0.60	4.87	17.33	13.95	215.13
	7.5	5.59	0.46	5.17	19.67	15.50	192.08
	15	5.33	0.36	5.21	21.00	16.60	160.43
	22.5	5.06	0.28	5.56	22.00	18.90	152.08
	30	4.97	0.24	6.01	22.67	21.78	149.74
	Average	5.38	0.39	5.36	20.53	17.35	173.89

The ISUHC and ISCO are shown in Figure 5-14 and Figure 5-15, respectively. The UHC of MF25 with CEGR is shown to increase as the EGR ratios increase because of the higher NIMEP COV attained. The increased UHC and CO seen from MF25 at low EGR with both cooling methods can be ascribed to the increased ignition delay and decreased cetane number increasing wall impingent and combustion chamber quenching reducing the amount of complete fuel conversion during the combustion process. With diesel and CEGR, the ISUHC and ISCO are seen to increase as EGR ratio increases; this can be

accredited to the increased ignition delay and the reduced combustion temperature increasing quenching. It can be seen that MF25 using HEGR maintains similar if not slightly reduced levels of ISCO and ISUHC as the HEGR ratio increases when compared to MF25 with CEGR. With high amounts of HEGR, reduced ISCO and ISUHC values were attained with MF25 when compared to diesel using CEGR. Again, at low EGR ratios, the MF25 using HEGR had higher levels of ISCO and ISUHC than diesel because of the cetane number and low intake charge temperature. However, when the HEGR ratio increased, the higher in-cylinder temperature aided in improving the combustion conversion process. MF25 was able to attain similar levels of ISCO and ISUHC throughout the tested HEGR ratio range by MF providing oxygen during the combustion process and allowing CO_2 to be formed, increasing the amount of complete combustion seen. Typically, when using HEGR and diesel, it is expected to see ISCO and ISUHC increase; as the EGR ratio increases, the reduced oxygen content and the hot nature of the recirculated exhaust gas reduces the density of the oxygen entering the combustion chamber (Pradeep and Sharma, 2007).

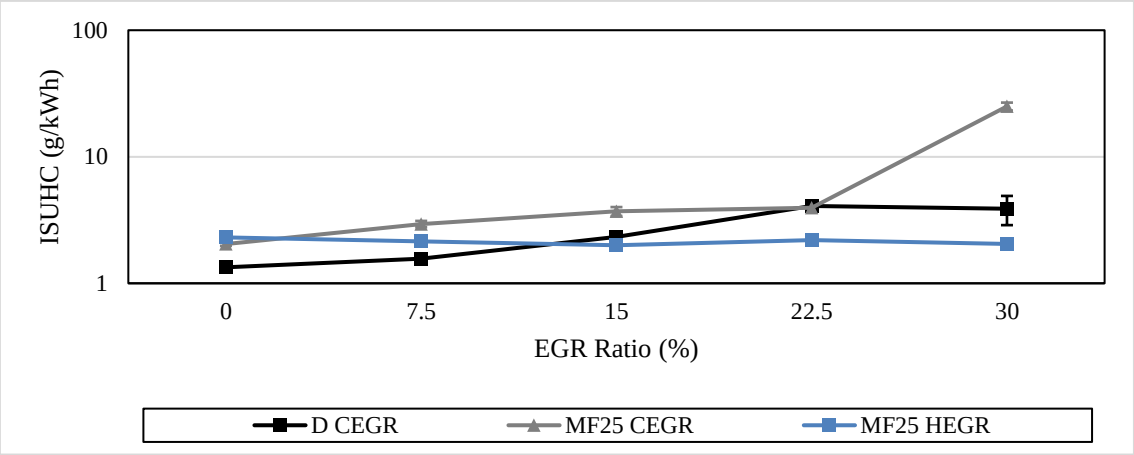

Figure 5-14 Fuelling and EGR Strategy ISUHC Comparison. Engine Operating at 5 bar IMEP, 1800 rpm, 650 bar IP, AHR50 8.

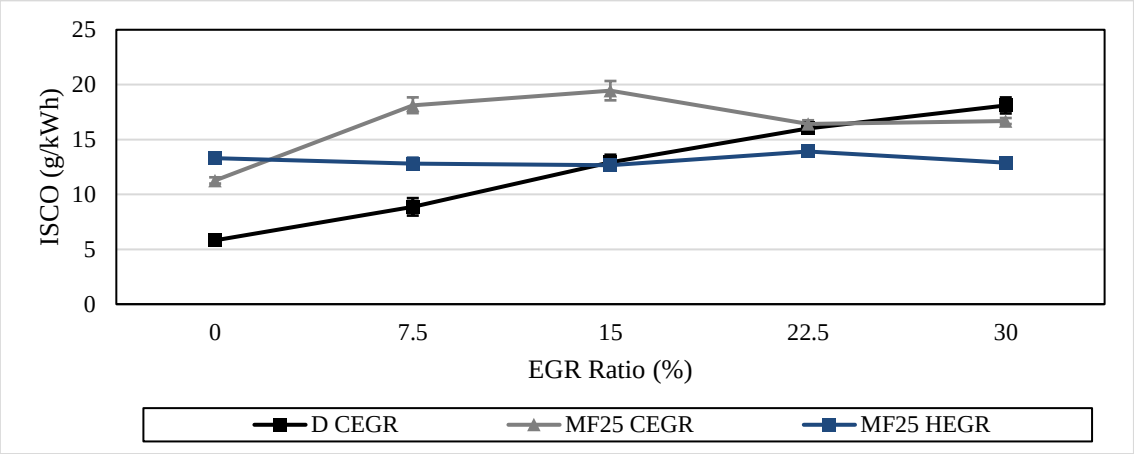

Figure 5-15 Fuelling and EGR Strategy ISCO Comparison. Engine Operating at 5 bar IMEP, 1800 rpm, 650 bar IP, AHR50 8.

Figure 5-16 displays the NO_x emitted from the various fuel and EGR strategies. It can be seen that at low EGR ratios, MF25 attained a higher ratio of NO_x because of the reduced combustion duration attained from MF self-supplying oxygen during the combustion process and reducing the duration. At 15% EGR MF25 with CEGR produced lower NO_x than diesel, this can be accredited to the ignition delay increasing mixture preparation. At this point, MF25 with HEGR had a higher NO_x ratio than diesel; this can be attributed to the higher in-cylinder temperature reducing the ignition delay and combustion duration, increasing combustion temperature. Past 22.5% EGR, MF25 with HEGR and CEGR

emitted lower NO_x than diesel with CEGR; this demonstrates that the increased ignition delay of MF25 outweighed the difference of in-cylinder temperature attained from the two exhaust gas recirculation conditioning methods.

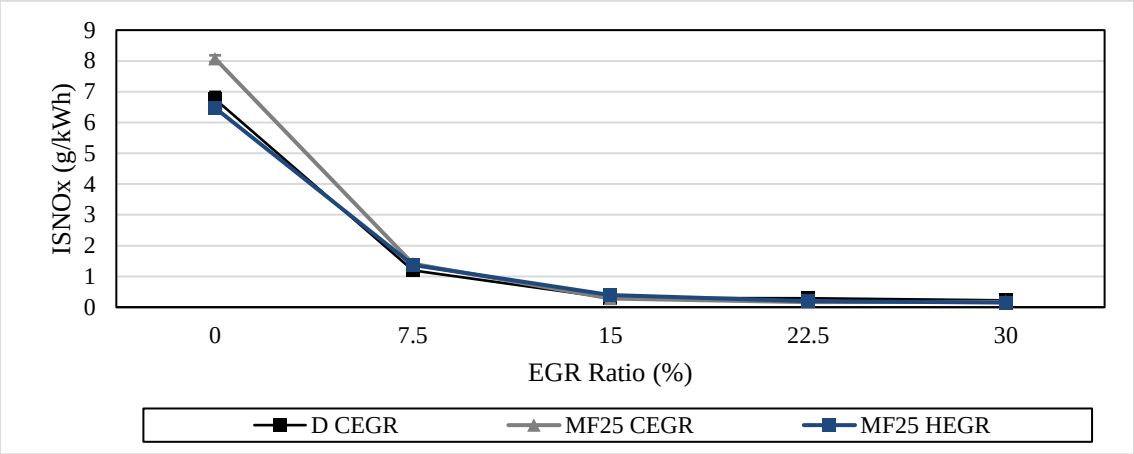

Figure 5-16 Fuelling and EGR Strategy $ISNO_x$ Comparison. Engine Operating at 5 bar IMEP, 1800 rpm, 650 bar IP, AHR50 8.

When comparing the diesel CEGR and MF25 HEGR results, it was found that the increased in-cylinder temperature aided in providing reduced ISUHC and ISCO values while the cetane number aided in providing reduced $ISNO_x$.

5.4 Conclusion

In this chapter, a CI engine was tested with a selection of MF/diesel blends. These fuels were tested assessing the impact of different engine parameters (IP, AHR50 CA, CEGR, HEGR) in reference to the gaseous emissions emitted. Experiments were completed at a load of 5 bar IMEP and an engine speed of 1800 rpm. The blends tested were MF5, MF15 and MF25. The following are the most predominant findings from the investigation:

- Throughout all of the test conditions, $ISNO_x$ was seen to increase with the higher fraction of MF used. The average increase of $ISNO_x$ with use of MF25 in comparison to neat diesel was 17.75%. $ISNO_x$ is formed when high local

combustion temperature is attained. The oxygenated nature of MF would aid in increasing the speed of combustion due to the higher rate of premixed combustion and MF self-supplying oxygen to the combustion process. This, in turn, would increase the maximum combustion pressure, temperature, which would increase NO_x formation.

- The amount of ISUHC produced from these test sweeps also increased with the fraction of MF used. By averaging the results seen from each fuel, it was found that the UHC increased by 4.56%, 22.71% and 47.4% with the use of MF5, MF15 and MF25, respectively. This increase in ISUHC can be ascribed to the reduced lower heating value and cetane number of MF as well as the higher latent heat of vaporisation and auto-ignition temperature compared to diesel. This combination would result in more fuel being injected and less fuel undergoing the complete combustion process. This can be seen to be accurate as the use of hot EGR, which increased intake gas temperature aided in promoting higher combustion efficiency, reducing ISUHC production when compared to the results seen from CEGR testing. Hot EGR increased intake gas temperature, increasing in-cylinder temperature, which reduced the quenching effect seen on the flame towards the combustion chamber wall increasing carbon conversion efficiency during combustion.
- The level of ISCO generated from the tests was seen to increase with the increase of MF fraction. Results found that ISCO increased by 8.33%, 21.21% and 31.8% with the use of MF5, MF15 and MF25 when compared to the average value found with neat diesel. In a similar manner to ISUHC, the level of ISCO is dependent on the fuel hydrocarbon combustion conversion. Ideally, CO_2 should be formed

from the combustion process, but CO is produced when not enough oxygen present; CO_2 is known to increase when the combustion temperature exceeds 1100°C. From the high NO_x seen, it can be concluded that the majority of the combustion process occurs in this temperature region with MF increasing combustion temperature. The self-oxygenated nature of MF would also aid in producing CO_2, which highlights that another characteristic of MF is reducing combustion efficiency. Similar to UHC, this can also be attributed to the increased fuel consumption required by the use of MF forcing more fuel to be introduced and the lower cetane number restricting combustion towards the end of the process when the flame front is exposed to adverse conditions. The use of HEGR was found to provide benefits in reducing the amount of ISCO generated. When comparing the performance of MF25 EGR testing, it was found that only CEGR 0% was able to attain lower ISCO values that the whole range of HEGR values tested. Typically increasing the EGR ratio reduces combustion stability reducing the amount of available oxygen within the cylinder. However, the use of HEGR aided by increasing the intake gas temperature, which increased combustion stability; the oxygenated nature of MF was also able to provide oxygen to the combustion process, further increasing combustion stability.

- Overall, it was found there were benefits to be attained from using HEGR with the increasing MF blends. The increased manifold temperature aided in reducing ignition delay and although the oxygen content of MF did provide increased $ISNO_x$, there was no particular difference observed in the NO_x values when comparing the performance of MF25 using CEGR and HEGR. However, the

increased manifold temperature was found to provide great reductions of ISUHC and ISCO when comparing the MF25 CEGR and HEGR results.

These results do not reflect in favour of the use of MF within a CI engine at the low/medium load of 5 bar IMEP. However, with the injection timing fixed to 7.5°BTDC, others have found the gaseous emissions of MF perform well at medium/high loads with the low loads like these experiments showing poor performance (Xiao et al., 2016). This investigation has highlighted some key characteristics of MF, which has allowed for some hypothesis to be generated. However, before a concise conclusion can be attained, it is necessary to consider the effect that MF/diesel blends have over particulate emissions. One of the key concerns regarding CI engines is the level of PM generated so it is important to investigate this area to conclude if any alternative fuels can provide a reduction of particulate emissions when compared to diesel.

CHAPTER 6

6. Particulate Matter Emissions of 2-Methylfuran and Diesel Blends

This chapter investigates the impact of altering various engine parameters on the particulate matter emissions of various 2-methylfuran and diesel blends.

6.1 Introduction

In comparison to SI engines, CI engines have always performed poorly regarding PM output. Lots of time and economic resources have been invested in researching PM reduction techniques for diesel CI engines. In addition, regulations regarding particulate pollution have become much more stringent in recent years, and this is a trend that is expected to continue in the future. Keeping these factors in mind, it is essential to assess the particulate matter performance of any viable alternative fuels.

This chapter studies the particulate matter emissions of a selection of 2-methylfuran and diesel fuel blends. The experiments completed for this investigation evaluated the effect of altering a single engine parameter at a time. These variables varied in this section were AHR50 CA, IP, cold EGR and hot EGR.

Particles can be classified as nucleation mode particles or accumulation mode particles and this has been appropriately described in the literature review. Nucleation mode particles only contribute from 0.1-10% of the total particulate mass. However, this mass can accommodate up to 90% of the total number of particles (Ristovski et al., 2003). Because of the large number concentration and the fact that nucleation particles are mostly composed of semi-volatile or volatile condensates, it is essential to investigate

what effect varying engine conditions and fuels have on this aerosol mode. In the opposite regard to nucleation mode particles, accumulation mode particles are known for having a comparatively low particle count while constituting for the majority of particle range mass. Accumulation particles are made up of solid particles like carbon, which can then have condensates like hydrocarbons or sulphur derivatives adsorb onto their body. The high mass of these particles means that they are a crucial area to consider as they draw significant concerns regarding human health.

6.2 Experimental Procedure

As with the previous chapter, the experiments were completed with the separated cylinder system. This system was employed to provide the author with more control when completing experiments, setting points and also to reduce the consumption of the fuel blends tested. The MF ratios used in this investigation were MF5, MF15 and MF25, with MF being mixed with 300ppm lubricity improver prior to being blended with diesel.

For each testing condition, the engine was operated at 1800 rpm and 5 bar IMEP. The testing of each engine parameter was completed over two consecutive days.

Tests were completed once the engine had been run for enough time for the intake air, engine coolant and oil temperature to plateau at the set temperatures and the engine had become thermally stable. Initially, all experiments were completed with neat diesel so that results of the MF testing could be discussed in reference to a current standard automotive fuel and serve as a suitable baseline. The test plan carried out was identical to the previous chapter with an overview of the experimental plan being shown in the appendix.

6.3 Results

6.3.1 Particle Size Distributions

The effects seen on the PSD from using the various MF blend ratios are shown in Figure 6-1, this displays a selection of graphs showing the particle emissions of the fuels at the AHR50 test points assessed. The graphs display a similar overall trend of particle size distribution density. They highlight that as MF content increases, the particle size distribution density at each measured point decreases. This can be accredited to the low cetane number and oxygen content of MF. The cetane number increased fuel entrainment via the increased ignition delay, and the oxygen content increased premixed combustion, reducing soot precursor formation, this is discussed in more detail in the following section.

For each fuel tested, it can be seen that the particle density of each measured point increases as the AHR50 increases. This increase is attributed to the combustion event reducing the amount of premixed combustion seen as the AHR50 value moves further from TDC.

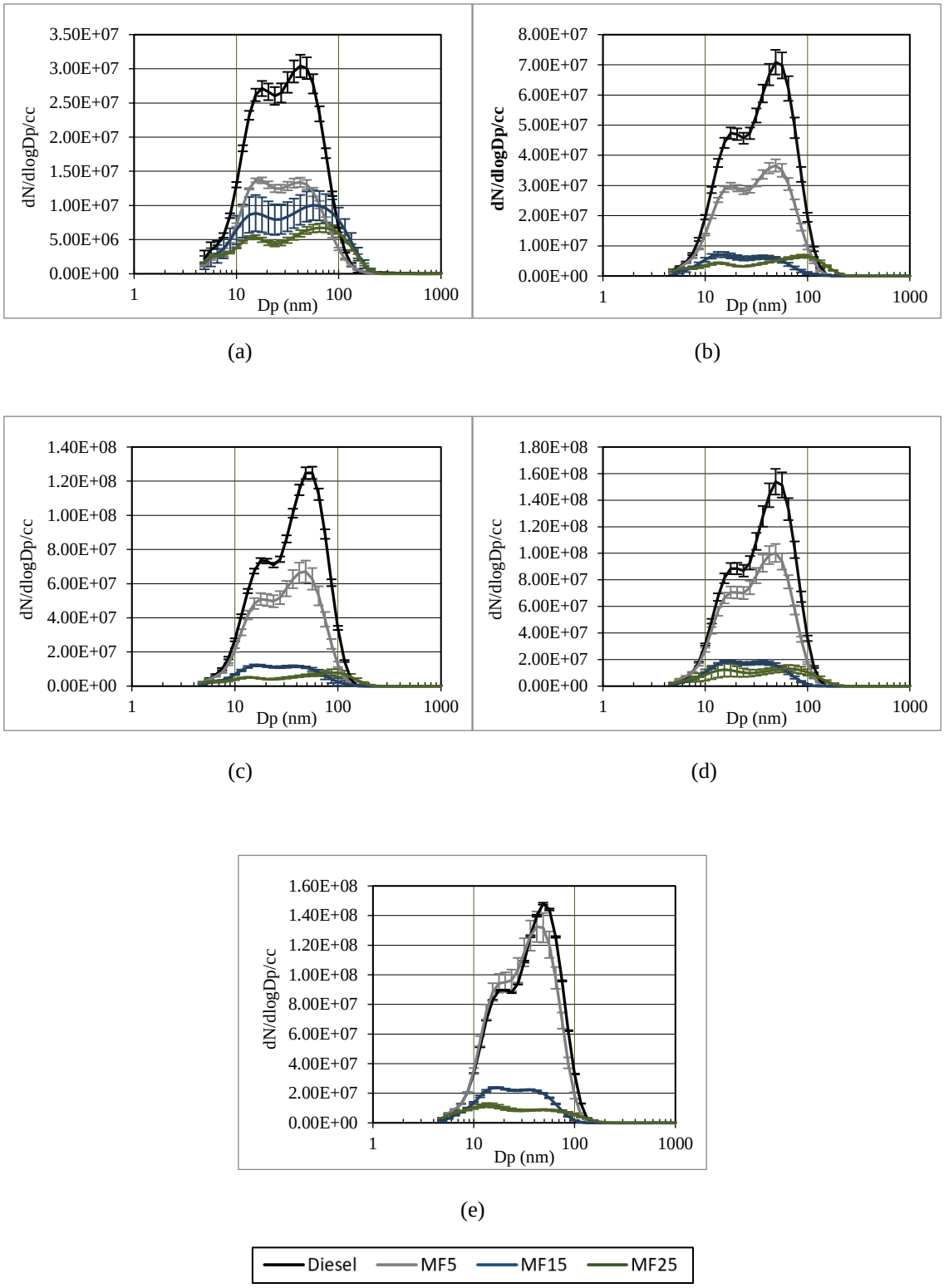

Figure 6-1 AHR50 Testing Particle Size Distribution Graphs. Engine Operating at 5 bar IMEP, 1800 rpm, 650 bar IP, 10% EGR. (a) - AHR50 0. (b) - AHR50 3. (c) - AHR50 6. (d) - AHR50 9. (e) - AHR50 12

6.3.2 Particle Number

When considering particle matter as a whole, the concentration of the PM emitted is a key component to consider.

Figure 6-2 displays the HRR of diesel at the various AHR50 values tested; this displays increased premixed combustion as AHR50 advanced to TDC from ATDC, the trends seen in this graph were similar for all of the fuels tested during the AHR50 tests. Figure 6-3 and Figure 6-4 displays the total particle concentration of nucleation and accumulation mode particles resulting from the AHR50 variation testing for all of the fuels. By investigating each fuel individually in both figures, it can be seen that the particle concentration reduces as the AHR50 value is advanced closer to TDC. This can be attributed to the early injection timing (advanced AHR50 closer to TDC) leading to a longer ignition delay resulting in (i) increased fuel/air mixing (more available time for fuel and air to mix) and (ii) an increase of premixed combustion, both reducing the probability of rich in fuel regions where particles are formed. In addition, the improved combustion efficiency of advanced combustion also leads to increasing premixed combustion, resulting in a shorter combustion duration, which also contributes to reduced particle emissions.

Total particle concentration as well as mean acc and nuc particle size reduces as the MF fraction increases. The oxygen content of MF is one of the key factors responsible for reducing the particle number (PN) by providing oxygen during the oxygen-limited premixed combustion phase. This will aid in producing hydroxyl radical (OH), which can reduce the formation of soot precursors (Song et al., 2002). The reduction of C-C bonds seen in diesel fuel (Takahashi and Glassman, 1984) and oxygen content of MF aided to reduce particulates (Mohankumar and Senthilkumar, 2017). In addition, the increase of

MF ratio over diesel will also aid in reducing the PM by reducing the number of aromatic components in the fuel (which is a critical process in soot formation) and the amount of sulphur within the fuel blends. Sulphur within fuels can aid in increasing nucleation particles by forming SO_2, which is then possible to oxidise and form SO_3 (Zhu et al., 2010). The introduction of MF in the MF-diesel fuel blends plays a significant role for retarded combustion (e.g. the retard values of AHR50) leading to a large decrease in particle concentration. Retarded combustion is more likely to generate local rich in fuel regions where the oxygen supplied from the fresh charge cannot be accessed and the MF aids in oxidising the particle precursors and particles to significantly reduce PM emissions. However, the introduction of MF does not play as much of a significant role in reducing the particle concentration at the advanced AHR50, and the particle concentration levels were comparatively low for diesel fuel throughout the AHR50 test range.

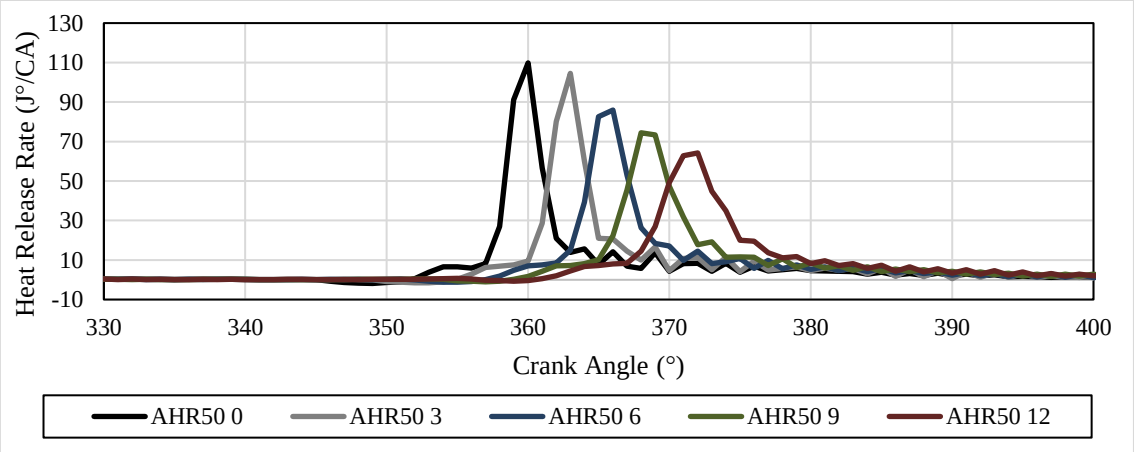

Figure 6-2 Diesel AHR50 Tests HRR. Engine Operating at 5 bar IMEP, 1800 rpm, 650 bar IP, 10% EGR.

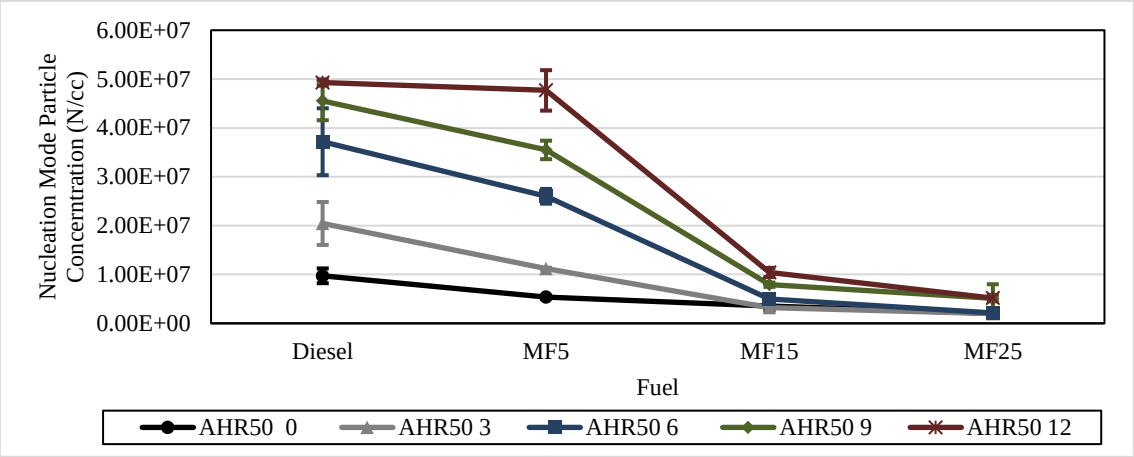

Figure 6-3 AHR50 Nucleation Mode Particle Concentration. Engine Operating at 5 bar IMEP, 1800 rpm, 650 bar IP, 10% EGR.

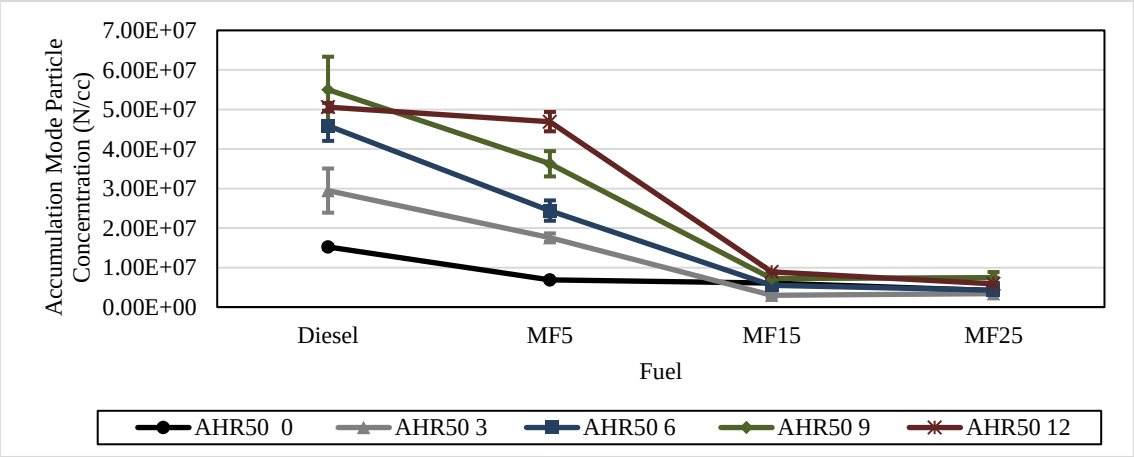

Figure 6-4 AHR50 Accumulation Mode Particle Number. Engine Operating at 5 bar IMEP, 1800 rpm, 650 bar IP, 10% EGR.

Figure 6-5 displays the total particle concentration seen during the injection pressure testing. When assessing neat diesel, it can be seen that the higher injection pressure reduces the particle formation as typically expected (Agarwal et al., 2013). This is attributed to the reduced fuel droplet size increasing entrainment and the longer spray penetration length, increasing the surface area of combustion chamber utilised during premixed combustion. This trend of reduced concentration when injection pressure is increased is also seen for MF5 combustion. However, the MF15 and MF25 results require

further analysis. When assessing the particle concentration of MF25, it can be seen that the 500 bar IP had the lowest concentration with IP950 and 1100 being very close to the 500 bar IP. It can be hypothesised that wall impingement is being seen from the injection pressure of the 650 and 800 IP's along with the increased ignition delay of MF25. However, at an IP of 950 and 1100 bar, the total particle concentration dramatically reduces and can be attributed to the higher premixed combustion being attained. Figure 6-6 highlights that the ignition delay of each fuel reduces as IP increases. It can be concluded that the high particle entrainment and reduced ignition delay of 950 and IP1100 aiding in heavily reducing MF25's particle concentration values by providing high entrainment and a low ignition delay.

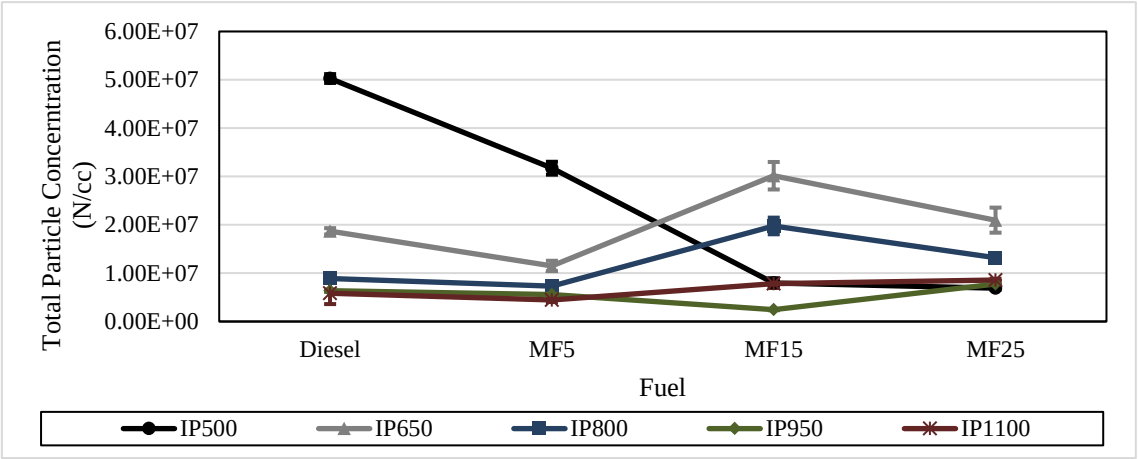

Figure 6-5 Injection Pressure Testing Total Particle Concentration. Engine Operating at 5 bar IMEP, 1800 rpm, 15% EGR, AHR50 8.

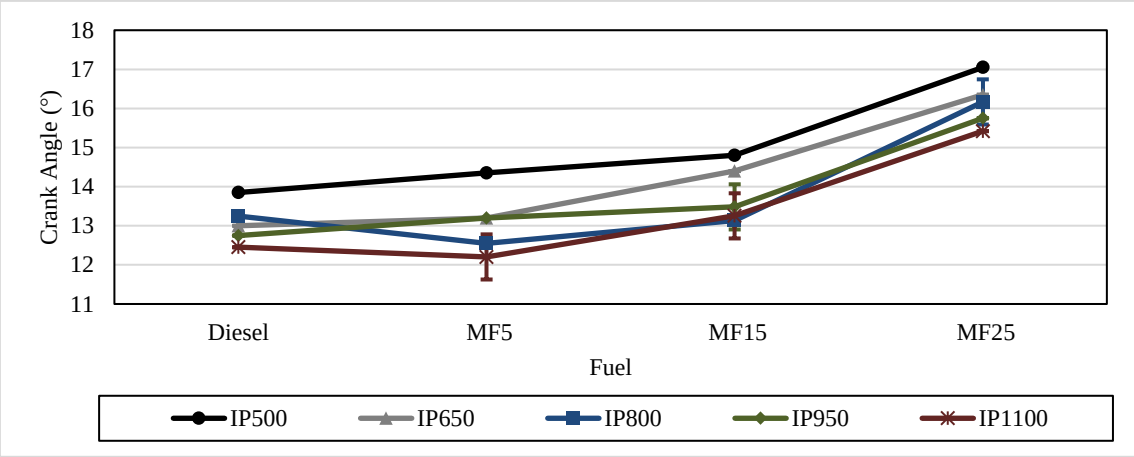

Figure 6-6 Injection Pressure Testing Ignition Delay. Engine Operating at 5 bar IMEP, 1800 rpm, 15% EGR, AHR50 8.

Figure 6-7 and Figure 6-8 display the particle concentration of the cold EGR tests. The results attained of 30% CEGR fuelled with MF25 have been removed as they are much larger than the rest of the data, the values for nucleation and accumulation particles under the test condition were 4E+08 and 1.1+E8, respectively.

When using neat diesel and increasing EGR ratio, it is expected to see a particle concentration increase. This is attributed to the reduction of available oxygen within the cylinder and the increased specific heat of the exhaust gas introduced into the cylinder (Wang et al., 2016). With the MF blends, these factors play a role, but the properties of MF also need to be considered. High MF blend ratios using high amounts of CEGR were found to produce increased particle concentration, this can be attributed to reduced combustion stability brought about from the cetane number of the blend, the low in cylinder gas temperature prior to combustion and the reduced amount of available oxygen within the cylinder. This can mainly be credited to the lower cetane number along with the reduced available oxygen and low in-cylinder gas temperature. These factors either contribute to combustion initiation difficulty or increase the combustion susceptibility to

premature extinguishing, both reduce the amount of fuel, particle precursors and particles oxidation obtained.

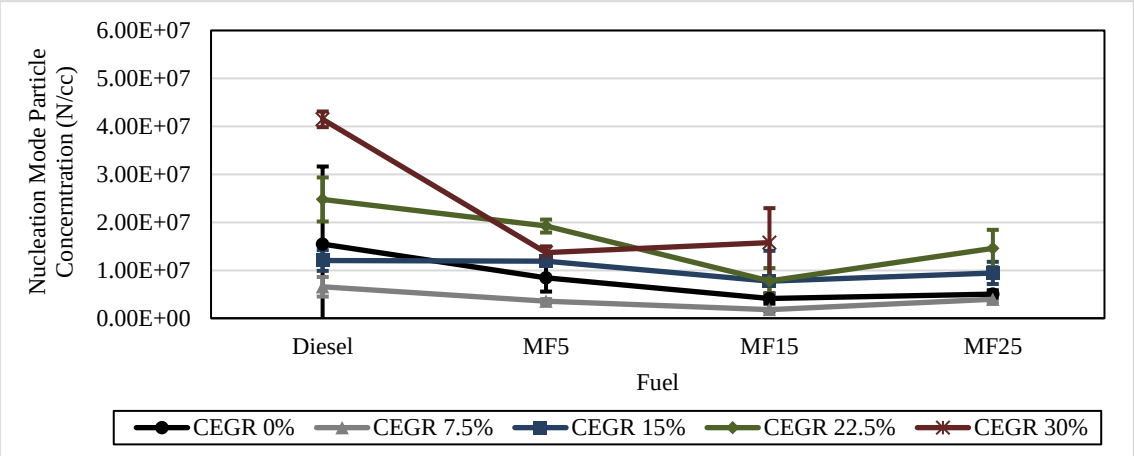

Figure 6-7 Cold EGR Nucleation Mode Particle Concentration. Engine Operating at 5 bar IMEP, 1800 rpm, 650 bar IP, AHR50 8.

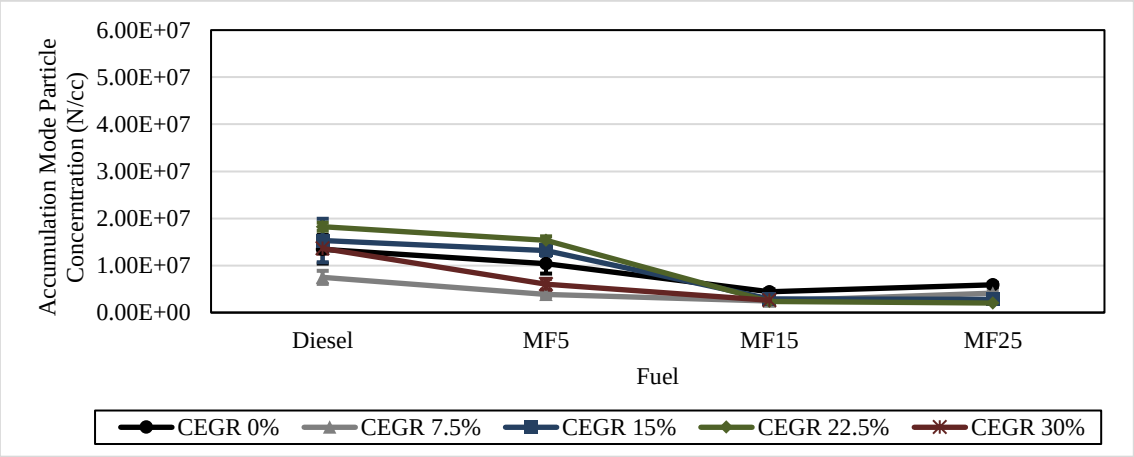

Figure 6-8 Cold EGR Nucleation Mode Particle Concentration. Engine Operating at 5 bar IMEP, 1800 rpm, 650 bar IP, AHR50 8.

The combustion instability seen when using high amounts of CEGR highlighted the requirement for a different control method when using high MF blends and high amounts of EGR. This requirement demonstrated the necessity to investigate the use of HEGR. By evaluating Figure 5-5, it can be seen that HEGR can increase the manifold temperature by up to 30°C-60°C depending on the EGR ratio used.

Figure 6-7 and Figure 6-8 display the nucleation and accumulation mode particle attained from the CEGR testing, these results can be compared to Figure 6-9 and Figure 6-10 which display the nucleation and accumulation trends attained from the HEGR testing.

The overall trends highlight reduced particle concentration in both modes when operating hot EGR and cold EGR. The reduction becomes more prevalent as the EGR ratio, and MF blend ratio are increased. This reduction in particles can be attributed to the increased combustion stability brought about by the increase of in-cylinder gas temperature, which in turn increases fuel, particle precursors and particle oxidation. It should be noted that at lower MF blend ratios, high particle concentration was seen when using HEGR. As combustion stability was not an issue with neat diesel, MF5 and MF15 there was no benefit attained from increased in-cylinder temperature. For these fuels, there were negative results of increased particle concentration in both modes when employing HEGR. This particle increase can be attributed to the phenomena ‘thermal throttling’ where the increase of intake gas temperature decreases the density of the intake gas and reduces the amount of available oxygen within the cylinder prior to combustion, decreasing soot oxidation (Kamimoto and Bae, 1988, Ladommatos et al., 2000).

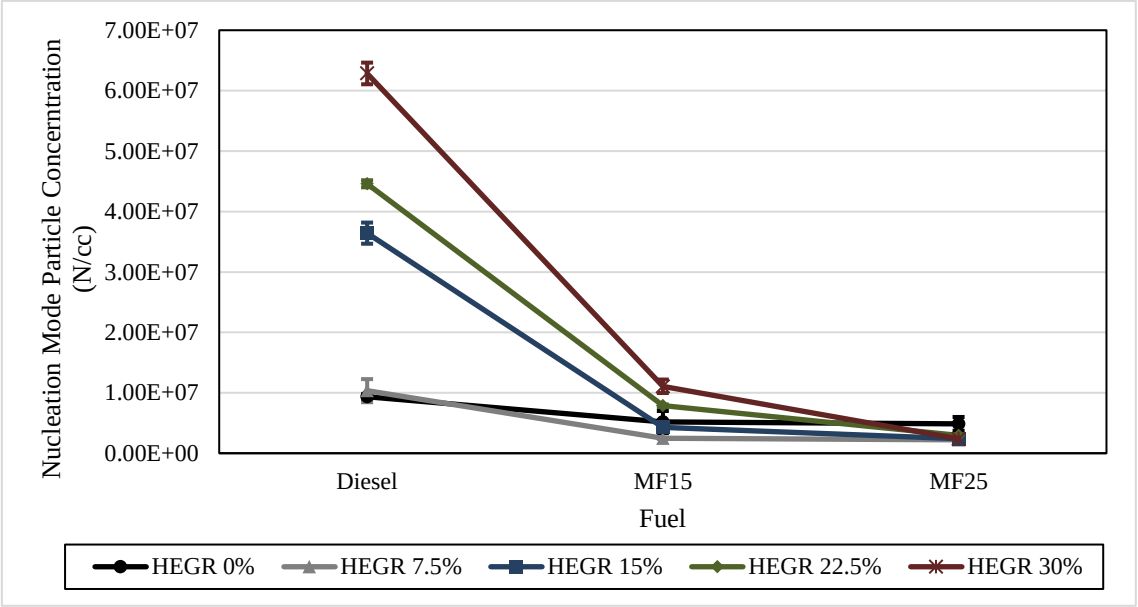

Figure 6-9 Hot EGR Nucleation Mode Particle Concentration. Engine Operating at 5 bar IMEP, 1800 rpm, 650 bar IP, AHR50 8.

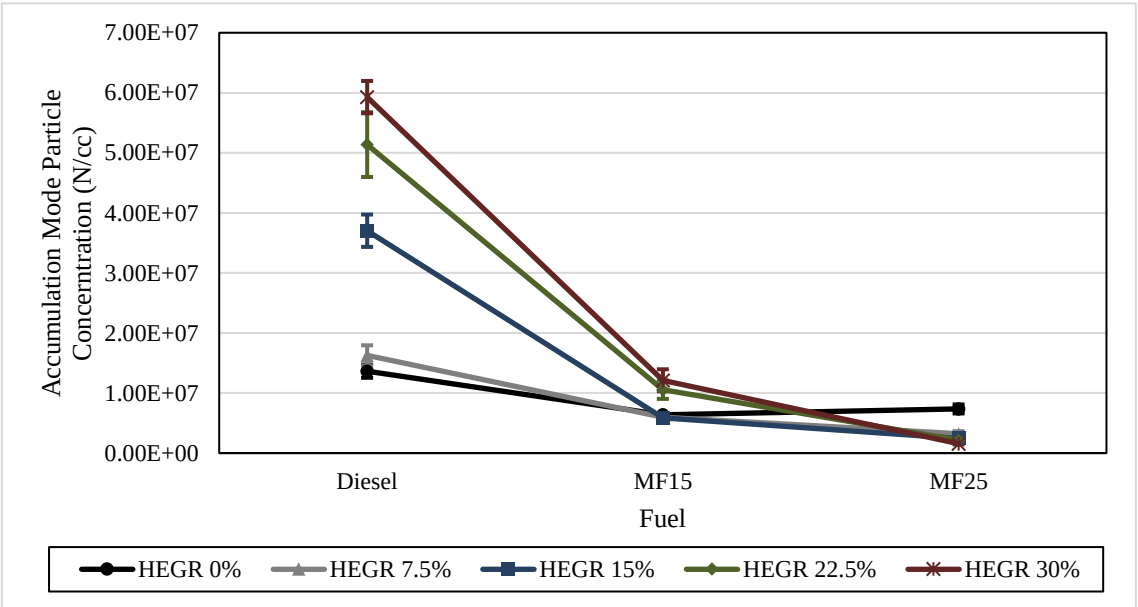

Figure 6-10 Hot EGR Accumulation Mode Particle Concentration. Engine Operating at 5 bar IMEP, 1800 rpm, 650 bar IP, AHR50 8.

6.3.3 Particle Surface Area and Mass

The concentration of particles generated in each mode has a direct effect on the particle surface area and mass. Figure 6-11 and Figure 6-12 display the surface area and mass of both particle modes during the AHR50 testing, both follow a similar trend to the total particle concentration graphs shown in Figure 6-3 and Figure 6-4 (the retard of AHR50 increases particle mass and SA). The addition of MF also reduced the mean mass and SA of particles. By comparing the combustion duration attained by the different fuels and test conditions, see Table 6-1, it can be seen that the combustion duration for neat diesel ranged from 21.33 CAD with AHR50 0 to 17.67 CAD with an AHR50 of 12, whereas with MF25 these values were 19.33 and 17. This reduced range in combustion duration can be attributed to the oxygenated nature of MF aiding in increasing combustion speed and temperature and also aiding to oxidise soot. The reduced particle mass and SA can be attributed to this reduced concentration attained, with a reduced number of particles produced the likelihood of particle interaction decreases, which in turn reduces the likelihood of agglomeration providing reduced particle mass and SA.

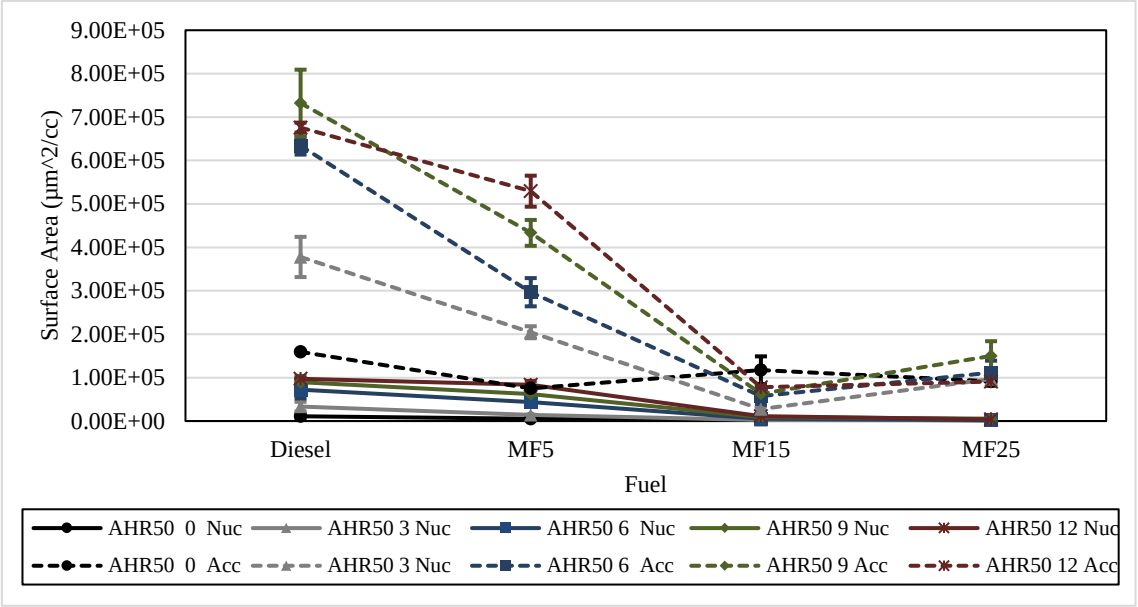

Figure 6-11 AHR50 Sweep Particle Surface Area. Engine Operating at 5 bar IMEP, 1800 rpm, 650 bar IP, 10% EGR.

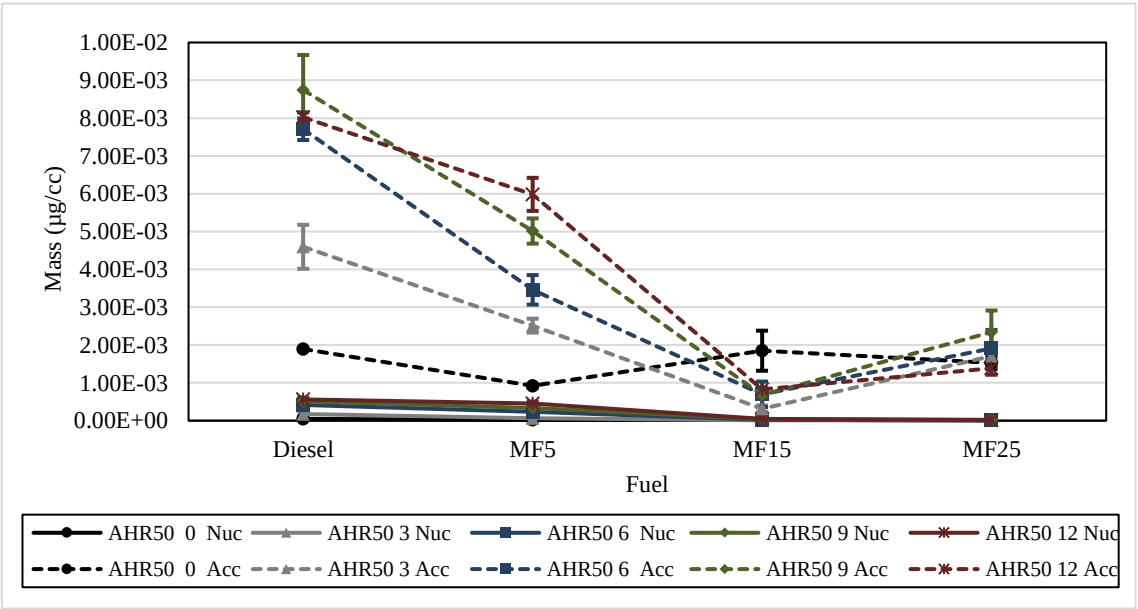

Figure 6-12 AHR50 Sweep Particle Mass. Engine Operating at 5 bar IMEP, 1800 rpm, 650 bar IP, 10% EGR.

Table 6-1 AHR50 Testing SOC, EOC and Combustion Duration Values. Engine Operating at 5 bar IMEP, 1800 rpm, 650 bar IP, 10% EGR.

		SOI (°)	Ignition Delay (°)	AHR10(°)	AHR50(°)	AHR90(°)	Combustion Duration (°)
Diesel	**AHR50 0**	341.00	17.00	358.00	360.00	379.33	21.33
	AHR50 3	344.90	16.10	361.00	363.00	381.00	20.00
	AHR50 6	347.60	15.40	363.00	366.00	383.00	20.00
	AHR50 9	349.80	15.53	365.33	369.00	384.00	18.67
	AHR50 12	351.75	16.25	368.00	372.00	385.67	17.67
	Average	347.01	16.06	363.07	366.00	382.60	19.53
MF5	**AHR50 0**	341.00	17.00	358.00	360.00	379.00	21.00
	AHR50 3	344.90	15.77	360.67	363.00	381.00	20.33
	AHR50 6	346.45	16.55	363.00	366.00	382.00	19.00
	AHR50 9	348.70	16.30	365.00	369.00	384.00	19.00
	AHR50 12	351.58	15.42	367.00	372.00	385.33	18.33
	Average	346.53	16.21	362.73	366.00	382.27	19.53
MF15	**AHR50 0**	338.40	19.60	358.00	360.00	378.33	20.33
	AHR50 3	342.95	18.05	361.00	363.00	379.00	18.00
	AHR50 6	346.15	16.85	363.00	366.00	381.00	18.00
	AHR50 9	348.15	17.18	365.33	369.00	382.67	17.33
	AHR50 12	349.50	17.50	367.00	372.00	385.00	18.00
	Average	345.03	17.84	362.87	366.00	381.20	18.33
MF25	**AHR50 0**	336.30	21.70	358.00	360.00	377.33	19.33
	AHR50 3	341.30	19.70	361.00	363.00	378.00	17.00
	AHR50 6	344.30	18.70	363.00	366.00	380.00	17.00
	AHR50 9	344.90	19.77	364.67	369.00	381.00	16.33
	AHR50 12	345.05	21.28	366.33	371.33	383.33	17.00
	Average	342.37	20.23	362.60	365.87	379.93	17.33

As explained, for most of the experiments as AHR50 was advanced and the MF fraction in the fuel blend increased, the total particle concentration, mass and SA reduced for both modes. However, when comparing the accumulation mode SA and mass in Figure 6-13 and Figure 6-14, it can be seen that the values increased between MF15 and MF25 with the MF25 values increasing as the AHR50 value retarded. By assessing Table 6-1 it can be seen that the average value of ignition delay increased increasing MF fraction; it should also be noted that MF is a more viscous fluid than diesel. Therefore, the increased ignition delay and increased spray penetration length attained from the high viscosity of MF would

result in a higher amount of wall impingement (Ghurri et al., 2012). These quenched particles would not attain complete combustion and would then have the opportunity to interact with one another, leading to larger aggregates, increasing particle mass and SA.

The mass and SA values of the cold EGR testing are shown in Figure 6-13 and Figure 6-14. Again, the MF25 30% EGR values were substantially higher because of the combustion instability and have been omitted from the graphs to allow better comparison between the other test conditions and fuels. For reference, the nucleation and accumulation mode SA was 4E+8 and 1E+6 µm^2/cc, respectively, the mass of the nucleation and accumulation particles were both 1E-02. By comparing the SA and mass values from the cold EGR testing, similar trends were seen. The values decrease as the MF fraction increased; this can be attributed to the oxygen content of MF oxidising soot and reducing particle concentration. This, in turn, reduced particle interaction which would then lead to lower SA and mass values. With the diesel and MF5 fuels, it can also be seen that the general trend is that increasing the EGR ratio increased the mass and SA of both modes, which is expected as the soot oxidation within the cylinder is reduced. However, with MF15 and MF25, it can be seen that increasing the EGR decreased the SA and mass. Figure 6-15 shows the ignition delay and combustion duration of each test condition. It should be noted that this testing was completed at low/medium engine load with high amounts of lambda, and this trend of high EGR and MF blends may change under increased loads and decreased lambda environments.

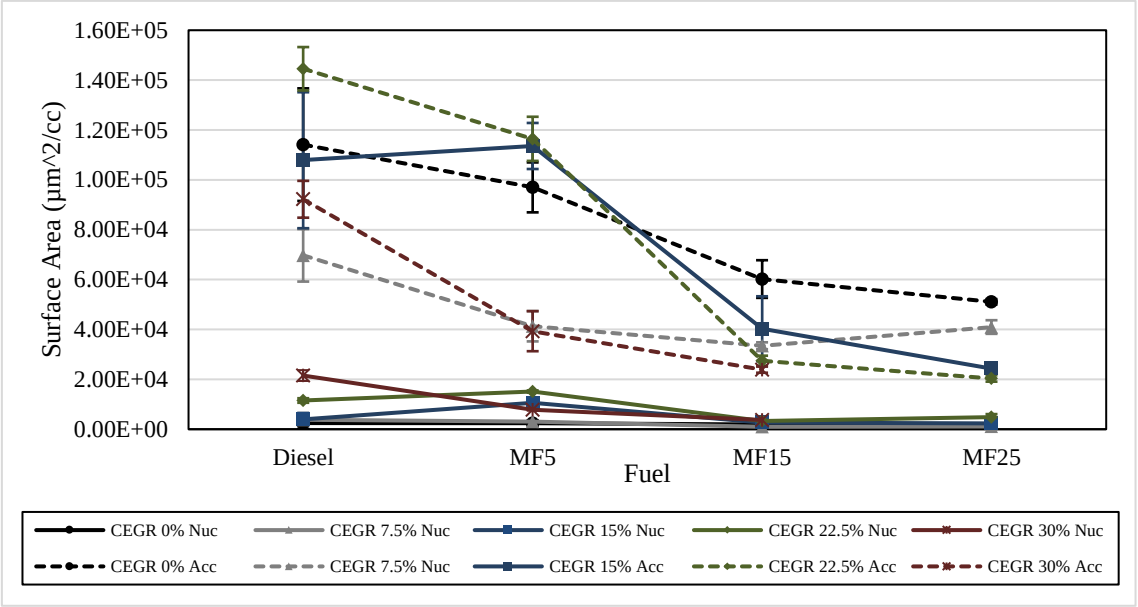

Figure 6-13 Cold EGR Particle Surface Area. Engine Operating at 5 bar IMEP, 1800 rpm, 650 bar IP, 10% EGR.

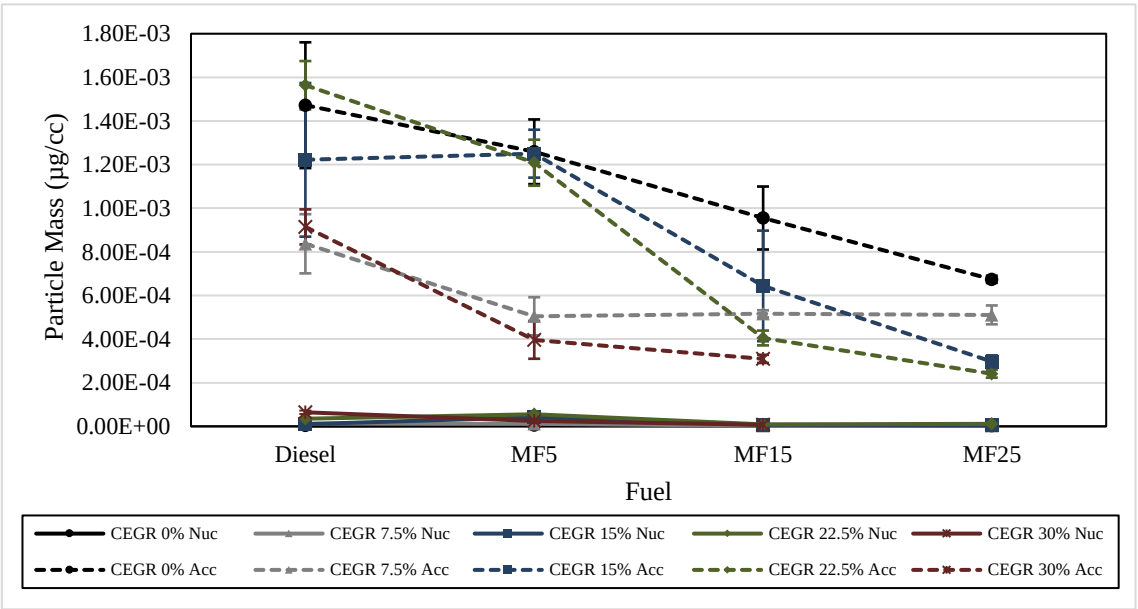

Figure 6-14 Cold EGR Particle Mass. Engine Operating at 5 bar IMEP, 1800 rpm, 650 bar IP, AHR50 8.

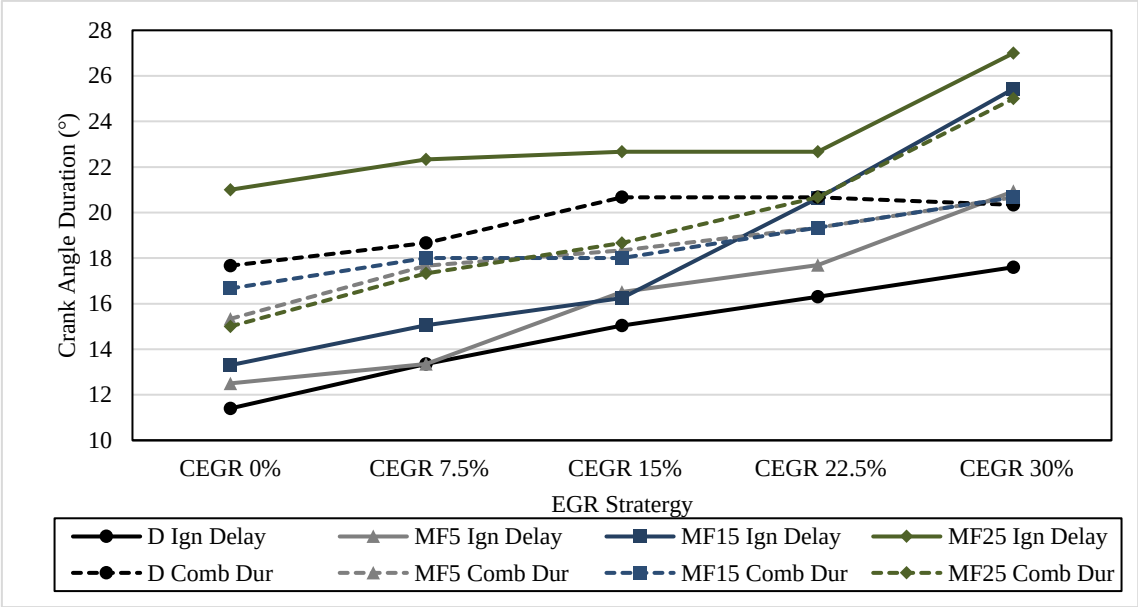

Figure 6-15 Cold EGR Ignition Delay and Combustion Delay. Engine Operating at 5 bar IMEP, 1800 rpm, 650 bar IP, AHR50 8.

6.3.4 Particulate Matter Emissions of MF25 Hot EGR Compared to Neat diesel Cold EGR

From the analysis undertaken in this chapter so far, it has been found that MF can provide reduced particle emissions, however, when using high amounts of CEGR and high MF blends it was found that combustion instability became an issue. To reduce this instability, HEGR was used to increase in-cylinder temperature prior to combustion. This section compares the use of diesel using CEGR to MF25 using HEGR. The purpose of this section is to conclude if MF25 with HEGR can attain lower particle and gaseous emissions, as well as increased overall performance than diesel with CEGR, even though HEGR is known to increase PM.

Figure 6-16 and Figure 6-17 display a comparison of the particle concentration when diesel was tested employing cold EGR and MF25 was used with hot EGR. By assessing the concentration of 0% and 7.5% EGR, it can be seen that there was a negligible difference between the two fuels which can be ascribed to the similarity in manifold

temperature. When comparing the two fuels with increased EGR, it was seen that MF25 was able to provide significantly reduced particle concentration in both modes. Results highlight that the positive aspect of using MF to promote soot oxidation outweighs the negative aspects seen from using hot EGR and reducing in-cylinder gas density, which typically results in increased PM. By comparing the diesel CEGR and MF25 HEGR results in Table 6-2, it can be seen that nearly all of the considered particle characteristics (particle concentration, SA and mass) were reduced when comparing diesel using CEGR and MF25 using HEGR. The overall particle concentration number was reduced by 78.8% with a 83.5% reduction in nucleation mode and a 74.2% reduction in accumulation mode. This in turn, significantly reduced the accumulation mode mass and SA and CMD.

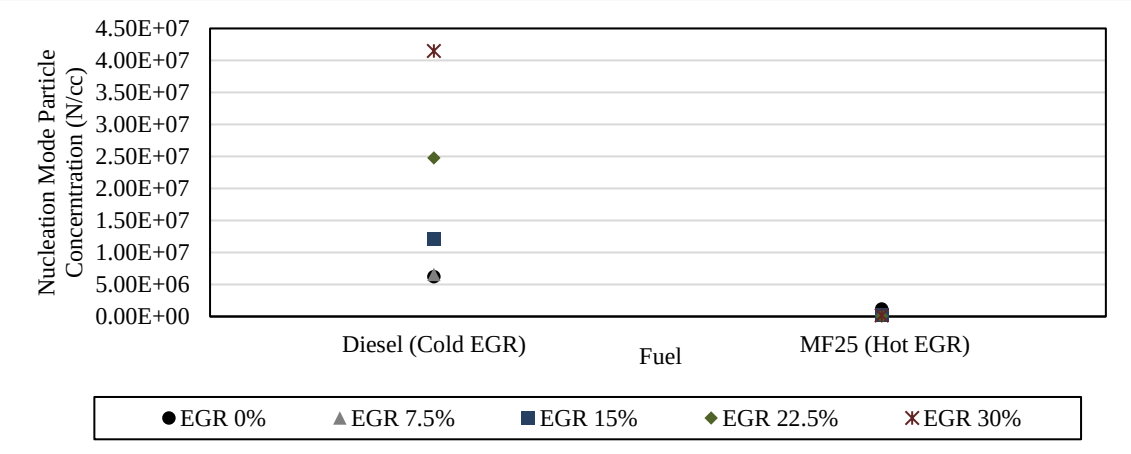

Figure 6-16 Neat Diesel Cold EGR and MF25 Hot EGR Nucleation Comparison. Engine Operating at 5 bar IMEP, 1800 rpm, 650 bar IP, AHR50 8.

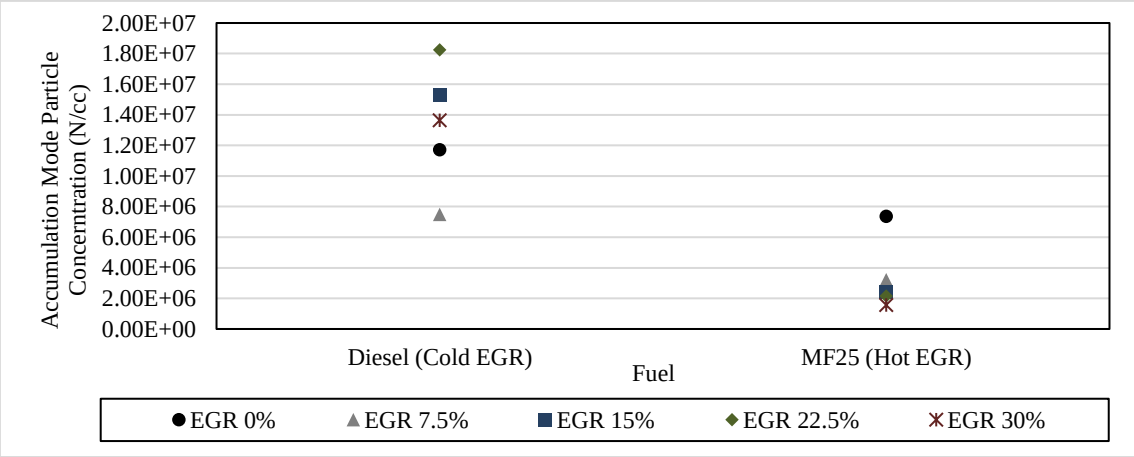

Figure 6-17 Neat Diesel Cold EGR and MF25 Hot EGR Accumulation Comparison. Engine Operating at 5 bar IMEP, 1800 rpm, 650 bar IP, AHR50 8.

Table 6-2 Fuelling and EGR Strategy Particulate Average Value Comparison. Engine Operating at 5 bar IMEP, 1800 rpm, 650 bar IP, AHR50 8.

Fuelling and EGR Strategy	D CEGR Average	MF25 CEGR Average	MF25 HEGR Average
Total Concentration (N/cc)	3.0E+07	1.1E+08	6.36E+06
Overall Count Median diameter (nm)	18.94	17.78	19.3
Nucleation Mode Concentration (N/cc)	1.8E+07	2.1E+00	2.97E+06
Nucleation Mode Count Median diameter (nm)	8.90	10.30	9.49
Nucleation Mode Geometric Standard deviation of diameter	1.63	1.61	1.6
Nucleation mode surface area (µm^2/cc)	8.4E+03	1.8E+05	1.25E+03
Nucleation mode mass (µg/cc)	2.5E-05	1.1E-03	3.46E-06
Accumulation Mode Concentration (N/cc)	1.3E+07	2.6E+07	3.35E+06
Accumulation Mode Count Median diameter (nm)	38.20	41.05	40.02
Accumulation Mode Geometric Standard deviation of diameter	1.69	1.73	1.71
Accumulation mode surface area (µm^2/cc)	1.0E+05	2.6E+05	3.1E+04
Accumulation mode mass (µg/cc)	1.2E-03	3.1E-03	3.84E-04

6.4 Conclusion

In this section, a CI engine was tested with a range of MF/diesel blends, altering a selection of engine parameters. The fuels tested were diesel, MF5, MF15 and MF25. The parameters investigated were AHR50 CA, IP, CEGR and HEGR. Experiments were completed at 5 bar IMEP, 1800 rpm and a single injection strategy was used.

From the particulate matter analysis, it was found that the low cetane number of MF aided in increasing the amount of mixture preparation. This factor coupled with the oxygenated nature of MF resulted in a more homogenous mixture that was able to provide high amounts of soot oxidation throughout the cylinder during combustion. Although all of the various test engine parameters altered the PM produced, it was found that the characteristics of the fuel had the most influence over PM. From the AHR50 testing, it was found that MF5, MF15 and MF25 would aid in reducing total particle concentration by 28%, 82% and 87%, respectively, when compared to the neat diesel values.

By further comparing the results of the AHR50 testing, it was found that the reduced concentration also aided in reducing particle surface area and mass because of reduced particle to particle interaction. The mean MF25 SA and mass values of the AHR50 testing displayed a reduction of 95% and 96% in the nucleation mode and 79% and 71% in the accumulation mode when compared to the diesel mean values.

The cold EGR testing highlighted MF's sensitivity to increased EGR ratio. This found that at high ratios, stable combustion was difficult to attain because of in-cylinder oxygen deprivation and the temperature of the intake gas. In turn, this resulted in high amounts of UHC to be formed, providing unacceptably high amounts of PM at 30% CEGR. To solve this challenge, HEGR was used to increase the intake manifold temperature and increase combustion stability. Although HEGR is known to increase PM by reducing oxygen concentration, the oxygenated nature, low cetane number and high auto-ignition temperature of MF outweighed these factors by increasing the mixture preparation time and the rate of soot oxidation. The use of HEGR also improved the NIMEP COV and the ISFC of MF25. Similar values of ISFC were attained when comparing diesel CEGR and MF25 HEGR results with MF25 attaining improved values of NIMEP COV. The result

of increased combustion stability, in-cylinder temperature and the use of oxygenated fuel resulted in significantly reduced PM, which was lower than the values attained from diesel using CEGR. The use of HEGR and MF25 also provided improved UHC, CO and NO_x values at high EGR ratios with improved values over diesel and MF25 with CEGR. This highlights the suitability of using MF within a CI engine while using HEGR to improve combustion characteristics which in turn reduced the gaseous and particulate emissions.

CHAPTER 7

7. Load Testing with Split Injection Using Furan Fuels mixed with Diesel

7.1 Introduction

This chapter investigates the performance of three biofuel/diesel blends at a range of engine loads. The results of the various biofuel blends were compared against each other and with neat diesel as the baseline fuel.

The results attained from the previous sections highlighted the positive aspects of MF usage, this displayed the necessity to investigate the performance of MF under a broader range of engine operation conditions (e.g. engine load), comparing the performance to diesel and other biofuels. MTHF was also chosen to be investigated in this chapter as it has suitable chemical characteristics for CI use and would allow for a comparison between two furan-based fuels. The third biofuel evaluated was biodiesel; this was selected because it is the conventional CI biofuel choice. Similar to the use of diesel in this section, the use of biodiesel would give useful performance benchmarks to understand whether the use of the furan fuels in a CI engine could provide improved combustion and emission performance to current options.

Keeping the RED incentive in mind and the expectation of 27% of transport fuel to be acquired from renewable sources by 2030, it was decided to use a ratio of 25% biofuel and 75% fossil diesel for the three biofuel blends.

7.2 Experimental Procedure

Tests were completed with the engine set to the conventional 4-cylinder configuration with no separated cylinder. This was chosen as it allowed for multiple injection events to be used, which would allow higher engine loads to be attained. The biofuel/diesel blends were mixed by volume with 300ppm of lubricity improver added to the biofuels before being mixed with diesel.

The loads for the testing were completed at BMEP values of 1.4, 3, 6 and 9 bar with the engine speed fixed to 1800 rpm. These loads were chosen as they fall into the Worldwide Harmonised Light Vehicle Test Procedure (WLTP) load testing region of a typical vehicle equipped with this engine and can allow for future comparison.

To reduce the complexity of the test matrix, it was decided to only include a pilot and main injection event during the experiments. The pilot SOI timing was fixed at 20°BTDC with the pilot volume accounting for 20% of the total fuel injection volume. The main injection event would account for the remaining 80% of the volume and would be altered to provide a constant AHR50 value of 8°ATDC. The EGR and intake pressure were the same for all of the fuels tested but varied for each engine load to simulate real-world conditions. From the experience gained with the MF25 testing in the previous section, it was decided to use HEGR during the 1.4 and 3 bar BMEP engine loads for the biofuels to improve combustion stability. For all other test points, cold EGR was used, including neat diesel testing at 1.4 and 3 bar BMEP as diesel was known to be combustion stable at these loads. The test matrix used for these experiments is shown in Table 7-1 to highlight the various EGR ratios, intake manifold and injection pressures used at each load point.

Table 7-1 Load Testing Experiment Matrix

Test Number	BMEP (bar)	Injection Pressure (bar)	EGR in Intake Manifold (%)	Manifold Pressure (bar)	Pilot SOI (°BTDC)	Pilot Injection Quantity Ratio (%)	AHR50 (°ATDC)	Main Injection Quantity Ratio (%)
1	1.4	600	40 (cold with diesel, hot with blends investigated)	0.95	20	20	8	80
2	3	800	30 (cold with diesel, hot with blends investigated)	0.98	20	20	8	80
3	6	1000	20	1	20	20	8	80
4	9	1200	10	1	20	20	8	80

Before tests were completed, the engine was run until the oil and coolant temperature had stabilised at the set temperatures and the engine had become thermally stable.

7.3 Results

7.3.1 Combustion Performance

Figure 7-1 shows the in-cylinder heat release rate for all the tested fuels at the different loads.

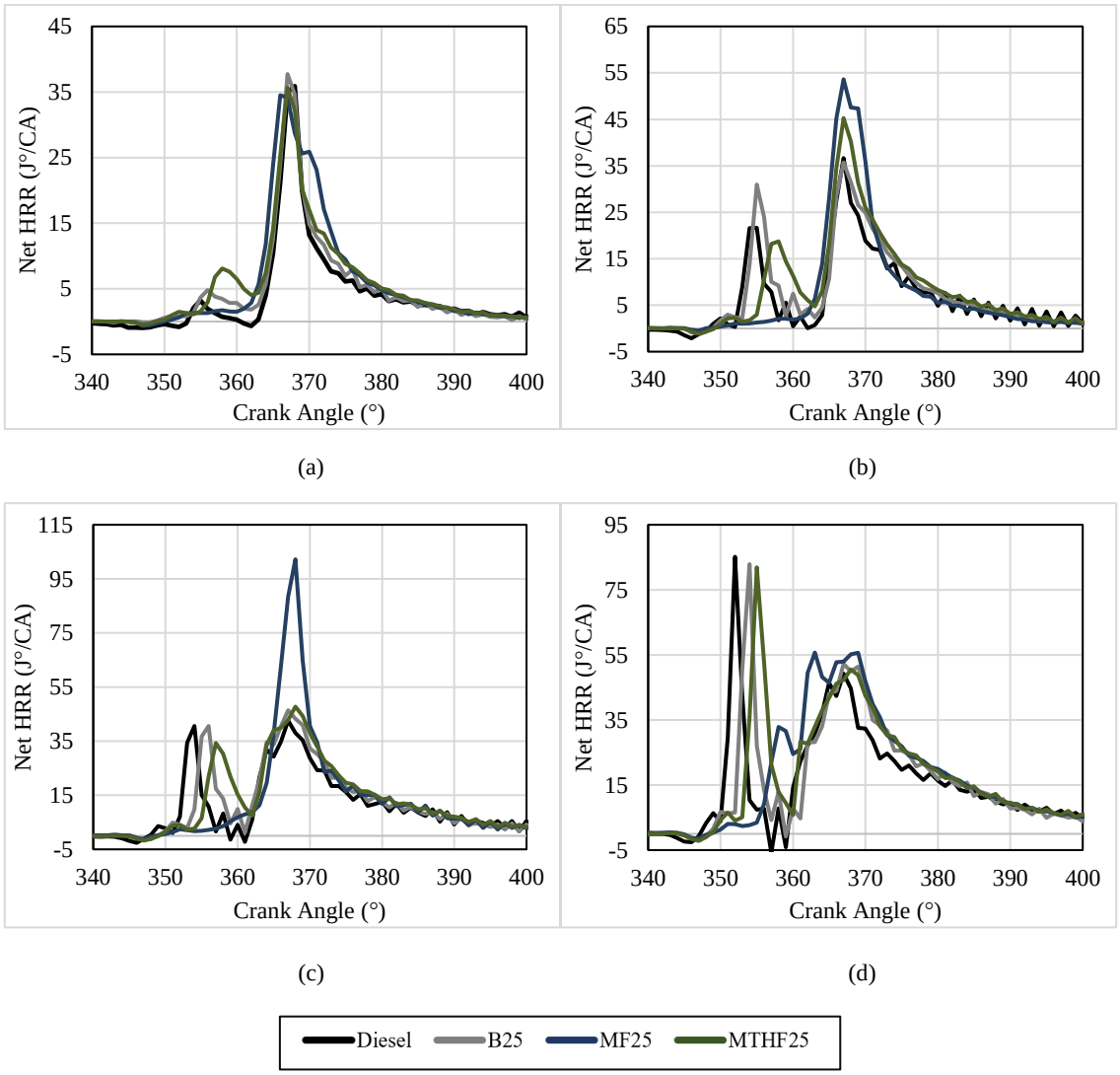

Figure 7-1 Rate of Heat Release. Engine Operating at 1800 rpm. (a) – 1.4 bar BMEP, 600 bar IP, 40% EGR. (b) – 3 bar BMEP, 800 bar IP, 30% EGR. (c) – 6 bar BMEP, 1000 bar IP, 20% EGR. (d) – 9 bar BMEP, 1200 bar IP, 10% EGR.

Unlike the HRR displayed in the SC research chapters, the majority of the graphs shown in Figure 7-1 highlight two separate HRR peaks that can be attributed to the pilot and main injection events used for this testing. It can be seen that MF25 was not able to attain a pilot HRR peak at the three lowest loads. A single HRR peak instead of multiple is considered as a negative characteristic for several reasons. From an in-cylinder pressure perspective, attaining multiple HRR peaks aids in reducing the P-Rate, this is a crucial factor when taking into account in-cylinder noise, vibration and harshness (NVH) as well

as the NO_x emissions generated. P-Rate needs to be considered because of its implications on combustion chamber design, material choice and consumer satisfaction.

From the SC EGR testing, it was found that when using a high amount of EGR, the in-cylinder temperature before combustion played a key role in attaining stable combustion. Higher manifold temperature could be used to increase in-cylinder gas temperature prior to combustion and improve combustion initiation susceptibility. This knowledge was the fundamental reason why HEGR was used for the biofuel blends at the two lower load points, where the high amounts of EGR were being used. As discussed, when using MF25 at the three lowest loads, pilot HRR was not attained. Therefore, and it was necessary to investigate this phenomenon in more detail. Table 7-2 displays a comparison of manifold temperature between the SC and conventional engine configuration. The first two test points displayed in rows 2 and 3 of Table 7-2 show two similar test points, the first being from the load testing, 3 bar BMEP with HEGR, and the second being from the SC HEGR testing. These points had similar engine load, exhaust pre-turbocharger temperature, HEGR ratio and were both fuelled with MF25. However, it can be seen that there was a 30°C reduction of manifold temperature when using the OEM EGR system with the intercooler cooling turned off when compared to the SC using its own HEGR system with no cooling. The reduced manifold temperature and high EGR ratio would be one of the contributing reasons to the lack of pilot HRR seen from the first three loads in Figure 7-1. However, the lack of pilot HRR attained from the 6 bar BMEP load highlights a more predominant reason behind this issue. The last two test cases displayed in Table 7-2 again shows similar operating conditions of the 6 bar BMEP split load condition and SC CEGR operating at 22.5% EGR. There are some differences in the operating conditions, including torque, manifold temperature and EGR ratio, but these differences are in favour

of the 6 BMEP load if manifold temperature and EGR ratio were the only considerations regarding the lack of pilot HRR. These results highlight that manifold temperature is not the most predominant reason regarding the lack of pilot HRR, with other areas including cetane number and latent heat of vaporisation being key characteristics to consider.

For the three lowest load points of the MF25 testing, the SOC CA was 4°ATDC, with the pilot injection beginning at 20°BTDC. Taking this information and the knowledge attained from comparing the load testing to the CEGR and HEGR SC testing, it is apparent that the fuel reactivity and motoring pressure is a crucial area regarding the use of high MF blends within a CI engine. To attain multiple HRR peaks at lower loads with MF25 advanced control techniques would be required, e.g. fresh gas charge heating.

Table 7-2 Comparison Between Temperatures Seen from Hot EGR SC Testing Point and Load Testing Point. Engine Operating at 1800 rpm, AHR50 8.

	Fuel	BMEP (bar)	IMEP (bar)	Injection Pressure (bar)	Torque (Nm)	Exhaust Header Temperature (°C)	EGR in Manifold (%)	Intake Manifold Temperature (°C)
Split	MF25	3	-	800	50.41	269.41	29.34	73.86
Hot	MF25	-	5	650	39.01	266.36	30.83	103.32
Split	MF25	6	-	1000	104.92	269.41	21.74	44.41
Cold	MF25	-	5	650	51.89	248.36	22.03	36.40

An investigation of the pilot injection characteristics was undertaken. Key differences were seen from the pilot HRR with the use of different fuels, and these were most predominant at 9 bar BMEP. Taking this into account, the pilot HRR results were compared and are shown in Table 7-3. For these results, the pilot SOC is defined as the CA at which the HRR becomes higher than 10J/CA, and the pilot end of combustion (EOC) is defined as the following CA where HRR becomes lower the 10J/CA. The pilot combustion of MF25 is displayed but cannot be discussed in the same detail as the other

fuels as the pilot and main HRR peaks merged, removing the possibility to sufficiently characterise the combustion events separately. From the results displayed by the other three tested fuels in Table 7-3, it can be seen that diesel and B25 had the same ignition delay, whereas MTHF25 had an additional 2 CA delay. This can be attributed to the cetane number of MTHF as diesel typically has a cetane value of 52, biodiesel can have a value from 47-52 and MTHF has a value of 15. Table 7-3 also highlights that the pilot combustion duration of B25 was 1 CA longer than diesel and MTHF was 2 CA longer than diesel. The increased duration of pilot combustion resulted in a smaller and delayed maximum pilot HRR values for those fuel blends. This can be attributed to the ignition delay increasing mixture homogeneity. The low cetane number would have also reduced combustion susceptibility, and these two factors can be seen to outweigh the oxygenated nature of MTHF, which would have aided in reducing the pilot combustion duration.

Table 7-3 9 BMEP Pilot Combustion Characteristics. Engine Operating at 1800 rpm, 1000 bar IP, 20% EGR.

Fuel	Pilot SOI (CA)	Pilot Start of HRR (CA)	Pilot Combustion Delay (CA)	Pilot End of HRR (CA)	Pilot Combustion (CA Duration)	Pilot Maximum HRR (J/CA)	Pilot Maximum HRR CA
Diesel	339	352	13	356	4	85.16	353
B25	340	353	13	358	5	82.9	355
MF25	340	359	19	-	-	32.8	359
MTHF25	340	354	15	360	6	81.91	356

As each fuel was tested under the same load conditions, it was possible to compare performance characteristics further and evaluate the effect that the fuel properties had on these areas. These characteristics include the BSFC and BTE, which are shown in Figure 7-2 and Figure 7-3, respectively.

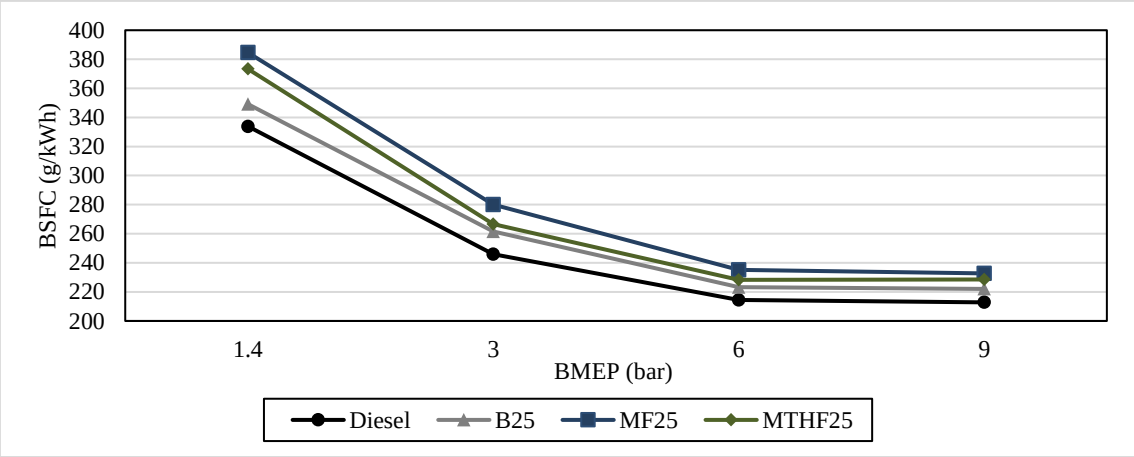

Figure 7-2 BSFC of Tested Fuels During Load Testing. Engine Operating at 1800 rpm. 1.4 bar BMEP - 600 bar IP, 40% EGR. 3 bar BMEP - 800 bar IP, 30% EGR. 6 bar BMEP - 1000 bar IP, 20% EGR. 9 bar BMEP - 1200 bar IP, 10% EGR.

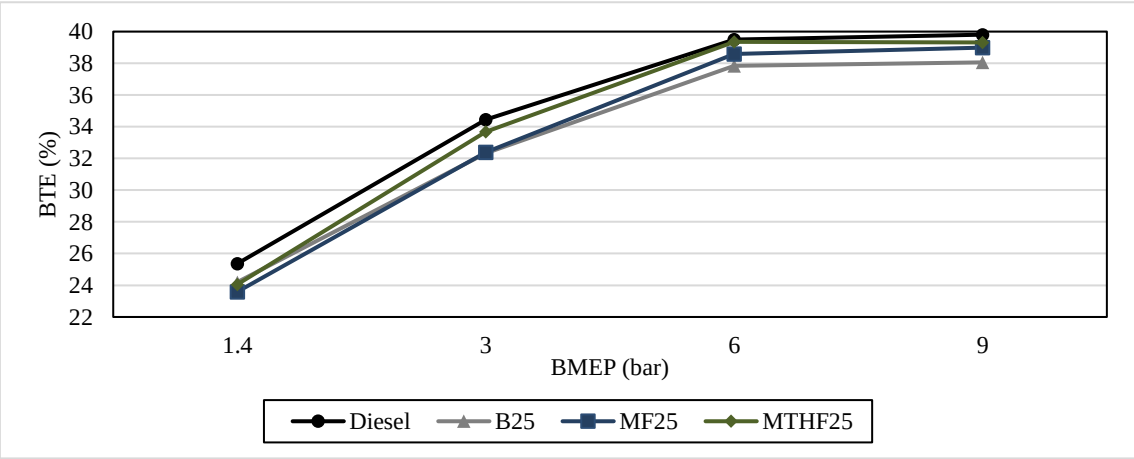

Figure 7-3 BTE of Tested Fuels During Load Testing. Engine Operating at 1800 rpm. 1.4 bar BMEP - 600 bar IP, 40% EGR. 3 bar BMEP - 800 bar IP, 30% EGR. 6 bar BMEP - 1000 bar IP, 20% EGR. 9 bar BMEP - 1200 bar IP, 10% EGR.

By comparing the BSFC results, it can be seen that diesel consumed the lowest amount of fuel and B25 attained the lowest fuel consumption of the biofuel blends. The increased fuel consumption seen from the use of the blends fuel was brought about by their reduced lower heating value, with MF having the lowest value and MTHF having the second lowest of the tested fuels. This increased BSFC is typically expected from biofuels

because it is known that their oxygen content consumes space within their molecular structure but does not provide any calorific value.

Further analysis of BTE (Figure 7-3) is required to understand how efficiently the fuels are combusted, taking into account their differences in heating values. It can be seen how the brake thermal efficiency of diesel fuel is slightly higher than those obtained from the biofuel blends, particularly at low loads. At higher loads, the in-cylinder temperature was higher, increasing MF and MTHF combustion efficiency/susceptibility and reducing the BSFC deficit when compared to the diesel values. B25 produced reduced thermal efficiency throughout the load range when compared to diesel. The two furan fuels were found to produce increased efficiency over biodiesel at higher loads, with the difference becoming more predominant as the load increased.

7.3.2 Gaseous Emissions

The gaseous emissions were investigated to understand further the differences between the performance of the fuels as they play a significant role in highlighting the suitability of a fuel for road use. The $BSNO_x$ emissions are shown in Figure 7-4, which highlights the general trend of the biofuel blends producing reduced $BSNO_x$ over neat diesel at high engine load. As discussed in the previous sections, $BSNO_x$ formation is directly linked to local equivalence ratio and combustion temperature. In the combustion section, the MF25 blend was unable to attain a pilot combustion until the highest load. This lack of pilot combustion did increase the ignition delay for the main combustion event. This highlights that the HRR attained was closely relatable to CDC combustion with a single combustion phase resulting in a substantial rise in HRR. This created higher in-cylinder temperature and NO_x for MF25 at 3 and 6 bar BMEP. At the two highest loads, it can be seen that B25 and MTHF25 produce lower $BSNO_x$ than diesel. This can be accredited to the lower

reactivity of the fuels increasing the ignition delay of the pilot combustion and increasing the mixture homogeneity. This resulted in a reduced max HRR value and also reduced the pilot P-Rate aiding in reducing the $BSNO_x$.

It should also be noted that the use of HEGR for the blend fuels with the two lowest load points will have aided in increasing the NO_x formation for all biofuel blends. However, when CEGR was employed at 6 and 9 bar BMEP, only one fuel at one load point emitted higher NO_x than diesel (MF25 at 6 bar BMEP). This highlights that an additional investigation into the optimal EGR strategy of biofuel/diesel blends at low loads would be advantageous.

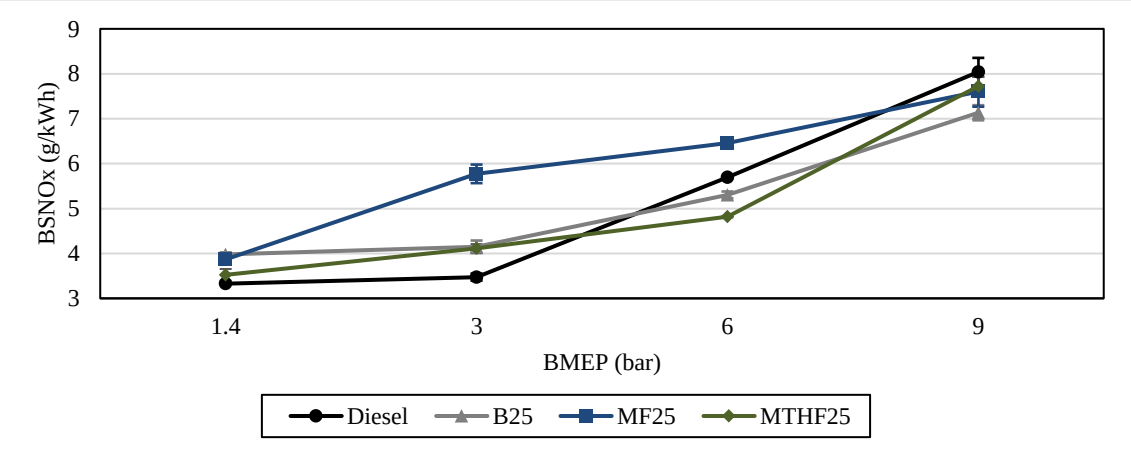

Figure 7-4 $BSNO_x$ of Tested Fuels During Load Testing. Engine Operating at 1800 rpm. 1.4 bar BMEP - 600 bar IP, 40% EGR. 3 bar BMEP - 800 bar IP, 30% EGR. 6 bar BMEP - 1000 bar IP, 20% EGR. 9 bar BMEP - 1200 bar IP, 10% EGR.

Similar to the $BSNO_x$ emissions, the BSCO and BSUHC produced show promising results for biofuel/diesel blends at higher loads when compared to diesel. When considering the three gaseous emissions at the low loads, the results attained by diesel highlight the positive aspects of the fuel by attaining relatively low values of the monitored emissions. The furan-based fuels were seen to perform particularly poorly because of their combustion instability brought about by the low cetane number of the

fuels. At the high load points, the BSUHC and BSCO of the furan fuels were similar to that of diesel while being able to produce lower $BSNO_x$ values, which is considered one of the more significant concerns regarding CI engines.

The BSCO emissions and combustion efficiency are displayed in Figure 7-5 and Figure 7-6, respectively. Results show a decrease in combustion efficiency of MF25 at the lowest load. At this point, the combustion efficiency is significantly reduced mainly due to the cetane number latent heat of vapourisation and auto-ignition temperature of the fuel, despite the use of HEGR to overcome this. The lack of pilot HRR at this load would have also increased the BSCO formation by increasing ignition delay and wall impingement. The two furan fuel blends were seen to consistently produce reduced combustion efficiency over diesel at each load point. This can mainly be attributed to the cetane number of the two fuels allowing the flame fronts to be quenched prematurely as they moved towards the boundary of the combustion chamber. B25 was seen to provide the lowest CO of all the fuels tested throughout the load range. As discussed in the literature review, CO is mainly produced when incomplete combustion is attained. Biodiesel has a cetane number similar to diesel while also being oxygenated. By using this in a mixture with diesel, it resulted in a fuel that has similar cetane number as diesel while providing additional oxygen to the combustion process, resulting in an environment where the complete combustion process has a higher chance of success, providing reduced BSCO formation.

Bearing the effects of complete combustion in mind, the performance of the fuels in reference to the BSUHC emitted is displayed in Figure 7-7, this reinforces the points discussed concerning the cetane number of fuels, and the effect oxygenated fuels can have on the fuel conversion process during combustion.

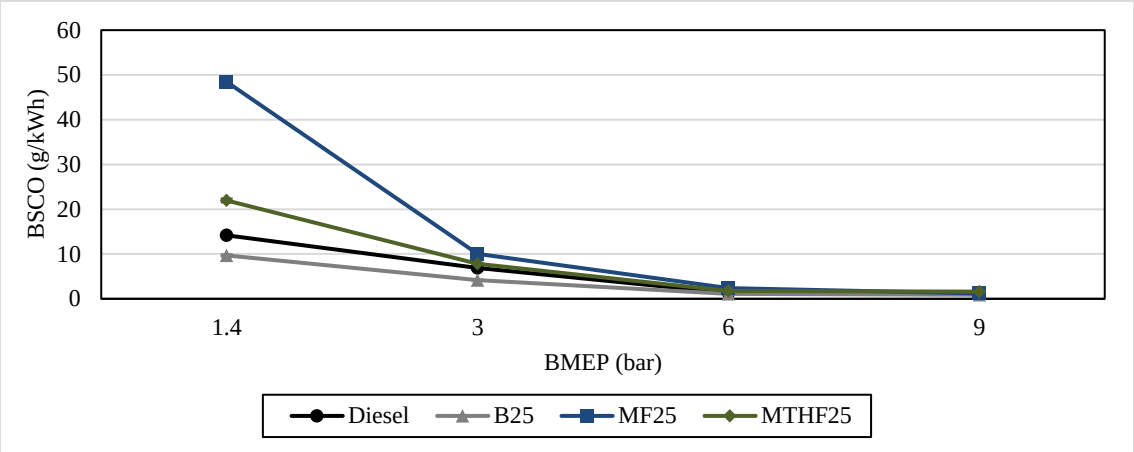

Figure 7-5 BSCO of Tested Fuels During Load Testing. Engine Operating at 1800 rpm. 1.4 bar BMEP - 600 bar IP, 40% EGR. 3 bar BMEP - 800 bar IP, 30% EGR. 6 bar BMEP - 1000 bar IP, 20% EGR. 9 bar BMEP - 1200 bar IP, 10% EGR.

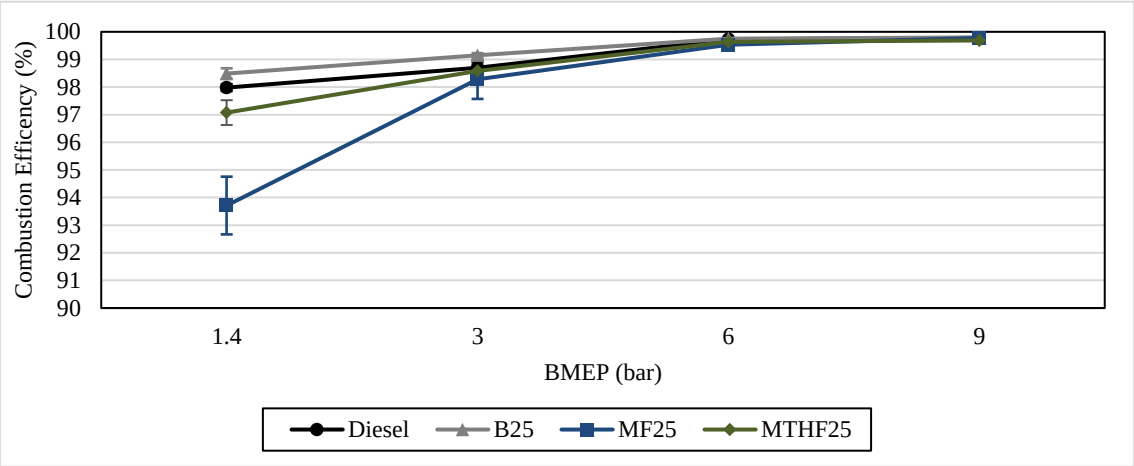

Figure 7-6 Combustion Efficiency of Tested Fuels During Load Testing. Engine Operating at 1800 rpm. 1.4 bar BMEP - 600 bar IP, 40% EGR. 3 bar BMEP - 800 bar IP, 30% EGR. 6 bar BMEP - 1000 bar IP, 20% EGR. 9 bar BMEP - 1200 bar IP, 10% EGR.

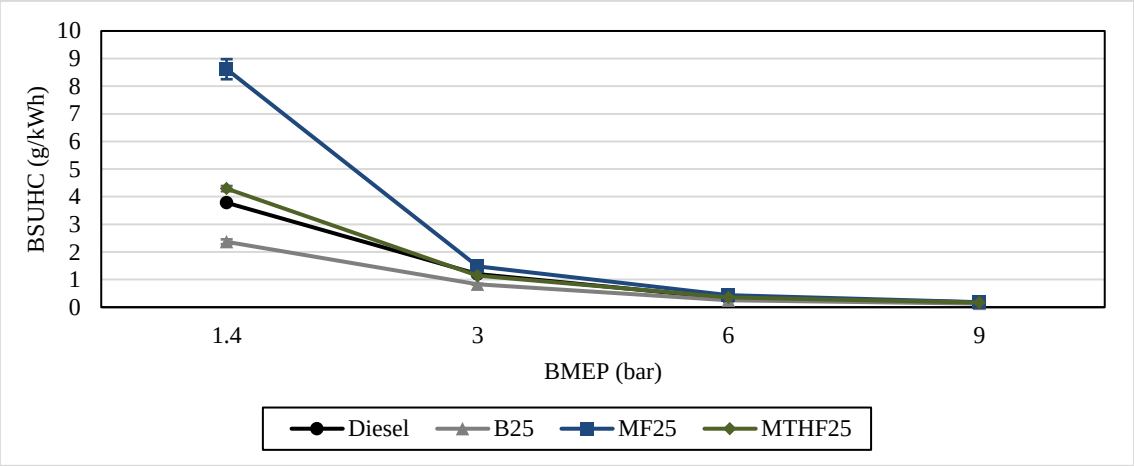

Figure 7-7 BSUHC of Tested Fuels During Load Testing. Engine Operating at 1800 rpm. 1.4 bar BMEP - 600 bar IP, 40% EGR. 3 bar BMEP - 800 bar IP, 30% EGR. 6 bar BMEP - 1000 bar IP, 20% EGR. 9 bar BMEP - 1200 bar IP, 10% EGR.

Overall, B25 was the most successful blend fuel investigated when considering the gaseous emissions. It provided slightly increased NO_x values at the two lower load points while providing reduced values at the two higher load points. However, the CO and UHC produced by B25 were consistently lower than diesel through the test points, highlighting the benefits that biofuels can provide regarding gaseous emission and CI engine use.

7.3.3 Particulate Emissions

As with gaseous emissions, particulate emissions are a crucial area when evaluating the performance of a fuel and should be considered when assessing the suitability of an alternative fuel.

The particle size distribution of the fuels under the tested load conditions is shown throughout Figure 7-8. The main observation attained from these graphs is that there is an overall increase in particulates as the load is increased, this is attributed to the additional fuel injection volume required to attain higher loads, and thus the additional carbon injected into the combustion chamber. Overall, the performance of the fuels at the

loads highlighted that MTHF25 typically attained lower particle concentration values with respect to the diesel and B25 particle levels, with MTHF25 9 bar BMEP attaining higher values. MF25 was able to consistently attain the lowest particle size concentration values.

Oxygenated fuels provide additional oxygen during the premixed combustion phase, reducing the oxygen-deprived combustion regions, decreasing particle emissions by promoting fine fuel/air mixing, in turn, this increases the amount of nucleation seen. Table 7-4 displays the nucleation and accumulation mode concentration along with the nuc/acc ratio of each fuel at the load points. The table highlights that at the two lowest load points, the three blend fuels obtained increased nucleation values when compared to the performance of diesel, while at the two higher loads B25 and MF25 saw a decrease in their nucleation/accumulation ratio. The increased ratio of nuc/acc at the two lower loads can be accredited to the amount of available oxygen within the cylinder during combustion, and the additional soot oxidation available from the use of the biofuels, both mainly reducing accumulation particles. In Figure 7-8a and Figure 7-8b an increase in nucleation can be seen from B25 at <5nm at 1.4 and 3 bar BMEP. This increase could be encouraged by two possible reasons. Firstly, biodiesel has an increased viscosity and lower volatility than diesel which could result in air entrainment reducing, producing increased SOF. Secondly, the oxygenated nature of biodiesel may cause carbonaceous particles to change from fine to ultra or nano-particles (Helmantel, 2008).

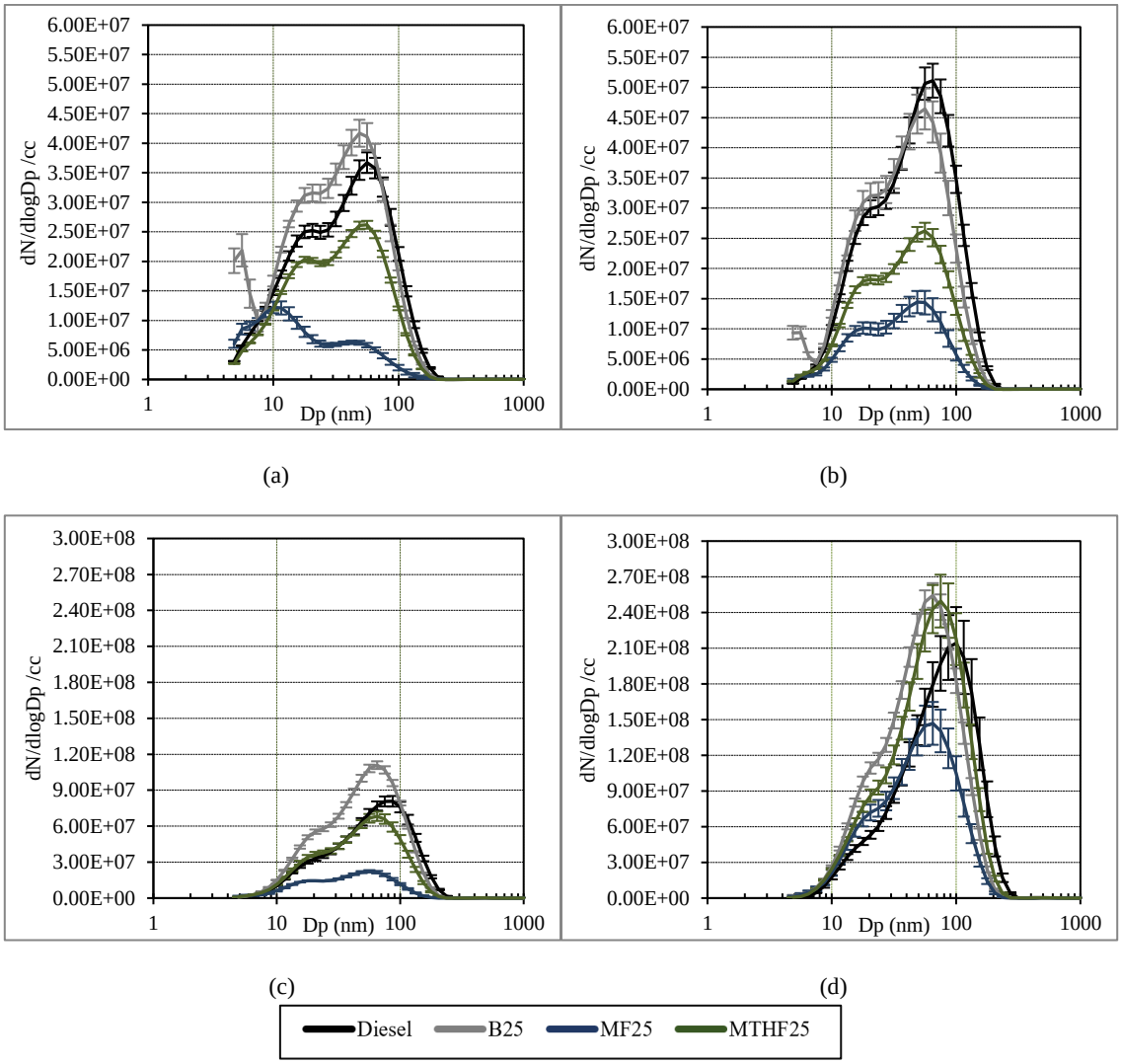

Figure 7-8 Particle Size Spectral Density. Engine Operating at 1800 rpm. (a) – 1.4 bar BMEP, 600 bar IP, 40% EGR. (b) – 3 bar BMEP, 800 bar IP, 30% EGR. (c) – 6 bar BMEP, 1000 bar IP, 20% EGR. (d) – 9 bar BMEP, 1200 bar IP, 10% EGR.

.

Table 7-4 Particle Properties Attained From Testing Different Fuels under Various Loads. Engine Operating at 1800 rpm. 1.4 bar BMEP - 600 bar IP, 40% EGR. 3 bar BMEP - 800 bar IP, 30% EGR. 6 bar BMEP - 1000 bar IP, 20% EGR. 9 bar BMEP - 1200 bar IP, 10% EGR.

BMEP Load (bar)	Fuel	Total Concentration (N/cc)	Total Concentration Reduction Over Diesel at Load Point (%)	Nucleation Mode Concentration (N/cc)	Accumulation Mode Concentration (N/cc)	Nucleation / Accumulation Ratio	**Nuc** Mode CMD Reduction Over Diesel at Load Point (%)	Acc Mode CMD % Reduction Over Diesel at Load Point (%)	Nuc Mode SA Reduction Over Diesel at Load Point (%)	Acc Mode SA Reduction Over Diesel at Load Point (%)	Nuc Mode Mass Reduction Over Diesel at Load Point (%)	Acc Mode Mass Reduction Over Diesel at Load Point (%)
1.4	Diesel	3.27E+07	0	6.03E+06	2.27E+07	0.27	0	0	0	0	0	0
1.4	B25	3.83E+07	-17.13	1.06E+07	2.54E+07	0.42	9.76	6.12	-48.93	13.13	-44.44	24.32
1.4	MF25	9.97E+06	69.51	6.59E+06	3.47E+06	1.9	30.31	5.66	45.65	88.80	60.91	90.68
1.4	MTHF25	2.39E+07	26.91	8.55E+06	1.41E+07	0.6	-7.04	-4.82	-63.88	46.09	-76.19	53.15
3	Diesel	4.07E+07	0.00	5.70E+06	2.83E+07	0.2	0.00	0.00	0.00	0.00	0.00	0.00
3	B25	3.86E+07	5.16	1.23E+07	2.39E+07	0.52	25.29	1.82	-29.53	33.08	-1.94	42.31
3	MF25	1.20E+07	70.52	3.82E+06	7.31E+06	0.52	32.95	5.17	68.32	81.94	78.08	85.55
3	MTHF25	2.18E+07	46.44	5.95E+06	1.54E+07	0.39	24.66	12.01	36.91	61.12	50.46	65.97
6	Diesel	6.22E+07	0.00	1.58E+07	3.62E+07	0.44	0.00	0.00	0.00	0.00	0.00	0.00
6	B25	8.27E+07	-32.96	1.39E+07	6.60E+07	0.21	10.63	28.29	42.71	-8.65	55.77	0.57
6	MF25	1.81E+07	70.90	4.10E+06	1.27E+07	0.32	28.85	32.99	88.09	83.08	92.11	86.17
6	MTHF25	5.27E+07	15.27	2.06E+07	2.72E+07	0.76	4.07	5.99	-10.68	40.48	-0.85	47.37
9	Diesel	1.52E+08	0.00	2.20E+07	9.93E+07	0.22	0.00	0.00	0.00	0.00	0.00	0.00
9	B25	1.83E+08	-20.39	1.39E+07	1.55E+08	0.09	-16.59	33.27	0.00	20.94	-35.85	33.12
9	MF25	1.11E+08	26.97	1.16E+07	9.57E+07	0.12	6.48	37.00	45.13	52.80	38.87	58.95
9	MTHF25	1.77E+08	-16.45	4.05E+07	1.15E+08	0.35	-5.63	9.40	-147.88	14.45	-203.40	24.88

Diesel and biodiesel are not fixed chemical formulas, but they do have accepted ranges. For biodiesel, this range is brought about from the various production methods and feedstocks that can be used, this results in carbon ranges from C12-24 (Chen et al., 2013). Further reading of biodiesel production methods highlighted that a likely formula for the biodiesel used would be $C_{19}H_{35}O_2$ (Barabás and Todoruţ, 2011). Shell fuels provided the normalised C, H and O values for the diesel provided, these were 1, 1.883 and 0.059, respectively, by using these ratios it was possible to determine that the likely chemical formula of the diesel supplied was $C_{17}H_{32}O$.

By assessing the size spectral density results of the B25 and diesel testing it can be seen that B25 typically attained a higher number of particles at each monitored size range and this can be accredited to a selection of properties. The first property is the additional length of the biodiesel chain compared to diesel. This increased length is a known characteristic to increase PM production (Mohankumar and Senthilkumar, 2017). Although biodiesel is oxygenated, the chemical formula above also displayed an increased carbon content which is known to enhance soot formation. This increase of carbon is seen to outweigh the oxidation that would be available from the use of biodiesel, again increasing the PM seen in Figure 7-8 (Mohankumar and Senthilkumar, 2017). Although the chemical structure of the diesel and biodiesel tested are not known, it is also worthwhile highlighting that an increase in double bonds within a chemical structure will also increase PM formation so this may have also been a factor as the formula of biodiesel is known to typically have a higher amount of double bonds over fossil diesel (Wang et al., 2016).

Similar to the results attained in the previous particulate matter research chapter, the use of MF attained significantly reduced PM throughout the measured range when compared to diesel at each load point. It can also be seen that MTHF was typically able to attain reduced values over diesel but not to the same extent as MF. MF and MTHF have very similar chemical formulas and properties, but a selection of small differences would have contributed to MF's additional PM reduction. As described within the biodiesel discussion, longer fuel chains, and additional carbon molecules promote PM, as does the use of ring structure over chains (Mohankumar and Senthilkumar, 2017). When compared to diesel, MF and MTHF have a significantly reduced number of molecules, 12 and 16, respectively. Although furan fuels are ring structures, it can be seen that they have a heavily reduced number of molecules which can be seen to outweigh the negative of using a ring structure as significant PM reductions were seen with the furan fuels. The higher cetane number of MTHF with respect to MF highlights reduced BSCO and BSUHC formation over MF, which would suggest reduced PM emissions via increased combustion efficiency. However, the chemical structure of MTHF has more of an influence over the PM generation than the cetane number. C/H ratio is known to be a critical factor regarding PM formation with formation typically increasing as C/H ratio increases (Mohankumar and Senthilkumar, 2017). The significant chemical difference between MF and MTHF is the additional hydrogen within MTHF; this results in MTHF having a lower C/H ratio than MF. Fuels with higher C/H ratios are known to increase PM by decreasing the oxidation rate of OH radicals (Takahashi and Glassman, 1984). However, the reduction of hydrogen in MF results in less double bonds being seen within the chemical structure, which is known to inhibit soot oxidation (Ruwe et al., 2018). The reduced size of MF would also mean that more MF molecules would be used to attain the

same injection volume of MTHF. This would result in more MF molecules and more oxygen being in the volume; this is one of the key areas that would be providing the reduced PM. By evaluating the PM results seen between MF and MTHF, it can be concluded that the increased oxygen was more influential over reducing PM than the lower C/H ratio of MTHF as well as the double bonds attained from the reduced hydrogen content of MF.

The data displayed in Table 7-4 highlights that B25 attained a higher number concentration than diesel under three of the loads, this increase in particle number resulted in an increase in nucleation surface area which then increased the nucleation particle mass. At the lowest and highest load, the CMD of MTHF25 nucleation mode particles was seen to be larger than the diesel values; this resulted in MTHF25 nucleation particles also attaining a significant increase in SA and mass. Overall MF25 produced the most favourable results while consistently reducing particle concentration and CMD in both modes, this, in turn, resulted in greatly reduced SA and mass.

7.4 Conclusion

From the completed testing in this research section, it can be seen that using furan-based fuels as an additive with diesel in a CI engine can draw a selection of benefits.

Loads tests at 1.4, 3, 6 and 9 bar BMEP and an engine speed of 1800 rpm were completed investigating two furan fuels, MF and MTHF, mixed with diesel. The results were compared to diesel and a biodiesel blend to provide a reference point to the furan blends fuel performance. The blend ratio used for this testing was 25% by volume and split injection with a pilot and main injection event was used to attain high engine loads safely. The EGR was set at 40,30, 20 and 10% at loads 1.4, 3, 6 and 9 bar BMEP, respectively,

and HEGR was used for the two lowest loads when the engine was fuelled with the blend fuels.

By analysing the combustion performance of the fuels under the various loads, it was found that MF25 was very sensitive to combustion at low load and was not able to attain a pilot combustion at the three lowest loads. The single combustion event attained during the MF25 6 bar BMEP testing resulted in an in-cylinder pressure that was 0.5MPa higher than the diesel value. The in-cylinder performance of B25 and MTHF25 were very similar to that of neat diesel, as the pilot injection timing was fixed it was possible to evaluate the ignition delay between the fuels, this found that B25 did attain a slight increase of ignition delay over diesel and MTHF25's delay was even more pronounced than that of B25. This can be accredited to the slightly lower cetane number of biodiesel and considerably lower cetane number of MTHF resisting combustion initiation.

By assessing the fuel consumption, load and fuel heating value of the fuels, it was possible to find the BTE and BSFC. Diesel had the highest lower heating value and attained the lowest fuel consumption at each load point resulting in diesel attaining the highest BTE and lowest BSFC at each point. By reviewing Figure 7-2 and Figure 7-3, it can be seen that the BTE and BSFC values began to plateau at 6 bar BMEP, the increased efficiency of BTE means that there were reduced fuel losses and therefore the fuel being injected was being utilised to a greater extent. The plateau highlighted that without additional control techniques, the BSFC and BTE would not dramatically change past 6 bar BMEP.

Overall, the gaseous emissions highlighted poor furan blend performance at low load. At 1.4 bar BMEP, MTHF had a 1% reduction in combustion efficiency, whereas MF25 had a 4% reduction when compared to the diesel performance. This can be attributed to the

cetane numbers of the fuel blends used and the in-cylinder temperature prior to combustion as the combustion efficiency of the furan blend fuels dramatically improved a 3 bar BMEP. The combustion efficiency attained by the furan blends had a similar performance to diesel at 6 and 9 bar BMEP. The reduced cetane number meant that combustion was more challenging to initiate and more susceptible to premature quenching. Biodiesel was found to have an improved combustion efficiency over diesel throughout the load range. This can be attributed to biodiesel having a similar cetane number to diesel while being able to provide oxygen during the combustion process and improving the likelihood of attaining more complete combustion at the local regions of combustion and towards the cylinder perimeter. As expected, the BSCO and BSUHC trends were similar to the combustion efficiency but inversed. At low load, the furan fuels emitted high amounts of CO and UHC, but past 6 bar BMEP, all fuels emitted similar values with B25 consistently being the lowest emitting fuel of both emissions. When considering the NO_x, it was found that all of the biofuels had increased NO_x formation at lower loads when compared to diesel but provided a reduction at the two highest loads, except MF25 at 6 BMEP which can be attributed to the lack of pilot combustion and high in-cylinder pressure attained from the single combustion event. The purpose of pilot injection was to improve mixture homogeneity and reduce HRR peaks.

The particulate matter emissions presented positive results for the furan-based blends. It was anticipated that the increased oxygen content of the biofuels would increase the soot oxidation. However, the increased length and complexity of the biodiesel molecule resulted in increased PM emissions in the nucleation and accumulation mode, which in turn increased the particle mass and surface area. Bearing the oxygen content in mind, biodiesel also had the lowest oxygen content of the three biodiesels so the effect of soot

oxidation with B25 would have been the lowest out of all the biofuel blends. The reduced complexity and length of the furan-based fuels greatly aided in reducing the particulates when compared to diesel, these fuels were able to attain lower particle concentrations in both the nucleation and accumulation mode, which reduced the mass and SA of the particles. It was found that MF25 was also able to emit lower particle concentration over MTHF25 as MF have a reduced number of double bonds.

Overall, the load testing displayed that many benefits can be attained from the use of furan-based fuels with diesel in a CI engine. When comparing B25 and diesel, it was found that B25 could provide similar in-cylinder performance with reduced gaseous emissions. However, the particulate emissions were found to increase, which highlights that this blend is not an ideal candidate to replace the use of neat diesel. It was found that MF25 could produce greatly improved PM results, but the cetane number of MF provided poor low load combustion performance which in turn produced poor gaseous emission qualities. MTHF25 was found to perform to the highest standard when compared to the overall diesel performance. MTHF25 was able to provide similar in-cylinder performance qualities to diesel while providing reduced gaseous emissions at high loads and reduced particulate emissions throughout the load range.

CHAPTER 8

8. Summary, Conclusions and Future Work

The research undertaken in this thesis focussed on using biofuels and diesel blends within an automotive compression ignition engine. Furan based fuels were the main research area with 2-methylfuran being the focus point of this research and an additional investigation taking 2-methyltetrahydrofuran into account. The research consists of four major sections to understand the suitability of the furan-based fuels in reference to current diesel fuel and the anticipated biofuel/diesel blend that will be used in the future if a more suitable alternative is not found. This chapter provides an overview of the significant findings of each of the four sections along with an additional section discussing suitable future work taking the results of this thesis into account.

8.1 Summary

Testing was completed on a four-cylinder compression ignition engine with a displacement of 2.2l. The engine was equipped with a VNT, common rail injection system and HPEGR. For some tests, the engine was operated in a conventional manner with all four cylinders being fuelled with the same fuel via the onboard common rail system, for other tests a novel engine configuration was designed. The unique configuration separated the gas flow and fuel injection of a single-cylinder so that it could operate with separate fuelling from an off-board common rail system, the separated cylinder also had its own HPEGR system.

Overall, this thesis used a statistical analysis of a single MF/diesel blend (MF10) to conclude the suitability of in-depth testing and the possible benefits attainable in comparison to neat diesel use. Further testing investigated the performance of MF5,

MF15 and MF25 when altering the AHR50 CA, injection pressure, CEGR and HEGR values individually in sweep tests. These found that as the MF fraction increased the ignition delay, ISUHC, ISCO, $ISNO_x$ and ISFC increased while the particle concentration mass and SA of both nucleation and accumulation mode particles reduced. The CEGR sweep testing highlighted MF's sensitivity to manifold temperature. The use of high MF blends and HEGR was compared to diesel performance with CEGR and highlighted similar in-cylinder results, with MF25 still being able to attain reduced PM, ISCO and ISUHC with similar $ISNO_x$ values. Further load testing was completed assessing the performance of MF25, MTHF25, B25 and diesel at various engine loads. The in-cylinder results found B25 and MTHF25 to perform similarly to diesel, but with an additional pilot ignition delay, MF25 was found to be unable to attain a pilot HRR at low loads producing a single combustion event rather than a pilot and main heat release event. The gaseous emissions results found MF to typically attain higher BSCO, BSUHC and $BSNO_x$ over diesel throughout the load range. MTHF25 was found to attain marginally higher BSCO, BSUHC and $BSNO_x$ than diesel at the two lowest load points with the gaseous emissions becoming lower than diesel at the two highest load points. At the high load points, all B25 emissions were lower than diesel. For the particulate matter, the general trends found B25 to produce marginally higher particle concentration at each measured point, typically MTHF25 produced marginally lower concentrations and MF25's concentration was considerably lower than the diesel results.

The overall findings of this thesis have demonstrated the success of using statistical analysis. The in-depth testing completed on MF demonstrated a large reduction in PM formation but higher gaseous emissions and fuel consumption highlight that it is not suitable to use blends of diesel and MF within a CI engine without using another fuel or

advanced control techniques to improve performance. The load testing highlighted that there were PM benefits attainable from using MTHF within a CI engine with reduced gaseous emissions being attained when compared to diesel at high loads. The results demonstrate that further in-depth testing with MTHF/diesel blends would be highly beneficial.

8.2 Conclusions

A summary of the experimental findings for each research chapter will be discussed in the following section.

8.2.1 Statistical Analysis of a 2-Methylfuran and Diesel Blend

The literature had highlighted some favourable fuels characteristics for using MF as a blend within a CI engine. As there was little knowledge about this area it was decided to complete a statistical analysis of a single fuel blend to evaluate if any benefits could be attained from using MF as a fuel component with diesel fuel over using neat diesel, the blend chosen was MF10 as this ratio fell in line with the RED EU biofuel blend ratio incentive.

The statistical analysis that was used focussed on the different engine inputs, SOI, IP and EGR, each at three different settings, e.g. SOI at 7.5, 10 and 12.5°BTDC. Tests were completed with the engine operating as a conventional four-cylinder engine operating a 1.4 bar BMEP using a single injection per combustion event. A systematically reduced test matrix was used to monitor the effects on three outputs, NO_x, soot and BTE. Signal-to-Noise ratio analysis was then completed to characterise the importance of each input on each output and also to find what engine settings would provide the optimum engine condition for each output.

Further analysis provided quantitative data about the importance of each input; the data allowed for an overall optimum point to be found to satisfy all of the outputs simultaneously. The test condition was then run with MF10 and also with neat diesel so that the performance of the fuels at this condition could be compared. The results found that the lower cetane number of MF increased the ignition delay and reduced the maximum in-cylinder pressure by 0.85 bar; this reduced pressure reduced the $BSNO_x$ formation by 17.24%. However, the delay and cetane number also decreased combustion efficiency by 1.12%. This reduced combustion efficiency and reduced lower heating value of MF increased the BSFC by 4.3% with both factors increasing the BSCO and BSUHC by 33% and 47%, respectively. It was found that MF10 had a reduced particle concentration number of 30% and 59% in the nucleation and accumulation mode. The particle reductions can be ascribed to the cetane number and oxygen content of MF increasing mixture preparation and enhancing the precursor and particle oxidation rate.

8.2.2 Gaseous Emission Behaviour of 2-Methylfuran and Diesel Blends

The statistical analysis research chapter highlighted that there are positive aspects to the use of MF within a CI engine, and a thorough investigation was required to understand possible ways to overcome the negatives aspects. This research chapter completed investigations altering a single engine condition at a fixed load. This was undertaken with various MF/diesel blends to understand the effect that the parameter alterations had the on gaseous emissions of the various fuel blends. The fuels blends investigated were 5, 15 and 25% MF (b/v) and the engine parameters evaluated were AHR50 CA, IP, CEGR and HEGR. The test load was fixed at 5 bar IMEP with a single injection and tests were completed with the separated cylinder fuelling strategy to provide the user with more

control and flexibility when setting the engine operating point. Tests were also completed on neat diesel to serve as a baseline.

Analysis of the results found that NO_x was seen to increase with MF fraction increase with MF25 on average attaining a 20% increase in $ISNO_x$ over diesel. This was found as the lower cetane number, and auto-ignition temperature of MF resulted in a higher ignition delay time, the oxygenated nature of MF aided in improving premixed combustion by self-supplying O_2, increasing combustion speed, cylinder pressure and temperature and thus $ISNO_x$ emissions. The ISUHC and ISCO produced also increased as MF fraction increased and can be accredited to the low cetane number of MF. This increased ignition delay, promoting wall impingement and reducing combustion efficiency. Throughout the test range, ISUHC was seen to increase on average by 7%, 29% and 51% and ISCO was seen to increase on average by 9%, 24% and 39% with the use of MF5, MF15 and MF25, respectively.

It was found that moving the AHR50 CA closer to TDC from ATDC increased $ISNO_x$ and reduced ISUHC and ISCO and increasing the IP also did the same. Increasing the EGR reduced NO_x and increased CO and UHC by reducing combustion speed and efficiency. The most influential testing found from altering the engine conditions was the sensitivity of the manifold temperature when using HEGR and high MF blends. It was found that HEGR was needed to be used at high EGR and MF ratios to ensure that increased combustion stability could be attained. This aided in reducing the ISCO and ISUHC formation. Overall, it was found that altering the engine parameter did alter the emissions output, however, the fuel characteristics had more influence.

8.2.3 Particulate Matter Emissions of 2-Methylfuran and Diesel Blends

Similar to the analysis of gaseous emissions, the test sweeps were completed investigating AHR50 CA, IP, CEGR and HEGR with the same fuel blends and test conditions as the previous chapter.

Overall results found that particle matter significantly reduced with the increase of MF fraction, particle number was seen to decrease on average by 40%, 75% and 81% when MF5, MF15 and MF25 were tested. On average the nucleation mode SA was found to reduce by 46%, 86% and 93% and the mass was found to reduce by 50%, 89% and 95% with the use of MF5, MF15 and MF25 when compared to the diesel PM. The accumulation mode found SA to reduce by 46%, 68%, 77% and the mass by 46%, 59% and 72% when using MF5, MF15 and MF25. These reductions can be attributed to the cetane number and oxygen content of MF. The cetane number increased the ignition delay and mixture preparation while the oxygenated content increased combustion temperature and ensured fuel, particle precursors and particle oxidation was obtained.

Once the particulate analysis was completed, it was then possible to complete an overall investigation of the gaseous and particulate emissions produced. As combustion stability was a known issue with MF, it was decided to assess the performance of MF25 with HEGR in comparison to diesel with CEGR. An initial evaluation into the NIMEP COV found the mean MF25 HEGR value to be 5.3% which was a vast improvement over MF25 CEGR attaining 15.2% and even an improvement over diesel with CEGR having a NIMEP COV of 5.82%. The decreased NIMEP COV and higher in-cylinder temperature when using HEGR resulted in the MF25 HEGR ISFC reducing by 15% when compared to MF25 with CEGR and only being 4% higher than diesel with CEGR. With MF25 using HEGR the ISCO and $ISNO_x$ mean values were relatively similar to the diesel value with

the ISCO being 4.96% higher and the $ISNO_x$ being 2.12% lower. The MF25 HEGR values were much lower than MF25 with CEGR and showed a significant improvement with using increased manifold temperature. The average ISUHC value of MF25 with HEGR was found to improve when compared to the diesel CEGR mean value with a 19% reduction. The mean particulate concentration analysis found MF25 with HEGR to reduce total PM by 78.8% with nucleation reducing by 83.5% and accumulation reducing by 74.2% when compared to the diesel CEGR mean values.

8.2.4 Load Testing with Split Injection Using Various Biofuels

This final investigation studied the effect of various biofuel/diesel fuel blends at a range of engine operating conditions. The engine was operated using the conventional four-cylinder configuration, the fuels tested were biodiesel, MTHF and MF. The biofuels were each tested at a blend ratio of 25% biofuel/ 75% diesel (b/v). B25 was tested along with neat diesel to serve as a baseline. The loads tested were 1.4, 3, 6 and 9 bar BMEP with pilot and main injections being used to attain the loads. Based on the outcomes from previous chapters, HEGR was used with the biofuel blends at the two lowest loads to try and reduce combustion instability. CEGR was used with diesel throughout the tested load range.

Regarding combustion performance, B25 and MTHF25 were found to perform similarly to diesel; however, both had a slight ignition delay over diesel. MTHF25 had a longer ignition delay than B25 because of the lower cetane number of MTHF. The increased delay did result in the pilot combustion occurring within a smaller volume of the combustion chamber than diesel. However, the increased delay increased the mixture preparation time and reduced the pilot HRR peak value as a more homogeneous pilot combustion was attained. The use of a pilot injection for MF25 did not provide a separate

pilot HRR peak for the three lowest loads, and a sustained ignition delay was seen from MF25 at the highest load. This highlighted that even with HEGR, at the two lowest loads, MF25 was sensitive to in-cylinder pressure dictating combustion initiation.

An investigation into the gaseous emissions found that MF25 and MTHF25 had lower combustion efficiencies than diesel and B25 at the lowest load resulting in the BSCO and BSUHC being considerably higher than diesel and B25. At 1.4 bar BMEP, the use of MF25 increased BSCO and BSUHC by 127.78% and 228.63% over the diesel values, whereas MTHF25 increased BSCO and BSUHC production by 37.56% and 34.32%. At loads of 3 bar BMEP and upwards the BSUHC and BSCO results for all of the fuels were very similar, with those emitted from the B25 fuel blend being the lowest. These outcomes can again be accredited to the cetane number and oxygen content of the fuels; it was found that the low cetane number of the furan-based fuels outweighed the oxygen content. However, B25 with a similar cetane number to diesel was able to attain lower BSCO and BSUHC values while providing additional oxygen to the combustion process. The cetane number of biodiesel also rejected wall quenching to a similar extent as diesel while increasing the combustion efficiency from the oxygen content. At low loads, it was found that the biofuel blends generated higher $BSNO_x$ than diesel, for B25 and MTHF25 this was attributed to the use of HEGR as the maximum in-cylinder pressure was lower for these two fuels when compared to diesel. MF25 attained the highest $BSNO_x$ values of all the test fuels and points at 3 and 6 bar BMEP because of the lack of pilot HRR resulting in a single HRR peak, resulting in a high amount of in-cylinder heat. The conclusion that HEGR caused the $BSNO_x$ for the biofuels to be higher at low loads is reasonable as the biofuels attained lower NO_x than diesel at the two higher loads (which used CEGR for all test points), except MF25 a 6 bar BMEP which did not attain a pilot HRR peak.

The main factors found to control the particle matter of the various fuels was fuel composition and structure. The overall trend of the results found that MTHF25 attained lower particulate matter values than diesel, while B25 typically attained higher results than diesel and MF25 provided the lowest results throughout the load range tested. When comparing the percentage reduction of the average total particle concentration of the biofuels against diesel it was found that MTHF25 provided a 4.44% reduction, MF25 attained a 47.5% reduction and B25 provided an increased its PN value of 18.75%. Oxygenated fuels are acknowledged to reduce PM by increasing soot oxidation. It was believed that the increased molecule length of biodiesel and the increased number of carbon atoms within the molecule increased the soot production outweighing the oxygenated nature of the fuel and producing more PM than diesel at each respective load point. MTHF25 and MF25 were believed to reduce PM as they have a reduced molecule complexity and are oxygenated fuel compounds. Increased C/H ratio and double bonds are both factors that are known to increase PM. MF has a higher oxygen ratio in the fuel molecule than MTHF. MF also contains double bonds and has a higher C/H ratio. This highlights that an increase in the oxygen ratio is more influential than the double bonds and C/H ratio of MF in regard to PM formation.

8.3 Recommendations for Future Work

The outcomes of this study can allow the author to provide recommendations for further work that would build from the knowledge gained in this study.

8.3.1 Statistical Analysis of Other Alternative Fuels

The statistical analysis undertaken was successful at highlighting that MF may be suitable to use within a CI engine and that additional investigation would be worthwhile. The advances made in fuel production mean that there is a range of alternative fuels that could

be assessed. The use of a statistical analysis allowed focus to be drawn upon specific criteria's that are known to be an issue for CI engines to determine whether any fuels investigated could provide improved results over the use of neat diesel. This would allow for time-efficient experimentation to be completed that would test a wide range of fuels and determine which would be suitable to investigate further.

This statistical method could be used to assess the suitability of any alternative fuel. Furan fuels worth investigating include, but are not limited to 2,5-dimethylfuran, 5-hydroxymethyl-2-furaldehyde and furfural. Biofuels that could be investigated outside of the furan family include long-chain carbon alcohols, including pentanol hexanol and octanol (Institution Of Mechanical, 2020), as well as di-methyl ether (DME), rape-seed methyl ester (RME), FAEE and FAME produced from various feedstock and manufacturing methods.

8.3.2 Engine Parameter Sweeps of Other Furan Fuels

Any fuels that highlight suitability from the statistical analysis should then be assessed by altering set engine parameters. Completing these testing sweeps aids in further extending the knowledge of a specific fuel's performance, highlighting any sensitivities to set engine characteristics and also displaying their overall combustion performance along with gaseous and particulate emissions. In terms of new engine technology and control methods that are being released, there is now a wide range of parameters that would be worthwhile reviewing including VNT position, intake and exhaust valve timing, along with novel control techniques including varying compressor geometry as well as intake and exhaust valve lift profiles. The results attained from this thesis highlight that MTHF would be a suitable initial fuel to complete engine sweep testing.

8.3.3 Further 2-Methylfuran Analysis

2-methylfuran shows promise as an alternative fuel, the EGR testing and split load testing demonstrated than novel control techniques would be required, especially at low load. In terms of high MF blend and high EGR ratio testing, it would be worthwhile investigating having two separate HPEGR systems, one with HEGR and the other using CEGR. Along with this, two separate air intake systems could be used, with only one utilising a intercooler to reduce fresh intake charger temperature, the other could have a heater integrated into its design. This would give the user much more flexibility regarding intake manifold temperature, allowing for increased temperature to be attained without having to necessarily use a HEGR.

The use of MF/diesel blends while using LTC combustion modes is a very promising area, the low cetane number of MF would correspond well to the heavily advanced injection timing of LTC modes and the oxygen content of biofuels can aid in reducing the increased CO and UHC formation seen when using LTC modes (Zehni et al., 2017), this would, in turn, provide a reduction in the emitted PM. If using an RCCI engine then MF could be injected into the intake port of the engine and diesel injected directly into the cylinder to commence combustion. It would also be worthwhile reviewing MF's sensitivity to multiple injection events by completing further pilot injection sweeps altering the pilot injection volume, timing and number of pilot events to try and encourage pilot combustion at lower loads.

Considering the suitability of MF/diesel blends for road-going vehicles, it would be worthwhile investigating MF's performance with DPF regeneration. Although MF's performance with a plain DPF has been undertaken, further analysis regarding DPF's

coated with different catalysts would provide a worthwhile insight (Bhardwaj et al., 2013).

Finally, a study into using MF and MTHF blended with diesel could be undertaken. By assessing the results from the load testing, it can be seen that incorporating an MF/MTHF blend with diesel fuel may produce a blend that is capable of providing the high combustion quality of MTHF, the low gaseous emissions of both fuels and the greatly reduced particles that can be attained from MF. It may also be worthwhile reviewing the performance of a high MF/diesel blend using high cetane number biofuel (e.g. di-n-buthylether) in the blend as well to increase the overall cetane number of the blended fuel. This may increase combustion performance and gaseous emission while maintaining some level of the heavily reduced PM attained from using MF within a CI engine.

CHAPTER 9

9. Appendix

9.1 ATI Vision User Interface

Left-Hand Screen

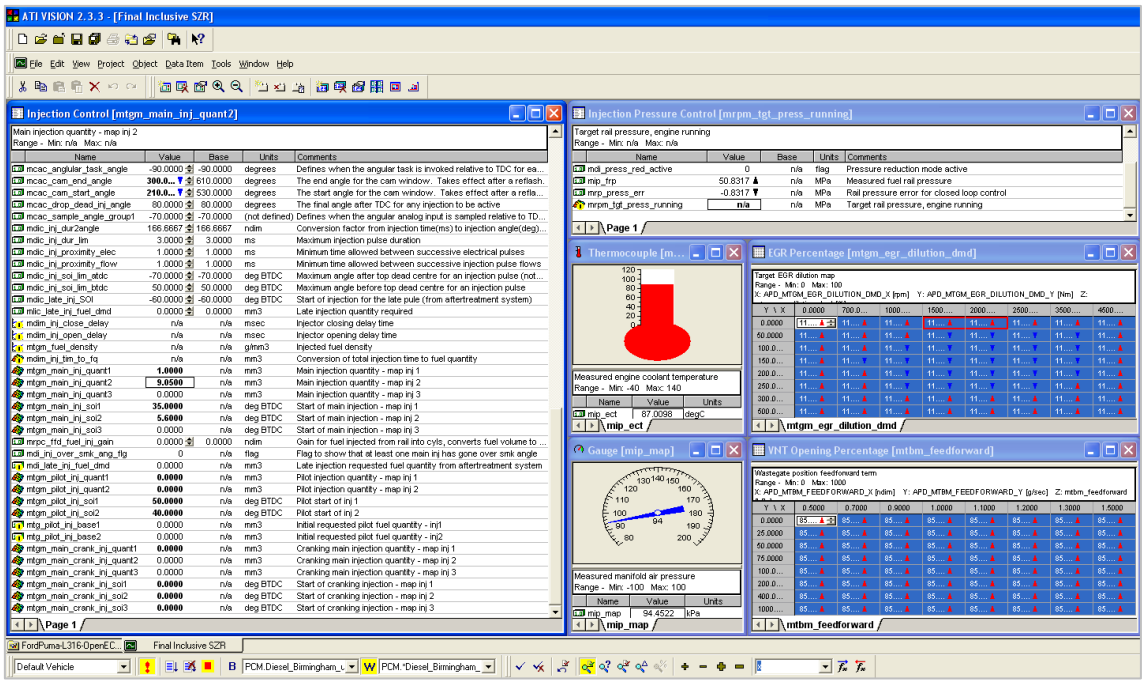

Right-Hand Screen

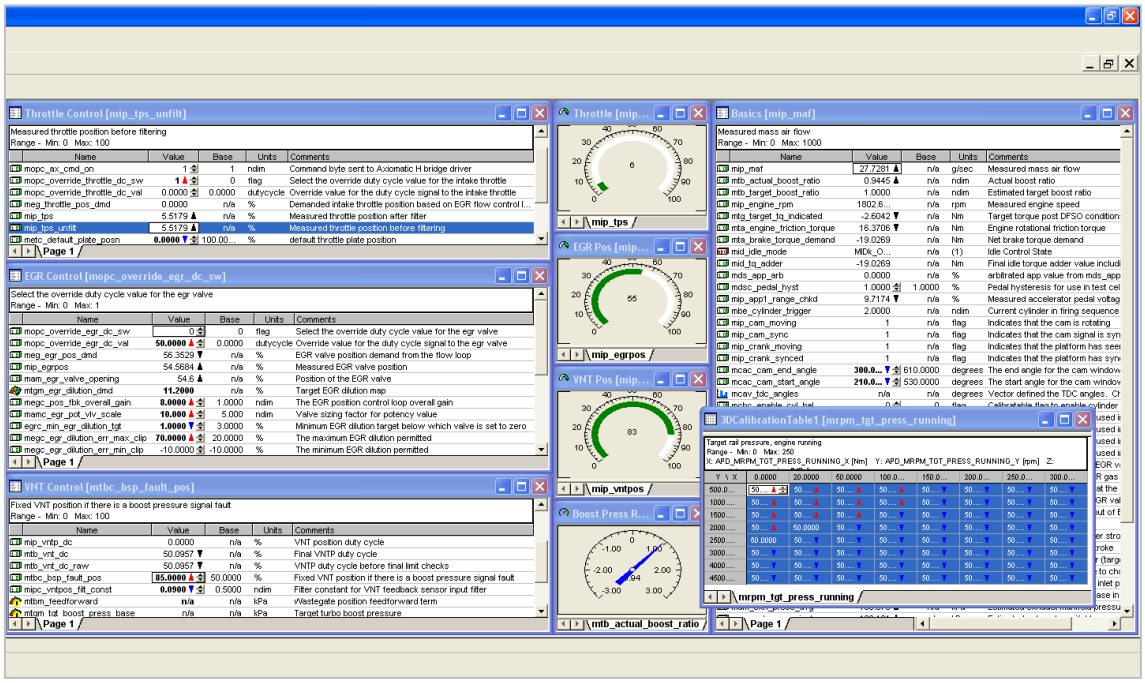

9.2 Single Cylinder Valve Wiring Diagram

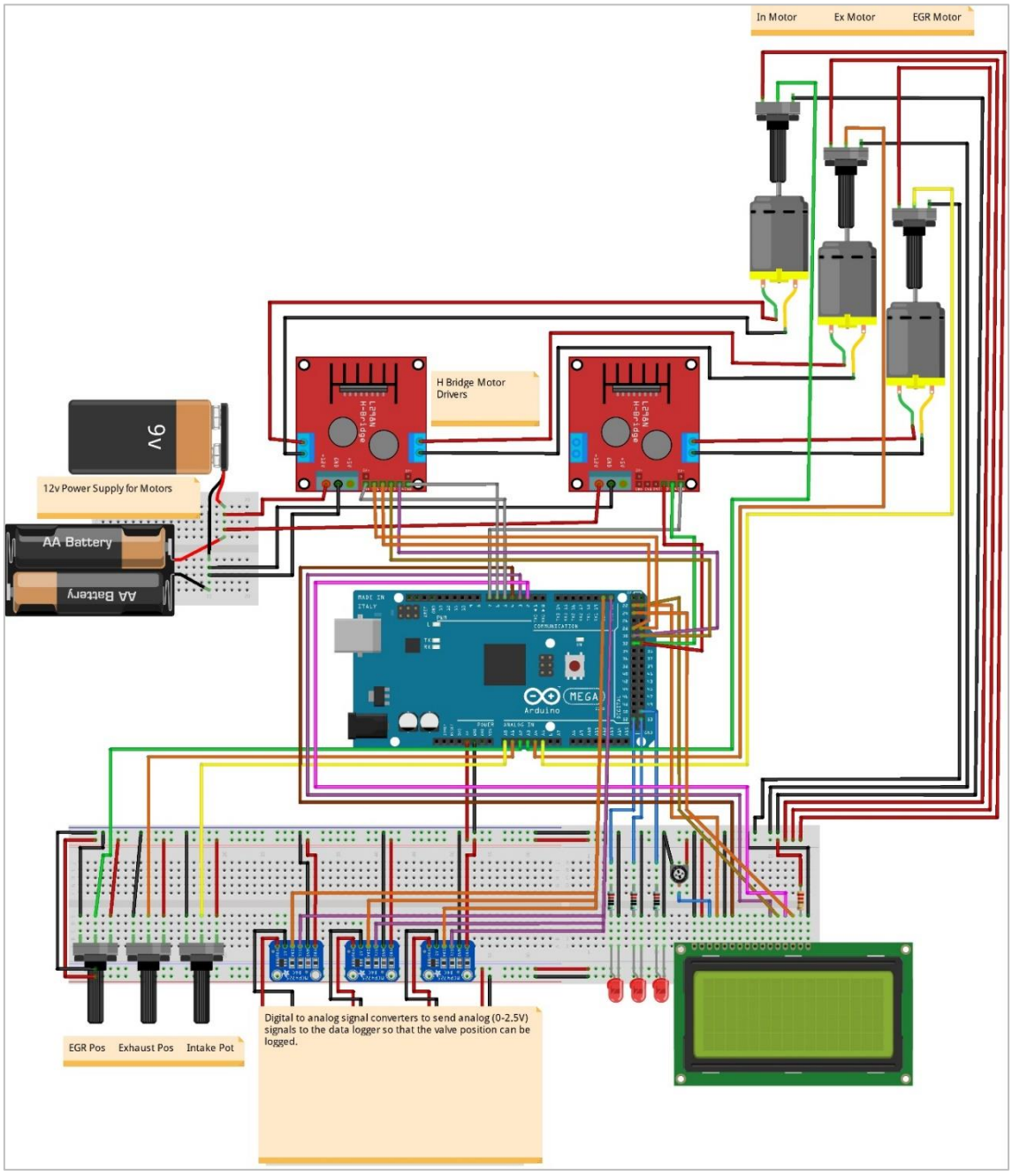

9.3 Injection System Intercooler Fan Control Wiring Diagram

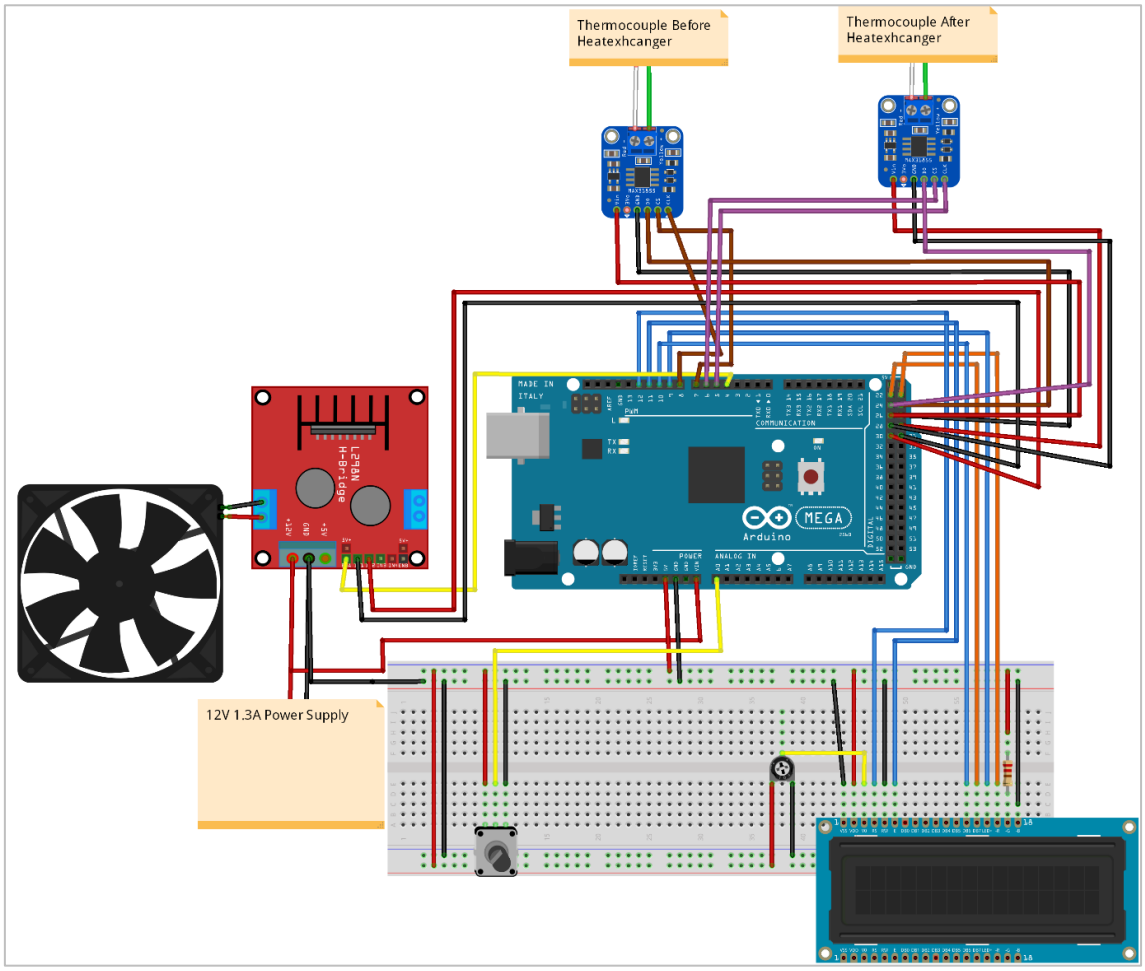

9.4 Cambustion DMS500 Exhaust Gas Sample Path

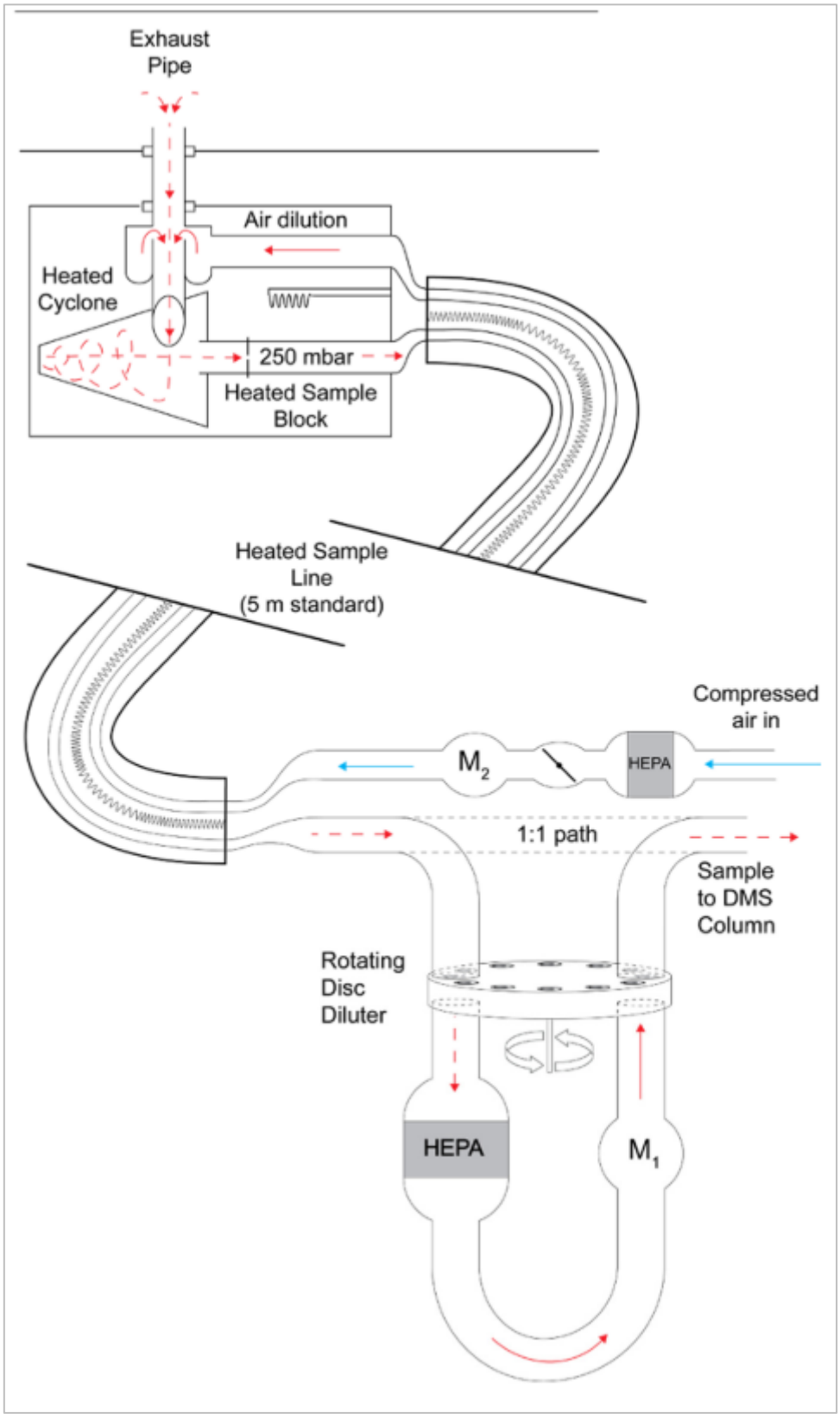

(Cambustion, 2007)

9.5 Test Plans Used for Single Cylinder Gaseous and Particle Emissions Testing in Chapter 5 & 6

Effect of Injection Timing

Test Number	IMEP (bar)	Injection Pressure (bar)	EGR in Intake Manifold (%)	Manifold Pressure (bar)	AHR50 (°ATDC)	Exhaust Back Pressure (bar)
1	5	650	15	0.95	**0**	1.15
2	5	650	15	0.95	**3**	1.15
3	5	650	15	0.95	**6**	1.15
4	5	650	15	0.95	**9**	1.15
5	5	650	15	0.95	**12**	1.15

Effect of Injection Pressure

Test Number	IMEP (bar)	Injection Pressure (bar)	EGR in Intake Manifold (%)	Manifold Pressure (bar)	AHR50 (°ATDC)	Exhaust Back Pressure (bar)
1	5	**500**	10	0.95	8	1.15
2	5	**650**	10	0.95	8	1.15
3	5	**800**	10	0.95	8	1.15
4	5	**950**	10	0.95	8	1.15
5	5	**1100**	10	0.95	8	1.15

Effect of Cold EGR Percentage

Test Number	IMEP (bar)	Injection Pressure (bar)	EGR in Intake Manifold (%)	Manifold Pressure (Bar)	AHR50 (°ATDC)	Exhaust Back Pressure (bar)
1	5	650	**0**	0.95	8	1.15
2	5	650	**7.5**	0.95	8	1.15
3	5	650	**15**	0.95	8	1.15
4	5	650	**22.5**	0.95	8	1.15
5	5	650	**30**	0.95	8	1.15

Effect of Hot EGR Percentage

Test Number	IMEP (bar)	Injection Pressure (bar)	EGR in Intake Manifold (%)	Manifold Pressure (bar)	AHR50 (°ATDC)	Exhaust Back Pressure (bar)
1	5	650	**0**	0.95	8	1.15
2	5	650	**7.5**	0.95	8	1.15
3	5	650	**15**	0.95	8	1.15
4	5	650	**22.5**	0.95	8	1.15
5	5	650	**30**	0.95	8	1.15

9.6 Particle Matter Comparison of Diesel using Cold EGR, MF25 using Cold EGR and MF25 using Hot EGR. Discussion in Chapter 6.

	EGR Ratio	Total Concentration (N/cc)	Overall Count Median diameter (nm)	Nucleation Mode Concentration (N/cc)	Nucleation Mode Count Median diameter (nm)	Nucleation Mode Geometric Standard deviation of diameter	Nucleation mode surface area (µm^2/cc)	Nucleation mode mass (µg/cc)	Accumulation Mode Concentration (N/cc)	Accumulation Mode Count Median diameter (nm)	Accumulation Mode Geometric Standard deviation of diameter	Accumulation Mode surface area (µm^2/cc)	Accumulation Mode mass (µg/cc)
Diesel Cold EGR Ratio (%)	**0**	1.7E+07	23.39	6.2E+06	5.92	1.63	1.1E+03	2.1E-06	1.2E+07	35.46	1.87	1.0E+05	1.3E-03
	7.5	1.4E+07	22.09	6.6E+06	11.01	1.63	3.8E+03	1.2E-05	7.5E+06	41.35	1.70	7.0E+04	8.4E-04
	15	2.6E+07	18.68	1.2E+07	7.87	1.61	3.9E+03	1.0E-05	1.5E+07	35.22	1.74	1.1E+05	1.2E-03
	22.5	4.2E+07	17.30	2.5E+07	9.49	1.66	1.2E+04	3.4E-05	1.8E+07	40.21	1.60	1.4E+05	1.6E-03
	30	5.3E+07	13.23	4.1E+07	10.23	1.61	2.2E+04	6.4E-05	1.4E+07	38.75	1.53	9.2E+04	9.1E-04
	Average	3.0E+07	18.94	1.8E+07	8.90	1.63	8.4E+03	2.5E-05	1.3E+07	38.20	1.69	1.0E+05	1.2E-03
MF25 Cold EGR Ratio (%)	**0**	1.0E+07	19.29	2.4E+00	7.41	1.66	1.4E+03	3.4E-06	5.9E+06	34.65	1.91	5.1E+04	6.7E-04
	7.5	7.7E+06	20.37	2.4E+00	7.30	1.63	1.1E+03	2.6E-06	4.1E+06	41.90	1.73	4.1E+04	5.1E-04
	15	1.0E+07	12.95	2.2E+00	7.22	1.61	2.3E+03	5.0E-06	2.8E+06	38.91	1.76	2.4E+04	3.0E-04
	22.5	1.5E+07	11.71	1.9E+00	8.34	1.59	4.9E+03	1.1E-05	2.0E+06	44.60	1.63	2.0E+04	2.4E-04
	30	5.3E+08	24.61	1.8E+00	21.26	1.59	8.9E+05	5.4E-03	1.1E+08	45.20	1.63	1.2E+06	1.4E-02
	Average	1.1E+08	17.78	2.1E+00	10.30	1.61	1.8E+05	1.1E-03	2.6E+07	41.05	1.73	2.6E+05	3.1E-03
MF25 Hot EGR Ratio (%)	**0**	5.8E+05	1.02	7.9E+05	1.20	0.03	2.0E+02	8.9E-07	4.4E+05	1.71	0.03	1.1E+03	1.6E-05
	7.5	9.3E+05	2.17	6.0E+05	2.17	0.02	4.7E+02	1.7E-06	5.2E+05	3.58	0.08	2.7E+03	4.3E-05
	15	1.1E+06	0.62	2.3E+06	1.10	0.00	2.3E+02	1.1E-06	7.0E+05	6.83	0.15	1.6E+03	2.8E-05
	22.5	3.1E+06	0.36	3.9E+06	0.18	0.00	1.2E+03	2.8E-06	1.1E+05	0.70	0.02	1.3E+03	1.8E-05
	30	8.5E+07	2.23	6.9E+07	1.19	0.02	2.4E+05	1.6E-03	3.0E+07	2.99	0.14	2.5E+05	1.9E-03
	Average	1.8E+07	1.28	1.5E+07	1.17	0.01	4.8E+04	3.3E-04	6.3E+06	3.16	0.08	5.1E+04	4.0E-04

9.7 Load Testing Particulate Matter Full Table. Discussion in Chapter 7.

BMEP Load (bar)	Fuel	Total Concentration (N/cc)	Nucleation Mode Concentration (N/cc)	Accumulation Mode Concentration (N/cc)	Total Concentration Reduction Over Diesel at Load Point (%)	Nucleation Mode Concentration (%)	Accumulation Mode Concentration (%)	Nucleation / Accumulation Ratio	Nucleation Mode Count Median diameter (nm)	Accumulation Mode Count Median diameter (nm)	Nuc Mode CMD Reduction Over Diesel at Load Point (%)	Acc Mode CMD % Reduction Over Diesel at Load Point (%)	Nucleation mode surface area (µm^2/cc)	Accumulation mode surface area (µm^2/cc)	Nuc Mode SA Reduction Over Diesel at Load Point (%)	Acc Mode SA Reduction Over Diesel at Load Point (%)	Nucleation mode mass (µg/cc)	Accumulation mode mass (µg/cc)	Nuc Mode Mass Reduction Over Diesel at Load Point (%)	Acc Mode Mass Reduction Over Diesel at Load Point (%)
1.4	Diesel	3.27E+07	6.03E+06	2.27E+07	0	18.43	69.19	0.27	14.35	48.56	0	0	6.09E+03	3.58E+05	0	0	2.52E-05	5.55E-03	0	0
1.4	B25	3.83E+07	1.06E+07	2.54E+07	-17.13	27.74	66.23	0.42	12.95	45.59	9.76	6.12	9.07E+03	3.11E+05	-48.93	13.13	3.64E-05	4.20E-03	-44.44	24.32
1.4	MF25	9.97E+06	6.59E+06	3.47E+06	69.51	66.08	34.78	1.9	10	45.81	30.31	5.66	3.31E+03	4.01E+04	45.65	88.80	9.85E-06	5.17E-04	60.91	90.68
1.4	MTHF25	2.39E+07	8.55E+06	1.41E+07	26.91	35.82	59.24	0.6	15.36	50.9	-7.04	-4.82	9.98E+03	1.93E+05	-63.88	46.09	4.44E-05	2.60E-03	-76.19	53.15
3	Diesel	4.07E+07	5.70E+06	2.83E+07	0	13.99	69.55	0.2	23.76	54.54	0	0	1.49E+04	5.35E+05	0	0	9.81E-05	8.58E-03	0	0
3	B25	3.86E+07	1.23E+07	2.39E+07	5.16	31.91	61.84	0.52	17.75	53.55	25.29	1.82	1.93E+04	3.58E+05	-29.53	33.08	1.00E-04	4.95E-03	-1.94	42.31
3	MF25	1.20E+07	3.82E+06	7.31E+06	70.52	31.84	60.9	0.52	15.93	51.72	32.95	5.17	4.72E+03	9.66E+04	68.32	81.94	2.15E-05	1.24E-03	78.08	85.55
3	MTHF25	2.18E+07	5.95E+06	1.54E+07	46.44	27.32	70.59	0.39	17.9	47.99	24.66	12.01	9.40E+03	2.08E+05	36.91	61.12	4.86E-05	2.92E-03	50.46	65.97
6	Diesel	6.22E+07	1.58E+07	3.62E+07	0	25.36	58.19	0.44	24.09	74.48	0	0	4.87E+04	1.04E+06	0	0	3.55E-04	1.75E-02	0	0
6	B25	8.27E+07	1.39E+07	6.60E+07	-32.96	16.81	79.8	0.21	21.53	53.41	10.63	28.29	2.79E+04	1.13E+06	42.71	-8.65	1.57E-04	1.74E-02	55.77	0.57
6	MF25	1.81E+07	4.10E+06	1.27E+07	70.90	22.59	69.87	0.32	17.14	49.91	28.85	32.99	5.80E+03	1.76E+05	88.09	83.08	2.80E-05	2.42E-03	92.11	86.17
6	MTHF25	5.27E+07	2.06E+07	2.72E+07	15.27	39.15	51.59	0.76	23.11	70.02	4.07	5.99	5.39E+04	6.19E+05	-10.68	40.48	3.58E-04	9.21E-03	-0.85	47.37
9	Diesel	1.52E+08	2.20E+07	9.93E+07	0	14.41	65.18	0.22	22.54	77.27	0	0	4.72E+04	3.39E+06	0	0	2.65E-04	6.31E-02	0	0
9	B25	1.83E+08	1.39E+07	1.55E+08	-20.39	7.6	85.18	0.09	26.28	51.56	-16.59	33.27	4.72E+04	2.68E+06	0.00	20.94	3.60E-04	4.22E-02	-35.85	33.12
9	MF25	1.11E+08	1.16E+07	9.57E+07	26.97	10.47	86.03	0.12	21.08	48.68	6.48	37.00	2.59E+04	1.60E+06	45.13	52.80	1.62E-04	2.59E-02	38.87	58.95
9	MTHF25	1.77E+08	4.05E+07	1.15E+08	-16.45	22.96	65.23	0.35	23.81	70.01	-5.63	9.40	1.17E+05	2.90E+06	-147.88	14.45	8.04E-04	4.74E-02	-203.40	24.88

10. References

ABD-ALLA, G. H. 2002. Using exhaust gas recirculation in internal combustion engines: a review. *Energy Conversion and Management,* 43**,** 1027-1042.

ADEWALE, P., DUMONT, M.-J. & NGADI, M. 2015. Recent trends of biodiesel production from animal fat wastes and associated production techniques. *Renewable and Sustainable Energy Reviews,* 45**,** 574-588.

ADEY, A. J., CUNLIFFE, F. & MARDELL, J. E. 1981. Rotary Fuel Injection Pump Developments for High Speed Diesel Engines. SAE International.

ADLER, J. & BANDHAUER, T. 2017. Performance of a Diesel Engine at High Coolant Temperatures. *Journal of Energy Resources Technology,* 139**,** 062203-062203-13.

AGARWAL, A. K., DHAR, A., GUPTA, J. G., KIM, W. I., LEE, C. S. & PARK, S. 2014. Effect of fuel injection pressure and injection timing on spray characteristics and particulate size–number distribution in a biodiesel fuelled common rail direct injection diesel engine. *Applied Energy,* 130**,** 212-221.

AGARWAL, A. K., DHAR, A., SRIVASTAVA, D. K., MAURYA, R. K. & SINGH, A. P. 2013. Effect of fuel injection pressure on diesel particulate size and number distribution in a CRDI single cylinder research engine. *Fuel,* 107**,** 84-89.

AGARWAL, A. K., SINGH, A. P. & MAURYA, R. K. 2017. Evolution, challenges and path forward for low temperature combustion engines. *Progress in Energy and Combustion Science,* 61**,** 1-56.

AGARWAL, A. K., SINGH, S. K., SINHA, S. & SHUKLA, M. K. 2004. Effect of EGR on the exhaust gas temperature and exhaust opacity in compression ignition engines. *Sadhana-Academy Proceedings in Engineering Sciences,* 29**,** 275-284.

AHMED, A., AL-AMIN, A. Q., AMBROSE, A. F. & SAIDUR, R. 2016. Hydrogen fuel and transport system: A sustainable and environmental future. *International Journal of Hydrogen Energy,* 41**,** 1369-1380.

AHMED, S. A., ZHOU, S., ZHU, Y., FENG, Y., MALIK, A. & AHMAD, N. 2019. Influence of Injection Timing on Performance and Exhaust Emission of CI Engine Fuelled with Butanol-Diesel Using a 1D GT-Power Model. *Processes,* 7**,** 299.

ALFARRA, M. 2004. *Insights into atmospheric organic aerosols using an aerosol mass spectrometer.* University of Manchester Manchester, UK.

ANASTASOV, A. 2009. Biodiesel—Basic Characteristics, Technology and Perspectives. *Biotechnology & Biotechnological Equipment,* 23**,** 755-759.

ANDREWS, G., ABDELHALIM, S. & WILLIAMS, P. 1993. The influence of lubricating oil age on emissions from an IDI diesel. SAE Technical Paper.

ARO, E.-M. 2016. From first generation biofuels to advanced solar biofuels. *Ambio,* 45**,** 24-31.

AVL 1996. AVL 733S Dynamic Fuel Meter - Operating Manual. *In:* GMBH, A. L. (ed.).

AYANDOTUN B. WASIU, A. R. A. A. A. M. R. H. 2012. The Effect of Carbon Dioxide Content-natural Gas on the Performance Characteristics of Engines: A Review. *Journal of Applied Sciences,* 12**,** 2346-2350.

BARABÁS, I. & TODORUŢ, I.-A. 2011. Biodiesel quality, standards and properties. *Biodiesel-quality, emissions and by-products***,** 3-28.

BARLOW, M., SMITH, D. & STEWARD, D. 1983. Fuel composition. *European patent EP0082689*.

BASCOM, R. C., BROERING, L. C. & WULFHORST, D. E. 1971. Design factors that affect diesel emissions. SAE Technical Paper.

BENAJES, J., MOLINA, S., GARCÍA, A. & MONSALVE-SERRANO, J. 2015. Effects of low reactivity fuel characteristics and blending ratio on low load RCCI (reactivity controlled compression ignition) performance and emissions in a heavy-duty diesel engine. *Energy,* 90**,** 1261-1271.

BERRY, I. J. & BRUNT, M. F. J. 1996. Improved Control of EGR During Speed/Load Transients. SAE International.

BHARDWAJ, O. P., KREMER, F., PISCHINGER, S., LÜERS, B., KOLBECK, A. F. & KOERFER, T. 2013. Impact of Biomass-Derived Fuels on Soot Oxidation and DPF Regeneration Behavior. SAE International.

BHUIYA, M. M. K., RASUL, M. G., KHAN, M. M. K., ASHWATH, N., AZAD, A. K. & HAZRAT, M. A. 2016. Prospects of 2nd generation biodiesel as a sustainable fuel – Part 2: Properties, performance and emission characteristics. *Renewable and Sustainable Energy Reviews,* 55**,** 1129-1146.

BODEN, T. A., MARLAND, G. & ANDRES, R. J. 2011. Global, Regional, and National Fossil-Fuel CO2 Emissions, 1751 - 2008 (Version 2011).

BOHAC, S. V., HAN, M., JACOBS, T. J., LÓPEZ, A. J., ASSANIS, D. N. & SZYMKOWICZ, P. G. 2006. Speciated hydrocarbon emissions from an automotive diesel engine and DOC utilizing conventional and PCI combustion. SAE Technical Paper.

BUCHMAN, M. R. & WINTER, A. 2017. Investigating the Effect of Intake Manifold Size on the Transient Response of Single Cylinder Turbocharged Engines. SAE International.

BULLIS, K. 2015. *Why We Don't Have Battery Breakthroughs* [Online]. MIT Technology Review. Available: https://www.technologyreview.com/s/534866/why-we-dont-have-battery-breakthroughs/ [Accessed 28/11/2018 2018].

BURTSCHER, H. & MATTER, U. 2000. Particle formation due to fuel additives. *SAE transactions*, 1334-1338.

CAMBUSTION 2007. DMS 500 User Manual v4.14. *In:* LTD, C. (ed.).

CAO, L., BHAVE, A., SU, H., MOSBACH, S., KRAFT, M., DRIS, A. & MCDAVID, R. M. 2009. Influence of Injection Timing and Piston Bowl Geometry on PCCI Combustion and Emissions. *SAE International Journal of Engines,* 2, 1019-1033.

CARLEY, L. 2003. *Exhaust Gas Recirculation (EGR)* [Online]. AA1Car.com: AA1Car Auto Diagnosis Repair Information. Available: https://www.aa1car.com/library/egr.htm [Accessed 18/04/2019 2019].

CHANG, C. T. & FARRELL, P. V. 1997. A Study on the Effects of Fuel Viscosity and Nozzle Geometry on High Injection Pressure Diesel Spray Characteristics. SAE International.

CHEN, G., SHEN, Y., ZHANG, Q., YAO, M., ZHENG, Z. & LIU, H. 2013. Experimental study on combustion and emission characteristics of a diesel engine fueled with 2,5-dimethylfuran–diesel, n-butanol–diesel and gasoline–diesel blends. *Energy,* 54, 333-342.

CHHEDA, J. N., HUBER, G. W. & DUMESIC, J. A. 2007. Liquid-Phase Catalytic Processing of Biomass-Derived Oxygenated Hydrocarbons to Fuels and Chemicals. *Angewandte Chemie International Edition,* 46, 7164-7183.

CHRISTIE, M. & WARD, A. Aftertreatment and Emissions Control for Improved GHG and Air Quality. ERC 2017 Symposium: Impact of Future Regulations on Engine Technology, Madison, USA, 14th–15th June, 2015.

COUNCIL, N. R. 2008. *Transitions to alternative transportation technologies: A focus on hydrogen*, National Academies Press.

CUATTO, T., PASSERONE, C., SANSOE, C., GREGORETTI, F., JURECSKA, A. & SANGIOVANNI-VINCENTELLI, A. 2000. A case study in embedded systems design: An Engine Control Unit. *Design Automation for Embedded Systems,* 6, 71-88.

DAHODWALA, M., JOSHI, S., KOEHLER, E., FRANKE, M. & TOMAZIC, D. 2015. Experimental and Computational Analysis of Diesel-Natural Gas RCCI Combustion in Heavy-Duty Engines. SAE International.

DANGAR, H. & RATHOD, G. P. 2013. Combine effect of exhaust gas recirculation (EGR) and varying inlet air pressure on performance and

emission of diesel engine. *IOSR Journal of Mechanical and Civil Engineering (IOSR-JMCE),* 6**,** 26-33.

DEARN, K. D., MOORCROFT, H., SUKJIT, E., POAPONGSAKORN, P., HU, E. Z., XU, Y. F. & HU, X. G. 2018. The tribology of fructose derived biofuels for DISI gasoline engines. *Fuel,* 224**,** 226-234.

DENNY, M., HOLST, F., HELMANTEL, A., PERSSON, H., TUNESTÅL, P. & ANDERSSON, Ö. 2019. Impact of closely-coupled triple-pilot and conventional double-pilot injection strategies in a LD diesel engine. *Fuel,* 246**,** 141-148.

DERFER, J. M. B., C.E; BURK, F.C; HESS, R.E; LOVELL,W.G; RANDALL,R.A; SABINA, J.R 1958. *Knocking Characteristics of Pure Hydrocarbons.,* West Conshohocken, PA, ASTM International.

DIESEL, R. 1898. *Internal Combustion Engine*. United States patent application.

DIESELNET. 2019. *Emission Standards: Europe: Cars and Light Trucks* [Online]. Available: https://www.dieselnet.com/standards/eu/ld.php [Accessed].

DRAGONE, G., FERNANDES, B. D., VICENTE, A. A. & TEIXEIRA, J. A. 2010. Third generation biofuels from microalgae.

DU, J., CHEN, X., LIU, L., LIU, D. & MA, X. 2019. Mechanism of combustion noise influenced by pilot injection in PPCI diesel engines. *Applied Sciences,* 9**,** 1875.

DUDLEY, B. 2019. British Petroleum Energy Outlook 2019 Edition. 2019 ed.

DWIVEDI, G., JAIN, S. & SHARMA, M. P. 2011. Impact analysis of biodiesel on engine performance—A review. *Renewable and Sustainable Energy Reviews,* 15**,** 4633-4641.

EDWARDS, P. P., KUZNETSOV, V. L., DAVID, W. I. F. & BRANDON, N. P. 2008. Hydrogen and fuel cells: Towards a sustainable energy future. *Energy Policy,* 36**,** 4356-4362.

EL-DIN, M. R. N., MISHRIF, M. R., GAD, M. S. & KESHAWY, M. 2019. Performance and exhaust emissions of a diesel engine using diesel nanoemulsions as alternative fuels. *Egyptian Journal of Petroleum,* 28**,** 197-204.

ELDEEB, M. A. & AKIH-KUMGEH, B. 2018. Recent Trends in the Production, Combustion and Modeling of Furan-Based Fuels. *Energies,* 11.

EPA., U. 2016. *Basic Information about NO2* [Online]. United States Environmental Protection Agency. Available: https://www.epa.gov/no2-pollution/basic-information-about-no2 [Accessed 17/02/2020 2020].

FENELEY, A. J., PESIRIDIS, A. & ANDWARI, A. M. 2017. Variable Geometry Turbocharger Technologies for Exhaust Energy Recovery and Boosting-A Review. *Renewable and Sustainable Energy Reviews,* 71**,** 959-975.

FLAIG, F. 2013. *Pressure in diesel engines; Why higher injection pressure saves fuel and also increases performance and torque.* [Online]. Bosch. Available: https://www.bosch-presse.de/pressportal/de/en/pressure-in-diesel-engines-42396.html [Accessed 15/01/2018 2018].

FLUENT, A. 2012. 14.5 Theory Guide. *Canonsburg, PA, USA: ANSYS Inc*.

FOMOCO 2018. Ford Mondeo. *In:* LIMITED, F. M. C. (ed.) *Ford Mondeo Sales Brochure.* Brentwood: Ford Motor Company Limited.

GAO, Z., WAGNER, R. M., SLUDER, C. S., DAW, C. S. & GREEN, J. B. 2011. Using a phenomenological computer model to investigate advanced combustion trajectories in a CIDI engine. *Fuel,* 90**,** 1907-1918.

GATHERGOOD, N., GRANADOS, M. L. & ALONSO, D. M. 2018. *Furfural: An entry point of lignocellulose in biorefineries to produce renewable chemicals, polymers, and biofuels*.

GHURRI, A., KIM, J.-D., KIM, H. G., JUNG, J.-Y. & SONG, K.-K. 2012. The effect of injection pressure and fuel viscosity on the spray characteristics of biodiesel blends injected into an atmospheric chamber. *Journal of mechanical science and technology,* 26**,** 2941-2947.

GIAKOUMIS, E. G., RAKOPOULOS, D. C. & RAKOPOULOS, C. D. 2016. Combustion noise radiation during dynamic diesel engine operation including effects of various biofuel blends: A review. *Renewable and Sustainable Energy Reviews,* 54**,** 1099-1113.

GILLINGHAM, K. 2018. *Hydrogen Internal Combustion Engine Vehicles: A Prudent Intermediate Step or a Step in the Wrong Direction?*

GROTE, M., PRESTON, J., CHERRETT, T. & TUCK, N. 2019. Locating residential on-street electric vehicle charging infrastructure: A practical methodology. *Transportation Research Part D: Transport and Environment,* 74**,** 15-27.

HANCOCK, E. G., SCI, HANCOCK, E. G. & SOCIETY OF CHEMICAL, I. 1985. *Technology of gasoline*.

HARDENBERG, H. O. & SCHAEFER, A. J. 1981. The Use of Ethanol as a Fuel for Compression Ignition Engines. SAE International.

HEBBAR, G. S. 2014. NOx from Diesel Engine Emission and Control Strategies-A Review. *International Journal of Mechanical Engineering and Robotics Research,* 3**,** 471.

HEITZIG, S., WEINEBECK, A. & MURRENHOFF, H. 2015. Testing and Prediction of Material Compatibility of Biofuel Candidates with Elastomeric Materials. SAE International.

HELMANTEL, A. 2008. Reduction of NOx Emissions from a Light Duty DI Diesel Engine in Medium Load Conditions with High EGR Rates. SAE International.

HEUSER, B., KREMER, F., PISCHINGER, S. & KLANKERMAYER, J. 2013. Optimization of Diesel Combustion and Emissions with Tailor-Made Fuels from Biomass. SAE International.

HEYWOOD, J. B. 1988. *Internal combustion engine fundamentals*, New York : McGraw-Hill, [1988] ©1988.

HIERETH, H. & PRENNINGER, P. H. W. 2007. Charging the internal combustion engine.

HILDINGSSON, L., KALGHATGI, G., TAIT, N., JOHANSSON, B. & HARRISON, A. 2009. Fuel octane effects in the partially premixed combustion regime in compression ignition engines. SAE Technical Paper.

HOPPE, F., BURKE, U., THEWES, M., HEUFER, A., KREMER, F. & PISCHINGER, S. 2016. Tailor-Made Fuels from Biomass: Potentials of 2-butanone and 2-methylfuran in direct injection spark ignition engines. *Fuel,* 167**,** 106-117.

HOUNTALAS, D., MAVROPOULOS, G. & BINDER, K. 2008. Effect of exhaust gas recirculation (EGR) temperature for various EGR rates on heavy duty DI diesel engine performance and emissions. *Energy,* 33**,** 272-283.

HUANG, J., XIA, J., JIANG, W., LI, Y. & LI, J. 2015. Biodiesel production from microalgae oil catalyzed by a recombinant lipase. *Bioresource Technology,* 180**,** 47-53.

ICKES, A. M. 2009. *Fuel Property Impact on a Premixed Diesel Combustion Mode.*

IEA 2019. The Future of Hydrogen. Partoc: IEA.

IGLESIAS FERNÁNDEZ, J. M. 2016. Study of Combustion Using a Computational Fluid Dynamics Software (ANSYS).

IIDA, N. 1993. Surrounding gas effects on soot formation and extinction-observation of diesel spray combustion using a rapid compression machine. *SAE Transactions***,** 787-797.

INSTITUTION OF MECHANICAL, E. 2020. *Internal Combustion Engines and Powertrain Systems for future Transport 2019*, Taylor & Francis.

ISERMANN, R., SCHAFFNIT, J. & SINSEL, S. 1999. Hardware-in-the-loop simulation for the design and testing of engine-control systems. *Control Engineering Practice,* 7**,** 643-653.

JAICHANDAR, S. & ANNAMALAI, K. 2011. The status of biodiesel as an alternative fuel for diesel engine-An Overview. *Journal of Sustainable Energy & Environment,* 2**,** 71-75.

JANSSEN, A., JAKOB, M., MÜTHER, M. & PISCHINGER, S. 2010. Tailor-made fuels from biomass—potential of biogenic fuels for reducing emissions. *MTZ worldwide,* 71**,** 54-60.

JANSSEN, A. J., KREMER, F. W., BARON, J. H., MUETHER, M., PISCHINGER, S. & KLANKERMAYER, J. 2011. Tailor-Made Fuels from Biomass for Homogeneous Low-Temperature Diesel Combustion. *Energy & Fuels,* 25**,** 4734-4744.

JONES, C. S. & MAYFIELD, S. P. 2012. Algae biofuels: versatility for the future of bioenergy. *Current Opinion in Biotechnology,* 23**,** 346-351.

JONKER, M. T. O. 2008. Absorption of polycyclic aromatic hydrocarbons to cellulose. *Chemosphere,* 70**,** 778-782.

JUTTU, S., THIPSE, S. S., MARATHE, N. V. & GAJENDRA BABU, M. K. 2007. Homogeneous Charge Compression Ignition (HCCI): A New Concept for Near Zero NOx and Particulate Matter (PM) from Diesel Engine Combustion. The Automotive Research Association of India.

KAMIMOTO, T. & BAE, M.-H. 1988. High combustion temperature for the reduction of particulate in diesel engines. *SAE transactions***,** 692-701.

KIMURA, S., AOKI, O., OGAWA, H., MURANAKA, S. & ENOMOTO, Y. 1999. New Combustion Concept for Ultra-Clean and High-Efficiency Small DI Diesel Engines. SAE International.

KITTELSON, D. B. 1998. Engines and nanoparticles: A review. *Journal of Aerosol Science,* 29**,** 575-588.

KNOTHE, G., KRAHL, J. & GERPEN, J. V. 2010. 2.4 The First "Biodiesel". *Biodiesel Handbook (2nd Edition).* AOCS Press.

KOKJOHN, S. L., HANSON, R. M., SPLITTER, D. A. & REITZ, R. D. 2011. Fuel reactivity controlled compression ignition (RCCI): a pathway to controlled high-efficiency clean combustion. *International Journal of Engine Research,* 12**,** 209-226.

KONG, F., ZHANG, L. Y., ZENG, J. & ZHANG, Y. H. 2007. Automatic measurement and control system for vehicle ECU based on CAN bus. *2007 Ieee International Conference on Automation and Logistics, Vols 1-6***,** 964-+.

LADOMMATOS, N., ABDELHALIM, S. & ZHAO, H. 2000. The effects of exhaust gas recirculation on diesel combustion and emissions. *International Journal of Engine Research,* 1**,** 107-126.

LADOMMATOS, N., ABDELHALIM, S. M., ZHAO, H. & HU, Z. 1996. The dilution, chemical, and thermal effects of exhaust gas recirculation on

diesel engine emissions-part 1: Effect of reducing inlet charge oxygen. SAE Technical Paper.

LADOMMATOS, N., ABDELHALIM, S. M., ZHAO, H. & HU, Z. 1997. The dilution, chemical, and thermal effects of exhaust gas recirculation on diesel engine emissions-Part 4: effects of carbon dioxide and water vapour. *SAE transactions*, 1844-1862.

LAPUERTA, M., ARMAS, O. & GARCÍA-CONTRERAS, R. 2007. Stability of diesel–bioethanol blends for use in diesel engines. *Fuel,* 86, 1351-1357.

LEI, J., BI, Y. & SHEN, L. 2010. Performance and emission characteristics of diesel engine fueled with ethanol-diesel blends in different altitude regions. *BioMed Research International,* 2011.

LI, J., YANG, W. M., AN, H., ZHOU, D. Z., YU, W. B., WANG, J. X. & LI, L. 2015. Numerical investigation on the effect of reactivity gradient in an RCCI engine fueled with gasoline and diesel. *Energy Conversion and Management,* 92, 342-352.

LI, X., JIA, P. & WANG, T. 2016. Furfural: A promising platform compound for sustainable production of C4 and C5 chemicals. *ACS catalysis,* 6, 7621-7640.

LI, Y., JIA, M., CHANG, Y., LIU, Y., XIE, M., WANG, T. & ZHOU, L. 2014. Parametric study and optimization of a RCCI (reactivity controlled compression ignition) engine fueled with methanol and diesel. *Energy,* 65, 319-332.

LIPMAN, T. E. 2020. Chapter 12 - Vehicle technologies for achieving near and longer term fuel economy and climate goals. *In:* DEAKIN, E. (ed.) *Transportation, Land Use, and Environmental Planning.* Elsevier.

LORNE, D. B., A. 2019. *Biofuels in the Road Transport Sector* [Online]. IFP Energies Nouvelles. Available: https://www.ifpenergiesnouvelles.com/article/biofuels-dashboard-2019 [Accessed 03/02/2020 2020].

LU, L., ADAM, M., KILBURN, M., SARATH, H., SOMERVILLE, M., JAHANSHAHI, S. & MATHIESON, J. 2013. Substitution of Charcoal for Coke Breeze in Iron Ore Sintering. *ISIJ International,* 53, 1607-1616.

LUKOIL 2016. Major Trends in Global Oil Market to 2030. http://www.lukoil.com/Business/Futuremarkettrends: Lukoil.

MACHRAFI, H. 2010. HCCI Combustion Chemistry, Reduced Kinetic Mechanisms and Controlling Strategies. *In:* LACKNER, M. W., F. AGARWAL, A. K. (ed.) *Handbook of Combustion.* Wiley.

MAIBOOM, A., TAUZIA, X. & HÉTET, J. F. 2008. Influence of high rates of supplemental cooled EGR on NOx and PM emissions of an automotive

HSDI diesel engine using an LP EGR loop. *International Journal of Energy Research,* 32**,** 1383-1398.

MAURO, S., ŞENER, R., GÜL, M. Z., LANZAFAME, R., MESSINA, M. & BRUSCA, S. 2018. Internal combustion engine heat release calculation using single-zone and CFD 3D numerical models. *International Journal of Energy and Environmental Engineering,* 9**,** 215-226.

MAURYA, R. K. & AGARWAL, A. K. 2011. Experimental investigation on the effect of intake air temperature and air–fuel ratio on cycle-to-cycle variations of HCCI combustion and performance parameters. *Applied Energy,* 88**,** 1153-1163.

MENDONCA, L. S., LUCEIRO, D. D., MARTINS, M. E. S. & BISOGNO, F. E. 2017. Development of an Engine Control Unit: Implementation of the Architecture of Tasks. *2017 Ieee International Conference on Industrial Technology (Icit)***,** 1142-1146.

MERKER, G. P., SCHWARZ, C. & TEICHMANN, R. 2011. *Combustion engines development: mixture formation, combustion, emissions and simulation*, Springer Science & Business Media.

MERKISZ, J. 2015. *Nanoparticle emissions from combustion engines / Jerzy Merkisz, Jacek Pielecha*, Cham : Springer, 2015.

MILLER, B. G. 2017. 6 - Clean Coal Technologies for Advanced Power Generation. *In:* MILLER, B. G. (ed.) *Clean Coal Engineering Technology (Second Edition).* Butterworth-Heinemann.

MOHAN, B., YANG, W. & CHOU, S. K. 2013. Fuel injection strategies for performance improvement and emissions reduction in compression ignition engines—A review. *Renewable and Sustainable Energy Reviews,* 28**,** 664-676.

MOHANKUMAR, S. & SENTHILKUMAR, P. 2017. Particulate matter formation and its control methodologies for diesel engine: A comprehensive review. *Renewable and Sustainable Energy Reviews,* 80**,** 1227-1238.

MUSCULUS, M. P., LACHAUX, T., PICKETT, L. M. & IDICHERIA, C. A. 2007. End-of-injection over-mixing and unburned hydrocarbon emissions in low-temperature-combustion diesel engines. SAE Technical Paper.

NATIONAL-INSTRUMENTS. 2020. *PCI-6251 Multifunction I/O Device* [Online]. National-Instruments. Available: https://www.ni.com/en-gb/support/model.pci-6251.html [Accessed 19/04/2020 2020].

NIEMAN, D. E., DEMPSEY, A. B. & REITZ, R. D. 2012. Heavy-Duty RCCI Operation Using Natural Gas and Diesel. SAE International.

O'CONNOR, J. & MUSCULUS, M. 2013. Post injections for soot reduction in diesel engines: a review of current understanding. *SAE International Journal of Engines,* 6**,** 400-421.

OBREGÓN, I., GANDARIAS, I. & ARIAS, P. L. 2018. 2-Methyl Tetrahydrofuran (MTHF) and its Use as Biofuel. *Furfural.*

OKOLIEOCHA, C., RAPS, D., SUBRAMANIAM, K. & ALTSTÄDT, V. 2015. Microcellular to nanocellular polymer foams: Progress (2004–2015) and future directions – A review. *European Polymer Journal,* 73**,** 500-519.

PACE, V., HOLZER, W., HOYOS, P., HERNÁIZ, M.J. AND ALCÁNTARA, A.R. 2014. 2-Methyltetrahydrofuran. *In Encyclopedia of Reagents for Organic Synthesis.*

PACITTI, G., AMPHLETT, S., MILLER, P., NORRIS, R. & TRUSCOTT, A. 2008. Real-time crank-resolved engine simulation for testing new engine management systems. *SAE International Journal of Passenger Cars-Mechanical Systems,* 1**,** 801-809.

PAN, M., SHU, G., PAN, J., WEI, H., FENG, D., GUO, Y. & LIANG, Y. 2014. Performance comparison of 2-methylfuran and gasoline on a spark-ignition engine with cooled exhaust gas recirculation. *Fuel,* 132**,** 36-43.

PARK, J., LEE, K. S., SONG, S. & CHUN, K. M. 2010. Numerical study of a light-duty diesel engine with a dual-loop EGR system under frequent engine operating conditions using the doe method. *International Journal of Automotive Technology,* 11**,** 617-623.

PARK, S.-K., CHOI, K.-S., WANG, H.-M., KIM, H.-M., LEE, D.-H., KIM, T.-J., LEE, J. & CHO, Y.-K. 2007. Effects of the Internal Shape of EGR Cooler on Heat Exchanger Efficiencies. SAE International.

PARK, Y. & BAE, C. 2014. Experimental study on the effects of high/low pressure EGR proportion in a passenger car diesel engine. *Applied Energy,* 133**,** 308-316.

PATIL, A. & TAJI, D. S. 2013. *Effect of Oxygenated Fuel Additive on Diesel Engine Performance and Emission: A Review*.

PICOTECH. 2020a. *PicoLog 1000 Manuals* [Online]. Pico Technology. Available: https://www.picotech.com/data-logger/picolog-1000-series/picolog-1000-manuals [Accessed 19/04/2020 2020].

PICOTECH. 2020b. *Thermocouple Data Logger* [Online]. Pico Technology. Available: https://www.picotech.com/data-logger/tc-08/thermocouple-data-logger [Accessed 19/04/2020 2020].

PIERPONT, D. A., MONTGOMERY, D. T. & REITZ, R. D. 1995. Reducing Particulate and NOx Using Multiple Injections and EGR in a D.I. Diesel. SAE International.

PRADEEP, V. & SHARMA, R. P. 2007. Use of HOT EGR for NOx control in a compression ignition engine fuelled with bio-diesel from Jatropha oil. *Renewable Energy,* 32**,** 1136-1154.

QIAN, Y., OUYANG, L., WANG, X., ZHU, L. & LU, X. 2015. Experimental studies on combustion and emissions of RCCI fueled with n-heptane/alcohols fuels. *Fuel,* 162**,** 239-250.

RAEIE, N., EMAMI, S. & KARIMI SADAGHIYANI, O. 2014. Effects of injection timing, before and after top dead center on the propulsion and power in a diesel engine. *Propulsion and Power Research,* 3**,** 59-67.

RAJAK, U., NASHINE, P., VERMA, T. N. & PUGAZHENDHI, A. 2019. Performance, combustion and emission analysis of microalgae Spirulina in a common rail direct injection diesel engine. *Fuel,* 255**,** 115855.

RANDOLPH, A. L. 1990. Methods of Processing Cylinder-Pressure Transducer Signals to Maximize Data Accuracy. SAE International.

REIJNDERS, J., BOOT, M. & DE GOEY, P. 2018. Particle nucleation-accumulation mode trade-off: A second diesel dilemma? *Journal of Aerosol Science,* 124**,** 95-111.

REN, Y., RANDALL, R. & MILTON, B. 1999. Influence of the resonant frequency on the control of knock in diesel engines. *Proceedings of the Institution of Mechanical Engineers, Part D: Journal of Automobile Engineering,* 213**,** 127-133.

RESITOGLU, I. A., ALTINISIK, K. & KESKIN, A. 2015. The pollutant emissions from diesel-engine vehicles and exhaust aftertreatment systems. *Clean Technologies and Environmental Policy,* 17**,** 15-27.

RISTOVSKI, Z., MORAWSKA, L., MOORE, M. R., AGRANOVSKI, V., SWANSON, C. & HUGHES, D. 2003. The impact of sulphur content of diesel fuel on ultrafine particle formation.

ROBERT BOSCH GMB, H. 2005. Diesel-engine management. 4th ed. completely revised and extended. ed. Plochingen : Chichester: Plochingen : Robert Bosch Gmbh

Chichester : Wiley.

ROMÁN-LESHKOV, Y., BARRETT, C. J., LIU, Z. Y. & DUMESIC, J. A. 2007. Production of dimethylfuran for liquid fuels from biomass-derived carbohydrates. *Nature,* 447**,** 982.

RUWE, L., MOSHAMMER, K., HANSEN, N. & KOHSE-HÖINGHAUS, K. 2018. Influences of the molecular fuel structure on combustion reactions towards soot precursors in selected alkane and alkene flames. *Physical Chemistry Chemical Physics,* 20**,** 10780-10795.

SAINI, S., MEGHENDRA, S. & KUMAR, A. 2018. Global warming and climate change: next generation biofuels and role of biotechnology. *Intl J Life Sci Pharma Res,* 8**,** 52-57.

SANDALCI, T., KARAGÖZ, Y., ORAK, E. & YÜKSEK, L. 2014. An Experimental Investigation of Ethanol-Diesel Blends on Performance and Exhaust

Emissions of Diesel Engines. *Advances in Mechanical Engineering,* 6**,** 409739.

SANTA CRUZ BIOTECHNOLOGY, I. 2015. *2-Methyltetrahydrofuran Safety Data Sheet* [Online]. Santa Cruz Biotechnology, Inc. Available: http://datasheets.scbt.com/sds/eghs/en/sc-238158.pdf [Accessed 06/02/2020 1.1].

SCHINDLER, C. S., W. SINGER, W. Notes on "Soot“ Measurement of Diesel Engines. Combustion Generated Particles, 2004 Zurich, Switzerland. 17.

SCHUBIGER, R., BERTOLA, A. & BOULOUCHOS, K. 2001. Influence of EGR on combustion and exhaust emissions of heavy duty DI-diesel engines equipped with common-rail injection systems. SAE Technical Paper.

SCHÖPPE, D., ZÜLCH, S., HARDY, M., GEURTS, D., JORACH, R. W. & BAKER, N. 2008. Delphi Common Rail system with direct acting injector. *MTZ worldwide,* 69**,** 32-38.

SELIM, M. Y. 2003. A study of some combustion characterstics of dual fuel engine using EGR. *SAE transactions***,** 1152-1160.

SEO, S. H., LEE, S. W., HWANG, S. H. & JEON, J. W. 2006. Development of network gateway between CAN and FlexRay protocols for ECU embedded systems. *2006 Sice-Icase International Joint Conference, Vols 1-13***,** 5168-+.

SHAHIR, V. K., JAWAHAR, C. P. & SURESH, P. R. 2015. Comparative study of diesel and biodiesel on CI engine with emphasis to emissions—A review. *Renewable and Sustainable Energy Reviews,* 45**,** 686-697.

SHARMA, Y. C., SINGH, B. & UPADHYAY, S. N. 2008. Advancements in development and characterization of biodiesel: A review. *Fuel,* 87**,** 2355-2373.

SINGH, R., PANDEY, A. & GNANSOUNOU, E. 2017. *Biofuels: Production and Future Perspectives*.

SJÖBERG, M., EDLING, L.-O., ELIASSEN, T., MAGNUSSON, L. & ÅNGSTRÖM, H.-E. 2002. GDI HCCI: Effects of Injection Timing and Air Swirl on Fuel Stratification, Combustion and Emissions Formation. SAE International.

SLUDER, C. S., WAGNER, R. M., LEWIS, S. A. & STOREY, J. M. 2001. High efficiency clean combustion in a Direct-Injection Diesel engine. Citeseer.

SMITH, K. R., JERRETT, M., ANDERSON, H. R., BURNETT, R. T., STONE, V., DERWENT, R., ATKINSON, R. W., COHEN, A., SHONKOFF, S. B., KREWSKI, D., POPE, C. A., THUN, M. J. & THURSTON, G. 2009. Public health benefits of strategies to reduce greenhouse-gas emissions: health implications of short-lived greenhouse pollutants. *The Lancet,* 374**,** 2091-2103.

SONG, J., CHEENKACHORN, K., WANG, J., PEREZ, J., BOEHMAN, A. L., YOUNG, P. J. & WALLER, F. J. 2002. Effect of Oxygenated Fuel on Combustion and Emissions in a Light-Duty Turbo Diesel Engine. *Energy & Fuels,* 16**,** 294-301.

SPEIGHT, J. G. 2011a. 2 - Production, properties and environmental impact of hydrocarbon fuel conversion. *In:* KHAN, M. R. (ed.) *Advances in Clean Hydrocarbon Fuel Processing.* Woodhead Publishing.

SPEIGHT, J. G. 2011b. Chapter 3 - Fuels for Fuel Cells. *In:* SHEKHAWAT, D., SPIVEY, J. J. & BERRY, D. A. (eds.) *Fuel Cells: Technologies for Fuel Processing.* Amsterdam: Elsevier.

SRIVASTAVA, D. K. & AGARWAL, A. K. 2008. Particulate matter emissions from single cylinder diesel engine: effect of engine load on size and number distribution. *SAE Int*.

STANISLAUS, A., MARAFI, A. & RANA, M. S. 2010. Recent advances in the science and technology of ultra low sulfur diesel (ULSD) production. *Catalysis Today,* 153**,** 1-68.

STATISTICS, N. 2019. Energy Trends September 2019. *In:* DEPARTMENT FOR BUSINESS, E. I. S. (ed.).

STONE, R. 1999. *Introduction to internal combustion engines*, Springer.

STRAUBEL, J. B. 2014. *Driving Range for the Model S Family* [Online]. Available: https://www.tesla.com/en_GB/blog/driving-range-model-s-family [Accessed 28/11/2018 2018].

SU, W. 2010. 11 - Alternative combustion system for heavy-duty diesel engines. *In:* ZHAO, H. (ed.) *Advanced Direct Injection Combustion Engine Technologies and Development.* Woodhead Publishing.

SURYAWANSHI, J. G. & DESHPANDE, N. V. 2005. Effect of Injection Timing Retard on Emissions and Performance of a Pongamia Oil Methyl Ester Fuelled CI Engine. SAE International.

SZYMKOWICZ, P. G. & BENAJES, J. 2018. Single-cylinder engine evaluation of a multi-component diesel surrogate fuel at a part-load operating condition with conventional combustion. *Fuel,* 226**,** 286-297.

TAKAHASHI, F. & GLASSMAN, I. 1984. Sooting Correlations for Premixed Flames. *Combustion Science and Technology,* 37**,** 1-19.

TAN, P.-Q., DENG, K. & LU, J.-X. 2004. Analysis of particulate matter composition from a heavy-duty diesel engine. *Proceedings of the Institution of Mechanical Engineers, Part D: Journal of Automobile Engineering,* 218**,** 1325-1331.

TAYLOR, C. F. 1977. *The internal-combustion engine in theory and practice*.

TIAN, Y., SUN, P., SUN, X. & CHEN, J. 2017. High-Pressure Common-Rail Fuel Injection System with Electronic Control System in Diesel Engine. *International Journal of Research in Engineering and Science (IJRES),* 5**,** 6.

TOMECZEK, J. & GRADOŃ, B. 1997. The Role of Nitrous Oxide in the Mechanism of Thermal Nitric Oxide Formation within Flame Temperature Range. *Combustion Science and Technology,* 125**,** 159-180.

TURNER, D., XU, H., CRACKNELL, R. F., NATARAJAN, V. & CHEN, X. 2011. Combustion performance of bio-ethanol at various blend ratios in a gasoline direct injection engine. *Fuel,* 90**,** 1999-2006.

TURNS, S. R. 1995. Introduction to combustion : concepts and applications / Stephen R. Turns. New York

London: New York

London : McGraw-Hill.

UCHIDA, H., KASHIMOTO, A. & IWAKIRI, Y. 2006. Development of wide flow range compressor with variable inlet guide vane. *R&D Review of Toyota Crdl,* 41**,** 9-14.

VARIOHM 2019. Pressure Sensor - EPT3100. *In:* EUROSENSOR, V. (ed.).

VENKAT REDDY, C. R., OSHEL, R. & VERKADE, J. G. 2006. Room-Temperature Conversion of Soybean Oil and Poultry Fat to Biodiesel Catalyzed by Nanocrystalline Calcium Oxides. *Energy & Fuels,* 20**,** 1310-1314.

WAN GHAZALI, W. N. M., MAMAT, R., MASJUKI, H. H. & NAJAFI, G. 2015. Effects of biodiesel from different feedstocks on engine performance and emissions: A review. *Renewable and Sustainable Energy Reviews,* 51**,** 585-602.

WANG, C., XU, H., DANIEL, R., GHAFOURIAN, A., HERREROS, J. M., SHUAI, S. & MA, X. 2013. Combustion characteristics and emissions of 2-methylfuran compared to 2,5-dimethylfuran, gasoline and ethanol in a DISI engine. *Fuel,* 103**,** 200-211.

WANG, Y. 2012. *Study of deposit formation inside diesel injectors nozzles.* Massachusetts Institute of Technology.

WANG, Y., LIU, H. & LEE, C.-F. F. 2016. Particulate matter emission characteristics of diesel engines with biodiesel or biodiesel blending: A review. *Renewable and Sustainable Energy Reviews,* 64**,** 569-581.

WEI, H., FENG, D., SHU, G., PAN, M., GUO, Y., GAO, D. & LI, W. 2014. Experimental investigation on the combustion and emissions characteristics of 2-methylfuran gasoline blend fuel in spark-ignition engine. *Applied Energy,* 132**,** 317-324.

WEINEBECK, A. 2019. *Impact of Biofuel Lubricity on Wear in Highly Loaded Contacts.* Doctor of Philosophy, RWTH Aachen Universtiy.

WILLIAMS, P. T., ANDREWS, G. E. & BARTLE, K. D. 1987. The role of lubricating oil in diesel particulate and particulate PAH emissions. SAE Technical Paper.

WU, C.-Y. 2007. Atmospheric Aerosol » Section 4. *In:* LI, Y. (ed.).

WU, X., MCLAREN, J., MADL, R. & WANG, D. 2010. Biofuels from lignocellulosic biomass. *Sustainable Biotechnology.* Springer.

XIAO, H., WANG, R., ZENG, P., HOU, B., XUE, Q. & RUAN, J. 2018. Effects of Pilot Injection on Combustion and Emissions Characteristics using 2-Methylfuran/Diesel Blends in a Diesel Engine. *Thermal Science*.

XIAO, H., WANG, R., ZENG, P., JIANG, A., HOU, B. & YANG, S. 2017. Particulate matter and unregulated emissions of diesel engine fueled with 2-methylfuran diesel blends. *Fuel,* 208**,** 168-173.

XIAO, H. L., YANG, X. L., HOU, B. B., WANG, R., XUE, Q. & JU, H. L. 2019. Combustion performance and pollutant emissions analysis of a diesel engine fueled with biodiesel and its blend with 2-methylfuran. *Fuel,* 237**,** 1050-1056.

XIAO, H. L., ZENG, P. F., LI, Z. Z., ZHAO, L. R. & FU, X. W. 2016. Combustion performance and emissions of 2-methylfuran diesel blends in a diesel engine. *Fuel,* 175**,** 157-163.

YAHUZA, I. & DANDAKOUTA, H. 2015. A performance review of ethanol-diesel blended fuel samples in compression-ignition engine. *Journal of Chemical Engineering & Process Technology,* 6**,** 1-6.

YOON, S. K., GE, J. C. & CHOI, N. J. 2019. Influence of fuel injection pressure on the emissions characteristics and engine performance in a CRDI Diesel engine fueled with palm biodiesel blends. *Energies,* 12**,** 3837.

YU, R., WONG, V. & SHAHED, S. 1980. Sources of hydrocarbon emissions from direct injection diesel engines. *SAE Transactions***,** 324-335.

ZAMBONI, G. & CAPOBIANCO, M. 2013. Influence of high and low pressure EGR and VGT control on in-cylinder pressure diagrams and rate of heat release in an automotive turbocharged diesel engine. *Applied Thermal Engineering,* 51**,** 586-596.

ZEHNI, A., KHOSHBAKHTI SARAY, R. & POORGHASEMI, K. 2017. Numerical comparison of PCCI combustion and emission of diesel and biodiesel fuels at low load conditions using 3D-CFD models coupled with chemical kinetics. *Applied Thermal Engineering,* 110**,** 1483-1499.

ZERAATI-REZAEI, S., AL-QAHTANI, Y. & XU, H. 2017. Investigation of hot-EGR and low pressure injection strategy for a Dieseline fuelled PCI engine. *Fuel,* 207**,** 165-178.

ZHANG, F. 2013. *Spray, combustion and emission characteristics of dieseline fuel.* University of Birmingham.

ZHANG, J. 2011. *Particle Matter Emission Control and Related Issues for Diesel Engines.* Ph.D, The University of Birmingham.

ZHANG, Q., CHEN, G., ZHENG, Z., LIU, H., XU, J. & YAO, M. 2013. Combustion and emissions of 2,5-dimethylfuran addition on a diesel engine with low temperature combustion. *Fuel,* 103**,** 730-735.

ZHANG, R. & KOOK, S. Effect of fuel injection pressure on size and structure of in-cylinder soot particles sampled from an automotive-size optical diesel engine. Proc. 18th Australasian Fluid Mechanics Conf., Launceston, Australia, 2012.

ZHAO, S. & YOU, F. 2019. Comparative life-cycle assessment of Li-ion batteries through process-based and integrated hybrid approaches. *ACS Sustainable Chemistry & Engineering,* 7**,** 5082-5094.

ZHENG, M., READER, G. T. & HAWLEY, J. G. 2004. Diesel engine exhaust gas recirculation—a review on advanced and novel concepts. *Energy Conversion and Management,* 45**,** 883-900.

ZHU, L., ZHANG, W., LIU, W. & HUANG, Z. 2010. Experimental study on particulate and NOx emissions of a diesel engine fueled with ultra low sulfur diesel, RME-diesel blends and PME-diesel blends. *Science of The Total Environment,* 408**,** 1050-1058.

ÇAĞATAY BAYINDIR, K., GÖZÜKÜÇÜK, M. A. & TEKE, A. 2011. A comprehensive overview of hybrid electric vehicle: Powertrain configurations, powertrain control techniques and electronic control units. *Energy Conversion and Management,* 52**,** 1305-1313.